INSA INSTITUT NATIONAL DES SCIENCES APPLIQUÉES CENTRE VAL DE LOIRE

GDAŃSK UNIVERSITY OF TECHNOLOGY

ÉCOLE DOCTORALE ÉNERGIE, MATÉRIAUX, SCIENCES DE LA TERRE ET DE L'UNIVERS
Gabriel Lamé Laboratory/ Faculty of Civil and Environmental Engineering

PHD THESIS COMPLETED IN « COTUTELLE » presented by:

Katarzyna SZEPIETOWSKA

to obtain the degree of:
Doctor of INSA Centre Val de Loire
and Gdańsk University of Technology

Discipline: Mechanical engineering

POLYNOMIAL CHAOS EXPANSION IN BIO- AND STRUCTURAL MECHANICS

Thesis supervisors:

Prof. Eric FLORENTIN	**INSA Centre Val de Loire**
Prof. Izabela LUBOWIECKA	**Gdańsk University of Technology**
Dr. Benoit MAGNAIN	**INSA Centre Val de Loire**

Reviewers:

Prof. Jerzy MAŁACHOWSKI	**Military University of Technology**
Prof. Philippe ROUCH	**Arts et Métiers ParisTech**

JURY:

Prof. Paweł KŁOSOWSKI	Gdańsk University of Technology	Jury president
Prof. Jerzy MAŁACHOWSKI	Military University of Technology	
Prof. Philippe ROUCH	Arts et Métiers ParisTech	
Prof. Eric FLORENTIN	INSA Centre Val de Loire	
Prof. Izabela LUBOWIECKA	Gdańsk University of Technology	
Prof. Krystyna KAZIMIEROWICZ-FRANKOWSKA	Institute of Hydro-Engineering of Polish Academy of Sciences	

Acknowledgements

First and foremost, I would like to express my deep gratitude to all my supervisors: Dr. hab. Inż. Izabela Lubowiecka, prof. nadzw. PG, Prof. Eric Florentin and Dr. Benoit Magnain. I am very grateful for their guidance, advice, availability, encouragement and patience. Furthermore, special thanks go to Prof. Izabela Lubowiecka for engaging me in the project concerning the mechanical approach to hernia repair and introducing me the world of biomechanics. In addition I thank Prof. Eric Florentin for introducing me to stochastic mechanics, enabling me to do my Phd in cotutelle and welcoming me to France. I thank Dr. Benoit Magnain for a lot of valuable help in realisation of the research.

I am also grateful to Prof. Paweł Kłosowski for his help and the opportunity to work in the Department of Structural Mechanics at Gdańsk University of Technology.

My sincere thanks also go to Prof. Czesław Szymczak and Dr. hab. Inż. Agnieszka Tomaszewska, prof. nadzw. PG for encouragement, sharing experience and stimulating discussions.

I thank Dr. Kamil Bury for discussions on medical aspects of the research on hernia repair, Dr. James Pfeffer for English corrections and Anna Pestka (Mleczek) for data needed to model the mechanics of timber corner joints.

The research presented in the thesis was partially supported by grant UMO-2015/17/N/ST8/02705 from the National Science Centre, Poland, and by the subsidy for the development of young scientists given by the Faculty of Civil and Environmental Engineering, Gdansk University of Technology. Computations were performed partially in TASK Computer Science Centre, Gdansk, Poland. The study on timber joints was partially supported by grant No. 2015/17/B/ST8/03260 given by the National Science Centre, Poland.

Last but not least, I would like to thank my family and friends for their support.

Contents

Symbols

A	cross sectional area of the cable
$\mathbf{A}^\top\mathbf{A}$, $\mathbf{A}^\top\mathbf{W}\mathbf{A}$	information matrix
$a_{\boldsymbol{\alpha}}$	coefficients of the polynomial chaos expansion
C	covariance function
$\mathbf{C}$	correlation matrix
D	variance
$D_{i_1,\ldots,i_s}$	partial variance
DoE	abbreviation of "Design of Experiment"
E	elastic modulus of the cable
E_1, E_2	elastic moduli of surgical mesh in two directions
E_1^{aw}, E_2^{aw}	elastic moduli of abdominal wall in two directions
E_L	Young's modulus of wood in longitudinal direction
$Err_{\%}$	reference error
$Err_{PC\%}$	error of the PC metamodel
Err_s	error in calculating Sobol' indices
$F(\mathbf{Z}, \omega)$	random field
FE	abbreviation of "finite element"
$f_{\mathbf{X}}$	probability density function of the input $\mathbf{X}$
f_{X_i}	marginal distribution of variable X_i
g	distributed load in the cable model
G_{12}^{aw}	shear modulus of abdominal wall
H	horizontal reaction in the cable model
H_0	initial force in the cable
H_n	Hermite polynomial
k_{aw}	stiffness of elastic foundation

k_f	stiffness of elastic springs
L_0	initial length of the cable
L_n	Legendre polynomial
l	span of the surgical mesh/cable
l_s	overlap of the surgical mesh onto the fascia
LHS	abbreviation of "latin hypercube sampling"
M	dimension of the input vector $\mathbf{X}$
MC	abbreviation of "Monte Carlo"
N_{KL}	number of terms of Karhunen-Loéve expansion
N_{MC}	number of simulations in Monte Carlo method
$NRMSE$	normalized root mean square error
P	size of the polynomial chaos basis
PC	abbreviation of "polynomial chaos"
PDF	abbreviation of "probability density function"
p	polynomial order
p_{ia}	intraabdominal pressure
R_i	reaction force in i-th support
r_i	radial change in position of support
R_{max}	maximum reaction force
$RMSE$	root mean square error
QoI	abbreviation of "quantity of interest"
SA	abbreviation of "sensitivity analysis"
S_i^{local}	local sensitivity index
$S_{i_1,\ldots,i_s}$	Sobol' sensitivity index
S_i^{Tot}	total Sobol' sensitivity index
t_i	forced displacement of i-th support
UQ	abbreviation of "uncertainty quantification"
u_{aw}	displacement of point in healthy abdominal wall
u_i	displacement of the centre of the implant in the global model
u_{max}	maximum deflection of the implant
w	weight function
$\mathbf{X}$	random input vector
Y	model response, quantity of interest

$\mathbf{Y}_{ex}$	vector of exact solutions
α_{aw}	orientation angle of the abdominal wall in lateral zone
α_{orient}	orientation angle of the surgical mesh
δ_i	angular change in position of support
Δ_p	displacement of the cable edge
λ_i	eigenvalue of C
μ_{cj}	coefficient of friction between wooden logs
φ_i	eigenfunction of C
$\Psi_{\boldsymbol{\alpha}}(\boldsymbol{\xi})$,$\Phi_{\boldsymbol{\alpha}}(\mathbf{X})$	multivariate polynomial basis
$\bar{\sigma}_{max}$	mean value of maximum principal stresses
$\bar{\sigma}_{min}$	mean value of minimum principal stresses
$\max \sigma_{max}$	maximum value of maximum principal stresses
$\min \sigma_{min}$	minimum value of minimum principal stresses
$\boldsymbol{\xi}$	standard input vector
Ξ	design of experiment
$\mathcal{A}$	truncation set
$\mathcal{H}_{\mathbf{X}}$	support of input vector $\mathbf{X}$
$\mathcal{H}_{X_k}$	support of random variable X_k
$\mathcal{LN}(\mu_{lni}, \sigma_{lni})$	lognormal distribution
$\mathcal{M}$	computational model
$\mathcal{M}^{PC}$	polynomial chaos metamodel
$\mathcal{M}_0$	mean
$\mathcal{M}_i(X_i)$, $\mathcal{M}_{i,j}(X_i, X_j)$, $\mathcal{M}_{1,2,\ldots,M}(\mathbf{X})$	terms of ANalysis of VAriance decomposition
$\mathcal{N}(\mu_i, \sigma_i)$	normal distribution
$\mathcal{T}$	isoprobabilistic transform
$\mathcal{U}([a, b])$	uniform distribution

Chapter 1

Introduction

The motivation of this study is the need for a mechanics-based approach to support the treatment of ventral hernia to help surgeons in solving the problem of hernia recurrences. Mathematical models are created to predict the mechanical behaviour of the implant-abdominal wall system and they can be used in the optimization of ventral hernia repair parameters. However, challenges such as the uncertainty related to natural variability of abdominal tissue mechanics and difficulties accurate measurement of material model parameters may occur in the modelling. Therefore, this study concerns an application of uncertainty quantification methods in the models of the implant-abdominal wall system.

1.1 Ventral Hernia

A ventral hernia is a bulge of tissues through a gap in the muscalo-fascial system. The hernia defect can be congenital, develop over time as a result of muscle weakness or be caused by trauma. Nowadays hernia commonly occurs at the place of an incision after other abdomen surgery (incisional hernia). In the study of Bensley et al. [10] hernia developed in 12% of patients after major abdominal surgery and in 3.3% after a laparoscopic operation. In France alone around 13 000 incisional hernia repairs are performed each year with an annual cost of around 84 million euros when estimated indirect cost related to sick leave etc. are included [56].

The treatment of ventral hernia is usually carried out by surgical intervention. An implant in the form of a surgical mesh is connected by the surgeon to the abdominal wall to cover the defect. It can be performed by an open or laparoscopic operation. Laparoscopic ventral hernia repair (LVHR) is less invasive and is believed to be superior to open repair in terms of short-term results [134, 142]. Although a smaller number

of postoperative complications were observed in patients treated by the laparoscopic method, the hernia recurrence rate is similar for both methods. Meshes for LVHR are typically made from polypropylene, polyester or expanded polytetrafluoroethylene [46]. It is desirable to reduce the number of hernia recurrences and pseudo-recurrences related to excessive bulging of the mesh. An increase of efficiency of hernia repair would have not only a clinical impact, but also a societal and economical one. It has been estimated that reduction of the recurrence rate only by 1% would save 32 million dollars just in the US [132]. Despite a number of studies, there is no consensus on the material and type of fixation which should be used in hernia repair [18].

Brown and Finch [20] wrote a medical review on surgical mesh choice which also described the history of surgical meshes as implants in hernia repair. The use of surgical meshes to reinforce the abdominal wall in hernia treatment began in 1958. Initially it was believed that a higher tensile strength of implant led to better persistence of the repair. However, patients after implantation of heavyweight surgical meshes suffered from pain and movement restriction. The trend in thinking about the desired properties of implants changed in the 1990s when biocompatibility of implants began to be investigated and lightweight meshes appeared [96]. Attention started to be paid to abdominal wall mechanics and physiology. Surgeons realized that knowledge about abdominal wall mechanics is crucial to finding efficient solutions for hernia repair [84]. Lightweight meshes are designed to mimic the mechanics of the abdominal wall. Their large pore size improves integration with human tissue and reduces problems of reaction to a foreign body when compared to heavy meshes with small pore size. Biocompatibility of implants in general in many medical applications is usually focused on biological and chemical interaction between prosthetic material and native tissue [182] but Mazza and Ehret [115] emphasized importance of mechanical biocompatibility in the case of implants in contact with soft biological tissues.

1.1.1 Mechanics based approach for ventral hernia repair

In order to improve hernia treatment it is important to understand the mechanics of the implant, abdominal wall, connection of the implant to the abdominal wall and the behaviour of the whole system of the abdominal wall and implant. An extensive review of studies on the mechanical approach to ventral hernia can be found in the paper by Deeken and Lake [41].

1.1.1.1 Surgical mesh

Klinge et al. [93] compared different meshes in terms of various mechanical properties such as tensile strength and stiffness after integration into the tissue. Saberski et al. [138] investigated the anisotropy of implants and identified elastic moduli in two directions of the implant. In [172] the effect of sample size and strain rate was tested in a uniaxial tensile test of surgical meshes. Biaxial tests with various ratios of applied stress were performed in [37]. Biaxial and cyclic tests on surgical meshes were performed in [42, 137]. Cyclic tests were also performed in [173], where the importance of incorporating preconditioning is discussed. The long-term behaviour of implanted meshes was studied in [72], where explanted meshes with ingrowth tissue were tested. In [136] an experiment protocol is proposed to simulate the behaviour of ingrown meshes. The studies above showed that surgical meshes are characterized by nonlinearity, anisotropy, dependence on loading rate and loading history, and change of mechanical behaviour after implantation (for example - due to the in-growth of tissue or resorption of implant components), which all make it challenging to determine the set of criteria which are important for mechanical compatibility with soft tissues [115]. Maurer et al. [114] proposed and experimental protocol composed of a set of test addressing the aforementioned characteristics of implants in order to compare different surgical meshes with each other.

Mechanical compatibility can also be explored by computer simulation of the abdominal wall-implant system [106, 107, 167], which requires a material model of the surgical mesh with identified parameters. In [97] and [174] the nonlinear behaviour of implants is approximated by a piecewise affine model. Such a simplified approach is used in the similar problem of technical textiles, which also show a nonlinear stress-strain relationship, e.g in [3, 191]. In [174] the implant material was modelled as orthotropic, whereas in [4, 105] a dense net material model appropriate for textile materials [94] was used. Transverse isotropic hyperelastic model parameters were identified for chosen surgical meshes in [71]. In [75] an orthotropic hyperelastic model is proposed and the change of effective porosity under deformation is investigated. Surgical meshes are usually modelled as homogenous membranes e.g. [67]. However, models of surgical mesh structure have also been proposed [68]. A structural model of textile surgical meshes was proposed in [135], but the study was conducted in the context of pelvic reconstruction. Coronary stents are another example of a device in contact with soft tissues wheremechanical behaviour is studied by numerical analysis [25].

1.1.1.2 Abdominal wall as a structure

The frontal abdominal wall (Figure 1.1) is composed of muscles, fascias, ligaments, fat and skin. There are four pairs of muscles. In the central part lie the rectus abdominis and in each lateral part, a composite of the external oblique, the internal oblique and the transversus abdominis. Muscles are covered by aponeuroses, which in the central part form the rectus sheath (Figure 1.2) covering the rectus abdominis and meet together in the midline creating linea alba. Therefore the abdominal wall as whole is a composite structure. What is more, some of the above-mentioned components are also consist of different layers, for example, linea alba is composed of 3 layers.

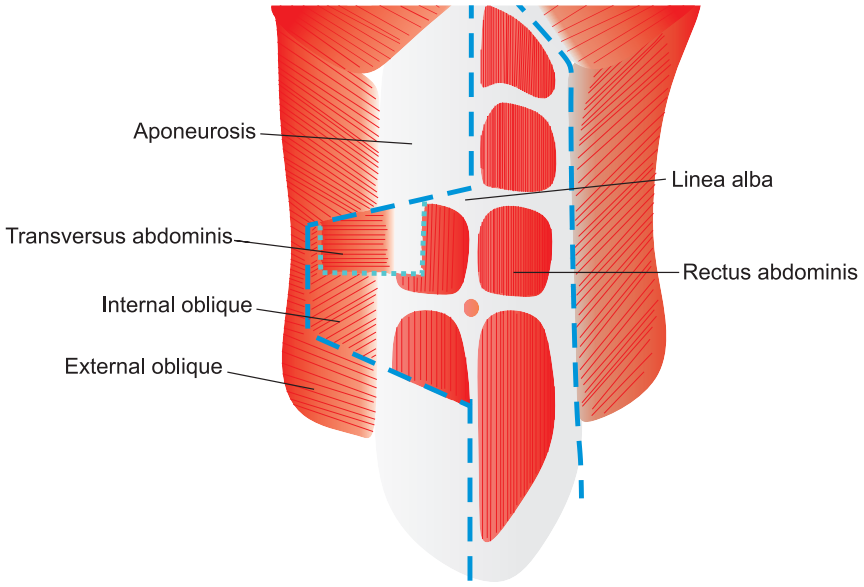

FIGURE 1.1: Scheme of human abdominal wall layers; picture inspired by [112]

Experimental measurement on biological tissues is challenging from both a practical as well as theoretical perspective [8]. Some characteristics of soft tissues which make them difficult to study from the mechanical point of view and to model are: nonlinearity, anisotropy, viscoelasticy, near incompressibility, dependence on the environment, growth and remodelling [79].

As reported in the literature, some single components of the abdominal wall were tested: linea alba [35, 36, 51, 60, 102], rectus sheath [1, 110, 113], fascia [65, 91], and abdominal wall muscles [22, 28, 67]. Other authors have investigated the abdominal wall as a whole composite [84, 130, 131, 153, 176]. The aforementioned studies investigated only passive behaviour of muscles but the active contribution has also been studied [23, 24, 59]. The literature devoted to experimental studies on abdominal wall mechanics or its components is summarized in Table 1.1, where a very short description of each work can be found together with information as to whether the specimen was human or animal and whether tested *in vivo*. It can be seen that the majority of existing research on

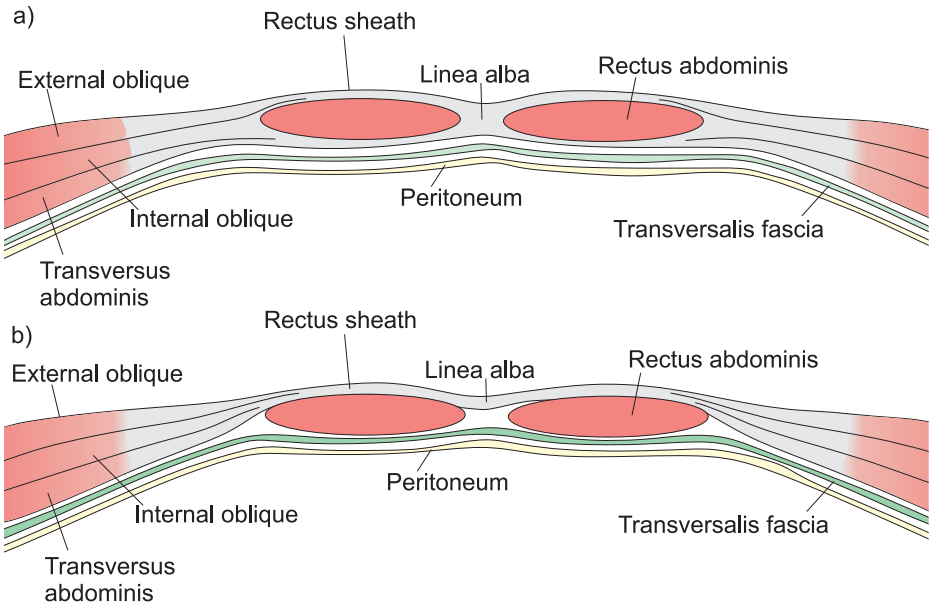

FIGURE 1.2: Cross-section of human abdominal wall and organization of rectus sheath, a) upper three-quarters of the rectus sheath b) lower one-quarter of the rectus sheath, picture inspired by [44]

abdominal wall mechanics was performed *ex vivo*. The issues related to *ex vivo* testing are: effect of freezing on mechanical behaviour of samples, effect of dehydration and rigor mortis, sourcing of samples mainly from aged donors in the case of human tissue where the behaviour can vary from that of younger tissues [41]. The mechanical behaviour of samples extracted post-mortem may not fully correspond to the behaviour of living tissues under physiological loading. Tests performed in the literature were conducted under different conditions, which make them difficult to compare.

tissue	**ref.**	**short description**	**material properties**	***in vivo***	**tissue species**
AW	[85]	*In vitro* multiaxial tensile test of abdominal wall (without skin and fat). Result: elongations in different directions for men and women	✗	✗	human
LA	[60]	Description of linea alba architecture, *in vitro* uniaxial tensile test of linea alba	Young's modulus of linea alba in 3 directions, in 2 areas and for men and women	✗	human

Literature about experimental works on abdominal wall mechanics. Continued on next page

Table 1.1 – continued from previous page					
tissue	**ref.**	**short description**	**material properties**	***in vivo***	**tissue species**
AW	[153], [154]	Identification of abdominal wall stiffness during inflation of the abdomen in patients undergoing laparoscopic surgery	Isotropic linear elastic model; Young modulus of whole abdominal wall calculated for transverse and longitudinal plane	✓	human
LA, RS, ST	[74]	*In vitro* uniaxial tensile test on linea alba, rectus sheath and scar tissue after median laparotomy	Rupture stress of LA, RS and ST	✗	human
F	[65]	*In vitro* uniaxial relaxation tests of fascia in two directions	model of Maxwell-Gurevich-Rabinovich	✗	human
OM	[23]	Study of transmission of forces during activity of oblique muscles	✗	✗	rabbit
EI IO	[24]	Ultrasound and electromyography measurements to study mechanics of abdominal wall contraction	✗	✓	human
LA	[51]	*In vitro* uni- and biaxial tensile tests on linea alba and comparison with *in vivo* study based on MRI images. Relation between uni- and biaxial tests and physiological loadings	Young's moduli and hyperelastic material law in 2 directions.	✗	human
RA EO OM	[67]	*In vitro* uni-axial tension tests of abdominal wall muscles in 2 directions	Transverse isotropic hyperelastic (Holzapfel-Gasser-Ogden) model of RA, EO and composites: EO with IO, IO with TA and composite of all oblique muscles (EO-IO-TA)	✗	rabbit
F	[91]	*In vitro* uniaxial tension test of fascia in 2 directions	Secant modulus, maximal stress and maximal stretch	✗	human

Literature about experimental works on abdominal wall mechanics. Continued on next page

Table 1.1 – continued from previous page					
tissue	**ref.**	**short description**	**material properties**	***in vivo***	**tissue species**
RA EO IO TA	[22]	Uniaxial tensile test of single muscles fibers and bundles of fibers	elastic modulus of single muscles fibers and bundels of fibers	✗	rat
RS	[113]	*In vitro* uni-axial tension test of anterior RS	Damage model of RS	✗	human
AW	[169]	Measurement of displacement of point in abdominal wall during various movements in order to calculate range of strains	✗	✓	human
RS	[1]	Uniaxial tensile test of anterior RS	Secant modulus at different strain levels, and failure stress and corresponding strain for different loading rates	✗	human
AW	[130]	*In vitro* study of strains in internal and external surfaces of abdominal wall subjected to pressure and contact loading. Study conducted for three states of abdominal wall: intact, with hernia and repaired with implant	✗	✗	pig
AW	[131]	Methodology of [130] applied to human abdominal wall subjected to pressure.	✗	✗	human

Literature about experimental works on abdominal wall mechanics. Continued on next page

Table 1.1 – continued from previous page					
tissue	**ref.**	**short description**	**material properties**	***in vivo***	**tissue species**
AW	[176]	Study of contributions of abdominal wall layers to abdominal wall response. Study included *in vitro* investigatons on strains in the abdominal wall surfaces subjected to pressure (similarly to [131]). The layers are sequentially dissected to investigate their influence on the global response. In addition, ultrasonographic elastography was conducted, which enabled identification of shear elastic modulus.	Shear modulus of RA	✗	human
OM RA LA	[28]	Uniaxial relaxation test.	Viscohyperelastic material law	✗	rabbit
RS	[111]	Uni- and biaxial tension test.	Ogden model (matrix) and exponential power law model (fibres)	✗	pig
LA	[36]	Uni- and biaxial tension test.	Fibre reinforced Ogden model	✗	pig
LA	[141]	Planar tension test.	Parameters of 3 hyperelastic material laws of linea alba in different areas: • Neo-Hookean • Ogden • Holzapfel-Gasser-Ogden	✗	pig

Literature about experimental works on abdominal wall mechanics. Continued on next page

Table 1.1 – continued from previous page					
tissue	**ref.**	**short description**	**material properties**	***in vivo***	**tissue species**
AW	[146]	Study based on concept of Song et al [153]. Deformation of abdominal wall subjected to intraabdominal pressure.	✗	✓	rabbit
AW	[177]	Use of ultrasound to perform elastographic measurements of abdominal wall muscles shear modulus and local stiffness during selected activities.	Shear modulus of RA, EO, IO, TA and local stiffness of LA, RA and lateral muscles in two directions	✓	human
RA, EO, OB	[59]	*In vitro* characterisation of active behaviour of AW muscles	Model of active behaviour of abdominal wall muscles.	✗	rabbit
LA	[102]	Tensile tests on linea alba in two directions performed under confocal microscope in order to find relation between mechanical properties and organisation of collagen and elastic fibers.	✗	✗	human and pig
LA	[35]	Uni- and biaxial tension test.	The slope of the most linear region of average stress-stretch curves	✗	human
AW	[144]	Study based on [153] and [146]. Inverse identification of abdominal wall properties	Isotropic hyperlastic two-parameter material law; abdominal wall as composite with spatial variation of parameters	✓	rabbit
LA,RS	[7]	Uniaxial tensile tests on linea alba and anterior and posterior rectus sheaths from the same donors	Tangent modulus for small and large deformations, Yeoh model parameters	✗	human

Table 1.1: Literature in chronological sequence about experimental works on abdominal wall (AW) mechanics and their components: linea alba (LA),rectus sheats (RS), rectus abdominis (RA), external oblique (EO), internal oblique (IO), transversus abdominis (TA), composite EO-IA-TA — oblique muscles (OM), scar tissue (ST), fascia (F)

Song et al. [153] identified the elasticity of the human abdominal wall *in vivo* by measuring the displacement of points on the abdominal wall during laparoscopic repair when the abdomen is filled with gas and internal pressure is known. Simón-Allué et al. developed this concept on an animal example [146] and proposed method to identify *in vivo* parameters of hyperelastic model with the spatial distribution within the abdominal wall [144]. Ultrasound is another possibility for *in vivo* characterization. Shear wave elastography has been used to evaluate the stiffness of muscles *in vivo* [45, 54]. Tran et al [177] used ultrasound to study the elasticity of the muscles of the abdominal wall.

The composite-laminate structure of the abdominal wall is discussed by Brown [21]. Sliding effects between muscles are investigated in [13] by numerical simulations with a finite element (FE) shell model of simplified geometry and with material parameters which are not based on any study of abdominal wall mechanical properties. Hernández-Gascón et al. [69] created a finite element model with realistic geometry based on MRI images with material properties based on previous *ex vivo* studies on animal samples. FE model with geometry based on CT scans with material parameters taken from literature *ex vivo* studies on human samples was proposed by Pachera et al. [124]. Both of the mentioned models were composed of solid tetrahedral elements (muscles) and membrane elements (aponeuroses). An FE solid model for purposes of identification by inverse analysis [144] was constructed based on measurements of the external geometry of the animal with the assumption of constant thickness. Lubowiecka et al. [109] proposed a membrane FE model of the abdominal wall and compared its response with measurements of patients undergoing peritoneal dialysis, during which intraabdominal pressure can be measured. The aforementioned FE models included only passive behaviour of abdominal wall muscles.

1.1.1.3 Connection of implant to abdominal wall

Recurrences of hernia are usually caused by connection failure. Therefore attention must be paid also to the fasteners joining the surgical mesh to the abdominal wall. Capacity of the following types of fasteners used in ventral hernia repair was identified as reported in literature: tacks and sutures [174] and glue [157]. The mechanical behaviour of suture connection has also been studied in order to prevent hernia as a postoperative complication by specifying sufficient closure after other abdominal operations. For example, Cooney et al. [34] tested different suture techniques on porcine linea alba subjected to pressure.

1.1.1.4 The system of abdominal wall with introduced implant

The behaviour of the system composed of the abdominal wall and implanted surgical mesh was investigated both experimentally and numerically. *Ex vivo* experimental work of abdominal wall tissues with implants was performed by Tomaszewska et al. [174] and Podwojewski et al. [130, 131]. Kahan et al. [86, 87] performed *in vivo* tests of performance of implants in the living porcine abdominal wall. Simón-Allué [147] investigated the behaviour of the rabbit abdominal wall with implanted surgical meshes *in vivo* and their FE model was validated. Also physical models exist, where the abdominal wall is replaced by artificial materials [63].

Mathematical models of the abdominal wall with a surgical mesh can be used to predict its mechanical behaviour and can be employed in the process of optimization of ventral hernia repair parameters (such as implant properties). Models proposed in the literature vary with complexity starting from simplification of the membrane structure of the surgical mesh to a 1-dimensional cable model [168], through FE membrane models of the surgical mesh with boundary conditions reflecting the behaviour of the abdominal wall [104, 105, 163] and FE models with simplified geometry of the abdominal wall [67] to complex models of the abdominal wall with realistic geometry and only passive behaviour of muscles and properties based on *ex vivo* identification in human or animal samples [70, 145, 171].

The procedure for optimisation of the choice of implant and its orientation was proposed by Lubowiecka et al. [106], where the objective function was to minimise the maximum force in the fasteners. This is because hernia recurrences are usually caused by connection failure. Szymczak et al. [167] extended the procedure to two-criterion optimisation and introduced also a criterion related to the implant deflection, which was motivated by the medical issues of excessive implant bulging after LVHR.

1.1.2 Need of probabilistic approach

The complexity of mechanical behaviour of both biological tissues and implants, and their interactions is not yet fully incorporated into the modelling of implant within the abdominal wall system. Based on the literature studies mentioned above, it can be concluded that many uncertainties appear in the modelling of athe bdominal wall into which a surgical mesh has been implanted. Accurate identification of soft tissues is challenging and standards of testing of such tissues have not yet been established. Morever existing models of the abdominal wall with hernia and implant are based on *ex vivo* tests on animal or human samples which may not correspond to the behaviour of

living human tissues. Additonally natural material such as soft tissues are characterized by natural variability, which could be observed in some of the aferomenitoned studies, e.g. [169]. Imposed loads, e.g. intraabdominal pressure [33] are also uncertain. Therefore, single deterministic simulations may not be sufficient to provide reliable information to clinicians and to predict well the required data such as the forces in the fasteners or the displacement of the surgical mesh. In order to address these issues, in this thesis uncertainties will be included in the modelling of the implant and abdominal wall and their influence on the uncertainty of the output will be investigated. To do so, uncertainty quantification and sensitivity analysis methods are employed.

1.2 Uncertainty Quantification

Real systems differ from their models. Data variability and errors as well as model and numerical errors occur in the simulations [100]. Manufactured or constructed objects also differ from their initial design. Therefore, uncertainties should be included in the modelling to better understand and predict the real behaviour of physical systems.

Uncertainty quantification (UQ) can be conducted with different objectives [100, 162]: reliability or risk analysis, validation and verification of models, inverse parameter identification and others. In this thesis, UQ methods are employed mainly to study response variation, which can be important for further optimization and drawing of conclusions for the surgeons. The second purpose of using UQ is sensitivity analysis, the result of which will be used to plan further research in an efficient manner.

A widely-used approach is to treat uncertain inputs as random variables (or processes, fields) [184]. Following [158] an uncertainty analysis flowchart is presented in Figure 1.3. The first step (A) is to define a model with a clearly defined input and output – quantity of interest. In the second stage (step B), inputs which are uncertain because of insufficient knowledge (epistemic uncertainty) or their natural variability (aleatoric uncertainty) are identified. In this step a random vector of inputs is created. Probabilistic models can be built from data statistics. However, sometimes sufficient data is not available. In such a case, expert judgement can be used. In step C, one of the uncertainty propagation methods is used. In the case of this thesis, that is Monte Carlo and the polynomial chaos expansion method. Also, sensitivity analysis can be performed (step C'). Identification of probabilistic models in the case of many inputs may be challenging and a sensitivity analysis is able to determine, which parameters contribute significantly to the output variation and which are insignificant. This enables reduction of the problem to smaller number of random variables.

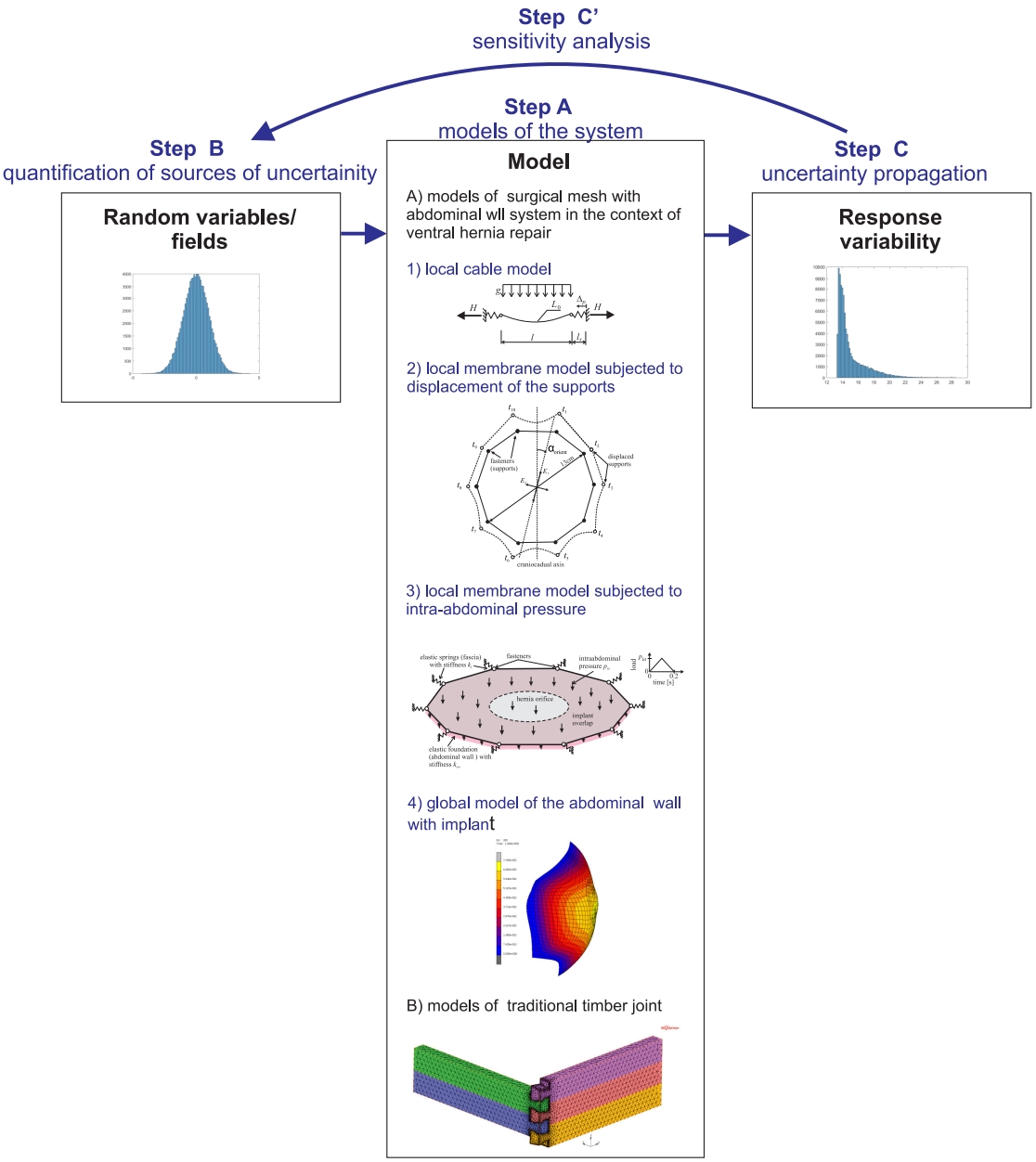

FIGURE 1.3: Sketch of the uncertainty analysis following the concept of [158]

Models of the abdominal wall and implant are usually nonlinear geometrically and physically. The majority of models used in this thesis are created in commercial FE software (MSC. Marc). These models require the application of nonintrusive UQ methods, which are easily applicable even in the case of "black-box" models. Nonintrusive methods are based on some number of deterministic runs of the model and do not require modifications of the model code. A widely used and easily applicable non-ntrusive method is the Monte Carlo (MC) method [50]. However, this method requires a large number of simulations, which make it very expensive computationally and therefore sometimes intractable. Methods based on creating metamodels can be used to reduce computational cost, for example the response surface [90, 183] and polynomial chaos (PC) expansion

[11, 55]. Metamodels substitute models containing information about physics of phenomena by analytical functions. PC is a method based on approximation of a computational model by series of multivariate polynomials. PC in a nonintrusive variant by regression is employed in this thesis. However, the accuracy of such nonintrusive methods depends on the number and choice of sampling points. Some error estimation methods have been developed [29] to address the need of verification of such metamodels. Finding a universally efficient method to provide a good balance between accuracy and computational cost is still an open question. Therefore different approaches are tested on models of the surgical mesh in order to find an efficient approach to PC in application to hernia related models.

Uncertainty quantification methods including PC have also already been employed in mechanics applied to medicine. Yang et al. applied PC to bone-implant healing model in intrusive [188] and nonintrusive way [189] with standard choice of regression points [159]. Huberts et al. [78] compared two nonintrusive approaches to PC on a cardiovascular pulse wave propagation model.

1.3 Objectives

The aim of this thesis is to investigate uncertainties in the modelling of surgical meshes within the abdominal wall and to evaluate the sensitivity of the response of the model to these uncertainties.

The majority of the models considered in this work represent the implant-abdominal wall system in the context of laparoscopic ventral hernia repair (LVHR). They have various levels of complexity and can be divided into two groups:

local models represent only the implant. The influence of the abdominal wall is included through boundary conditions:

1. cable model of the implant,
2. model of the membrane subjected to displacement of the supports,
3. model of the membrane subjected to intraabdominal pressure,

global models are concerned with the behaviour of the combined system of the implant and abdominal wall:

4. Membrane model of abdominal wall with implant.

The local model outputs on which this study is focused (quantities of interest) are pertinent to two medical problems of LVHR:

hernia recurrence – usually caused by connection failure. Therefore, this analysis is focused on the force in the fasteners connecting tissue to the implant;

excessive implant bulging [143], which can be considered as a kind of pseudo-recurrence [178]. Thus, attention is also paid to the deflection of the implant.

The force in the fasteners and the deflection of the implant were incorporated in two-criterion optimisation of the choice of implant [167]. In the case of the global model the quantity of interest is the difference between the displacement of the centre of the implant and the corresponding point in a healthy abdominal wall, as a measure of compatibility.

The models Considered are nonlinear and in some cases nonsmooth, which can be challenging for PC.

Different strategies for the choice of sampling points are considered and compared for two local models of surgical mesh. The goal is to establish a methodology for uncertainty propagation and global sensitivity analysis, which can be efficiently used in models related to ventral hernia. The conclusions drawn from the first examples are then used to perform uncertainty quantification and sensitivity analysis in other local and global models.

As an addition the expertise gained on nonlinear biomechanical models with high levels of uncertainty is applied in the context traditional timber joints. Mechanical analyses of such joints are important owing to the need of repair and renovation of buildings of historic value. Wood, being a natural material, exhibits natural variability of its mechanical properties, which depend on many factor such as moisture and region of origin. However in historic buildings full measurements of the parameter of the particular wood used is not possible. Therefore the study of uncertainty propagation and sensitivity analysis in the mechanical model of these joints represents a valuable contribution to conservation efforts.

1.4 Outline

The thesis is structured as follows:

Chapter 1 introduces the medical problem of ventral hernia repair, the state of the art of biomechanical studies in this context, the idea of uncertainty and the main objectives of the work.

Chapter 2 presents the theoretical background on uncertainty quantification and sensitivity analysis methods. Attention is focused mainly on the polynomial chaos expansion method and Sobol indices.

Chapter 3 introduces different approaches to choice of sampling points in the polynomial chaos expansion method and contains a comparison of these methods on one benchmark function and two local models of implants used in ventral hernia repair with versions containing different numbers of variables.

Chapter 4 presents the results of uncertainty propagation and sensitivity analysis in the models related to ventral hernia already presented in chapter 3. Also further local and global models are introduced. A method to choose regression points is chosen based on conclusions drawn in chapter 3. Additionally the propagation of uncertainties in models of traditional timber joints is studied.

Chapter 5 summarizes the work and includes conclusions and outline of future work

Chapter 2

Uncertainty quantification and sensitivity analysis

Let $\mathcal{M}$ be a computational model. $\mathcal{M}$ is a deterministic mapping:

$$y = \mathcal{M}(\mathbf{x}), \tag{2.1}$$

where $\mathbf{x} = [x_1, \ldots, x_M]^\top \in \mathbb{R}^M$, with number of variables $M \geq 1$, is an input and y is the output – the quantity of interest (QoI).

To represent uncertainty, let the input be written as a random vector $\mathbf{X}(\omega)$, $\omega \in \Omega$ with joint probability density function (PDF) $f_{\mathbf{X}}$, where Ω is space of random events ω. Hence the model response is also a random variable:

$$Y(\omega) = \mathcal{M}(\mathbf{X}(\omega)). \tag{2.2}$$

For simplicity, ω is skipped in the following text.

Since the majority of models of the implant-abdominal wall system are created in FE commercial "black-box" software, only non-intrusive methods are considered in this work. Non-intrusive probabilistic methods are based on a series of deterministic calculations. These types of method are more flexible and easier to apply because they do not require any code modification. $\mathcal{M}$ can be a black-box function, which is known by the outcomes of repeated single realizations, e.g. of computer FE code [158]:

$$y^{(i)} = \mathcal{M}(\mathbf{x}^{(i)}) \tag{2.3}$$

2.1 Uncertainty quantification methods

2.1.1 Sampling-based methods

2.1.1.1 Monte Carlo method

The Monte Carlo (MC) method [50] is one of the most widely-used methods. It is based on repeated evaluations of the deterministic model $\mathcal{M}$ done for N_{MC} sampling points generated with a given PDF. On the basis of these calculations, statistical information can be obtained. Let $\mathbf{X}_n = [X_{1n}, X_{2n}, \ldots, X_{Mn}]^\top$ be n-th sample point, $n = 1, 2, \ldots N_{MC}$. The mean $\mathcal{M}_0$ can be estimated by:

$$\mathcal{M}_0 \approx \mathcal{M}_0^{MC} = \frac{1}{N_{MC}} \sum_{n=1}^{N_{MC}} \mathcal{M}(\mathbf{X}_n) \tag{2.4}$$

and the variance D by

$$D \approx D^{MC} = \frac{1}{N_{MC}} \sum_{n=1}^{N_{MC}} \big(\mathcal{M}(\mathbf{X}_n)\big)^2 - (\mathcal{M}_0^{MC})^2. \tag{2.5}$$

$\mathcal{M}_{p\%}^{MC}$ is the estimator of the p-th percentile, where $p\%$ of N_{MC} realizations are such that $\mathcal{M}(\mathbf{X}_n) \leq \mathcal{M}_{p\%}$.

Usually, very high N_{MC} is required because of slow convergence. Thus despite the flexibility and power of MC, applying it can be sometimes intractable computationally, for example in the case of complex FE models, where one simulation is already computationally expensive. On the other hand, convergence of MC is independent of the number of variables [184].

2.1.1.2 Improved sampling strategies

In order to decrease computational cost some methods to accelerate convergence have been developed, for example:

Latin hypercube sampling (LHS) [116] – sample points drawn by LHS are better distributed in the sample space. The method consists of firstly dividing the PDF into N_{LHS} disjoint intervals with equal probability and then randomly drawing from each subset one value. The samples are then permuted to obtain points in M-th space. This method has been shown to be superior to simple sampling when certain monotonicity conditions of functions are satisfied.

Quasi Monte Carlo sampling (QMS) [122] – the concept behind QMC is to use low-discrepancy sequences [120] instead of random draws to provide better uniformity.

2.1.2 Spectral methods

Spectral methods represent the response as a series expansion [100] enabling the full PDF of the output to be obtained. The recent popularity and advancement of the spectral approach in uncertainty quantification in the field of mechanics started with work by Ghanem and Spanos, where the Stochastic Finite Element Method was proposed [55].

2.1.2.1 Karhunen-Loève expansion

The Karhunen-Loève expansion [89, 103] is one of the methods of random field (or process) discretization and dimension reduction.

Let $F(\mathbf{Z}, \omega)$ be a random field (or process), where Z is a spatial (or time) variable in domain $\mathcal{D}$. The Karhunen-Loève expansion of the $F(\mathbf{Z}, \omega)$ is:

$$F(\mathbf{Z}, \omega) = F_0(\mathbf{Z}) + \sum_{i=1}^{\infty} \sqrt{\lambda_i} \xi_i(\omega) \varphi_i(\mathbf{Z}), \tag{2.6}$$

where $F_0(\mathbf{Z})$ is the mean value of the field (or process) and the ξ_i are a set of uncorrelated, zero mean and unit variance random variables. When the field is Gaussian, the ξ_i are also independent. The λ_i, where $i = 1, 2, ..., \infty$, $(\lambda_1 \geq \lambda_2 \geq ...)$ and $\varphi_i(\mathbf{Z})$ are eigenvalues and orthogonal eigenfunctions respectively:

$$\int_{\mathcal{D}} C(\mathbf{Z}_1, \mathbf{Z}_2) \varphi(\mathbf{Z}) d\mathbf{Z}_1 = \lambda \varphi(\mathbf{Z}_2), \tag{2.7}$$

where C is covariance function.

The infinite expansion can be truncated to a finite number N_{KL} of terms

$$F(\mathbf{Z}, \omega) \approx F_0(\mathbf{Z}) + \sum_{i=1}^{N_{KL}} \sqrt{\lambda_i} \xi_i(\omega) \varphi_i(\mathbf{Z}) \tag{2.8}$$

A review of random field discretization methods can be found in [156, 161].

2.1.2.2 Polynomial chaos expansion

The polynomial chaos expansion (PC) method was proposed in the field of mechanics by Ghanem and Spanos [55]. The method was inspired by the Wiener-Hermite theory [181]. In order to improve convergence of PC in the case of non-Gaussian problems, Xiu and Karniadakis [185] proposed using polynomials from the Askey scheme which are orthogonal with respect to a given distribution measure. In the beginning [55], PC coefficients were computed in an intrusive manner by the Galerkin method. Later, non-intrusive approaches were also proposed: nonintrusive projection [101] and the regression method [11, 82].

The following description of PC is based on [14, 15, 38, 99, 159, 160].

The assumption is that the input variables X_i in $\mathbf{X}$ of the model $\mathcal{M}$ are independent. Therefore the joint PDF is the product of the marginal distributions $f_{\mathbf{X}} = \prod_{i=1}^{M} f_{X_i}$, where f_{X_i} is the marginal distribution of variable X_i. The general framework allowing arbitrary distributions, also with dependent random variables, can be found in [152]. Some methodologies of PC for dependent variables have also been proposed [121, 175]. A widely used approach is transformation of dependent random variables into independent ones, e.g. by the Nataf or Rosenblatt transforms or the Karhunen-Loève expansion.

The model output Y is expanded via the polynomial chaos expansion as follows:

$$Y = \mathcal{M}(\mathbf{X}) = \sum_{\boldsymbol{\alpha} \in \mathbb{N}^M} a_{\boldsymbol{\alpha}} \Phi_{\boldsymbol{\alpha}}(\mathbf{X}), \tag{2.9}$$

where $a_{\boldsymbol{\alpha}}$ are coefficients to be computed, and $\Phi_{\boldsymbol{\alpha}}$ is a multivariate polynomial basis constructed by multiplying univariate polynomials ϕ_{α_i} of order α_i:

$$\Phi_{\alpha_1,\ldots,\alpha_M}(\mathbf{X}) = \prod_{i=1}^{M} \phi_{\alpha_i}^{(i)}(X_i). \tag{2.10}$$

The multi-index $\boldsymbol{\alpha} = [\alpha_1, \ldots, \alpha_M]$ in (2.9) refers to the polynomial orders of the univariate components of each variable in the construction of the multivariate basis.

Orthonormal polynomials are used to construct the PC basis:

$$\langle \phi_i, \phi_j \rangle = \int_{\mathcal{H}_X} \phi_i(X)\phi_j(X) f_X(X) dX = \delta_{ij}, \tag{2.11}$$

where δ_{ij} is the Kronecker symbol $\delta_{ij} = \begin{cases} 1, & \text{if } i = j, \\ 0, & \text{if } i \neq j. \end{cases}$

The input random variables are transformed into reduced variables:

$$\mathbf{X} = \mathcal{T}(\boldsymbol{\xi}). \tag{2.12}$$

For example:

- if X_i is a normal variable $X_i \sim \mathcal{N}(\mu_i, \sigma_i)$, where μ_i is the mean and σ_i is the standard deviation, the transformation is:

$$X_i = \mu_i + \sigma_i \xi_i, \tag{2.13}$$

  where ξ_i is a standard normal variable $\xi_i \sim \mathcal{N}(0, 1)$

- if X_i is a uniform variable $X_i \sim \mathcal{U}([a_i, b_i])$ with support $[a_i, b_i]$, the transformation is:

$$X_i = \frac{a_i + b_i}{2} + \frac{b_i - a_i}{2} \xi_i, \tag{2.14}$$

  where $\xi_i \sim \mathcal{U}([-1, 1])$

- if X_i is a lognormal variable $X_i \sim \mathcal{LN}(\mu_{lni}, \sigma_{lni})$, where μ_{lni} and σ_{lni} are the mean and standard deviation, respectively, of the variable's natural logarithm, it can be transformed into a standard normal variable $\xi_i \sim \mathcal{N}(0, 1)$

$$X_i = e^{\mu_{lni} + \sigma_{lni} \xi_i}. \tag{2.15}$$

The model response is then expressed as a function of the reduced variables:

$$Y = \mathcal{M}(\mathbf{X}) = \mathcal{M} \circ \mathcal{T}(\boldsymbol{\xi}) = \sum_{\boldsymbol{\alpha} \in \mathbb{N}^M} a_{\boldsymbol{\alpha}} \Psi_{\boldsymbol{\alpha}}(\boldsymbol{\xi}). \tag{2.16}$$

In computational practice the infinite expansion needs to be truncated. Let $\mathcal{A}$ be a truncation set – a finite subset of $\mathbb{N}^M$. The classic method of truncation is applied in this work, which is to use all M-dimensional polynomials of a degree equal to or smaller than the established PC degree p:

$$\mathcal{A}^{M,p} = \{\boldsymbol{\alpha} \in \mathbb{N}^M : \sum_{i=1}^{M} \alpha_i \leq p\}. \tag{2.17}$$

Some remarks on practical implementations of the construction of multivariate polynomials with respect to this truncation rule can be found in the appendix section A.2.

The cardinality of such a truncation set $\mathcal{A}$ is $P = |\mathcal{A}^{M,p}| = \frac{(M+p)!}{M!p!}$. This is number of coefficients which have to be computed. The method can be intractable in case when M is high. PC suffers from the so-called curse of dimensionality. In order to decrease number of coefficients and consequently computational cost, some adaptive sparse PC algorithms have been proposed in the literature [14, 77].

Finally, the response can be approximated as:

$$Y \approx Y^{PC} = \mathcal{M}^{PC}(\boldsymbol{\xi}) = \sum_{\boldsymbol{\alpha} \in \mathcal{A}} a_{\boldsymbol{\alpha}} \Psi_{\boldsymbol{\alpha}}(\boldsymbol{\xi}). \tag{2.18}$$

$\mathcal{M}^{PC}$ can be considered to be a metamodel or surrogate model.

The polynomials used should be orthonormal (2.11). This can be achieved by employing polynomials from the Askey scheme in which the weighting function corresponds to the applied distribution [185]. Examples for popular distributions are presented in Table 2.1.

Distribution	PC Polynomial basis	Support
Gaussian	Hermite	$(-\infty, \infty)$
Gamma	Laguerre	$[0, \infty)$
Beta	Jacobi	$[a, b]$
Uniform	Legendre	$[a, b]$
Poisson	Charlier	$\{0, 1, 2, \dots\}$

TABLE 2.1: Distributions and corresponding polynomials. Adapted from [184]

In this work uniform, normal and lognormal, which can be transformed into normal, distributions are used. Therefore Hermite and Legendre polynomials are employed.

Hermite polynomials can be generated using recurrence equations:

$$\begin{aligned} H_0(x) &= 1 \\ H_1(x) &= x \\ H_{n-1}(x) &= xH_n(x) - nH_{n-1}(x) \end{aligned} \tag{2.19}$$

They are orthogonal with respect to the Gaussian probability measure:

$$\langle H_m, H_n \rangle = \int_{-\infty}^{\infty} H_m(X) H_n(X) w(X) dX = n! \delta_{nm}, \tag{2.20}$$

where the weight function is:

$$w(x) = \frac{1}{\sqrt{2\pi}} \mathrm{e}^{-x^2/2}. \tag{2.21}$$

To obtain an orthonormal basis, the normalized polynomials $H_n(x)/\sqrt{n!}$ should be used. Hence, for example $H_2(x) = (x^2 - 1)/\sqrt{2}$, $H_3(x) = (x^3 - 3x)/\sqrt{6}$.

Legendre polynomials are orthogonal with respect to the uniform distribution. They can also be generated by recurrence equations:

$$\begin{aligned} L_0(x) &= 1 \\ L_1(x) &= x \\ (n+1)L_{n+1}(x) &= (2n+1)xL_n(x) - nL_{n-1}(x) \end{aligned} \tag{2.22}$$

They are also orthogonal:

$$\langle L_m, L_n \rangle = \int_{-1}^{1} L_m(X)L_n(X)dX = \frac{2}{2n+1}\delta_{nm}. \tag{2.23}$$

When the uniform $\mathcal{U}(-1,1)$ distribution is assumed, the weight function is a constant $w(X) = 1/2$

$$\langle L_m, L_n \rangle = \int_{-1}^{1} L_m(X)L_n(X)w(X)dX = \frac{1}{2n+1}\delta_{nm}. \tag{2.24}$$

The basis function after normalization is

$$L_n(x)/\sqrt{\frac{1}{2n+1}} \tag{2.25}$$

The convergence rate of the Legendre approximation depends on the function smoothness [184]. The convergence of discontinuous functions especially is problematic. The Gibbs phenomenon concerns numerical artefacts related to approximation of discontinuous functions by smooth polynomials. Figure 2.1 illustrates this problem and shows the PC Legendre expansion of the sign function for different polynomial orders (with regression points equal to the roots of the Legendre polynomial of order $p+1$):

$$\operatorname{sgn}(x) = \begin{cases} -1, & x < 0 \\ 0, & x = 0 \\ 1, & x > 0 \end{cases}$$

Methods to compute coefficients can be divided into two main groups.

Intrusive methods require code modification. One such method – Galerkin projection – which requires implementation in FE code, was used by Ghanem and Spanos in their pioneering book on Stochastic Finite Elements [55].

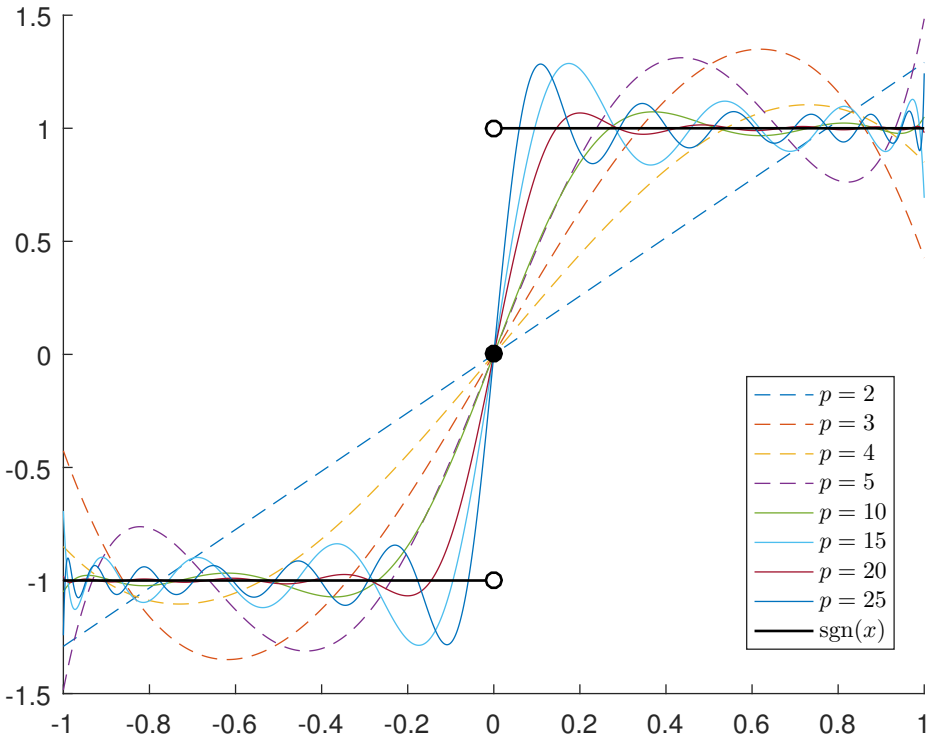

FIGURE 2.1: Legendre PC approximation of sign function for different PC orders p

Non-intrusive methods are based on deterministic computations, so the model can be given in black-box form. The two widely used methods in this category are:

- Non-intrusive spectral projection(NISP) [101]
- the regression approach [11]

The methodology established in this work will later be applied to complex models in biomechanics and structural mechanics. Therefore, owing to the greater feasibility of their application to more complex models, only non-intrusive methods are considered here. On the one hand these methods are easier to apply but on the other hand their accuracy depends on the choice of sampling points. The choice of points is discussed in chapter 3.

Non-intrusive spectral projection uses the orthogonality of the PC basis. For simplicity of notation $\mathcal{M}(\boldsymbol{\xi})$ will be written in the following text, since $\mathbf{X}$ is a function of $\boldsymbol{\xi}$. The k-th coefficient a_k can be obtained from

$$a_k = \frac{\langle \mathcal{M}(\boldsymbol{\xi}), \Psi_k(\boldsymbol{\xi}) \rangle}{\langle \Psi_k, \Psi_k \rangle}, \tag{2.26}$$

where the inner product (numerator) is defined as

$$I_k = \langle \mathcal{M}(\boldsymbol{\xi}), \Psi_k(\boldsymbol{\xi}) \rangle = \int_{\mathcal{H}_{\boldsymbol{\xi}}} \mathcal{M}(\boldsymbol{\xi}) \Psi_k(\boldsymbol{\xi}) f_{\boldsymbol{\xi}} d\xi_1 \dots d\xi_M, \tag{2.27}$$

where $\mathcal{H}_{\boldsymbol{\xi}}$ is the support of $\boldsymbol{\xi}$ and $f_{\boldsymbol{\xi}}$ is joint PDF. The exact values of the denominators are known for classic probability distributions and PC polynomials. Integration to calculate I_k can be done numerically.

Deterministic integration by quadrature is based on model realizations on N_Q nodes:

$$I_k \approx \sum_{i=1}^{N_Q} \mathcal{M}(\boldsymbol{\xi}^{(i)}) \ \Psi_k(\boldsymbol{\xi}^{(i)}) w^{(i)} \tag{2.28}$$

where the $w^{(i)}$ are weights and the $\boldsymbol{\xi}^{(i)}$ are integration points.

Different integration methods can be considered such as Monte Carlo Sampling, QMC sampling, full tensorization of one-dimensional quadrature formula, and cubature formulas based on the Smolyak method. QMS and Smolyak cubature are less computationally expensive but their performance depends on the smoothness. Huberts et al. [78] compared NISP with Smolyak cubature and the regression-based approach, with the same sampling points. They obtained generally better results when the regression-based method was used. This was explained by possible non-smoothness of the output and the high number of variables. Therefore, since some of the considered QoI are non-smooth (R_{max}), the regression-based approach will be used in the work, owing to its lower sensitivity to non-smoothness.

The response of the model can be expressed as a sum of a truncated series and a residual:

$$Y = \mathcal{M}(\mathbf{X}) = \sum_{\boldsymbol{\alpha} \in \mathcal{A}} a_{\boldsymbol{\alpha}} \Psi_{\boldsymbol{\alpha}}(\boldsymbol{\xi}) + \varepsilon. \tag{2.29}$$

In order to perform regression, N regression points are chosen in the space of reduced variables $\Xi = [\boldsymbol{\xi}^{(1)}, \dots, \boldsymbol{\xi}^{(N)}]$. A vector of exact solutions $\mathbf{Y}_{ex} = [\mathcal{M}(\mathbf{X}^{(1)}), \dots, \mathcal{M}(\mathbf{X}^{(N)})]^\top$ is obtained by computation of the model $\mathcal{M}$ on these N regression points after their isoprobabilistic transformation. The coefficients $a_{\boldsymbol{\alpha}}$ are collected into a vector $\mathbf{a} = [a_{\boldsymbol{\alpha}_0}, \dots, a_{\boldsymbol{\alpha}_{P-1}}]^\top$. Let $A_{ij} = \Psi_{\boldsymbol{\alpha}_j}(\boldsymbol{\xi}^{(i)})$, $i = 1, \dots, N$; $j = 1, \dots, P$. The coefficients $\mathbf{a}$ can be computed by solving the least squares problem minimizing ε:

$$\mathbf{a} = (\mathbf{A}^\top \mathbf{A})^{-1} \mathbf{A}^\top \mathbf{Y}_{ex}. \tag{2.30}$$

The matrix $\mathbf{A}^\top\mathbf{A}$ is called an information matrix and $(\mathbf{A}^\top\mathbf{A})^{-1}$ is a dispersion matrix, e.g. after [40].

The diagonal matrix $\mathbf{W}$ with weights $w(\xi^{(i)})$ on the diagonal may be introduced into the regression:

$$\mathbf{A}^\top\mathbf{W}\mathbf{A} = \mathbf{A}^\top\mathbf{W}\mathbf{Y}_{ex}. \tag{2.31}$$

After computation of coefficients, a $\mathcal{M}^{PC}$ is ready. The calculations even for a large number of sampling points can be conducted with a negligible computational cost with use of metamodel. It can be used to obtain response PDF. Some statistics, e.g. the mean $\mathcal{M}_0$ and the variance D, can be approximated directly from the PC coefficient:

$$\mathcal{M}_0 \approx \mathcal{M}_0^{PC} = a_{\mathbf{0}}, \tag{2.32}$$

$$D \approx D^{PC} = \sum_{\boldsymbol{\alpha}\in\mathcal{A}\setminus\{\mathbf{0}\}} a_{\boldsymbol{\alpha}}^2. \tag{2.33}$$

2.2 Sensitivity analysis

Sensitivity analysis (SA) is a tool which is widely used in modelling practice. According to the proposed definition of Saltelli et al. [139], SA studies the relationships between information flowing into the model and out of it. SA provides knowledge on how the variation of the model output depends on that of the model input. This information can be used in many ways. For example, SA can be employed to identify the most significant factors which consequently require further, more detailed study. SA can also be helpful in model reduction, when the number of variables is decreased but the model is still satisfactorily approximated.

Different sensitivity measures exist. Choosing the proper method depends on the problem at hand, the intended purpose of its solution and the complexity of the model used, in terms of, for example, its nonlinearity or monotonicity [81]). The methods are classically divided into two groups ([159, 162] among others):

Local SA – studies sensitivity of the output to small variations of the input around a particular base point [166] (section 2.2.1);

Global SA – studies sensitivity of the output to variations of the input across the domain [140] (section 2.2.2);

Sometimes screening methods are distinguished as a third group [139]. However, these methods can be also classified as local or global. Screening is based on a qualitative

ranking of variables without quantification of their relative importance. It is often used to identify which variables, out a large number, have a negligible effect.

In the literature other classifications of SA methods can also be found, for example:

Quantitative and qualitative methods [129]. The former quantify the effects of inputs through sensitivity measures (sensitivity indices) whereas in the latter, qualitative evaluation of importance is based on visualisation, e.g. scatter plots. Qualitative methods are usually used as a screening technique.

One-At-a-Time (OAT) and All-At-a-Time (AAT) methods [129]. In the OAT method only one model parameter is varied while others remain fixed. In AAT all parameters are varied at the same time. This enables the effects of interaction between parameters to be captured. Local SA methods are generally OAT. According to Pianosi et al. [129] global SA methods can be both OAT and AAT. However, this is not in agreement with the statement of Saltelli et al. [139] that varying all parameter at the same time is one of the properties of global SA methods (see section 2.2.2). Skowronek [148] gives an example of an OAT method dealing with probability distributions and allowing changes in the whole domain.

Mathematical, statistical and graphical [52]. Mathematical methods are based on deterministic analysis and estimate local influence of parameters around base points. They belong to the local SA group of methods. Statistical methods involve inputs with a given probability distribution and deal with the distribution of the output, which is also a property of global SA. Graphical methods are based on visualisation of sensitivity in the form of graphs etc. These methods can also be classified as qualitative methods.

Screening, sampling-based methods, metamodel-based methods [80, 81]. The screening family of methods aims only to give a qualitative ranking of variables. A quantitative measure can be obtained based on samples of input and output (sampling-based) or, if this is too computationally expensive, an approach based on metamodels can be used. For example, polynomial chaos expansion can be used as a metamodel to efficiently compute sensitivity indices.

2.2.1 Local sensitivity analysis

Local SA is usually based on derivatives and is applied in deterministic studies. The first-order local sensitivity measure [66] can be defined as follows:

$$S_i^{local} = \frac{x_i}{y}\frac{\partial y}{\partial x_i}, \tag{2.34}$$

where x_i/y is introduced to normalize the sensitivity coefficient.

Higher order sensitivity measures can also be defined in a similar way. Nevertheless, usually only linear sensitivity analysis is conducted.

Many methods have been developed to address the case, where analytical differentiation is not possible. One of the easiest is the brute-force method, also called the indirect method, which involves the use of finite differencing to approximate derivatives:

- one-sided forward difference

$$\frac{\partial y(\mathbf{x})}{\partial x_i} \approx \frac{y(\mathbf{x}+\mathbf{h}) - y(\mathbf{x})}{h} \tag{2.35}$$

- central differencing

$$\frac{\partial y(\mathbf{x})}{\partial x_i} \approx \frac{y(\mathbf{x}+\mathbf{h}) - y(\mathbf{x}-\mathbf{h})}{2h} \tag{2.36}$$

where h is a finite difference step and $\mathbf{h}$ is a vector of zeros of length M where the i-th element equals h. The latter method is believed to be more accurate, but requires more evaluations of the model. Accuracy depends on the size of h and can be degraded by numerical errors in the FEM model.

The other methods are the direct method, the variational method and the polynomial approximation method [179].

It should be noted that local sensitivity analysis studies the influence of small variations around a particular base point. To be able to estimate the sensitivity of more significant input changes corresponding to high uncertainties in non-linear models, global methods should be considered.

2.2.2 Global sensitivity analysis

Global methods can be characterized by two properties [139]:

1. They deal with variations over the whole domain of the PDF,
2. They deal with estimation of sensitivity indices by varying all factors at the same time.

Global SA methods are usually probabilistic and deal with random inputs and consequently random outputs [179].

The main quantitive global methods can be divided into two groups [159]:

Regression based – based on linear regression of the output on the input;

Variance based – based on variance decomposition according to the contributions of each variable.

The former do not give satisfactory results in the case of non-linear non-monotonic models [159] but Sobol' indices (section 2.2.2.2) – a variance based method – can be used in this case because they do not need any *a priori* assumptions about the model's properties [81]. However, this method can be very expensive computationally. To deal with this problem, it can be preceded by a screening method [80]. The computational cost can be also decreased by employing metamodels like PC or Gaussian processes [99]. Section 2.2.2.1 briefly introduces scatter plots – one the simplest graphical methods, which will be used in some examples for visualisation of importance of variables.

2.2.2.1 Scatter plots

Scatter plots [52, 139] are one the easiest qualitative global SA methods to visualise importance of variables. Points obtained from each simulation (e.g. from MC) are presented on a plot showing the relation between the input variable and the value of the output and consequently indicating the influence of the input variable in question. Scatter plots can be used for screening purposes to identify inputs whose uncertainty has negligible effect, to rank variables according to their importance [140] or to aid the decision as to which quantitative method should be used (e.g. because of linear or non-linear dependence)[52]. Nevertheless, in some particular cases scatter plots can lead to classification of important variables as non-influential (error type II, whereas error type I is to classify non-influential variable as important) [140].

For an illustration of this graphical method, let us use a simple example adopted from [140]. Let the model be:

$$Y = \sum_{i=1}^{4} X_i, \tag{2.37}$$

where X_i is a random normal variable $X_i \sim \mathcal{N}(0, \sigma_{X_i})$ and $i = 1, \ldots, 4$. Let $\sigma_{X_i} = i$. Figure 2.2 shows scatter plots obtained from 1000 MC iterations. Comparison of the patterns obtained leads to the conclusion that X_4 is the most influential variable and the rank of variables from the most influential to least influential is X_4, X_3, X_2, X_1. It

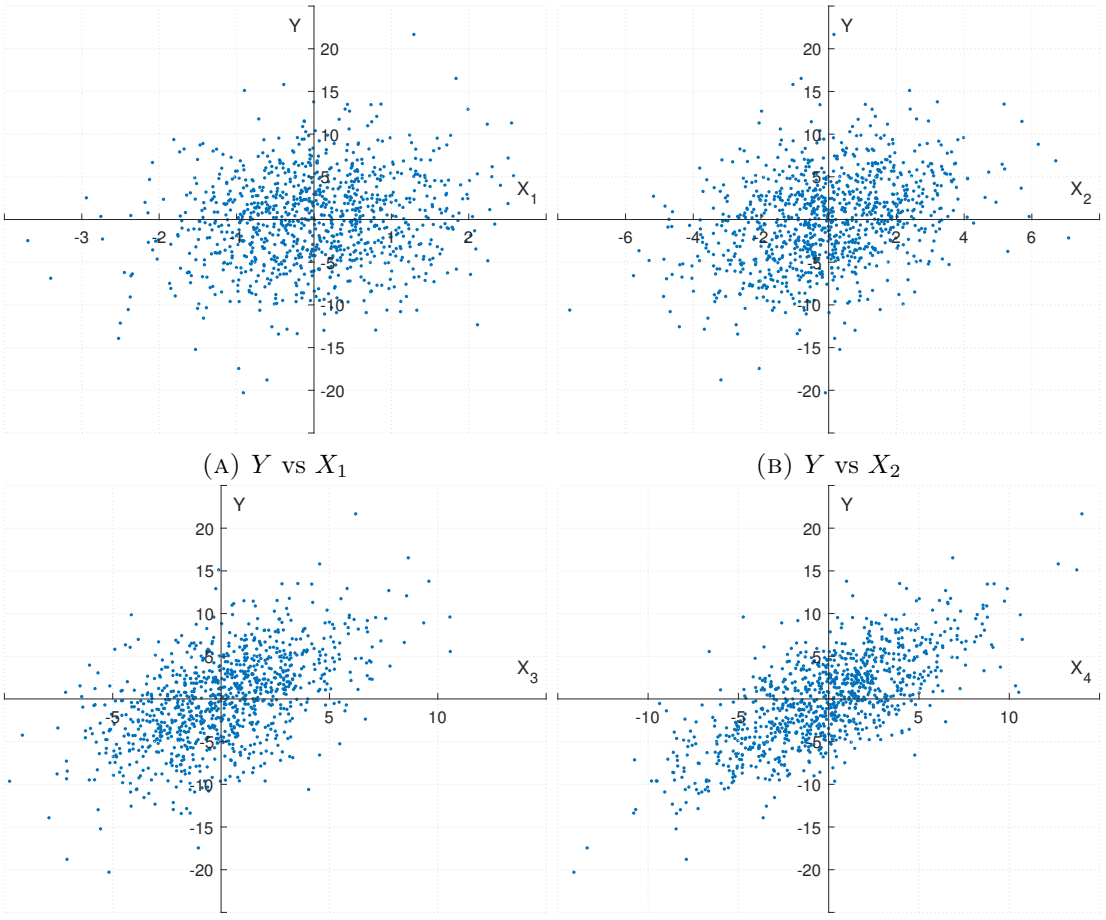

(A) Y vs X_1 (B) Y vs X_2

(C) Y vs X_3 (D) Y vs X_4

FIGURE 2.2: Scatterplots of X_i vs Y for model (2.37) following [140]

is interesting to note that local sensitivity shows the same sensitivity of Y on the all variables ($\partial Y/\partial X_i = 1$).

Scatter plots can be useful, but conclusions rely on the subjective judgement.

2.2.2.2 Sobol' sensitivity analysis

Sobol' indices are known to be good measures of sensitivity, since they do not require any assumptions about linearity or monotonicity [159]. The following description is based on [15, 150, 151, 159]. Similarly to the PC case, the assumption is again that all the variables $X_i, \ldots, X_M$ are independent, so $f_{\mathbf{X}}(\mathbf{X}) = \prod_{i=1}^{M} f_{X_i}(X_i)$. Some studies on sensitivity analysis of models with correlated variables can be found in the literature [98, 186].

The method is based on the ANalaysis of VAriance (ANOVA) decomposition of the model $\mathcal{M}$ (2.1). The representation:

$$\mathcal{M}(\mathbf{X}) = \mathcal{M}_0 + \sum_{i=1}^{M} \mathcal{M}_i(X_i) + \sum_{1 \le i < j \le M} \mathcal{M}_{ij}(X_i, X_j) + \cdots + \mathcal{M}_{1,2\ldots M}(\mathbf{X}). \tag{2.38}$$

is an ANOVA decomposition and is unique if:

$$\begin{gathered} \int_{\mathcal{H}_{X_k}} \mathcal{M}_{i_1 \ldots i_s}(X_{i_1}, \ldots, X_{i_s}) f_{X_k}(X_k) dX_k = 0 \\ \text{for} \quad 1 \le i_1 < \cdots < i_s \le M,\ k = i_1, \ldots, i_s \end{gathered} \tag{2.39}$$

and

$$\mathcal{M}_0 = \int_{\mathcal{H}_{\mathbf{X}}} \mathcal{M}(\mathbf{X}) f_{\mathbf{X}}(\mathbf{X}) dX_i \ldots dX_M, \tag{2.40}$$

where $\mathcal{H}_{\mathbf{X}}$ is the support of the random input vector $\mathbf{X}$. $\mathcal{H}_{X_k}$ and f_{X_k} are the support and the marginal PDF, respectively, of random variable random variable X_k.

The one-dimensional terms $\mathcal{M}_i(X_i)$ can be obtained by integration of formula (2.38) with respect to the probability measure over all variables except X_i over an associated domain $\mathcal{H}_{\mathbf{X} \setminus X_i}$:

$$\int_{\mathcal{H}_{\mathbf{X} \setminus X_i}} \mathcal{M}(\mathbf{X}) \prod_{k \ne i} f_{X_k} dX_k = \mathcal{M}_0 + \mathcal{M}_i(X_i). \tag{2.41}$$

The two-dimensional terms, $\mathcal{M}_{ij}(X_i, X_j)$ can be calculated by integration of formula (2.38) over all variables except x_i and x_j over an associated domain $\mathcal{H}_{\mathbf{X} \setminus \{X_i, X_j\}}$:

$$\int_{\mathcal{H}_{\mathbf{X} \setminus \{X_i, X_j\}}} \mathcal{M}(\mathbf{X}) \prod_{k \ne i,j} f_{X_k} dX_k = \mathcal{M}_0 + \mathcal{M}_i(X_i) + \mathcal{M}_j(X_j) + \mathcal{M}_{i,j}(X_i, X_j) \tag{2.42}$$

and so on, to get higher dimension terms.

D is the total variance:

$$D = \int_{\mathcal{H}_{\mathbf{X}}} \mathcal{M}(\mathbf{X})^2 f_{\mathbf{X}} dX_1 \ldots dX_M - \mathcal{M}_0^2. \tag{2.43}$$

After squaring and integrating 2.38, the variance decomposition is obtained:

$$D = \sum_{i=1}^{M} D_i + \sum_{1 \le i_1 < j \le M} D_{ij} + \cdots + D_{1,2,\ldots,M} \tag{2.44}$$

where the $D_{i_1 \ldots i_s}$ are the partial variances, defined as:

$$D_{i_1 \ldots i_s} = \int_{\mathcal{H}_{X_{i_1},\ldots,X_{i_s}}} \mathcal{M}^2_{i_1 \ldots i_s}(X_{i_1}, \ldots, X_{i_s}) f_{X_{i_1},\ldots,i_s} dX_{i_1} \ldots dX_{i_s} \tag{2.45}$$

The Sobol' sensitivity indices are defined as the ratios of variances:

$$S_{i_1,\ldots,i_s} = \frac{D_{i_1,\ldots,i_s}}{D}, \tag{2.46}$$

It can be noted, that all sensitivity indices are nonnegative and

$$\sum_{i=1}^{M} S_i + \sum_{1 \le i_1 < j \le M} S_{ij} + \cdots + S_{1,2,\ldots,M} = 1 \tag{2.47}$$

The Sobol' index $S_{i_1,\ldots,i_s}$ conveys information as to how much of the total ouput variance is due to each of the input variables $\{i_1, \ldots, i_s\}$. The first order indices S_i contain information about the influence of each variable taken alone, whereas their influence in combination is given by the higher order indices.

A more detailed analysis may require use of a total global sensitivity index, which is the sum of all sensitivity indices including the mixed terms that correspond to the i-th variable:

$$S_i^{Tot} = \sum_{i \subset \{i_1,\ldots,i_s\}} S_{i_1,\ldots,i_s}. \tag{2.48}$$

Alternatively:

$$S_i^{Tot} = 1 - S_{\sim i}, \tag{2.49}$$

where $S_{\sim i}$ is a sum off all partial indices which do not include the i-th variable.

It can be noted, that $0 \le S_i \le S_i^{Tot} \le 1$. The extreme cases are:

- $S_i = S_i^{Tot} = 0$ which means that the model $\mathcal{M}$ does not depend on X_i
- $S_i = S_i^{Tot} = 1$ which means that model $\mathcal{M}$ does not depend on variables other than X_i.

The Sobol' indices can be estimated by the Monte Carlo method.

Two sets of N_{MC} sampling points are generated independently and denoted with superscripts (1) and (2). The sets are then mixed and sampling points as follows are constructed:

- $\widetilde{\mathbf{X}}_{i\,n}^{(1)} = [X_{1n}^{(1)}, X_{2n}^{(1)}, \ldots, X_{(i-1)n}^{(1)}, X_{i\,n}^{(2)}, X_{(i+1)n}^{(1)}, \ldots, X_{M\,n}^{(1)}]^\top$ is the n-th sampling point from the set (1), where $X_{i\,n}^{(1)}$ is replaced by $X_{i\,n}^{(2)}$ from the set (2)
- $\widetilde{\mathbf{X}}_{i\,n}^{(2)} = [X_{1n}^{(2)}, X_{2n}^{(2)}, \ldots, X_{(i-1)n}^{(2)}, X_{i\,n}^{(1)}, X_{(i+1)n}^{(2)}, \ldots, X_{M\,n}^{(2)}]^\top$ is the n-th sampling point from the set (2), where $X_{i\,n}^{(2)}$ is replaced by $X_{i\,n}^{(1)}$ from the set (1).

The partial variance can be estimated by:

$$D_i^{MC} = \frac{1}{N_{MC}} \sum_{n=1}^{N_{MC}} \mathcal{M}(\mathbf{X}_n^{(1)}) \mathcal{M}(\widetilde{\mathbf{X}}_{i\,n}^{(2)}) - (\mathcal{M}_0^{MC})^2. \tag{2.50}$$

The partial Sobol' index computed by MC is:

$$S_i^{MC} = \frac{D_i^{MC}}{D^{MC}}. \tag{2.51}$$

The total Sobol' index can be obtained without the necessity of using all the required partial indices:

$$S_i^{Tot,MC} = 1 - \frac{D_{\sim i}^{MC}}{D^{MC}}, \tag{2.52}$$

where:

$$D_{\sim i}^{MC} = \frac{1}{N_{MC}} \sum_{n=1}^{N_{MC}} \mathcal{M}(\mathbf{X}_n^{(1)}) \mathcal{M}(\widetilde{\mathbf{X}}_{in}^{(1)}) - (\mathcal{M}_0^{MC})^2. \tag{2.53}$$

Estimation of Sobol' indices by MC is very expensive computationally, especially when M is high. To obtain all indices one has to compute the model for 2^M MC sets. Since very often computing a single set of MC computations is already expensive (usually more than 10^4 model evaluations), calculating even just the complete set of total sensitivity indices can be intractable by crude MC.

In order to reduce the huge computational cost of Sobol' index calculation, metamodel-based approaches can be used. Sudret [159], Crestaux et al. [38] have shown, that Sobol' indices can be calculated with use of PC coefficients. In such a case, the computational cost is barely greater than the cost of obtaining PC coefficients. This is very attractive when compared to crude MC.

Let $\mathcal{A}_{i_1,\ldots,i_s}$ be a set of $\boldsymbol{\alpha}$-tuples in $\mathcal{A}$, such that only indices $i_1, ..., i_s$ are non-zero:

$$\mathcal{A}_{i_1,..,i_s} = \{\boldsymbol{\alpha} \in \mathcal{A} : \alpha_k \neq 0 \Leftrightarrow k \in \{i_1, \ldots, i_s\}\}. \tag{2.54}$$

In other words, these are $\boldsymbol{\alpha}$-tuples corresponding to polynomials $\Psi_{\boldsymbol{\alpha}}$ depending only on all the input variables $X_{i_1}, ..., X_{i_s}$.

The truncated polynomial chaos expansion can be expressed as follows:

$$\begin{aligned}\mathcal{M}^{PC}(\boldsymbol{\xi}) = a_0 + \sum_{i=1}^{M}\sum_{\boldsymbol{\alpha}\in\mathcal{A}_i} a_{\boldsymbol{\alpha}}\Psi_{\boldsymbol{\alpha}}(\xi_i) + \sum_{1\le i_1<i_2\le M}\sum_{\boldsymbol{\alpha}\in\mathcal{A}_{i_1,i_2}} a_{\boldsymbol{\alpha}}\Psi_{\boldsymbol{\alpha}}(\xi_{i_1},\xi_{i_2}) + ..+ \\ + \sum_{1\le i_1<...<i_s\le M}\sum_{\boldsymbol{\alpha}\in\mathcal{A}_{i_1,...,i_s}} a_{\boldsymbol{\alpha}}\Psi_{\boldsymbol{\alpha}}(\xi_{i_1},...,\xi_{i_s}) + ... + \sum_{\boldsymbol{\alpha}\in\mathcal{A}_{1,...,M}} a_{\boldsymbol{\alpha}}\Psi_{\boldsymbol{\alpha}}(\boldsymbol{\xi}).\end{aligned} \tag{2.55}$$

Since the employed PC basis is orthonormal, the properties (2.39) and (2.40) are fulfilled. Hence, the terms in (2.55) can be identified as summands in (2.38):

$$\mathcal{M}_{i_1,..,i_s}(\xi_{i_1},...,\xi_{i_s}) = \sum_{\boldsymbol{\alpha}\in\mathcal{A}_{i_1,...,i_s}} a_{\boldsymbol{\alpha}}\Psi_{\boldsymbol{\alpha}}(\xi_{i_s},...,\xi_{i_s}). \tag{2.56}$$

The sensitivity indices $S^{PC}_{i_1,..,i_s}$ can be obtained with use of PC coefficients:

$$S^{PC}_{i_1,..,i_s} = \frac{1}{D^{PC}}\sum_{\boldsymbol{\alpha}\in\mathcal{A}_{i_1,...,i_s}} a^2_{\boldsymbol{\alpha}}. \tag{2.57}$$

Let $\mathcal{A}^{Tot}_i$ be a set that contains all $\boldsymbol{\alpha}$-tuples with the non-zero i-th index:

$$\mathcal{A}^{Tot}_i = \{\boldsymbol{\alpha}\in\mathcal{A} : \alpha_i \neq 0\}. \tag{2.58}$$

The total sensitivity indices can be obtained with the use of PC coefficients:

$$S^{Tot,PC}_i = \frac{1}{D^{PC}}\sum_{\boldsymbol{\alpha}\in\mathcal{A}^{Tot}_i} a^2_{\boldsymbol{\alpha}}. \tag{2.59}$$

Chapter 3

Comparison of regression point choice methods

3.1 Methods to choose regression points in non-intrusive polynomial chaos expansion

The accuracy of non-intrusive PC depends on the number and location of sampling points. A good balance between computational cost and satisfactory accuracy is needed. Finding an effective universal way to choose points is still an open question not only in PC but also in other non-intrusive uncertainty quantification methods, sensitivity analysis methods etc. The choice of points can be regarded as the design of an experiment (DoE). Techniques of DoE were originally developed for planning physical experiments. The main difference between a physical and computational experiment is that when we run a computer simulation twice we obtain the same result without the random noise that occurs in a physical experiment. Nevertheless, DoE has been extended to the computational field. Some authors call DoE of physical experiments classic DoE, whereas DoE of deterministic computational experiments is called modern DoE [57]. The general aim of both classic and modern DoE is the same, which is to obtain accurate information with a limited number of experiments.

Different approaches exist in the literature. An overview of methods of DoE used in the computational field can be found in [57], which concluded that there is no universally applicable way of determining which technique of DoE is preferable. Some methods were also compared by [30], where recommendations are given for functions with different properties (e.g. many local minima, rapid changes). Comparison of methods in the least squares polynomial approximation was done by [53]. They noticed better convergence

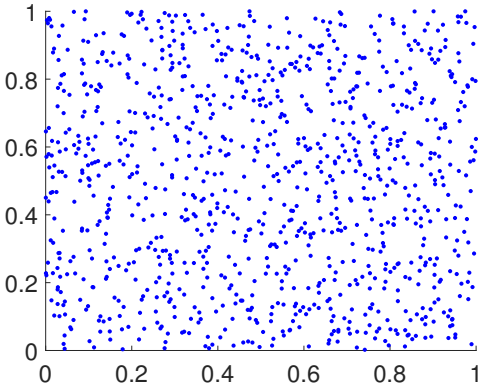

FIGURE 3.1: Simple random choice of uniformly distributed 1000 points in range from 0 to 1, 2 variables

of sparse grid points for very low dimensional problems, whereas QMS was believed to be better for higher dimensional problems in terms of convergence. Nevertheless, there are not many studies on the choice of sampling points in regression-based PC. Recently, Hadigol and Doostan [64] have investigated DoE methods in least square polynomial chaos expansion and have also proposed a new approach. The adaptive DoE approach was proposed for global sensitivity analysis in [27].

DoE methods widely used in PC can be divided into two main groups:

Random and quasi-random – regression points are drawn according to a distribution (section 3.1.1);

Based on optimality criteria – a deterministic choice based on optimization criteria, which will be discussed in more detail in section 3.1.2.

Some combined approaches are also considered in this work (section 3.1.3), which use both the optimality criteria and random choice elements.

3.1.1 Random and quasi-random choice

In the random and quasi-random methods, regression points are drawn in the following ways:

- pure randomly – (e.g. [53]) This is a simple and widely-used method in PC. DoE points are drawn randomly with respect to a distribution (Figure 3.1);
- by one of the improved sampling strategies (already described in section 2.1.1.2):
  - LHS – also widely used in PC [31] (Figure 3.2);

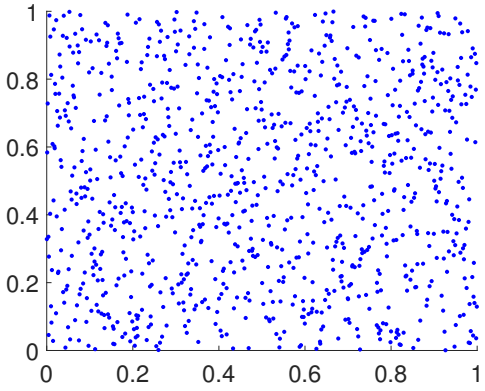

FIGURE 3.2: 1000 points generated by LHS, two variables

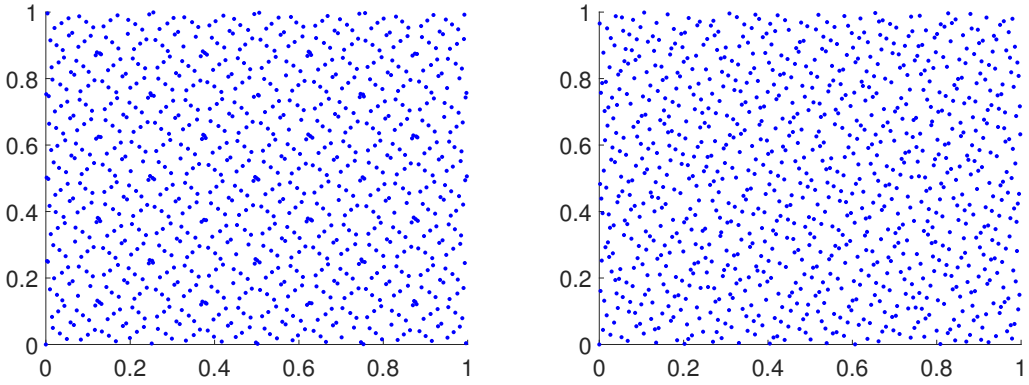

(A) Sobol' sequence (B) Halton sequence

FIGURE 3.3: 1000 points generated by QMS, two variables

– QMS [16, 53], e.g. Halton and Sobol' sequences (Figure 3.3). Sobol' sequences were shown to be the most efficient in a study [16] where the NISP method was used. With metamodels other than PC, Sobol' sequences, were also shown to be superior (in terms of the projection property over optimal latin hypercube design, centroidal Voronoi tessellation and Halton and Hammersley sequences) especially in case of higher dimensional problems [30].

3.1.2 Optimality criteria

The following optimality criteria are taken from the theory of optimal design of physical experiments [48].

Widely-used criteria in classic DoE are based on the information matrix (or, equivalently, its inverse – the dispersion matrix). It can be noted that the information matrix $\mathbf{A}^\top\mathbf{A}$ is determined by the DoE and does not depend on the model solution (observations $\mathbf{Y}_{ex}$) [49].

The most widely-used criterion is D-optimality. In classic DoE, the assumption is made of independent normal random error with constant variance $\mathrm{var}(\mathbf{Y}_{ex}) = \mathbf{I}\sigma^2$ [47, 190]. Under such an assumption, minimisation of the variance of the estimated coefficients leads to maximisation of the information matrix $\mathbf{A}^\top\mathbf{A}$ determinant:

$$\det(\mathbf{A}^{*\top}\mathbf{A}^*) = \max_{\Xi}((\det(\mathbf{A}^\top\mathbf{A})), \tag{3.1}$$

where $\boldsymbol{A}^*_{ij} = \Psi_{\boldsymbol{\alpha}_j}(\boldsymbol{\xi}^{(i)*})$, $i = 1, \ldots, N$; $j = 1, \ldots, P$.

This is equivalent to minimisation of the determinant of the dispersion $(\mathbf{A}^\top\mathbf{A})^{-1}$ matrix. Geometrically, coefficients and their errors are represented as an ellipsoid, which shows the confidence interval of each coefficient. Maximisation of the determinant of the information matrix corresponds to minimising the volume of the ellipsoid [40].

The D-criterion was firstly proposed by Smith [149]. Efficient algorithms for finding D-optimal design have been proposed in the literature, e.g. the Fedorov exchange algorithm [48].

In PC application, construction of DoE based on D-optimal design was proposed by Isukapalli [82] and today may be considered as one of the most widely-used approaches [27, 133, 159, 190]. The concept of D-optimality is part of recently developed methods of efficient sampling for the PC method, e.g. [43, 64].

Other criteria common in classic DoE, but not in PC, are:

A-optimality maximization of the trace of the dispersion matrix $(\mathbf{A}^\top\mathbf{A})^{-1}$ which corresponds to minimization of the average variance of the coefficients [40].

E-optimality maximization of the least singular value of the information matrix $\mathbf{A}^\top\mathbf{A}$,

G-optimality minimization of the largest diagonal term of $\mathbf{A}(\mathbf{A}^\top\mathbf{A})^{-1}\mathbf{A}^\top$

3.1.2.1 Univariate case

The D-optimal solution is known for some univariate polynomials of order p with an appropriate weight function (information matrix in form $\mathbf{A}^\top$ **WA** (2.31)), [5]:

For Hermite polynomials: the roots of the Hermite polynomial of order $p+1$, when $w(x) = \exp(-x^2)$ is applied (Figure 3.4),

For Legendre polynomials: the roots of the polynomial $(1-x^2)L'_p(x)$, for $w(x) = 1$, where L_p is the Legendre polynomial of order p.

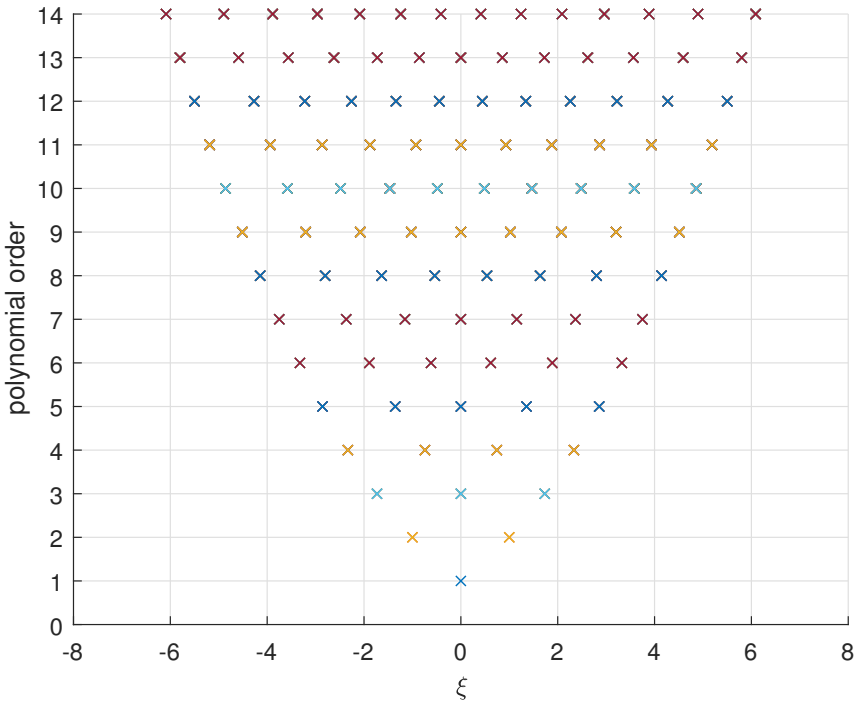

FIGURE 3.4: Roots of Hermite polynomials of different orders

It can be seen, that the D-optimal points of the Legendre polynomials are different from those of the Hermite polynomials. Nevertheless, in the application of PC, sometimes the roots of polynomial order $p+1$ are taken as a general rule for constructing a DoE for other PC bases, e.g. Legendre [159].

Let us consider the univariate problem $M = 1$, with the Hermite basis, PC order $p = 1$ and the minimum required number of regression points which in this case is two. The points are denoted ξ_1 and ξ_2. Then, $\mathbf{A}$ is in the following form:

$$\mathbf{A} = \begin{bmatrix} 1 & \xi_1 \\ 1 & \xi_2 \end{bmatrix}. \tag{3.2}$$

For this simple case it is easy to draw the change of the determinant of the information matrix as a function of positions of the points ξ_1 and ξ_2 (Figure 3.5).

It should be noted, that including the weight $w = \frac{1}{\sqrt{2\pi}} e^{-\boldsymbol{\xi}^{\mathbf{2}}/\mathbf{2}}$ changes the shape of the relation between the determinant of the information matrix and the position of the regression points. The maximum of $\det(\mathbf{A}^\top \mathbf{W} \mathbf{A})$ (Figure 3.5b) is indeed at the roots of the second-order Hermite polynomial $\xi^2 - 1$. Where no weight function is applied ($w = 1$) (Figure 3.5a) the maximum of $\det(\mathbf{A}^\top \mathbf{A})$ is on the border. If the support of ξ_1, ξ_2 is the range from -1 to 1, which corresponds to the Legendre polynomial (information matrix

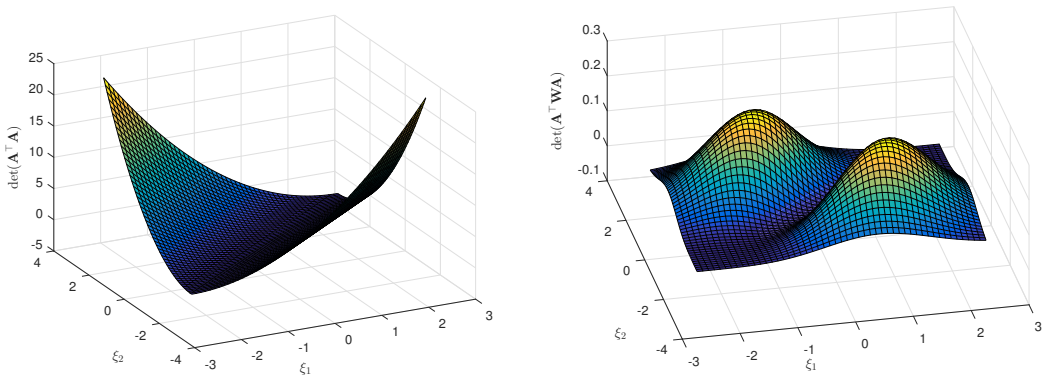

(A) $\det(\mathbf{A}^\top\mathbf{A})$ - without weight function ($\mathbf{W} = \mathbf{I}$)

(B) $\det(\mathbf{A}^\top\mathbf{WA})$ including weight function $w = \frac{1}{\sqrt{2\pi}}e^{-\boldsymbol{\xi}^2/2}$

FIGURE 3.5: Determinant of information matrix (3.2) as a function of 2 sampling points, $M = 1$, $p = 1$

is the same form, since first-order Hermite and Legendre polynomials are the same), the maximum would be at points $(-1, 1)$, which are the roots of $(1 - x^2)L'_p(x)$.

3.1.2.2 Multivariate case

Multivariate DoE can be constructed by a combination of D-optimal points of univariate polynomials [82]. However, there are $(p+1)^M$ such combinations, which is usually computationally intractable but good accuracy can be achieved for a much smaller number of regression points. The classic approach [11, 82] is to take points that are closest to the origin. This method will be denoted M1. The main disadvantage of M1 is that a rank-deficient information matrix can be easily obtained. This problem can be solved by adding more points into the DoE, but this unfortunately increases computational cost.

Although the D-optimal points of the univariate Legendre polynomials are not roots of the Legendre polynomial of order $p+1$, as in case of Hermite polynomial, a combination of such ponts is often used as a DoE, e.g. in [159]. That is why method M1 in the case of the Legendre basis will be investigated in two variants of the grid:

- of D-optimal points of the univariate polynomial (roots of $(1 - x^2)L'_p(x)$),
- roots of the Legendre polynomial of order $p + 1$.

The solution obtained by method M1 is not exactly D-optimal. Another method consists of finding the D-optimal set from combinations of roots of the polynomial of order $p+1$ [190]. This method will be denoted M2. Works, where such an approach is proposed, do not contain information about the inclusion of the weight function in case of the Hermite

PC basis, e.g. [190]. Figure 3.6 shows a DoE chosen by method M1 (Figure 3.6a) and D-optimal solutions found amongst combinations of roots of Hermite polynomial of order $p+1$. Different solutions are obtained depending on whether a weight function is applied (Figure 3.6c) or not (Figure 3.6b). In this case M1 is closer to the D-optimal solution with a weight function. The variant of method M2 without weight will be denoted M2a and with weight M2b.

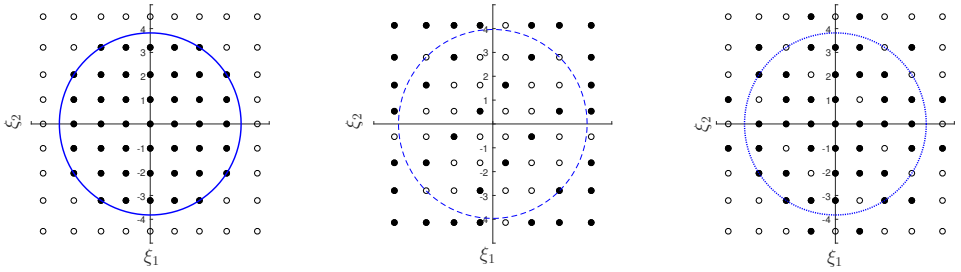

(A) Points chosen by method M1 proposed by [11]

(B) points chosen by method M2a - D-Optimal choice from a set of candidate points composed of the combination of polynomial roots of order $p+1$, information matrix without weight function

(C) points chosen by method M2a - D-Optimal choice from a set of candidate points composed of the combination of polynomial roots of order $p+1$, information matrix with weight function $w(x) = \exp(-x^2)$

FIGURE 3.6: Choice of points in the case of Hermite basis, $M = 2$, $p = 7$. Small circles denote combinations of roots of 1-D Hermite polynomial of order $p + 1$. Black circles denote those of the points which are chosen for the DoE. The blue circle shows the range of the points closest to the origin, which are used for the DoE in the M1 method

3.1.3 Combined approach

In method M3, the DoE will be randomly drawn from a grid of D-optimal points of univariate polynomials.

The solution obtained by method M2 may be not D-optimal generally. Different candidate sets that contain combinations of roots of polynomials of order $p + 1$ are to be considered. Figure 3.7 shows D-optimal solutions for a grid of points which is denser than a grid of the roots of the polynomial of order $p+1$. Again, the cases are shown with and without the weight function $w(x) = \exp(-x^2)$. Although combinations of roots of polynomials of order $p + 1$ are included in the denser and wider candidate set of points, they were not included in the D-optimal final set. Therefore, other candidate sets of points will be also considered in this work. Candidate sets of points will be generated simply randomly (method M4) or by LHS (method M5). In the case of the Hermite basis, both methods will be considered (a)without a weight function and (b)with a weight

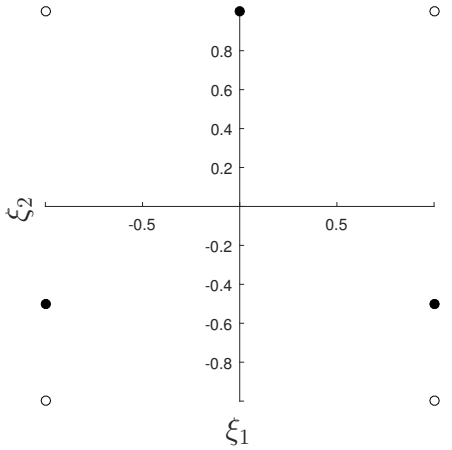

(A) D-optimal points chosen from a uniform range from -2 to 2 with a step 0.5 including weight $w(x) = \exp(-x^2)$

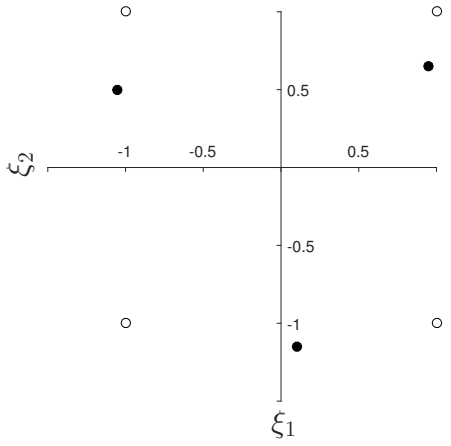

(B) D-optimal points chosen from a uniform range from -1.5 to 1.5 with a step 0.05 including weight $w(x) = \exp(-x^2)$

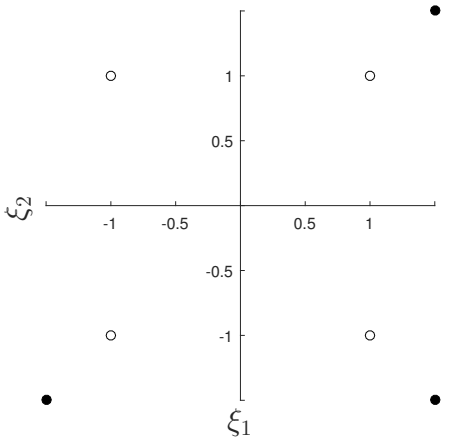

(C) D-optimal points chosen from a uniform range from -1.5 to 1.5 with a step 0.05 without weight

FIGURE 3.7: D-optimal points compared to the c-method M1, Hermite basis ($M = 2$, $p = 1$). Empty circles denote combination of roots of polynomial $p+1$ and black circles denote D-optimal solutions from a denser grid of candidate points

function $w(x) = \exp(-x^2)$. Figure 3.8 shows an example of such a solution in these two variants. The difference can be clearly seen.

3.1.4 Summary of methods

To sum up, the following methods are compared within this work:

S1 - Sobol' sequence [16];

S2 - Halton sequence [16];

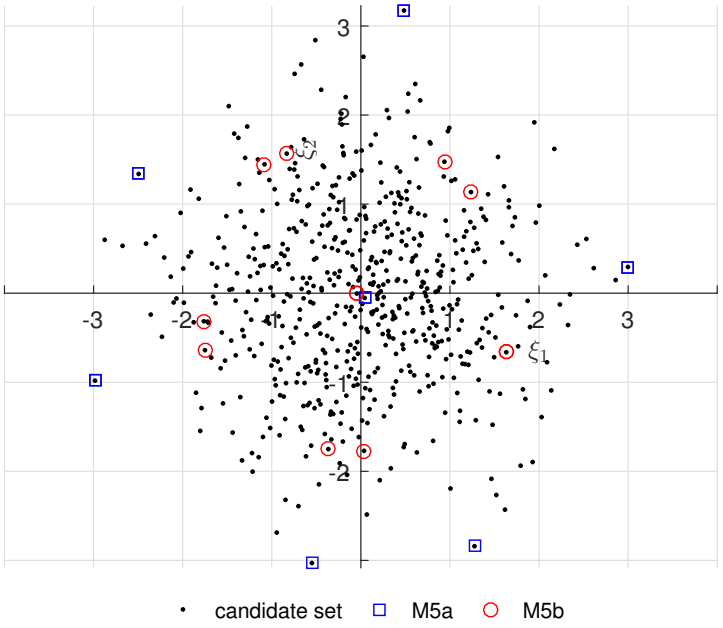

FIGURE 3.8: Example of D-optimal set from the candidate set drawn by the LHS method when D-optimality is conducted without (M5a) and with (M5b) weight function $w(x) = \exp(-x^2)$, Hermite basis, $M = 2$, $p = 2$

M1 - the closest to the origin from combination of roots of polynomial of order $p + 1$ [159]. Also method M1b is investigated, which is a combination of D-optimal points in the case of the uniform distribution instead of roots;

M2 - D-optimal design from D-optimal points of univariate polynomials (e.g. in case of normal distribution roots of Hermite polynomials or order $p + 1$). In the case of normal distribution in variants:

- without a weight function - M2a [190];
- with a weight function - M2b;

M3 - randomly drawn subset of univariate D-optimal points;

M4 - D-optimal design chosen from a random candidate set of points. In the case of normal distribution in variants:

- without a weight function - M4a ;
- with a weight function - M4b;

M5 - D-optimal design chosen from candidate set sampled by LHS method. In the case of normal distribution in variants:

- without a weight function - M5a [26];
- with a weight function - M5b.

Also the number of regression points should be appropriately chosen. The number of points depends on the size of the PC basis P (which depends on M and p). The recommendations in the literature vary, e.g $2P$, $P(M-1)$ [11], $2(P+1)$ [82].

3.2 Comparison of methods on numerical examples

The results presented in this chapter were partially published in [165] (comparison of methods in multivariate models) and [164] (choice of regression points in the 1-dimensional case and D-optimality)

In order to evaluate and compare solutions obtained by the PC method, the following error measures are introduced:

- The reference error $Err_{\%}$ is defined as:

$$Err_{\%} = \frac{|V^{ref} - V^{PC}|}{|V^{ref}|} \cdot 100, \tag{3.3}$$

  where V is one of the quantities: mean, standard deviation, percentile or sensitivity index, the superscript ^{PC} denotes that the quantity is estimated by PC and the superscript ^{ref} denotes the reference solution obtained analytically or by MC method.

- The error in calculating the Sobol' indices can be measured by Err_s:

$$Err_s = \sqrt{\sum_{i=1}^{M} (S_i^{Tot,ref} - S_i^{Tot,PC})^2}, \tag{3.4}$$

  where $S_i^{Tot,ref}$ is the reference value of the i-th random variable, obtained analytically or by MC.

- In some examples in order to evaluate the PC metamodel the root mean square error is calculated as:

$$RMSE = \sqrt{\frac{1}{N} \sum_{i}^{N} \left(\mathcal{M}(\boldsymbol{\xi}_i) - \mathcal{M}^{PC}(\boldsymbol{\xi}_i)\right)^2}, \tag{3.5}$$

  where $\boldsymbol{\xi}_i$ is sampling point

or as the normalized RMSE (in chapter 4)

$$NRMSE = \frac{RMSE}{\frac{1}{N}\sum_i^N \mathcal{M}(\boldsymbol{\xi}_i)}, \tag{3.6}$$

- The error of the PC metamodel at a given point $\boldsymbol{\xi}_i$ relative to the exact solution as a percentage is

$$Err_{PC\%} = \frac{\left|\mathcal{M}(\boldsymbol{\xi}_i) - \mathcal{M}^{PC}(\boldsymbol{\xi}_i)\right|}{|\mathcal{M}(\boldsymbol{\xi}_i)|} \cdot 100. \tag{3.7}$$

In this work only the error due to the PC approximation is studied.

3.2.1 Examples

PC is firstly applied to 1D examples (section 3.2.2) and then to multivariate problems (section 3.2.3).

The methods will be compared on the Sobol' function which is widely used in the literature concerning global sensitivity analysis:

$$Y = \prod_{i=1}^{M} \frac{|4X_i - 2| + d_i}{1 + d_i}, \tag{3.8}$$

where X_i, $i = 1, \ldots, M$ are uniformly distributed random variables over $[0, 1]$ and d_i are non-negative constants. In this work, M is set to 1 or 4 and the constants are $\mathbf{d} = [1, 2, 5, 10]^\top$ following [15]. This function is especially interesting in comparison with the implant models (e.g. model 2, section 3.2.1.2) because its nonsmoothness is similar to that of the maximum of reaction forces in the membrane model of an implant.

The methods described above will also be compared on two local models of implants used in hernia repair in the following variants:

1. Cable model of the implant (section 3.2.1.1):
   (a) one random variable E;
   (b) one random variable L_0;
   (c) four random variables $\mathbf{X} = [E, L_0, H_0, \Delta_p]^\top$;
2. Model of the membrane subjected to displacement of the supports (section 3.2.1.2):
   (a) with one random variable t_1;

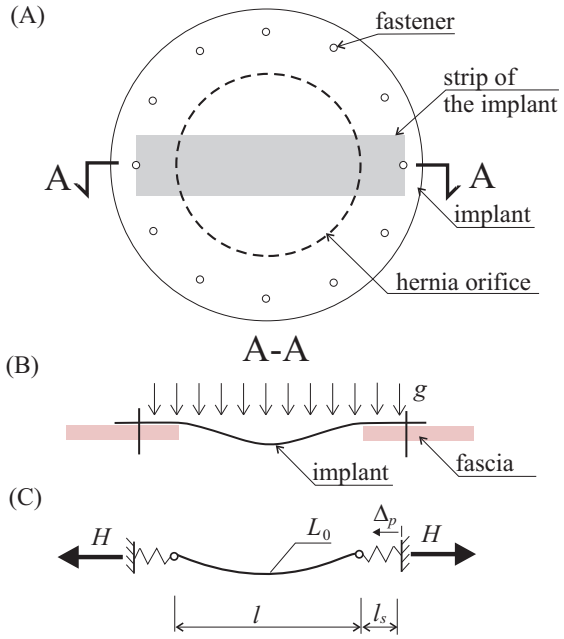

FIGURE 3.9: Scheme of the surgical mesh covering the hernia orifice with one strip for the cable model in top view (A) and lateral view (B), (C) scheme of cable model, adapted from [168]

(b) with one random variable t_4;

(c) with three random variables $\mathbf{X} = [t_i]^\top$; $i = 1, 2, 3$;

(d) with ten independent random variables $\mathbf{X} = [t_i]^\top$; $i = 1, 2, \ldots 10$.

3.2.1.1 Model 1: cable model of the implant

The simplest model of the implant-tissue system is a cable model (Figure 3.9). The model was proposed by Szymczak et al. [168] and the following description is based on that work [168]. The aim of this study was to develop a simple model and perform local sensitivity analysis in order to identify the most influential parameters and outline the direction of future studies. The one-dimension cable model refers to a strip of surgical mesh between two fasteners on the opposite sides of the hernia orifice that is tightened the most.

The cable is subjected to a uniformly distributed load g which simulates intraabdominal pressure. Because connection failure is one of the main reasons for hernia recurrence, the QoI is the horizontal reaction H. It can be found from the equilibrium equation. The width of the overlap of the mesh onto the fascia is denoted by l_s. The fact that the hernia orifice is not stiff is also taken into account by introducing Δ_p, which is the displacement of the cable edges resulting from the fascia elasticity. The final form of equation to be solved is:

parameter	unit	value
A	m^2	1.35e-5
g	N/m	148.8
l	m	0.1
l_s	m	0.04

TABLE 3.1: Values of cable model constants (3.9)

Variable	unit	when assumed constant	lower limit	upper limit
E	MPa	10.77	5.385	16.155
L_0	m	0.105	0.0945	0.1155
H_0	N	1	0	4
Δ_p	m	0.005	0.0025	0.0075

TABLE 3.2: Uniform random variables of model 1 and parameters of their distribution

$$H^3(1+\frac{l_s}{L_0})+H^2(-H_0+\Delta_p\frac{EA}{L_0})-\frac{EA}{L_0}\frac{g^2l^3}{24}=0, \tag{3.9}$$

where E is the elastic modulus of the cable material representing the implant material, L_0 is the initial length of the cable, H_0 is the initial force in the cable originated by tightening of the mesh, A is the cross sectional area of the cable and l the cable span.

For clearer derivations of the local sensitivity indices (section 4.1), let the equation (3.9) be expressed as:

$$H^3c_1+H^2c_2-c_3=0, \tag{3.10}$$

where $c_1=1+\frac{l_s}{L_0}$, $c_2=-H_0+\Delta_p\frac{EA}{L_0}$ and $c_3=\frac{EA}{L_0}\frac{g^2l^3}{24}$.

The values of the constant parameters are presented in Table 3.1.

In [168] variations of E, L_0, H_0 and Δ_p were studied with deterministic local sensitivity analysis. When one parameter changes, the others remain fixed. Different base points were considered because each may have a different local sensitivity index. Table 3.2 presents values of the parameters for the case where they were held fixed and, for the case in which they were varied, the range over which they did so. The same ranges are taken as limits of a uniform distribution in UQ and global SA analysis of the model. Firstly, univariate analyses are conducted when only E is a random uniform variable (model 1a) or only L_0 is a random uniform variable (model 1b). The purpose of these examples is that it is easy to show the relations between DoE and the error of the PC estimation in the univariate case. The main example (model 1c) has all four variables drawn from indepedent random uniform distributions. In this case, the outcomes of global SA can be compared with local SA results.

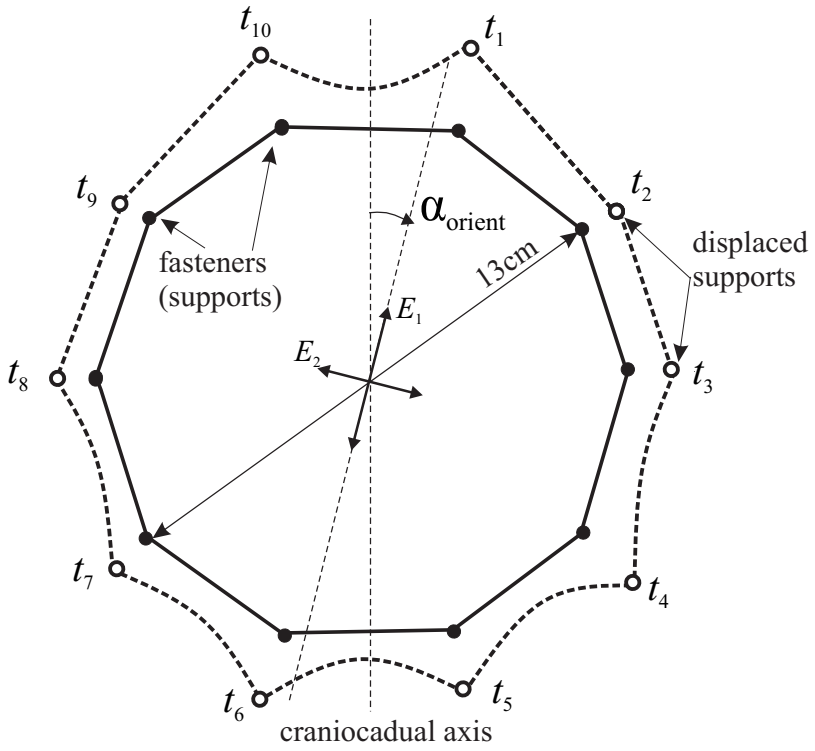

FIGURE 3.10: Scheme of model 2

.

3.2.1.2 Model 2: model of membrane subjected to displacement of the supports

The implant is modelled as a membrane structure. A finite element membrane model of a surgical mesh was proposed in [108] and also in [67, 147]. Lubowiecka [104] proposed subjecting the implant to forced displacements of its supports, which simulate displacements of the fasteners during daily movements of the torso. In that work values of these displacements were taken from the study of Szymczak et al. [169], where the strains of the external abdominal surface were identified. Podwojewski et al. [130] found that the ratio between the strains on the surfaces of the external and internal abdominal walls was 2.6 so the values of Szymczak at el. were reduced by this factor. Next, the model with some modifications was applied to the procedure of optimising implant choice and orientation of implant within an anisotropic abdominal wall [106]. A model in the same form is applied in this thesis.

The scheme of model is shown in Figure 3.10. It is assumed that the hernia orifice radius is equal to 2.5 cm. The overlap of the implant over human tissue according to surgical practice is 4 cm. Therefore, the total span of the implant is equal to 13 cm. It is assumed that the implant is connected to the fascia by 10 fasteners (tacks), which are modelled by 10 supports fixing all translations.

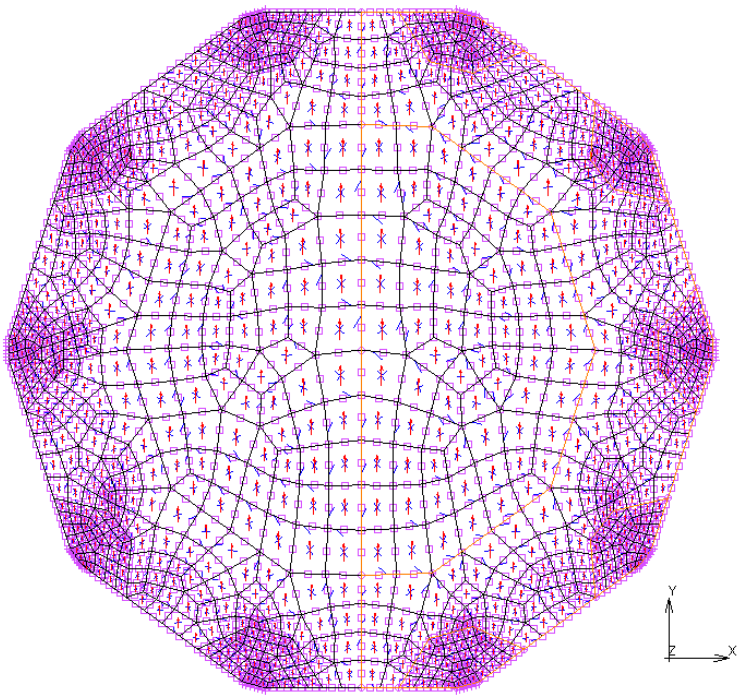

FIGURE 3.11: Finite Element mesh of model 2

.

The MSC.Marc commercial system was used. The FE model is composed of quadrilateral eight-node isoparametric membrane elements with three translational degrees of freedom at each node. A membrane has no bending stiffness. Figure 3.11 shows FE mesh, which was tested by convergence analysis. The mesh is finer next to the model supports. Static non-linear (large displacement and large strain) analysis was performed.

The material of the implant is assumed to be piecewise affine orthotropic. The parameters correspond to the commercial implant DynaMesh®-IPOM (Figure 3.12) surgical implant (FEG Textiltechnik mbH, Aachen, Germany and are taken from [174]. This is a knitted mesh made of polypropylene and polyvinylidene fluoride. The elastic modulus in the first (stiffer) direction of the implant E_1 is equal to 6.4 N/mm if the strain is smaller than 0.15 and 14 N/mm otherwise. In the perpendicular direction the elastic modulus E_2 is equal to 0.36 N/mm. The high orthotropy ratio (E_1/E_2) of this material can be seen: 18 for strain lower than 0.15 and 39 otherwise. Since the abdominal wall is anisotropic, the orientation of the orthotropic implant is significant as shown in [106]. α_{orient} (Figure 3.10) is the angle between the cranio-caudal axis and the first direction of the implant. In this chapter $\alpha_{orient} = 0$, which means that the first direction of implant is parallel to the cranio-caudal axis. In chapter 4 simulations have been done also for α_{orient} in the range from 0 to 180 degrees (if not stated, $\alpha_{orient} = 0$).

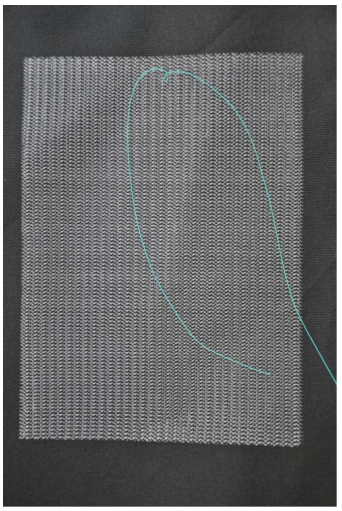

FIGURE 3.12: DynaMesh surgical mesh

support	t_1	t_2	t_3	t_4	t_5	t_6	t_7	t_8	t_9	t_{10}
μ [cm]	0.575	0.2	0.225	0.4	0.45	0.45	0.4	0.225	0.2	0.575
σ [cm]	0.115	0.343	0.123	0.793	0.215	0.215	0.793	0.123	0.343	0.115

TABLE 3.3: Mean and standard deviation of displacement of supports $t_i \sim \mathcal{N}(\mu_i, \sigma_i)$ in the model 2

It is assumed that the hernia is located in the central part of abdominal wall, which has consequences for the values of the forced displacements.

Due to uncertainties resulting, e.g., from the natural variability of the mechanical properties of the abdominal wall and difficulties in accurate *in vivo* measurement in humans, the values of the forced displacements (t_i, where $i = 1 \dots n$ and n is the number of supports, Figure 3.10) are assumed to be normal random variables. Their means and standard deviations (Table 3.3) are based on [104, 169].

Examples with different numbers of independent random variables are considered: with 1 random variable (t_1 in model 2a) and t_4 in model 2b), with 3 random variables $\mathbf{X} = [t_i]^\top$; $i = 1, 2, 3$ (model 2c). Support displacements that are not assumed to be random are constant and equal to their mean from Table 3.3. Also an example with random forced displacements in all supports is considered $\mathbf{X} = [t_i]^\top$; $i = 1, 2, \dots 10$ (model 2d).

Since hernia recurrences are usually caused by connection failure, the quantity of interest Y is the maximum reaction force, R_{max}, which corresponds to the maximum force in the implant-abdominal wall connection. Two approaches for calculating R_{max} are examined:

Approach 1 : one metamodel is created based directly on the outcomes of the maximum reaction

$$Y = R_{max}; \tag{3.11}$$

Although this approach is straightforward, it can be problematic since R_{max} may be a nonsmooth function, which can be challenging for PC approximation by smooth polynomials.

Approach 2 : firstly create a separate metamodel for each reaction R_i. The maximum R_{max} is calculated as the maximum of values obtained from each metamodel Y_i.

$$Y_i = R_i \tag{3.12}$$

$$Y = \max(Y_i) \quad \text{for} \quad i = 1, \ldots, n_{fas}. \tag{3.13}$$

The number of realisations of the metamodels which are carried out for random sampling points in order to calculate Y is 10^5. In this approach, calculating Sobol' sensitivity indices does not consist of straightforward post-processing of PC coefficients. Nevertheless, they can be still calculated with negligible computational cost by employing the metamodels of each reaction to perform the MC procedure for calculating sensitivity indices (2.50–2.52).

3.2.2 Results on 1D-dimensional examples

Firstly, some methods are compared in the univariate cases of the Sobol' function and univariate implant models (models 1a, 1b, 2a, 2b).

3.2.2.1 Position of regression points when $p = 1$

The aim of this section is to check the relation between errors and positions of sampling points in simple univariate cases. The quantity of interest optimality can be defined as minimisation of errors of the mean, standard deviation, etc., of the quantity of interest. Its correspondence to classic D-optimal choice is checked.

When $M = 1$ and $p = 1$ and the minimum number of points is taken (two points denoted ξ_1, ξ_2) the matrix $\mathbf{A}$ for both Hermite and Legendre PC takes the form (3.2). Such a low order and number of points can be considered insufficient, especially in the case of model response which is nonsmooth and non-linear. However the case with only two regression points enables simple visualization of the change of error with the position of regression points.

Figures 3.13–3.29 show $Err_{\%}$ of the mean and standard deviation in relation to the position of the two regression points denoted ξ_1 and ξ_2. The colour scale shows the value of $Err_{\%}$. The results can be compared with the graph of the determinant (Figure 3.5)

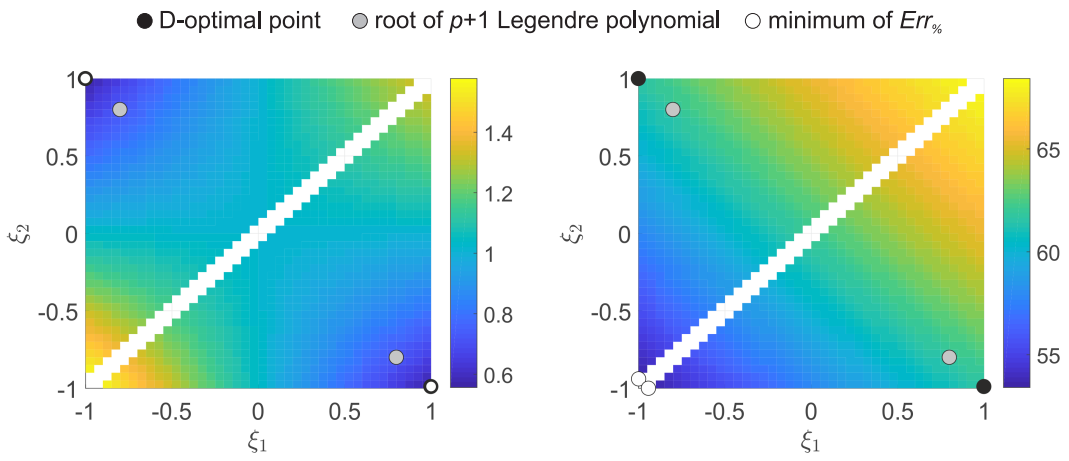

(A) mean (B) standard deviation

FIGURE 3.13: $Err_{\%}$ of H (3.9) in relation to the positions of regression points ξ_1, ξ_2, model 1a

of the information matrix as a function of the position of the points, which refers to the D-optimality criterion. On each figure the minimum of $Err_{\%}$ is marked by a white circle and the D-optimal points by a black circles. In the case of the uniform distribution, the roots of the polynomial of order $p+1$ (gray circle) are also marked. Figures 3.13–3.16 showing examples with uniformly distributed random variables were created with a pitch (distance between points) of 0.05 x 0.05. Examples with the normal distribution (Figures 3.18– 3.29), were performed in a wider range (from -3 to 3) with pitch 0.1 x 0.1.

Figure 3.13a shows the relation between $Err_{\%}$ and the position of regression points for the cable model (3.9) when E is a uniformly distributed random variable (model 1a). It can be seen that the shape obtained is similar to the shape of the determinant of the information matrix (Figure 3.5a). The minimum of $Err_{\%}$ is placed at the maximum of the determinant of the information matrix in the range <-1,1>. In contrast, the shape of the graph obtained for the standard deviation (Figure 3.13b) does not reproduce the shape of the determinant and its minimum is far from the D-optimal points.

When we choose L_0 as a random variable (model 1b), the relation between $Err_{\%}$ of the mean and the position of points (Figure 3.14) is different and is not as close to Figure 3.5a as in the previous example. Furthermore the position of neither the D-optimal points nor the roots of the polynomial of order $p+1$ coincide with the minimum of the mean. Nevertheless, although they are not at the exact minimum of $Err_{\%}$, they can be still considered a good choice from the point of view of the error of the standard deviation, because they are in the area of relatively low error $Err_{\%}$ when compared to the rest of domain. However, it should be noted that in this example $Err_{\%}$ of the mean is very small for for all pairs of ξ_1 and ξ_2.

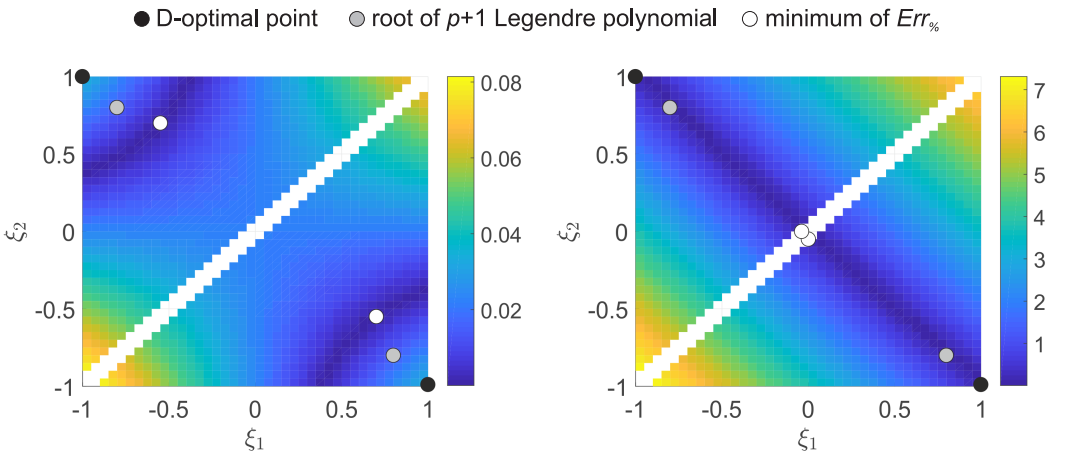

(A) mean (B) standard deviation

FIGURE 3.14: $Err_{\%}$ of H (3.9) in relation to the positions of regression points ξ_1, ξ_2, model 1b

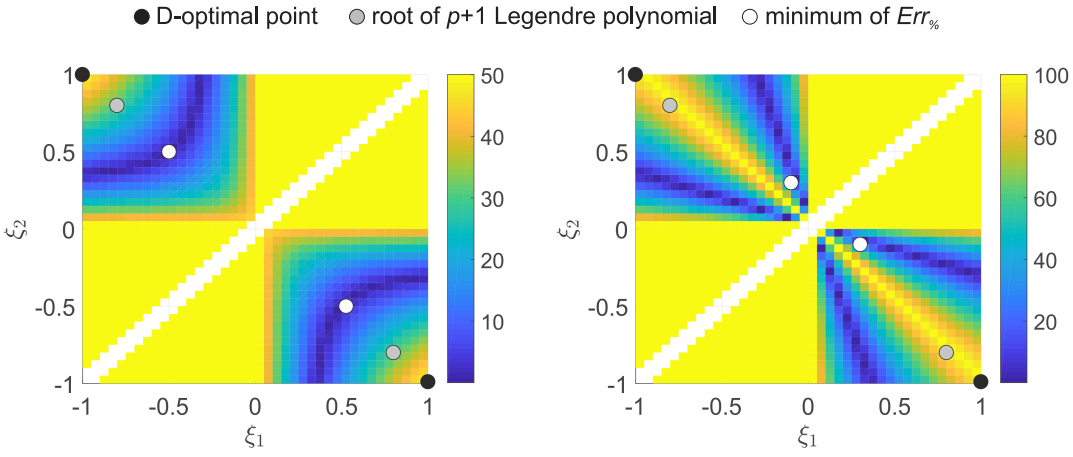

(A) mean (B) standard deviation

FIGURE 3.15: $Err_{\%}$ of mean of Sobol' function value Y (3.8) in relation to positions of regression points ξ_1, ξ_2, model 2a with uniform random variables

Figure 3.15 shows the results for the 1D Sobol' function (3.8), which is nonsmooth in a way similar to R_{max} of the membrane problem. In this case, the use of D-optimal points leads to a very large error. The roots of $p + 1$ order Legendre polynomials are better from the point of view of the mean, but lead to a huge error in the standard deviation.

The example of model 2a is carried out using both normal and uniform distributions. The outcomes obtained for the uniform distribution are presented in Figure 3.16. It can again be seen that in this example neither D-optimal points nor roots of $p + 1$ order are optimal when the objective is to minimise errors of the mean or standard deviation. Furthermore in this example an improper choice of points leads to quite large errors. Figures 3.18a and 3.19a show results where t_1 is a normal random variable. From the

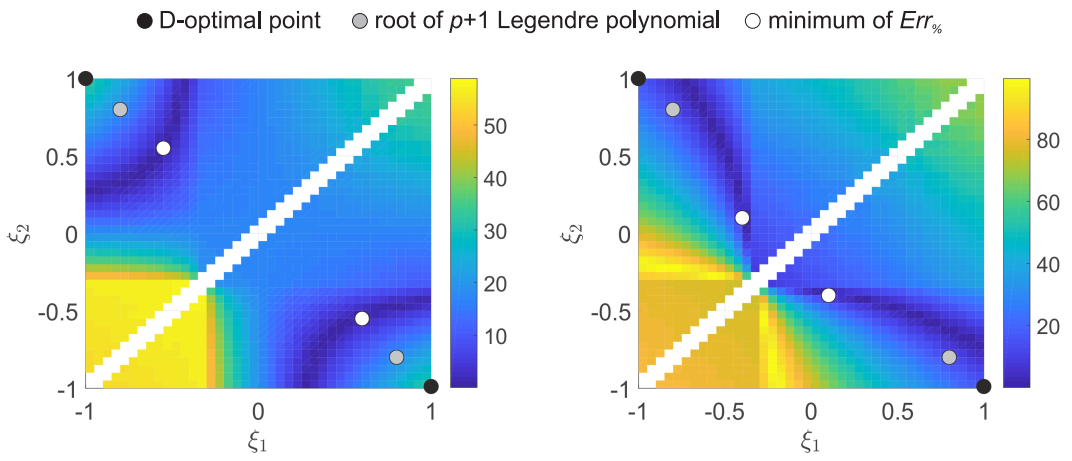

(A) mean (B) standard deviation

FIGURE 3.16: $Err_{\%}$ of standard deviation of R_{max} in relation to the positions of regression points ξ_1, ξ_2, model 2a with uniform random variables

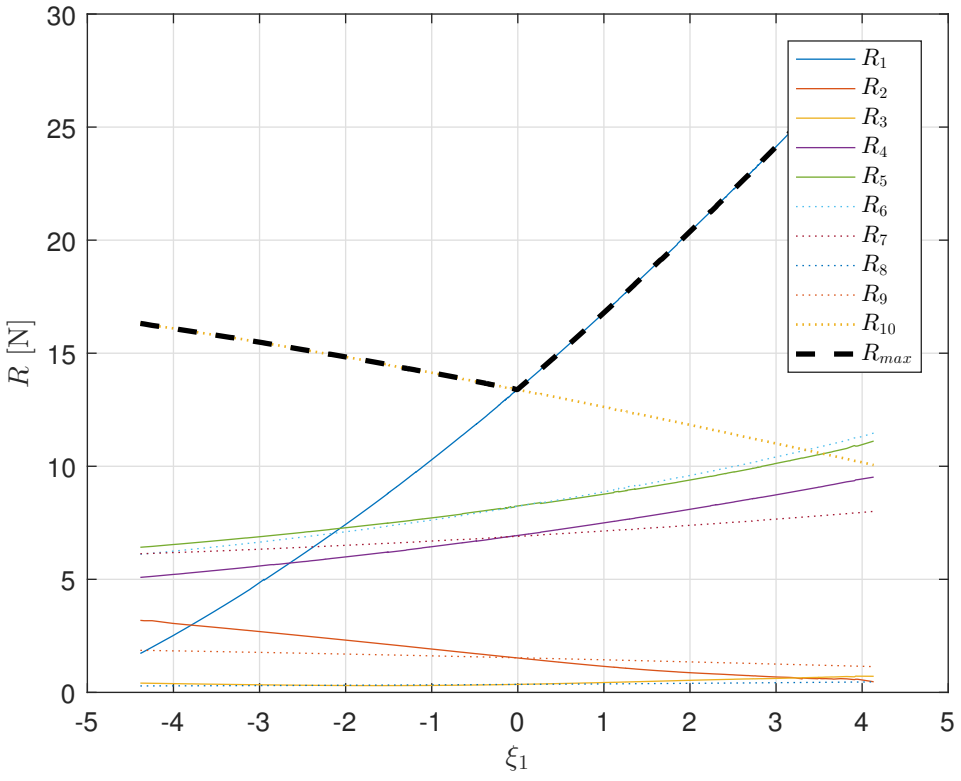

FIGURE 3.17: Reaction forces in the membrane model 2a

point of view of the mean, the position of D-optimal points is closer to the area of low $Err_{\%}$ than in the example with the uniform distribution.

Figure 3.17 shows the change of individual reactions and R_{max} with a change of the standard normal random variable corresponding to t_1. The nonsmoothness of R_{max} can be challenging, so two approaches are considered as described in section 3.2.1.2. Maps

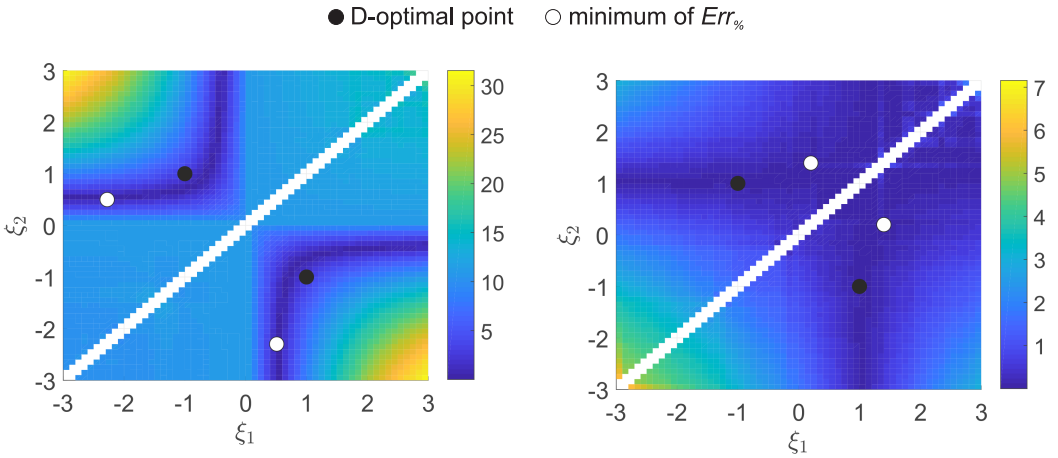

(A) approach 1 (B) approach 2

FIGURE 3.18: $Err_{\%}$ of the mean of R_{max} in relation to the position of the regression points ξ_1, ξ_2, model 2a with normal random variables

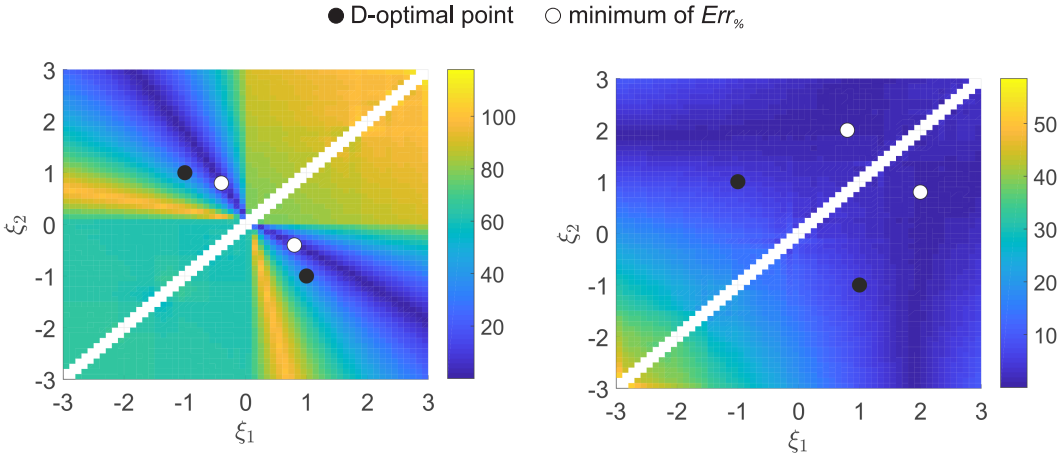

(A) approach 1 (B) approach 2

FIGURE 3.19: $Err_{\%}$ of the standard deviation of R_{max} in relation to the position of the regression points ξ_1, ξ_2, model 2a with normal random variables

of $Err_{\%}$ of the mean (Figure 3.18), standard deviation (Figure 3.19) and 95th percentile (Figure 3.20) of R_{max} when t_1 is the random variable (model 2a) are shown obtained by the two approaches of calculating R_{max} . The minimum values of $Err_{\%}$ and values at D-optimal points are also presented in Table 3.4. It can be seen that in model 2a, when t_1 is a normal random variable, the minima of $Err_{\%}$ as well as the values of $Err_{\%}$ at D-optimal points are lower when the QoI is calculated by the second approach (3.13) than by the first one (3.11). The maxima of $Err_{\%}$ of the mean and standard deviation obtained by the first approach are also higher than those obtained by the second. However, the maximum of $Err_{\%}$ of the 95th percentile is higher in the case of second approach (Figure 3.20).

Cases where the QoI is a single reaction are also presented for the following reactions

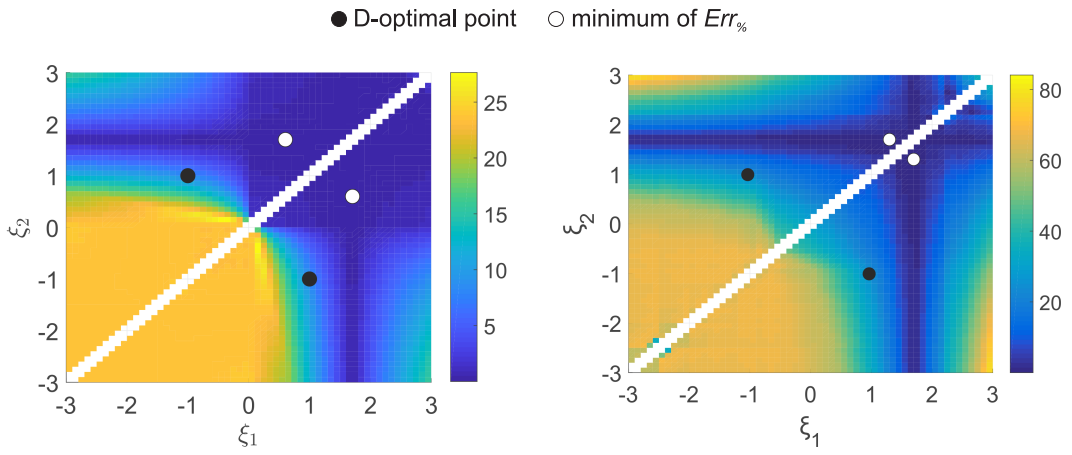

(A) approach 1 (B) approach 2

FIGURE 3.20: $Err_{\%}$ of the 95th percentile of R_{max} in relation to the position of the regression points ξ_1, ξ_2, model 2a

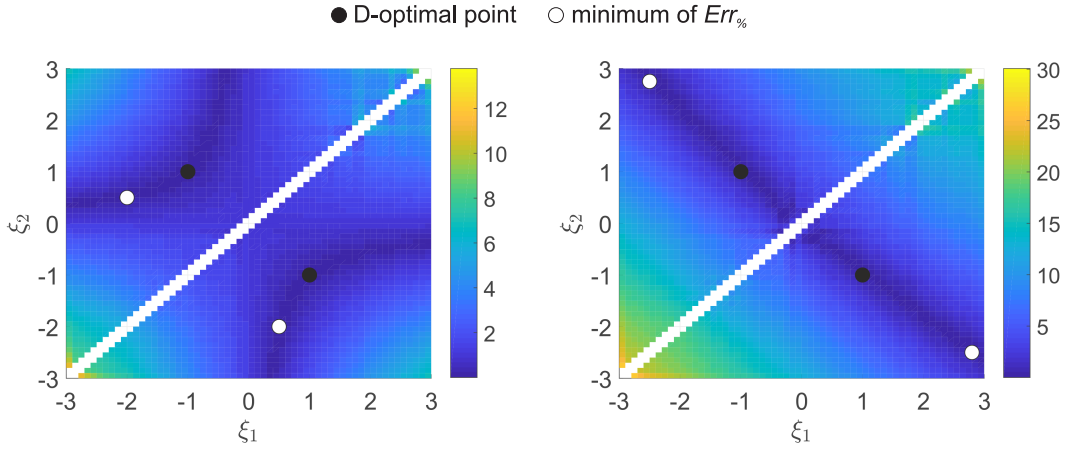

(A) mean (B) standard deviation

FIGURE 3.21: $Err_{\%}$ of the mean and standard relation of the single reaction R_1 in relation to the position of the regression points ξ_1, ξ_2, model 2a

R_1 (Figure 3.21), R_2 (Figure 3.21), R_3 (Figure 3.21) R_4 (Figure 3.21), R_5 (Figure 3.21). For these simpler QoIs, D-optimal points are a better choice in the case of the standard deviation than for R_{max} as QoI. The D-optimal points even coincide with the minimum of $Err_{\%}$ where R_3 (Figure 3.23b) is the QoI and are very similar to the minimum in case of R_5 (Figure 3.25b).

Maps of $Err_{\%}$ of the mean (Figure 3.27), standard deviation (Figure 3.28) and 95th percentile (Figure 3.29) of R_{max}, when t_4 is the random variable (model 2b) are shown for the two approaches of calculating R_{max}. The graph of R_{max} and the random variable t_4 is more strongly nonlinear(Figure 3.26). The obtained $Err_{\%}$ is higher than in the case of model 2a. As in the case of model 2a, application of second approach leads to lower errors, which is also shown in Table 3.4.

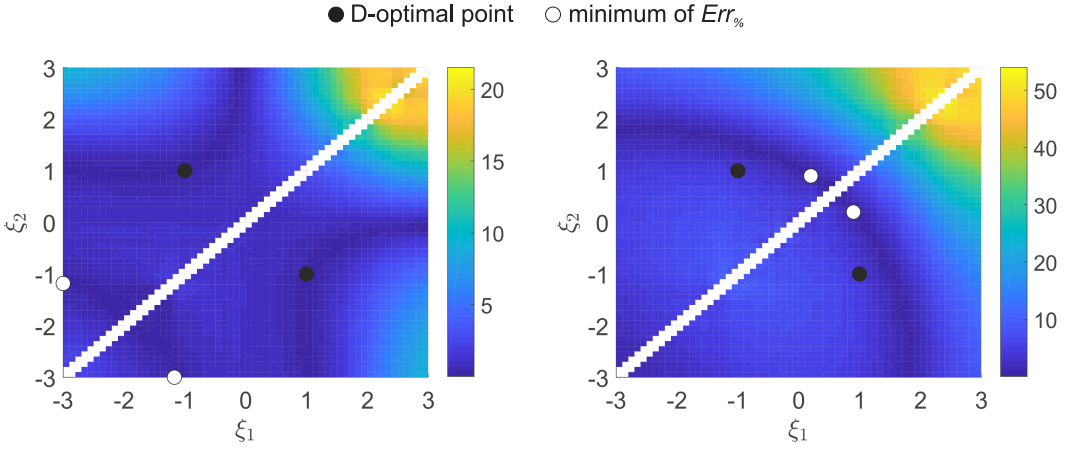

(A) mean (B) standard deviation

FIGURE 3.22: $Err_{\%}$ of the mean and standard relation of the single reaction R_2 in relation to the position of the regression points ξ_1, ξ_2, model 2a

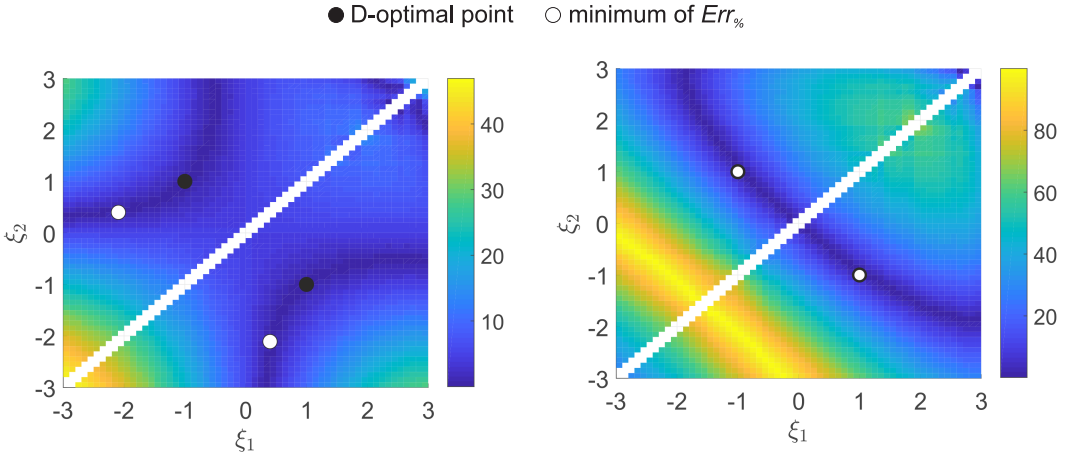

(A) mean (B) standard deviation

FIGURE 3.23: $Err_{\%}$ of the mean and standard deviation of the single reaction R_3 in relation to the position of the regression points ξ_1, ξ_2, model 2a

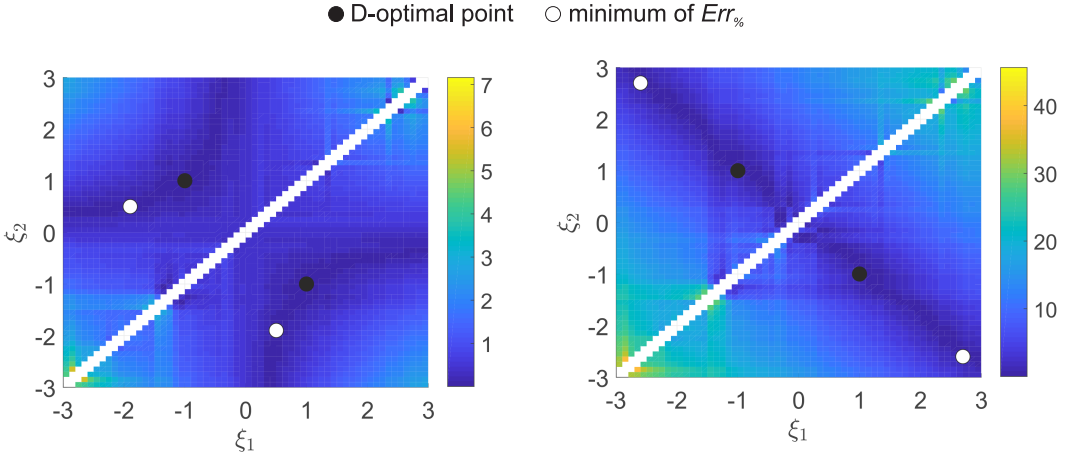

(A) mean (B) standard deviation

FIGURE 3.24: $Err_{\%}$ of the mean and standard relation of the single reaction R_4 in relation to the position of the regression points ξ_1, ξ_2, model 2a

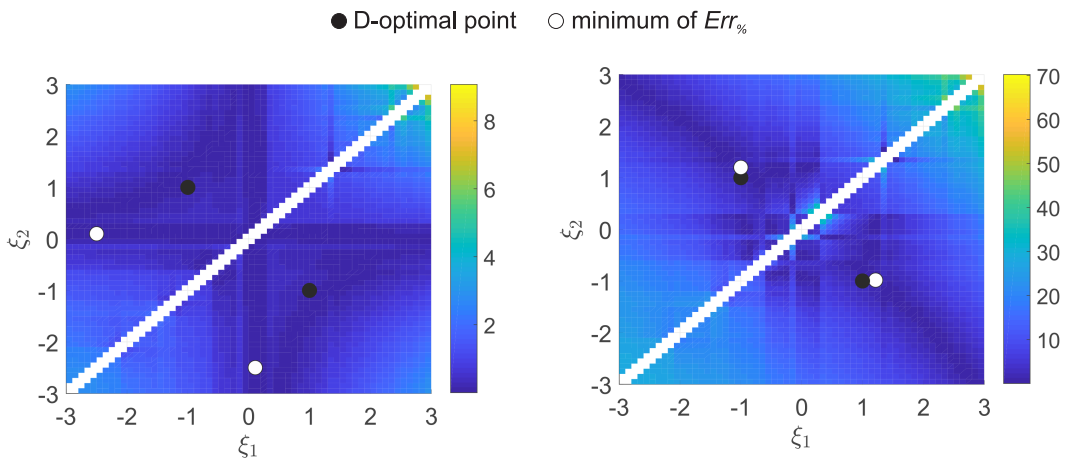

(A) mean (B) standard deviation

FIGURE 3.25: $Err_{\%}$ of the mean and standard relation of the single reaction R_5 in relation to the position of the regression points ξ_1, ξ_2, model 2a

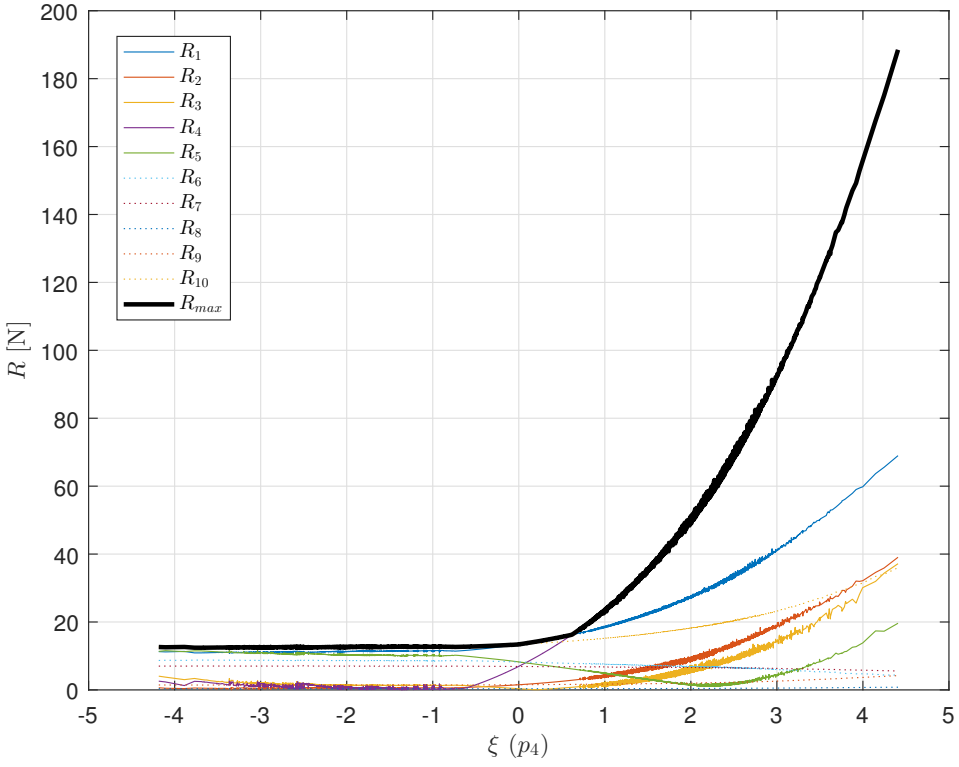

FIGURE 3.26: ξ corresponding to t_4 vs reaction forces in the membrane model 2b

The results showed that first creating separate metamodels for each reaction force leads to smaller errors in the cases considered. The D-optimal points in the majority of cases do not overlap with the minimum of the error. Nevertheless, the choice of these points as the DoE yields a relatively low error in the estimation of the mean values.

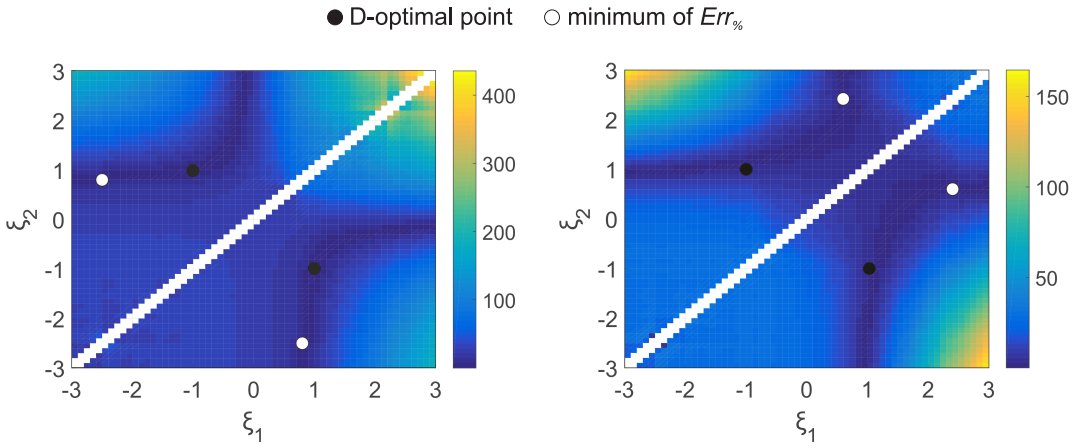

(A) approach 1 (B) approach 2

FIGURE 3.27: $Err_{\%}$ of the mean in relation to the position of the regression points ξ_1, ξ_2, model 2b

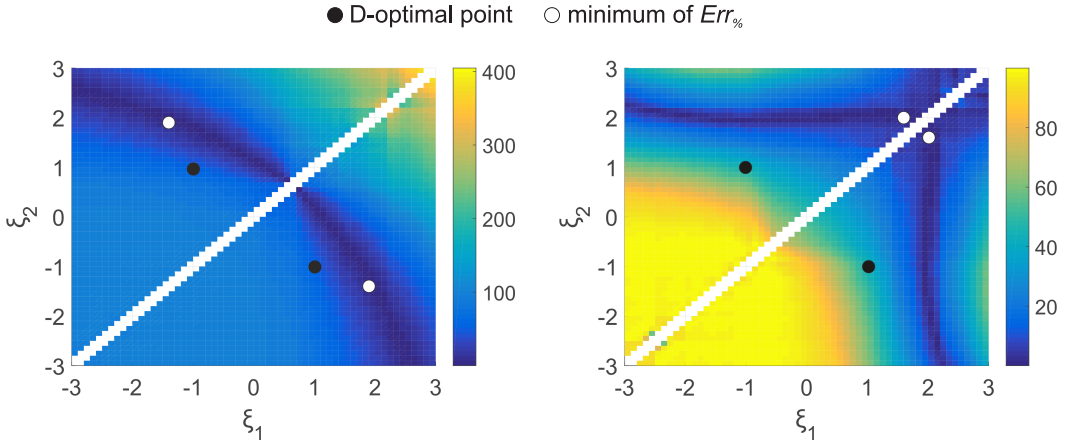

(A) approach 1 (B) approach 2

FIGURE 3.28: $Err_{\%}$ of the standard deviation in relation to the positions of regression points ξ_1, ξ_2, model 2b

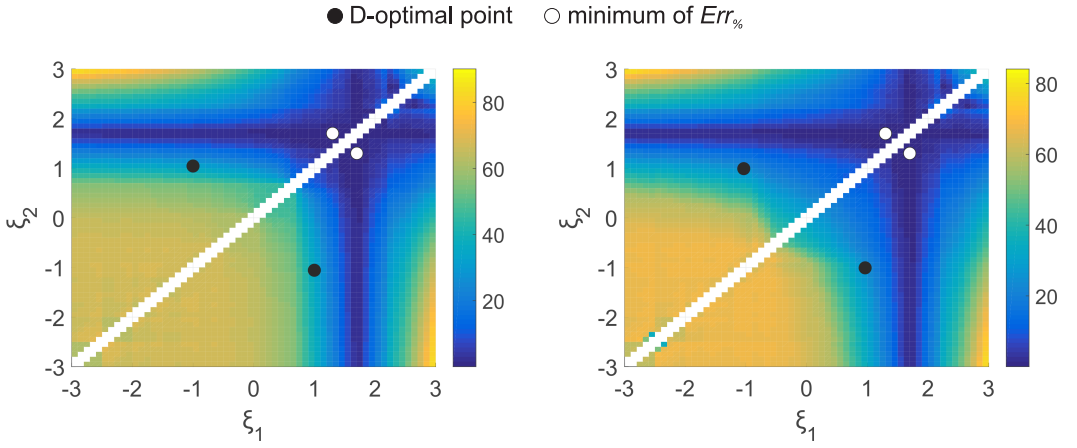

(A) approach 1 (B) approach 2

FIGURE 3.29: $Err_{\%}$ of the 95th percentile in relation to the positions of the regression points ξ_1, ξ_2, model 2b

variable	approach	points	mean	standard deviation	95th percentile
t_1	1	D-optimal	2.681	29.304	7.526
		minimum	0.018	0.026	0.000
	2	D-optimal	0.020	4.839	0.956
		minimum	0.000	0.006	0.000
t_4	1	D-optimal	0.723	48.699	31.555
		minimum	0.058	0.150	0.014
	2	D-optimal	2.620	41.661	22.046
		minimum	0.071	0.000	0.014

TABLE 3.4: $Err_{\%}$ at the D-optimal points and the minimum $Err_{\%}$, model 2 (a and b)

3.2.2.2 Higher order examples - two approaches for calculating R_{max} in the membrane model

The nonsmoothness of R_{max} can be challenging for PC. R_{max} can be directly chosen as the quantity of interest (3.11) or can be defined as the maximum of values calculated using PC metamodels created for each support individually (3.13). These approaches are called respectively approach 1 and approach 2.

Figure 3.30 shows metamodels of R_{max} obtained by PC of different orders p from 0 to 10 by approach 1 in model 2a. Figure 3.31 shows the same but in a narrower range of ξ. Metamodels were created using the roots of polynomial order $p+1$ as regression points. The fit of the metamodel to the exact solution obtained for 10^5 sampling points is poor for low orders of PC and this is also indicated by $RMSE$ value presented in Figure 3.33. $RMSE$ of metamodels with high order polynomials is lower. Nevertheless it can be observed in Figure 3.30 that in the range of standardized variables ξ is far from the zero value of metamodel predictions. Y^{PC} is far from the exact solution Y.

RMSE (Figure 3.33) is lower when the second approach is applied (with the exception of order 0, when both approaches lead to the same metamodel). Metamodels obtained by the second approach are presented in Figure 3.32.

The histogram of R_{max} obtained in model 2a by the MC method is presented in Figure 3.34. It can be compared with the distribution obtained by the PC approximation of different polynomial orders (Figures 3.35–3.44). Calculating R_{max} by the second approach leads to better agreement with the MC solution even when p is low, whereas the distribution obtained by approach 1 is further from the MC solution for low (e.g. Figure 3.35) and very high orders (e.g. Figure 3.44). The mean, standard deviation and

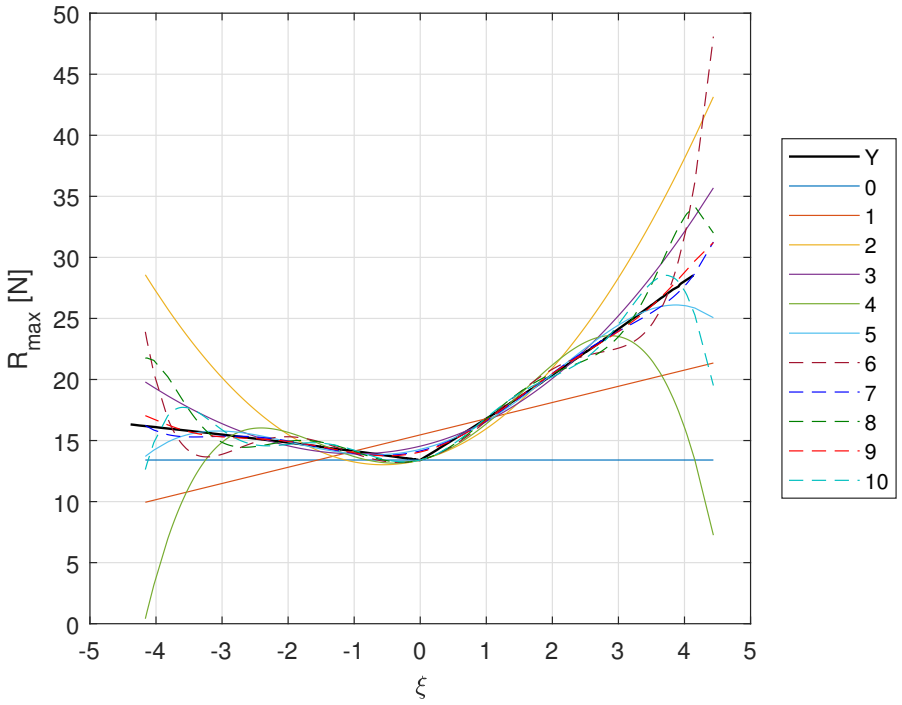

FIGURE 3.30: Metamodels obtained by approach 1 for different polynomials orders (form 0 to 10) compared with model solution Y, Model 2a

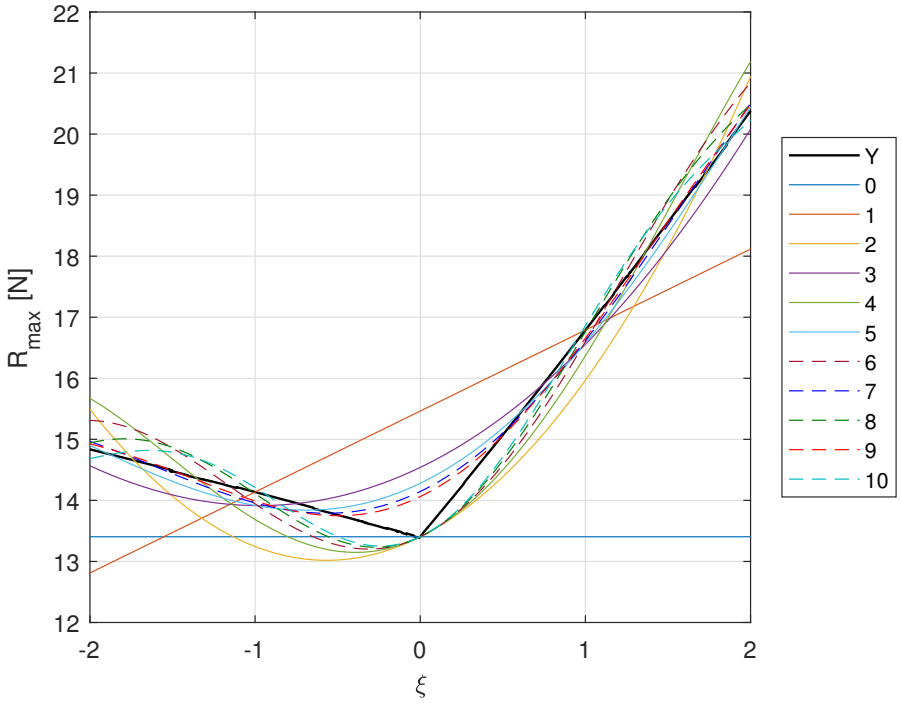

FIGURE 3.31: Data from Figure 3.30 presented for a narrower range of standard random variables ξ

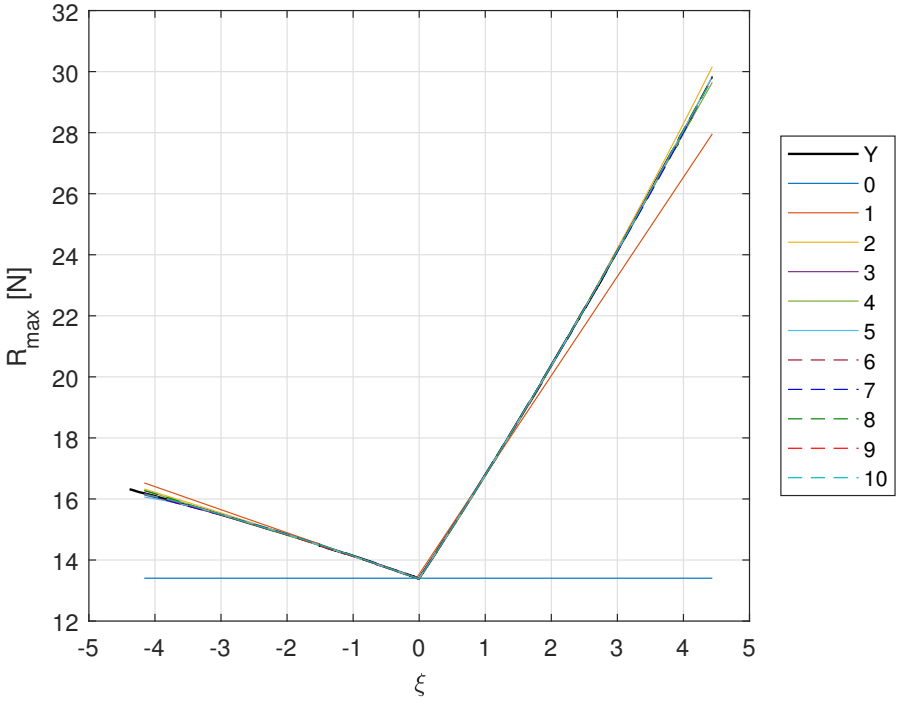

FIGURE 3.32: Metamodels obtained by approach 2 – Model 2a

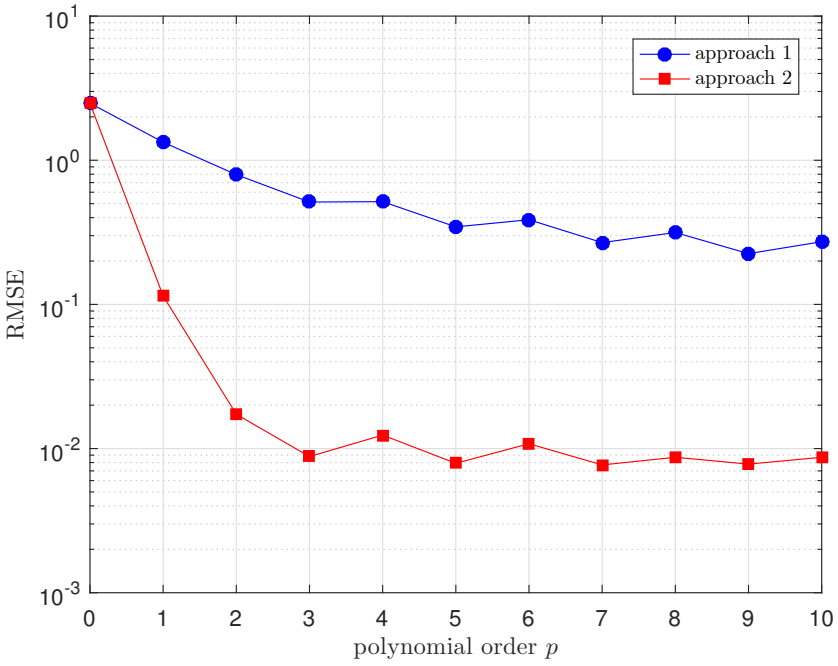

FIGURE 3.33: RMSE between the PC metamodel and the exact solution for different polynomial orders, model 2a

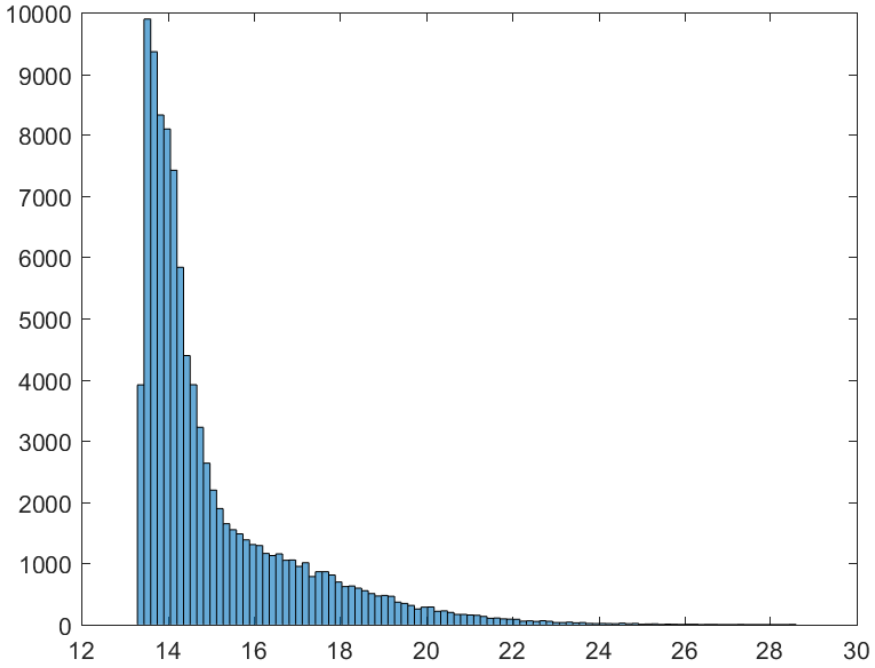

FIGURE 3.34: Histogram of R_{max} obtained by the MC method, model 2a

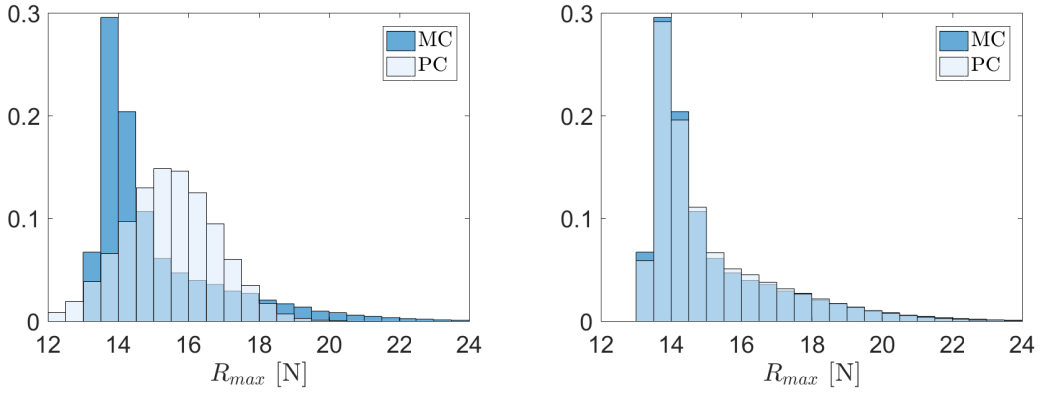

(A) approach 1 (B) approach 2

FIGURE 3.35: Normalized histograms of R_{max} obtained for PC order $p = 1$ compared with the MC solution, model 2a

95th percentile approximated by PC in the two approaches are compared in Figure 3.45. Convergence with increase of PC order can be observed.

A similar comparison of approaches is carried out for model 2b. Figure 3.46 and Figure 3.47 show metamodels obtained by PC of different orders by approach 1 and 2, respectively. A comparison of $RMSE$ is presented in Figure 3.48. In this case, the difference between approaches is smaller. Nevertheless, the accuracy of the metamodel obtained by the second approach is higher in this case as well. It is also visible in the histograms of Figures 3.49 –3.58 in which the MC solution is compared with the PC result in model

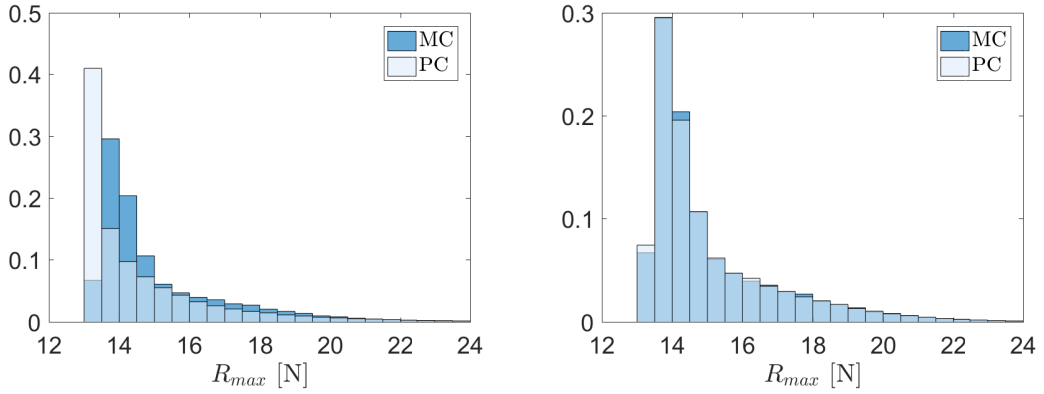

(A) approach 1 (B) approach 2

FIGURE 3.36: Normalized histograms of R_{max} obtained for PC order $p = 2$ compared with the MC solution, model 2a

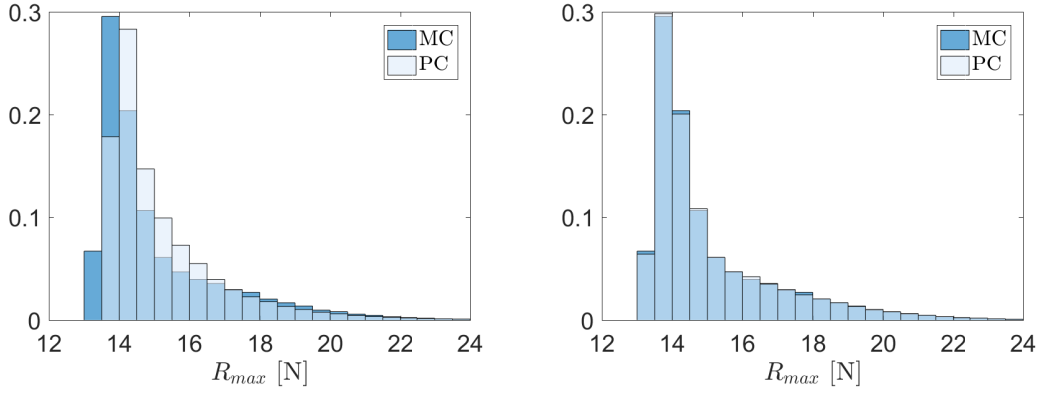

(A) approach 1 (B) approach 2

FIGURE 3.37: Normalized histograms of R_{max} obtained for PC order $p = 3$ compared with the MC solution, model 2a

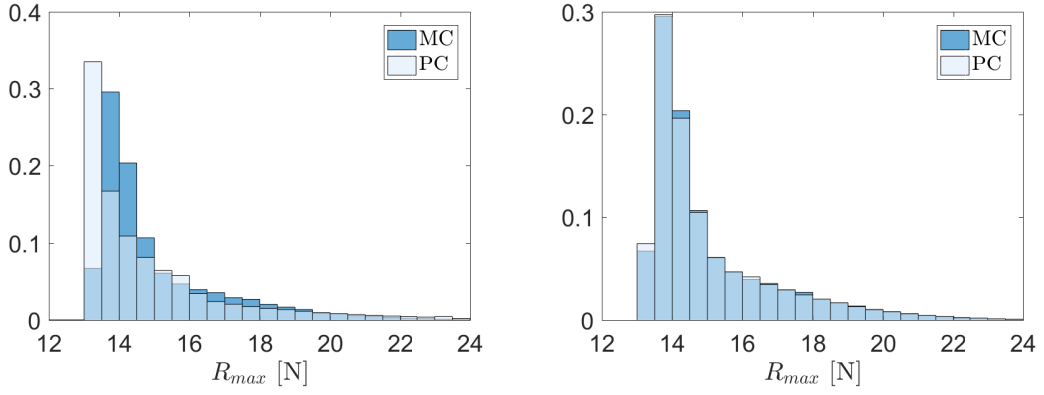

(A) approach 1 (B) approach 2

FIGURE 3.38: Normalized histograms of R_{max} obtained for PC order $p = 4$ compared with the MC solution, model 2a

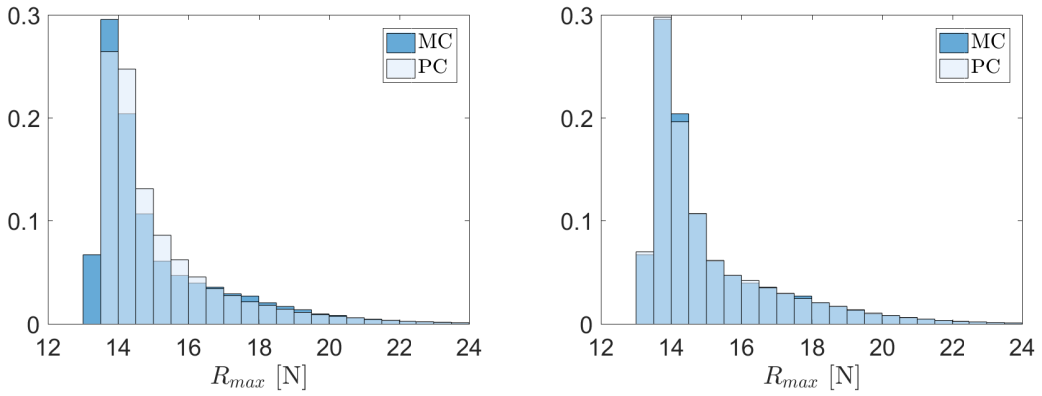

(A) approach 1 (B) approach 2

FIGURE 3.39: Normalized histograms of R_{max} obtained for PC order $p = 5$ compared with the MC solution, model 2a

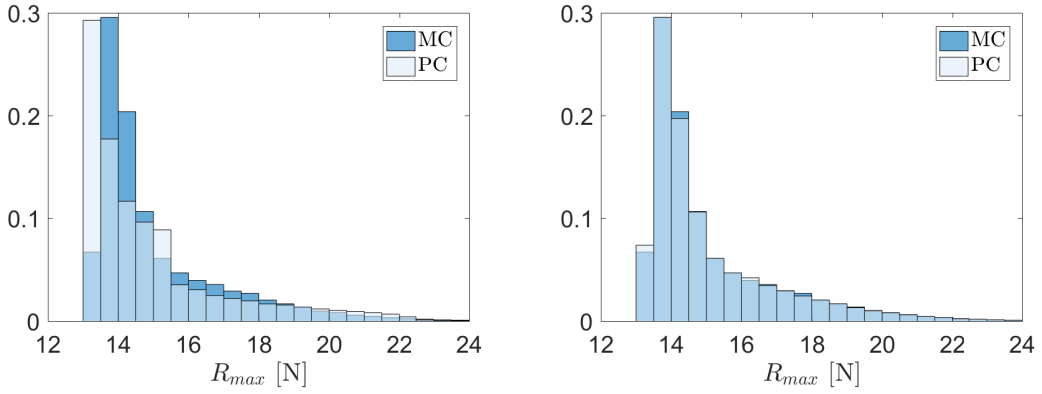

(A) approach 1 (B) approach 2

FIGURE 3.40: Normalized histograms of R_{max} obtained for PC order $p = 6$ compared with the MC solution, model 2a

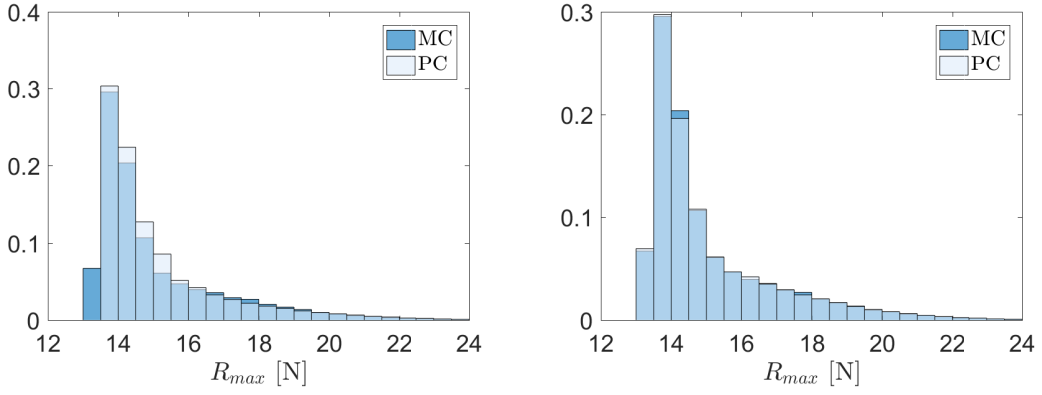

(A) approach 1 (B) approach 2

FIGURE 3.41: Normalized histograms of R_{max} obtained for PC order $p = 7$ compared with the MC solution, model 2a

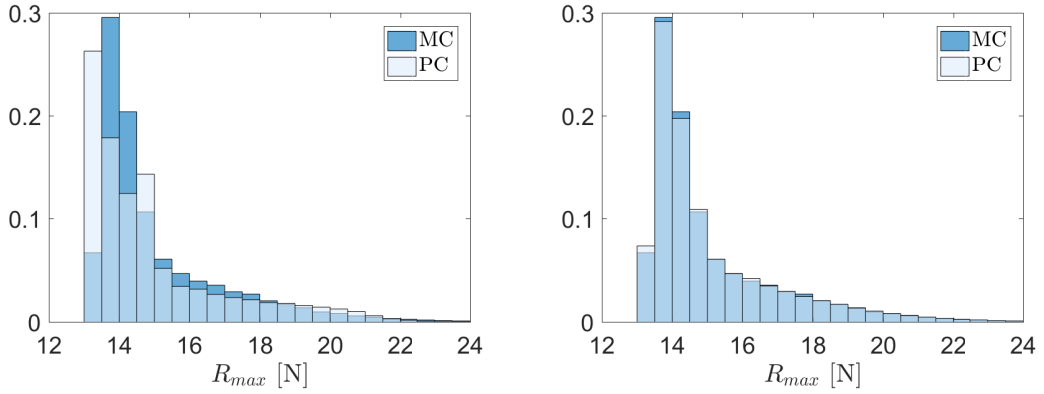

(A) approach 1 (B) approach 2

FIGURE 3.42: Normalized histograms of R_{max} obtained for PC order $p = 8$ compared with the MC solution, model 2a

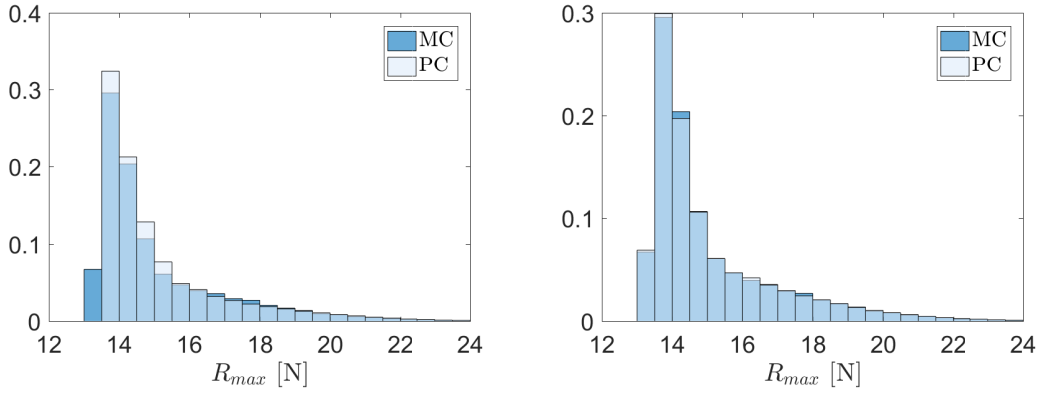

(A) approach 1 (B) approach 2

FIGURE 3.43: Normalized histograms of R_{max} obtained for PC order $p = 9$ compared with the MC solution, model 2a

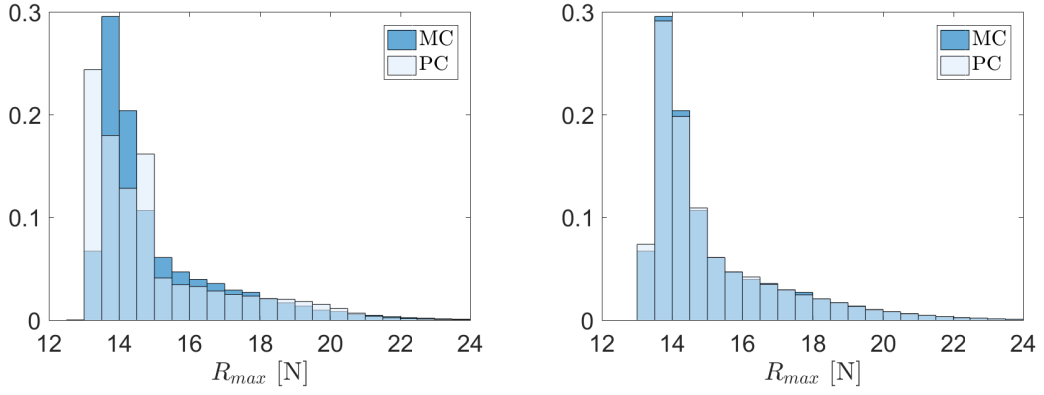

(A) approach 1 (B) approach 2

FIGURE 3.44: Normalized histograms of R_{max} obtained for PC order $p = 10$ compared with the MC solution, model 2a

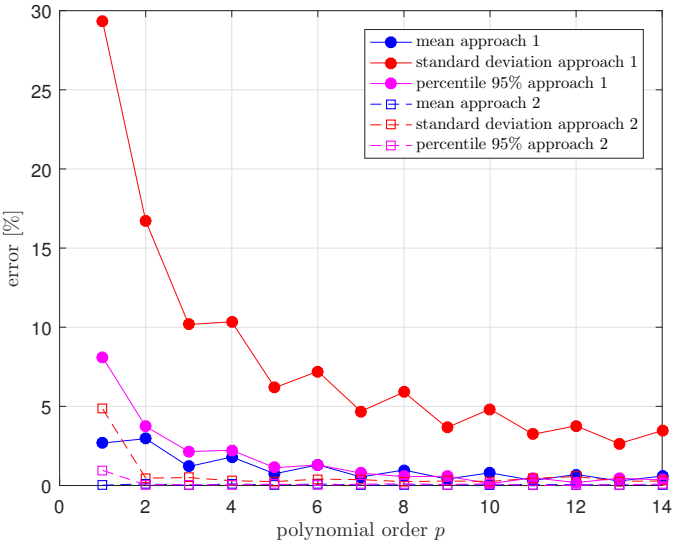

FIGURE 3.45: $Err_{\%}$ with change of polynomial order for approach 1 and 2, model 2a

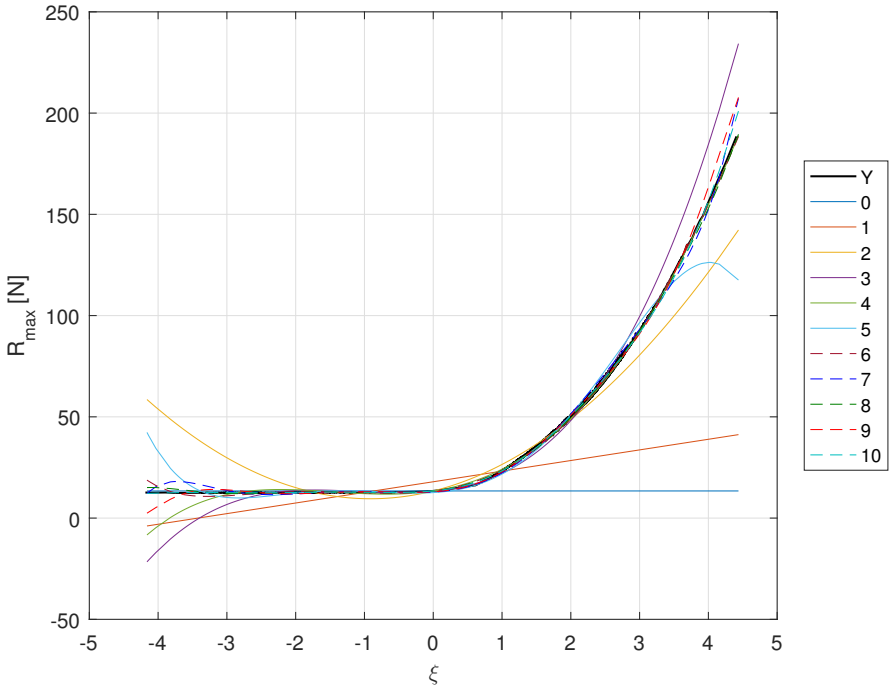

FIGURE 3.46: Metamodels obtained by approach 1—Model 2b

2b. Figure 3.59 shows the mean, standard deviation and 95th percentile obtained by the two approaches. $Err_{\%}$ is high when 1st order PC is applied for both approaches, but improved significantly when the order is higher.

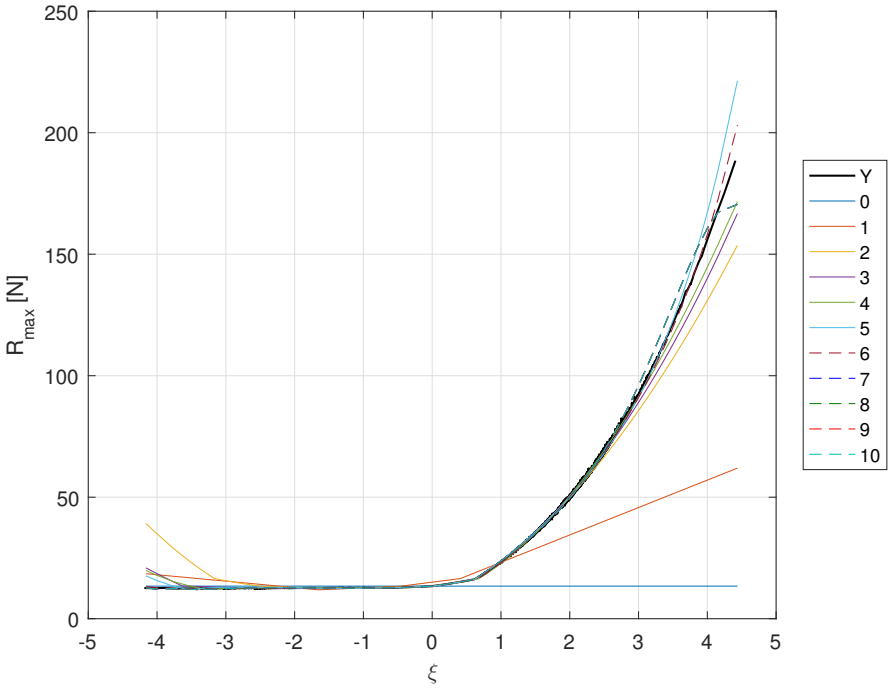

FIGURE 3.47: Metamodels obtained by approach 2—Model 2b

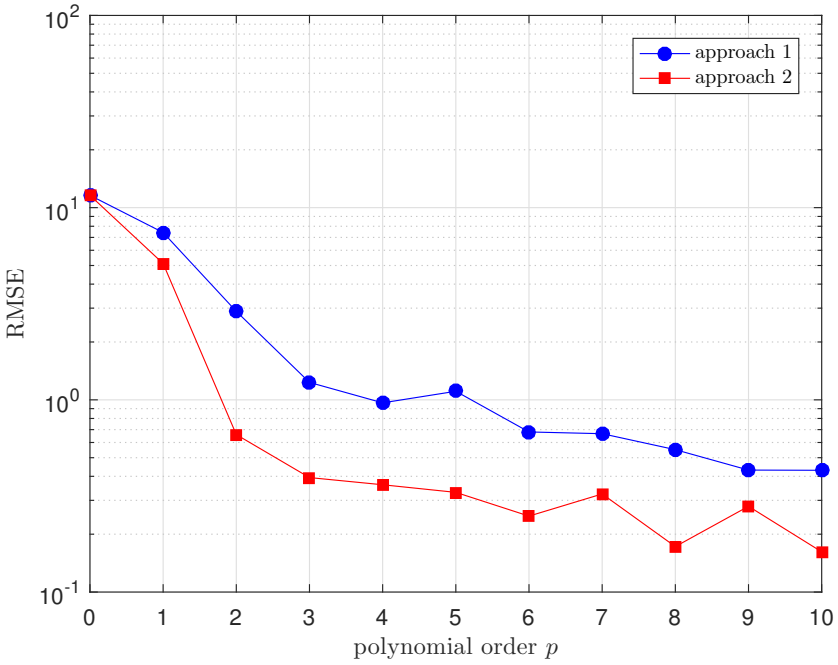

FIGURE 3.48: RMSE between PC metamodel and the exact solution for different polynomial orders, model 2b

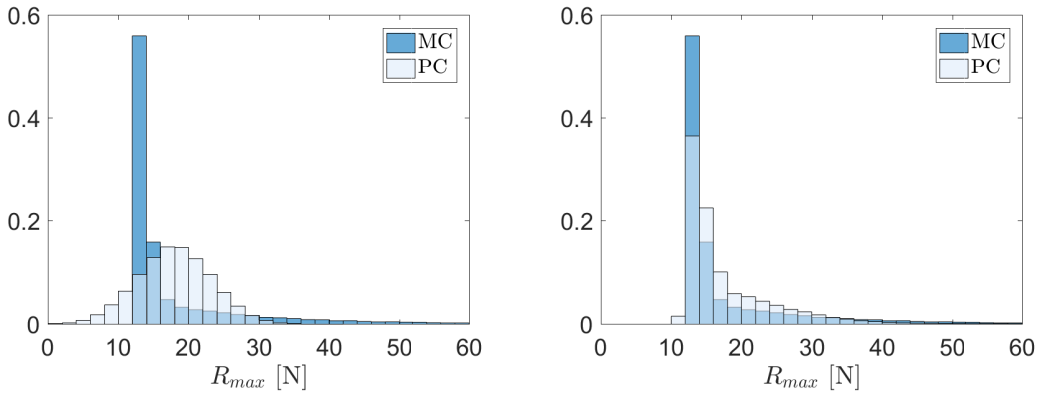

(A) approach 1 (B) approach 2

FIGURE 3.49: Normalized histograms of R_{max} obtained for PC order $p = 1$ compared with the MC solution, model 2b

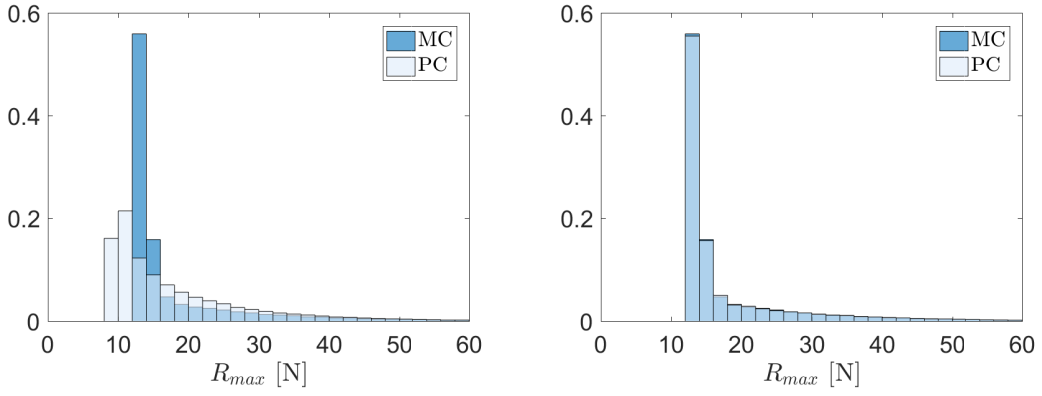

(A) approach 1 (B) approach 2

FIGURE 3.50: Normalized histograms of R_{max} obtained for PC order $p = 2$ compared with the MC solution, model 2b

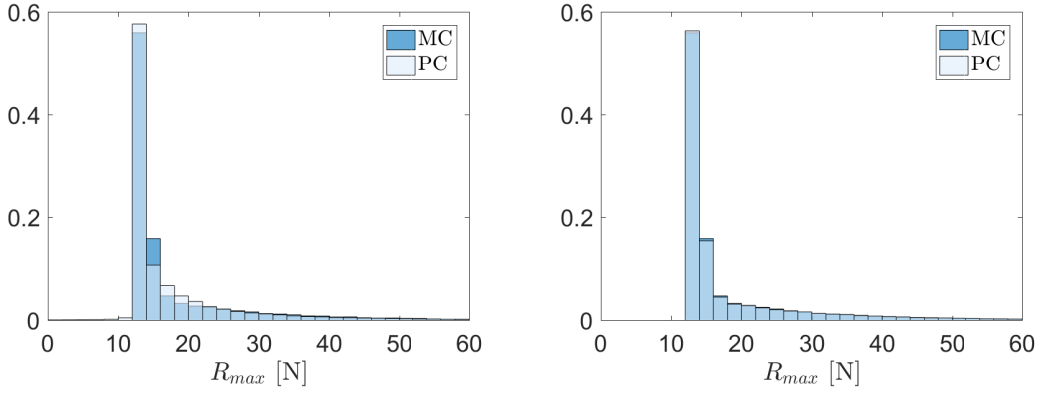

(A) approach 1 (B) approach 2

FIGURE 3.51: Normalized histograms of R_{max} obtained for PC order $p = 3$ compared with the MC solution, model 2b

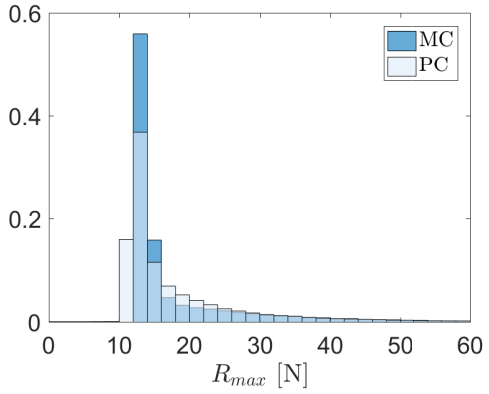

(A) approach 1

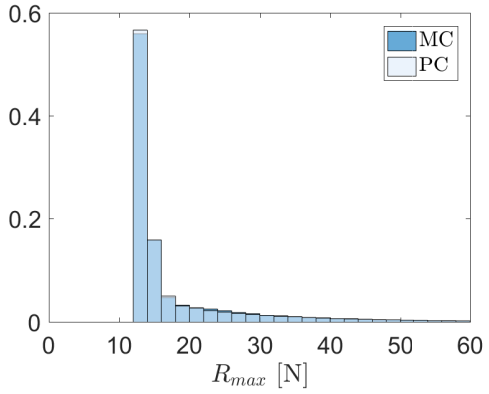

(B) approach 2

FIGURE 3.52: Normalized histograms of R_{max} obtained for PC order $p = 4$ compared with the MC solution, model 2b

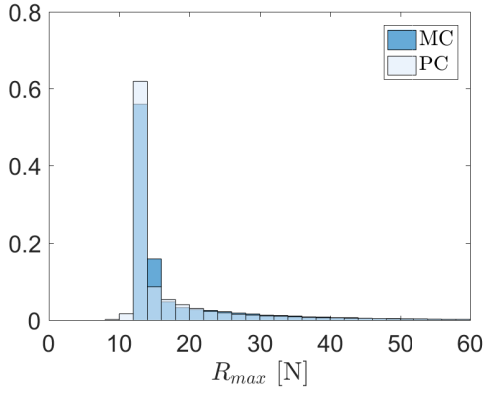

(A) approach 1

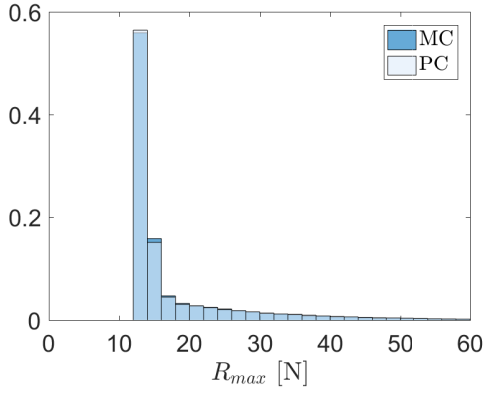

(B) approach 2

FIGURE 3.53: Normalized histograms of R_{max} obtained for PC order $p = 5$ compared with the MC solution, model 2b

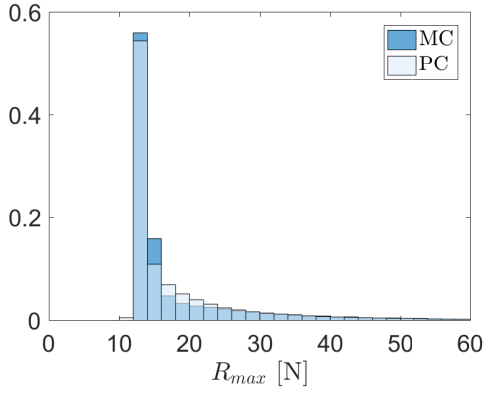

(A) approach 1

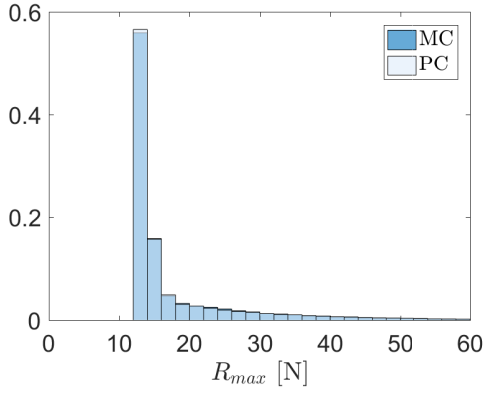

(B) approach 2

FIGURE 3.54: Normalized histograms of R_{max} obtained for PC order $p = 6$ compared with the MC solution, model 2b

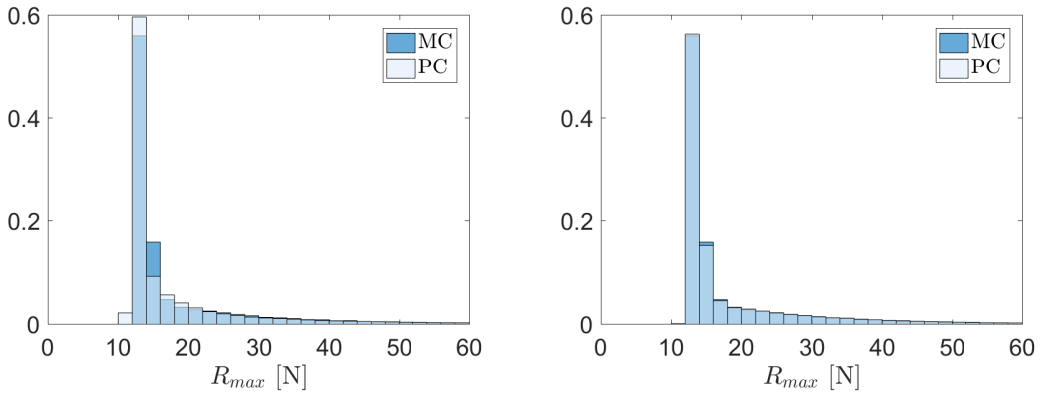

(A) approach 1 (B) approach 2

FIGURE 3.55: Normalized histograms of R_{max} obtained for PC order $p = 7$ compared with the MC solution, model 2b

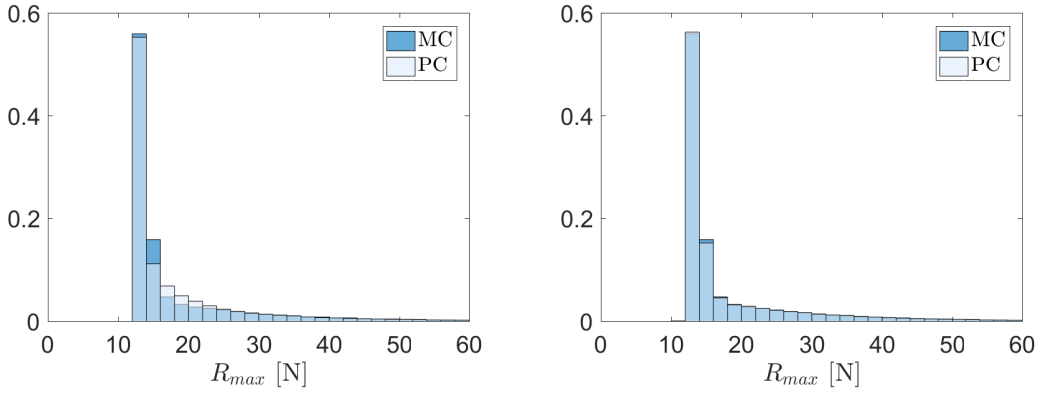

(A) approach 1 (B) approach 2

FIGURE 3.56: Normalized histograms of R_{max} obtained for PC order $p = 8$ compared with the MC solution, model 2b

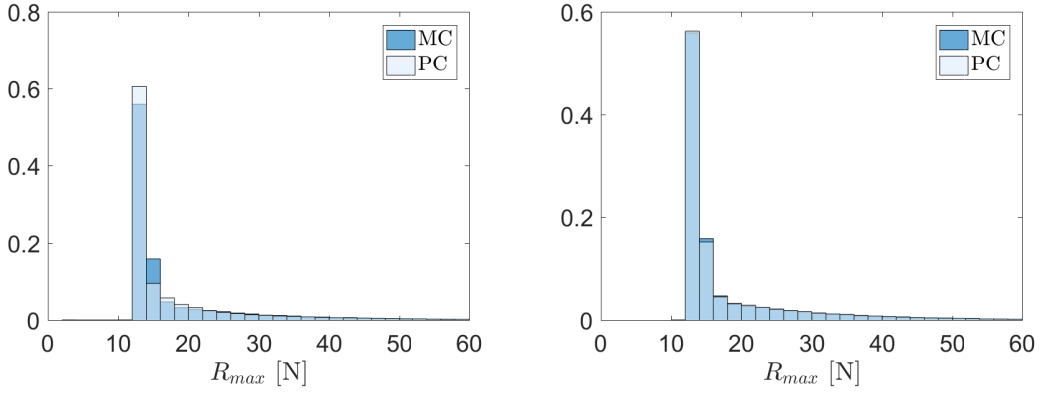

(A) approach 1 (B) approach 2

FIGURE 3.57: Normalized histograms of R_{max} obtained for PC order $p = 9$ compared with the MC solution, model 2b

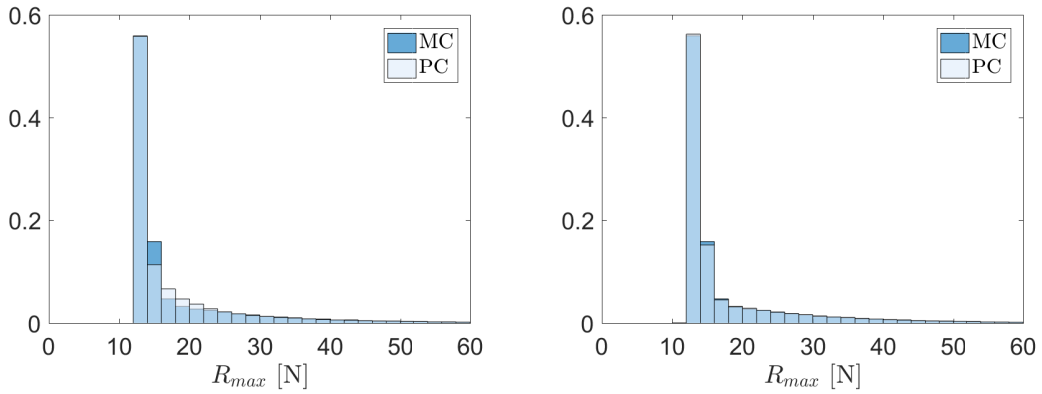

(A) approach 1 (B) approach 2

FIGURE 3.58: Normalized histograms of R_{max} obtained for PC order $p = 10$ compared with the MC solution, model 2b

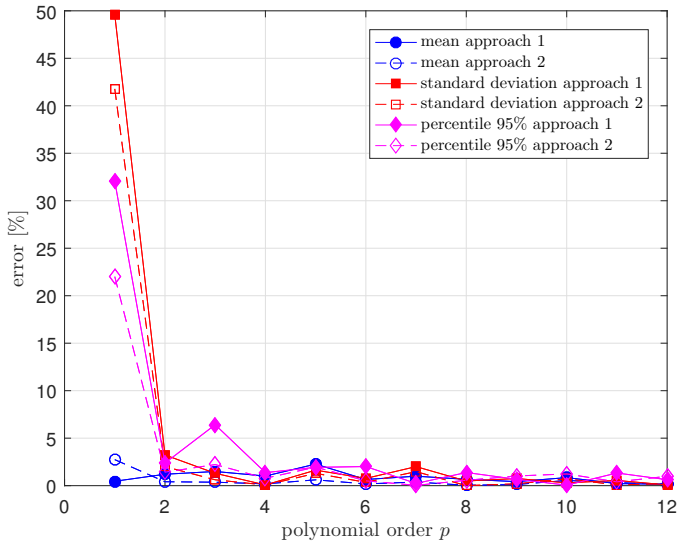

FIGURE 3.59: $Err_{\%}$ with a change of polynomial order for approach 1 and approach 2, model 2b

3.2.3 Results of comparison on multivariate examples

In the multivariate case it is possible also to compare sensitivity index values.

3.2.3.1 Sobol' function

Firstly, the Sobol' function is used with 4 random uniformly distributed variables. Additionally to the methods listed previously, the choice of combination of optimal points for 1D – Legendre polynomials is compared with the classic choice of roots of Legendre polynomials order $p + 1$. All methods are tested with the same number of regression points as used in [159], where the M1 method was applied on the present example of

the Sobol' function. The number of points was determined there by the necessity of obtaining a full rank information matrix. Despite the fact that the use of other methods is also possible for a smaller number of points, the same number is used here to exclude its influence on the results. Where a method included random drawing (M3, M4 and M5) it was performed repeatedly in order to arrive at a statistically valid average value.

The variables can be ranked by their importance, which is determined by S_i^{Tot} value. All methods give the same result as in the analytical solution variable ranking according to S_i^{Tot}. In addition, none of the methods lead to a large relative error $Err_{\%}$ for the most significant variables ($S_i^{Tot} \geq 0.1$, in this case S_1^{Tot} and S_2^{Tot}). Figure 3.60 shows the value of the sensitivity indices for each variable for different orders. In the case of methods M3, M4 and M5, the mean results from the repeated process of drawing are shown. The sequence of methods in respect of their closeness to the analytical solutions changes with the order of PC and depends on the variable. For example, method M1 is the worst for even orders. However, its modification by means of the use of D-optimal points for Legendre polynomial instead of roots of polynomial order $p+1$ results in a smaller distance to the analytical solution. Err_s is presented in Figure 3.61. It can be observed that choosing the D-optimal points of the Legendre polynomial is superior to choosing the roots of $p+1$ polynomial for method M1 but inferior for method M2. The standard deviation of the results obtained by methods including random draw (M3-M5) decreases with order and is quite low for each model (Table 3.5).

3.2.3.2 Cable model

Figure 3.62 show Err_s for all methods in the cable model with 4 random variables (model 1c). It should be noted, that the reference Sobol' sensitivity indices are approximated by MC. In this case taking combinations of roots of Legendre polynomial order $p+1$ gives better results than a combination of D-optimal points of univariate Legendre polynomials in the case of methods M1, M2 and M2.

3.2.3.3 Model of membrane subjected to forced displacement with 3 random variables (model 2c)

Figure 3.63 shows scatter plots obtained for MC (only every tenth value is shown for better clarity of the diagram). The low significance of $t_3(\xi_3)$ can be observed, whereas $t_1(\xi_1)$ appears to be important. The significance of $t_2(\xi_2)$ changes. These conclusions were confirmed by calculation of Sobol' indices by the MC method: $S_1^{Tot} = 0.9173$, $S_2^{Tot} = 0.1326$, $S_3^{Tot} = 9.05E-04$. S_3^{Tot} is omitted in the analysis of $Err_{\%}$ due to its small value.

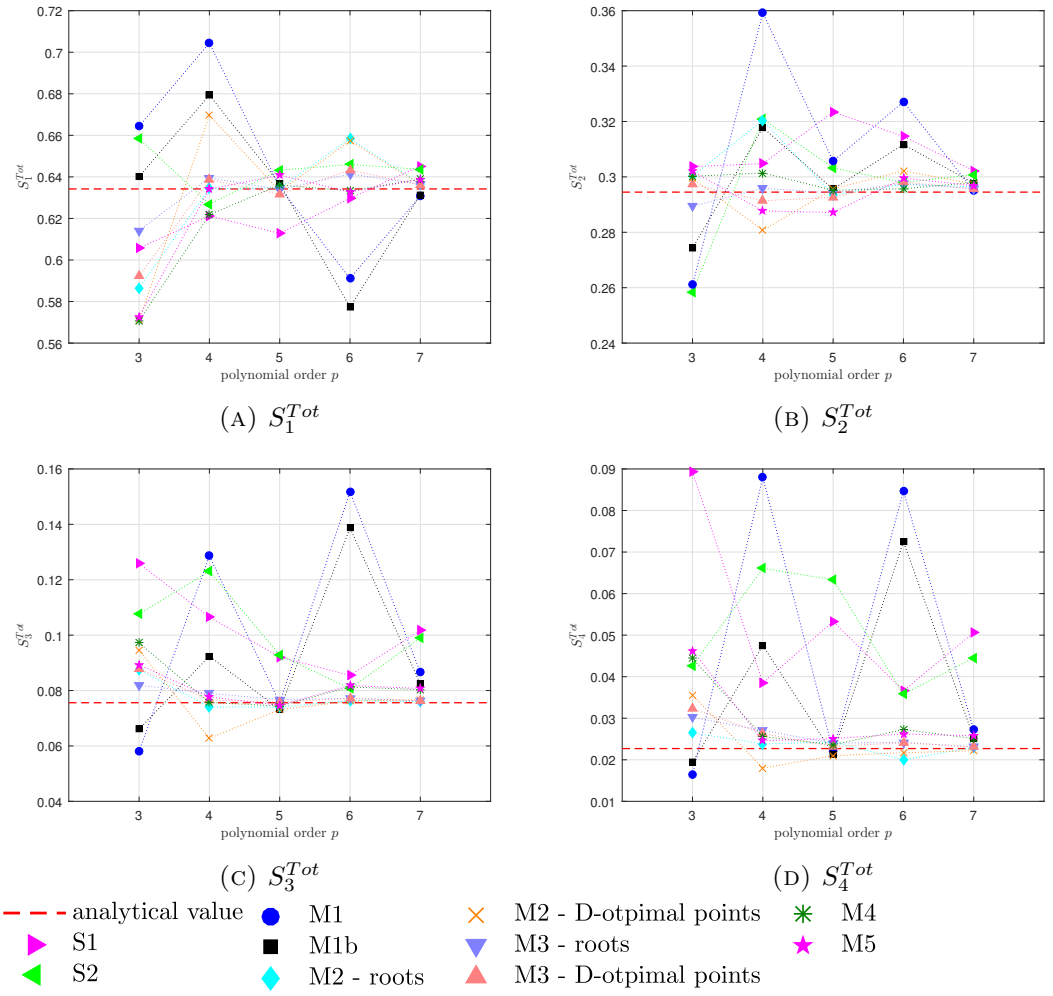

(A) S_1^{Tot} (B) S_2^{Tot}

(C) S_3^{Tot} (D) S_4^{Tot}

FIGURE 3.60: Values of total sensitivity indices of Sobol' function obtained for different methods and PC order

Method M1, which can be considered as the classic method, has been tested for different orders and approaches to calculating R_{max}. Figure 3.64 presents $Err_{\%}$ of the mean, standard deviation and 95th percentile of R_{max} obtained by approach 1 (3.11) and approach 2 (3.13). The difference between these two approaches is not as important as in the 1-dimensional case, shown in the previous section. For some orders approach 1 yields even better results. Figure 3.65 shows the relation between Err_s and order p for the two approaches. In the 3-dimensional case it is not clear which approach is better. In further simulations of other examples, only approach 1 is employed.

The infuence of the number of regression points is presented in Figures 3.66 and 3.67, which contain the results obtained by method S2 for different orders and number of points $c \cdot P$ proportional to the size of PC basis P.

However in this case increasing the order can lead to an increase in error. The order which minimizes the error is different for different quantities (mean, standard deviation,

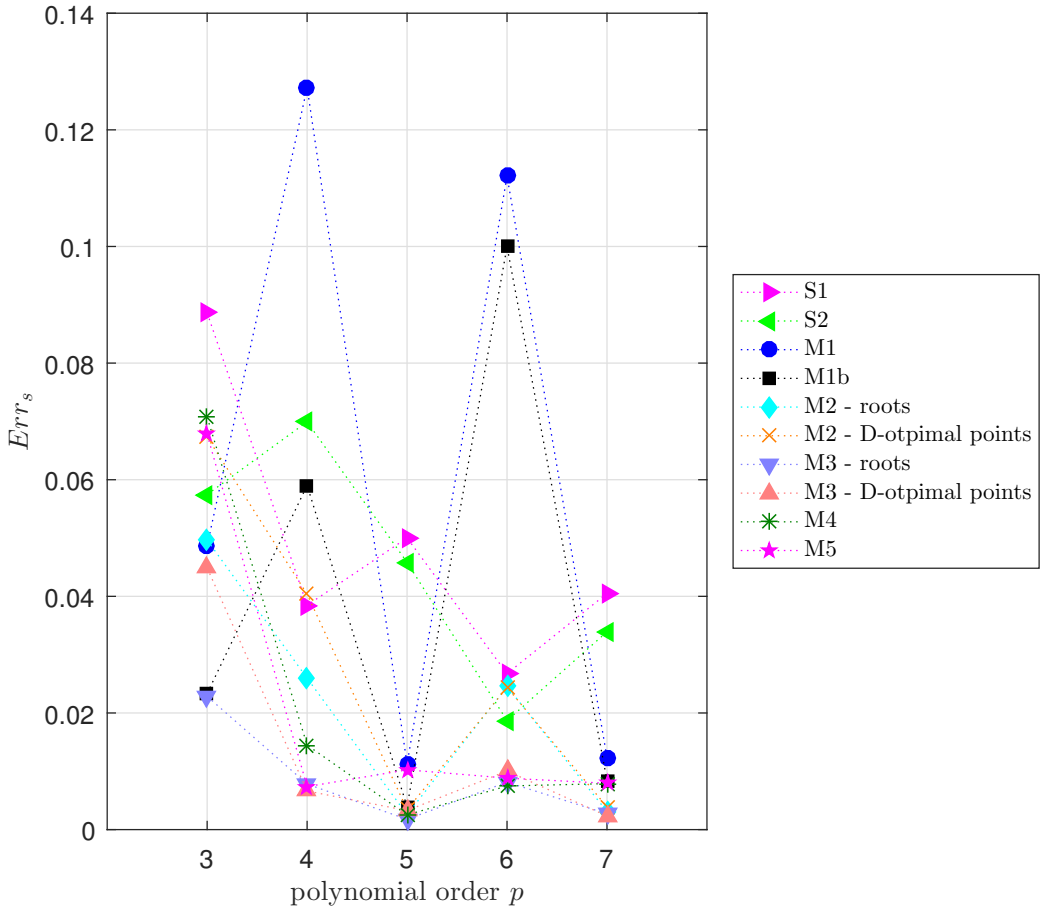

FIGURE 3.61: Err_s obtained for different methods, Sobol' function

95th percentile). It can also be seen, that above a certain threshold, further increases in the number of points do not significantly improve the accuracy of approximation of these statistics. This is inline with observations, which have already been made in the literature [11]. However, when Err_s is considered, such an observation can be made only for low orders. In case of high orders the situation is less stable.

The methods M2, M4 and M5 are considered in two variants:

(a) not including a weight function,

(b) including a weight function $w = \frac{1}{\sqrt{2\pi}} e^{-\xi^{\mathbf{2}}/\mathbf{2}}$.

Methods M2a and M2b, M4a and M4b, M5a and M5b were applied on the same initial candidate sets of points. Table 3.6 shows a comparison of results obtained by 3rd order PC, where in the case of methods involving random sampling, mean values are presented. In the majority of cases, the variant including weight leads to higher accuracy. Only in

analytical value		S_1^{Tot} 0.6342		S_2^{Tot} 0.2945		S_3^{Tot} 0.0756		S_4^{Tot} 0.0227	
method	order	mean	st. dev.	mean	st. dev.	mean	st. dev.	mean	st. dev.
M3a	3	0.6142	0.025	0.2894	0.0212	0.0819	0.012	0.0302	0.008
	4	0.6395	0.0142	0.2959	0.0126	0.079	0.0073	0.0271	0.0044
	5	0.6339	0.0052	0.2942	0.0047	0.0767	0.0026	0.024	0.0014
	6	0.6414	0.0044	0.2976	0.0038	0.0772	0.0022	0.0242	0.0013
	7	0.6365	0.0015	0.2957	0.0014	0.0763	0.0008	0.0231	0.0004
M3b	3	0.5922	0.0249	0.2973	0.0209	0.0878	0.0113	0.0323	0.0079
	4	0.6387	0.0206	0.2914	0.018	0.0766	0.0105	0.0263	0.0058
	5	0.6316	0.0062	0.2926	0.0054	0.0758	0.0028	0.0232	0.0016
	6	0.6433	0.0068	0.2982	0.006	0.0772	0.0031	0.0241	0.0017
	7	0.6361	0.0018	0.2956	0.0017	0.0763	0.0008	0.0231	0.0005
M4	3	0.5707	0.0258	0.3002	0.0248	0.0972	0.0157	0.0444	0.0155
	4	0.6218	0.0176	0.3014	0.0147	0.0757	0.0136	0.0256	0.004
	5	0.6361	0.0102	0.2952	0.0079	0.0744	0.0058	0.0236	0.004
	6	0.6333	0.0068	0.2957	0.0053	0.0813	0.0039	0.0273	0.0031
	7	0.6389	0.0048	0.298	0.0059	0.0803	0.003	0.0251	0.0015
M5	3	0.5726	0.0255	0.3020	0.0238	0.0893	0.0198	0.0463	0.0158
	4	0.6341	0.0280	0.2877	0.0269	0.0777	0.0119	0.0246	0.0041
	5	0.6408	0.0181	0.2871	0.0188	0.0747	0.0043	0.0251	0.0038
	6	0.6327	0.0148	0.2995	0.0127	0.0818	0.0044	0.0262	0.0023
	7	0.6388	0.0045	0.2968	0.0043	0.0807	0.0032	0.0258	0.0020

TABLE 3.5: Mean and standard deviation of results obtained by methods including random sampling, Sobol' function

the case of method M2 is the error of the 95th percentile smaller in the variant without weight. The superiority of the approach with weight can be also seen in the case of a single pair of calculations taken from the same set performed for the same candidate points. However, cases where some of the $Err_{\%}$ are lower without the weight can be found for some random draws and quantities.

Figures 3.68, 3.69, 3.70 show the error obtained using methods M2 and M5, respectively, for higher orders. The relation between variants with and without weight differs with the order of PC. Including the weight in creation of the D-optimal set seems to be a better choice when a low PC order is used.

A comparison of all methods for model 2c is given in Table 3.6. The sensitivity to the second variable is small, so the value of the relative error seems to be high. The Halton sequence (S2) outperforms the Sobol' sequence (S1) for all investigated quantities. This was also observed in previous examples. In the case of methods involving random sampling, variability with subsequent throws was not high, especially in the case of method M3.

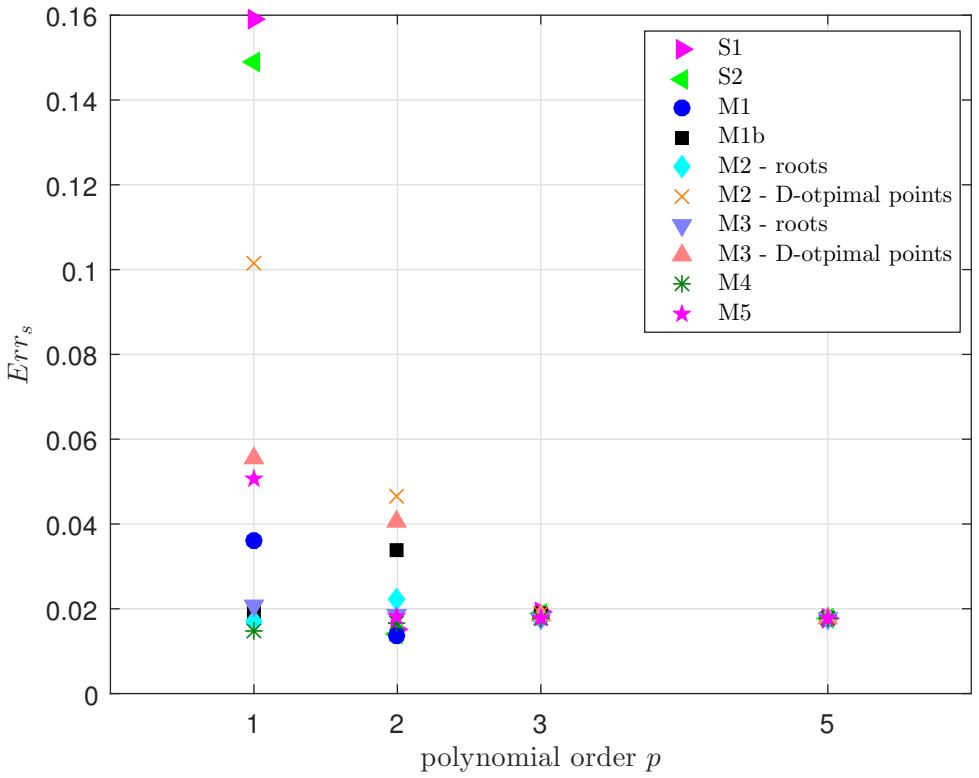

FIGURE 3.62: Err_s obtained for different methods, model 1c

Method M1 is the least convenient due to the rank deficiency problem because it requires a larger number of regression points. The D-optimal choice seems to work in both variants, but is generally better when weight is included. Therefore, in an example with 10 random variables (model 2d) the variants without weight in method M5 and M6 were excluded owing to the size of the problem leading to higher number of required simulations.

3.2.3.4 10 dimensional case

In this section methods will be compared on the 10-dimensional case of the model of the membrane subjected to forced displacement (model 2d).

In the case of 10 variables, the computational cost is higher owing to the larger size of P and also to the higher cost of a single simulation caused by the higher complexity of the problem. Furthermore, when the classic method M1 is applied to 10 variables, the rank deficient problems force the use of more variables $(M-1)\cdot P$ than suggested in the literature [11]. Table 3.7 shows the number of points which have to be taken to obtain the full rank matrix in comparison with size of PC basis P and the number of regression points $(M-1)\cdot P$ recommended in the literature. Errors of the mean, standard

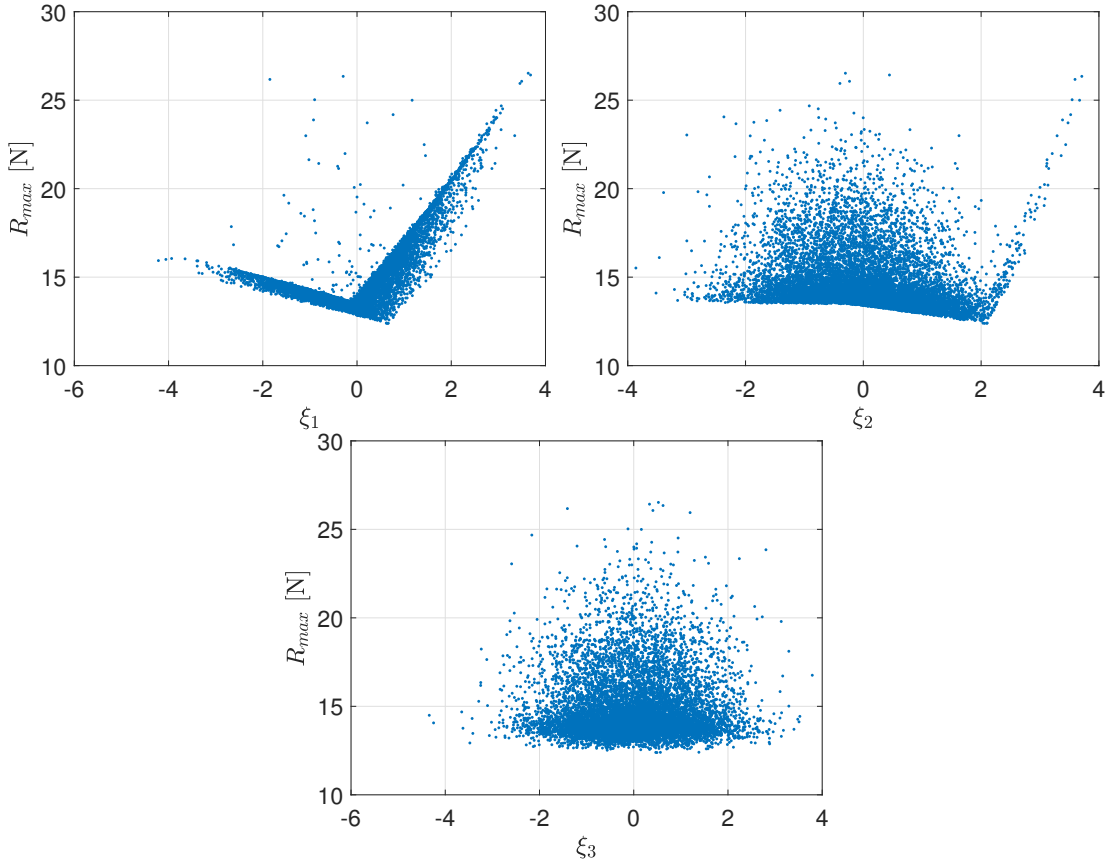

FIGURE 3.63: Scatter plots of model 2c with standardized variables ξ_i related to forced support displacement t_i

	$Err_{\%}$					Err_s
	Mean	Standard deviation	95th percentile	S_1^{Tot}	S_2^{Tot}	
S1	0.63	30.21	3.1	9.09	82.53	0.1416
S2	0.09	20.36	0.93	7.62	49.02	0.1037
M1	4.14	11.19	0.19	5.68	75.07	0.1208
M2a	1.36	16.55	3.84	2.22	49.31	0.0742
M2b	0.96	13.19	3.29	0.21	24.65	0.0357
M3	1.43	17.82	3.96	1.59	42.42	0.0636
M4a	6.42	12.84	5.58	41.12	174.26	0.47
M4b	0.23	1.66	2.17	2.07	25.09	0.04
M5a	1.49	8.08	3.84	18.16	67.24	0.2
M5b	0.16	2.39	2.14	1.4	30	0.05

TABLE 3.6: Errors in model 2c, $p = 3$, 40 regression points ($2P$). Calculations for the M1 method were carried out for 49 points because of the rank deficiency problem

.

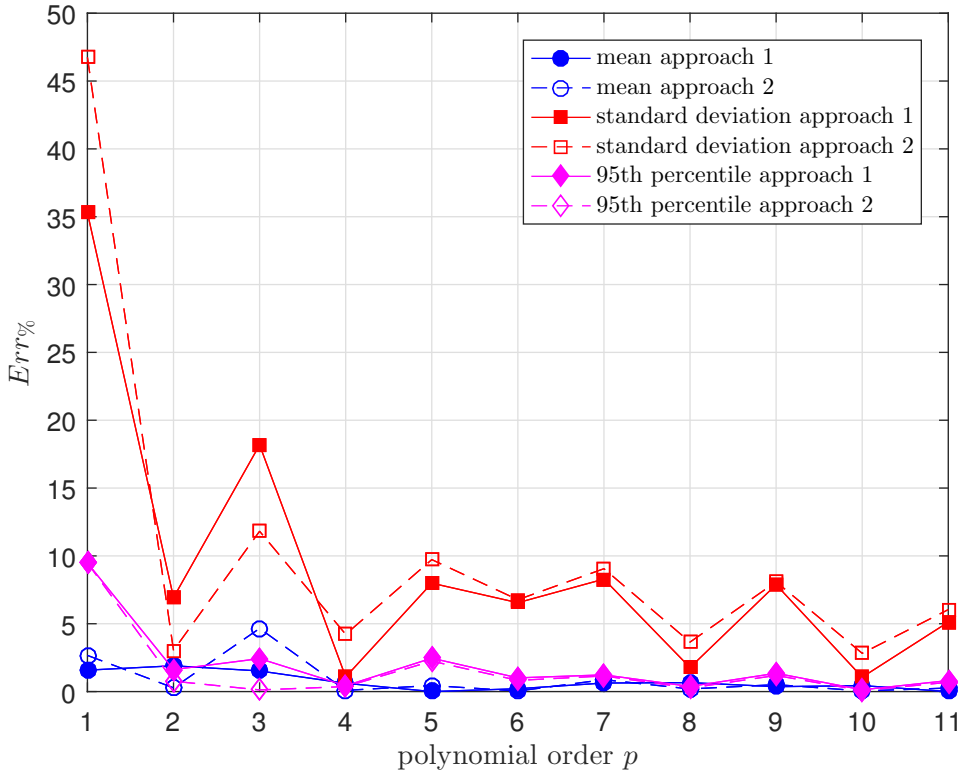

FIGURE 3.64: $Err_{\%}$ of the mean, standard deviation and 95th percentile of R_{max} using method M1 and two approaches to creating a metamodel of R_{max}, model 2c

order	1	2	3	4
P	11	66	296	1001
$(M-1)P$	99	594	2574	9009
number of points	258	147	7674	12693

TABLE 3.7: Number of simulations needed (regression points) in method M1 in the case $M = 10$ due to the rank deficient problem in comparison to P and recommended number of points $(M-1)P$

deviation, 95th percentile obtained by 3rd order PC are equal to 3.57%, 8.05%, 0.29% and 2.09% for the sensitivity index of random variable 4. The rank deficiency problem did not appear in the rest of the considered methods.

The comparison of methods is presented in Table 3.8. Calculations were made on a small $(2P)$ number of points. The method M1 is not presented in this table because of its computational cost. Quasirandom sequences and especially the Halton sequence (S2) out-perform other methods in terms of mean, 95th percentile and sensitivity index of the most significant variable S_4^{Tot}. Method M3 leads to lowest error of standard deviation and a relatively low error of other quantities.

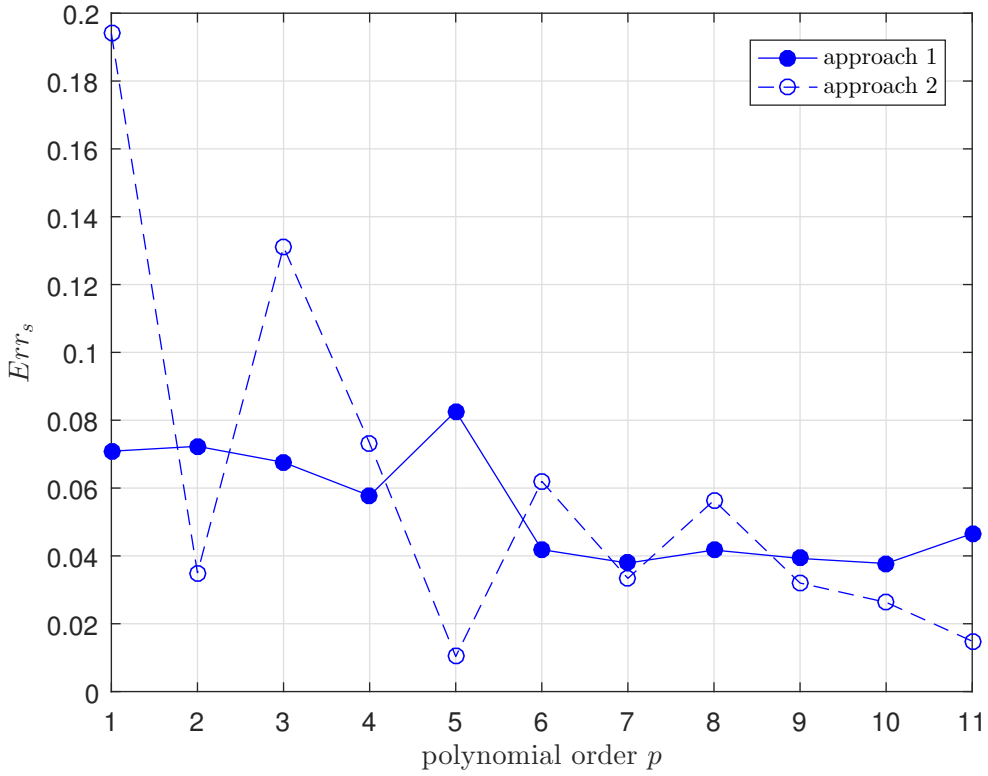

FIGURE 3.65: Err_S obtained by two approaches to creating a metamodel of R_{max} in model 2c

method	Mean	Standard deviation	95th percentile	S_4^{Tot}
S1	1.36	6.41	0.35	1.13
S2	0.87	7.41	0.96	1.24
M3	3.36	2.31	1.67	2.58
M4b	2.15	6.92	1.94	3.79
M5b	4.51	33.78	6.84	24.12

TABLE 3.8: $Err_{\%}$ for methods for model 2d (10 dimensional)

3.3 Conclusions

PC was applied to one analytical function and local models of the surgical mesh. Different methods of choosing regression points were compared and the error compared to the analytical or MC solution was calculated. The aim of this section was to find the DoE method that will be effective in application to hernia-related problems.

Despite nonlinearity and nonsmoothness of some of the quantities of interest, it was possible to obtain sufficient accuracy by regression-based PC.

The relation between errors and the position of sampling points is dependent on the studied problem, which makes it difficult to draw general conclusions about the most efficient

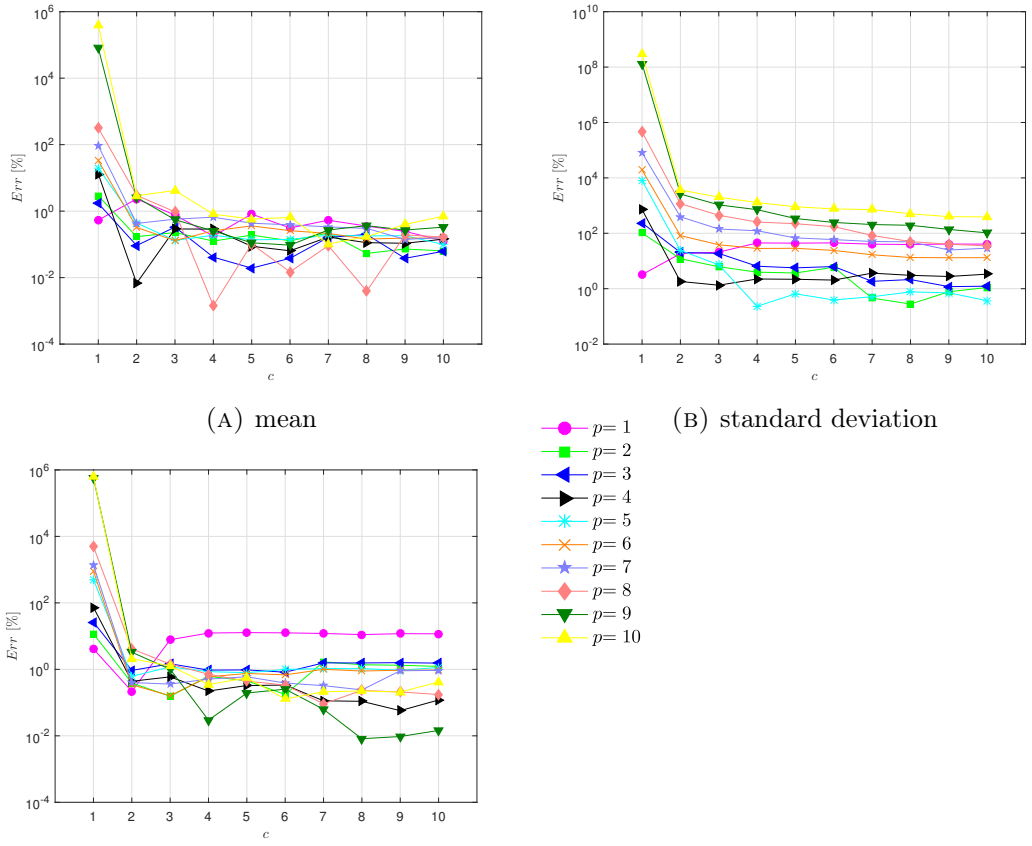

(A) mean

(B) standard deviation

(C) 95th percentile

FIGURE 3.66: Error obtained by method S2 for different orders and number of regression points $N = c \cdot P$, model 2c

DoE method. Nevertheless, some conclusions can be drawn from the perspective of the application of PC to similar models e.g a model with forced displacements corresponding to another hernia location or different surgical mesh types. Further examples will be presented in the next chapter.

All methods lead to low error in the case of the cable model (model 1) for polynomial order $p > 2$. Therefore conclusions are drawn mainly from the more demanding membrane model (model 2). Based on the results presented, the following observations can be made:

- PC constructed on DoE based on D-optimality can lead to relatively low error. Nevertheless, the accuracy depends on the initial candidate set.
- Method M1 leads to higher computational cost in the case of the higher dimensional problem owing to the rank-deficiency problem, which make it less attractive in comparison to other methods.

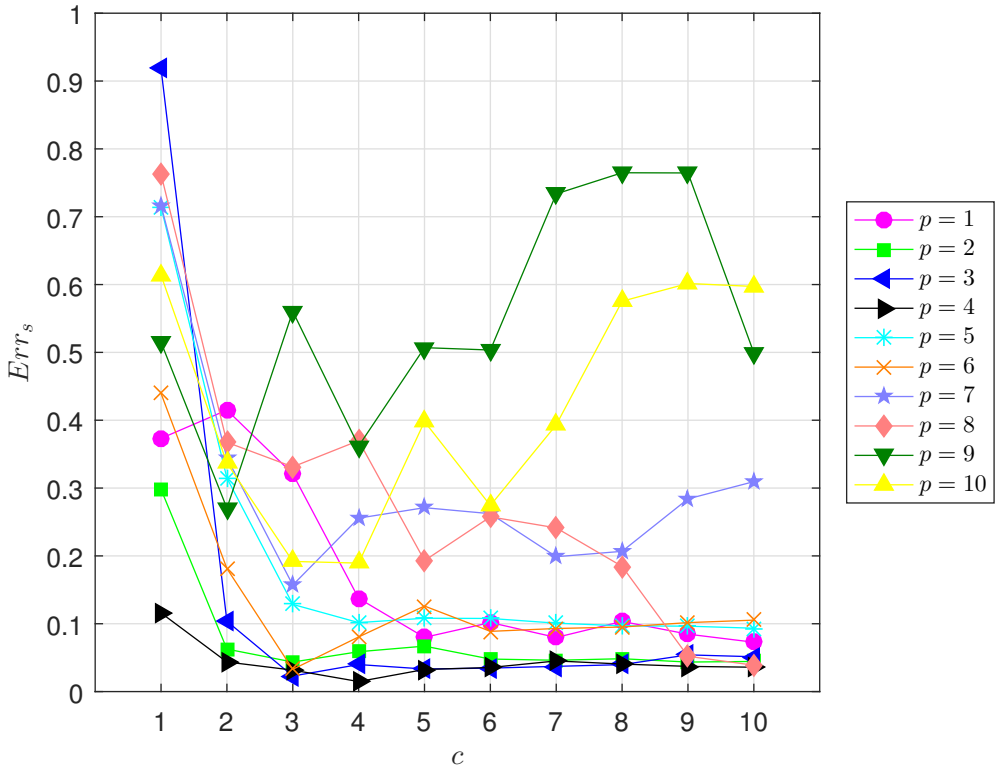

FIGURE 3.67: Err_s obtained by method S2 for different orders and number of regression points $N = c \cdot P$, model 2c

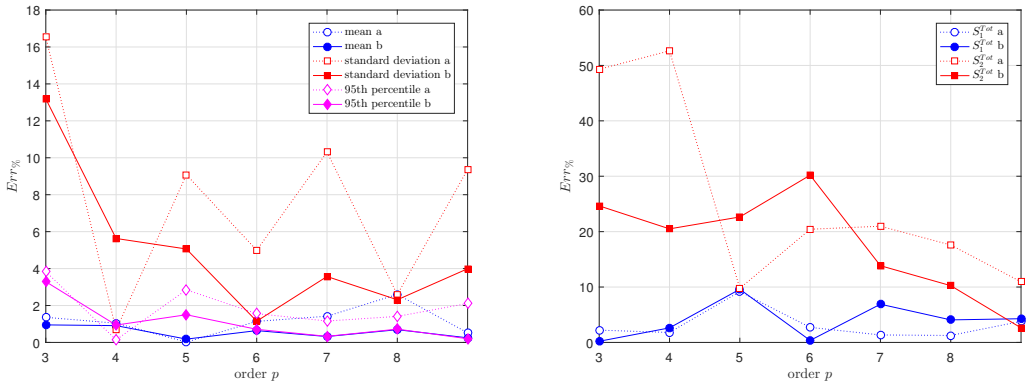

(A) mean, standard deviation, 95th percentile (B) sensitivity indices

FIGURE 3.68: Err_s, when method M2 was applied in variants without (a) and with (b) weight for different orders, example 2-3D)

- When a method incorporates the choice of D-optimal design of experiment (M2, M4, M5) in the case of normal distribution and low PC order it is beneficial to include a weight function corresponding to a Gaussian measure in the construction of the information matrix, the determinant of which will be maximized;
- Sobol' (S1) and Halton (S2) sequences are a better choice in the case of higher

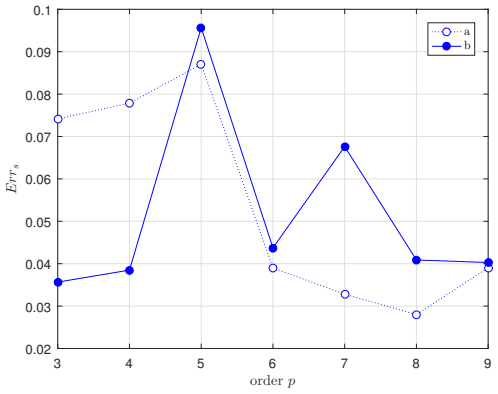

FIGURE 3.69: Err_s obtained by method M2 , example 2c

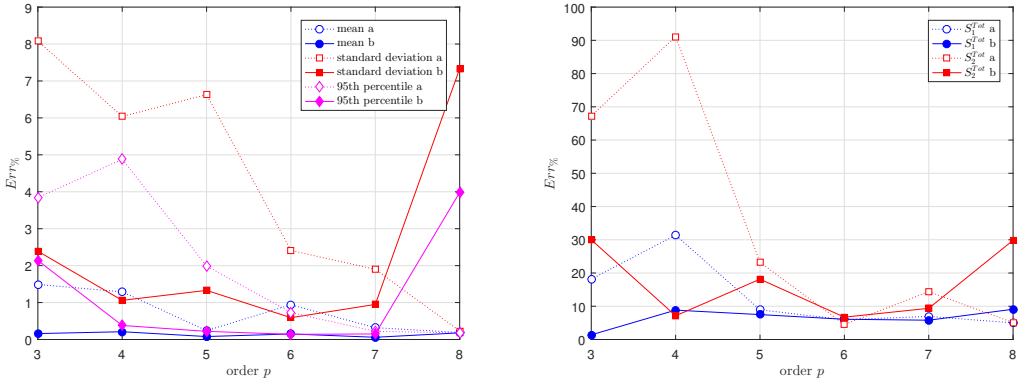

(A) mean, standard deviation, 95th percentile (B) sensitivity indices

FIGURE 3.70: Err_s, when method M5 was applied in the variant without (a) and with (b) weight for different orders (mean result from a couple of drawn LHS candidate sets of points, example 2-3D)

($M = 10$) dimensional models , but lead to a large error in the standard deviation in the lower ($M = 3$) dimensional case (this will be also shown in the example of the reduced model in chapter 4), which is in line with conclusions drawn by Cho et al. [30] and Gao et al. [53] on the superiority of QMS when M is high.

- In the lower dimensional case ($M = 3$) and normal distribution, methods based on the D-optimal set founded on a random candidate set with weight function (M4b, M5b) lead to the lowest error. However, for the higher M ($M = 10$) method M5b with a candidate set drawn by LHS leads to a large error of the standard deviation and sensitivity index when compared to other methods including method M4b.

- Method M3 (random choice from D-optimal 1D cases) leads to the lowest error of the standard deviation in the case of the model with 10 variables and also a satisfactory error of the other quantities.

- Approach 2 (3.11) to calculate metamodels of R_{max} was usually superior to approach 1 (3.13) in terms of the error of the statistical values and RMSE of the metamodel but not in the case of estimation of the total sensitivity indices.

In the case of all considered methods, the choice of DoE is made regardless of model response, which make it impossible to incorporate problem dependence. In further research some adaptive methods can be considered. However, the question of choice of criteria then occurs.

In the examples shown in the next chapter, the decision on the DoE is based on the number of variables.

Chapter 4

Results of uncertainty propagation and sensitivity analysis

In this chapter the results of uncertainty quantification and sensitivity analysis are presented. The results are shown for the models already introduced in chapter 2. UQ and SA is also performed on other models, where the DoE choice is based on expertise gained in chapter 2.

The following models are considered in this chapter:

1. local cable model of the implant with four random variables $\mathbf{X} = [E, L_0, H_0, \Delta_p]^\top$ (model 1c);
2. local model of the membrane subjected to displacement of the supports:
   - model 2d with 10 independent random variables $\mathbf{X} = [t_i]^\top$; $i = 1, 2, \dots 10$;
   - model 2e with a reduced number of random variables based on the global SA outcome of model 2d;
   - model 2f with 10 correlated random variables $\mathbf{X} = [t_i]^\top$; $i = 1, 2, \dots 10$;
3. local model of the membrane subjected to intraabdominal pressure:
   - model 3a with uncertain pressure and stiffness of the fascia and abdominal wall;
   - model 3b with imperfections;
4. Gloabl membrane model of abdominal wall with implant.

Both the local and global models are concerned with the period shortly after repair. No tissue overgrowth is taken into account.

In addition to the examples from the implant-abdominal wall system, an example is considered which addresses a topic from the civil engineering field (section 4.5). A model of corner joints in historic log houses is introduced together with a description of the background of the study and a brief account of the state of the art of historic timber structures.

4.1 Cable model (model 1)

This model has already been presented in section 3.2.1.1, where the choice of DoE was also discussed. In the following section attention will be paid to the outcome of sensitivity analysis.

Firstly, the local sensitvity is considered following [168]. The local sensitivity in the case of the cable model can be calculated by analytic differentiation. The derivation of the local sensitivity indices performed by [168] is briefly presented here. Let s be parameter, which can be one of the cable model parameters: L_0, H_0, Δ_p or E. The derivative of the left side of equation 3.10 with respect to s is

$$3H^2\frac{\mathrm{d}H}{\mathrm{d}s}c_1 + H^3\frac{\mathrm{d}c_1}{\mathrm{d}s} + 2H\frac{\mathrm{d}H}{\mathrm{d}s}c_2 + H^2\frac{\mathrm{d}c_2}{\mathrm{d}s} - \frac{\mathrm{d}c_3}{\mathrm{d}s} = 0, \tag{4.1}$$

Therefore:

$$\frac{\mathrm{d}H}{\mathrm{d}s} = \frac{-H^3\,\frac{\mathrm{d}c_1}{\mathrm{d}s} - H^2\,\frac{\mathrm{d}c_2}{\mathrm{d}s} + \frac{\mathrm{d}c_3}{\mathrm{d}s}}{3H^2c_1 + 2Hc_2} \tag{4.2}$$

Then the local sensitivity index S_s^{local} (2.34) with respect to parameter s is

$$S_s^{local} = \frac{s}{H}\frac{\mathrm{d}H}{\mathrm{d}s} \tag{4.3}$$

The local sensitivity indices are then given by:

$$\begin{aligned}
S_{L_0}^{local} &= \frac{H^3 l_s + H^2\Delta_p EA - \frac{EAg^2l^3}{24}}{L_0H^2\left[3H\left(1+\frac{l_s}{L_0}\right) + 2\left(-H_0 + \Delta_p\frac{EA}{L_0}\right)\right]} \\
S_{H_0}^{local} &= \frac{H_0}{3H\left(1+\frac{l_s}{L_0}\right) + 2\left(-H_0 + \Delta_p\frac{EA}{L_0}\right)} \\
S_{\Delta_p}^{local} &= \frac{\frac{-EA}{L_0}\Delta_p}{3H\left(1+\frac{l_s}{L_0}\right) + 2\left(-H_0 + \Delta_p\frac{EA}{L_0}\right)} \\
S_E^{local} &= \frac{-H^2\Delta_p EA + \frac{EAg^2l^3}{24}}{L_0H^2\left[3H\left(1+\frac{l_s}{L_0}\right) + 2\left(-H_0 + \Delta_p\frac{EA}{L_0}\right)\right]}
\end{aligned} \tag{4.4}$$

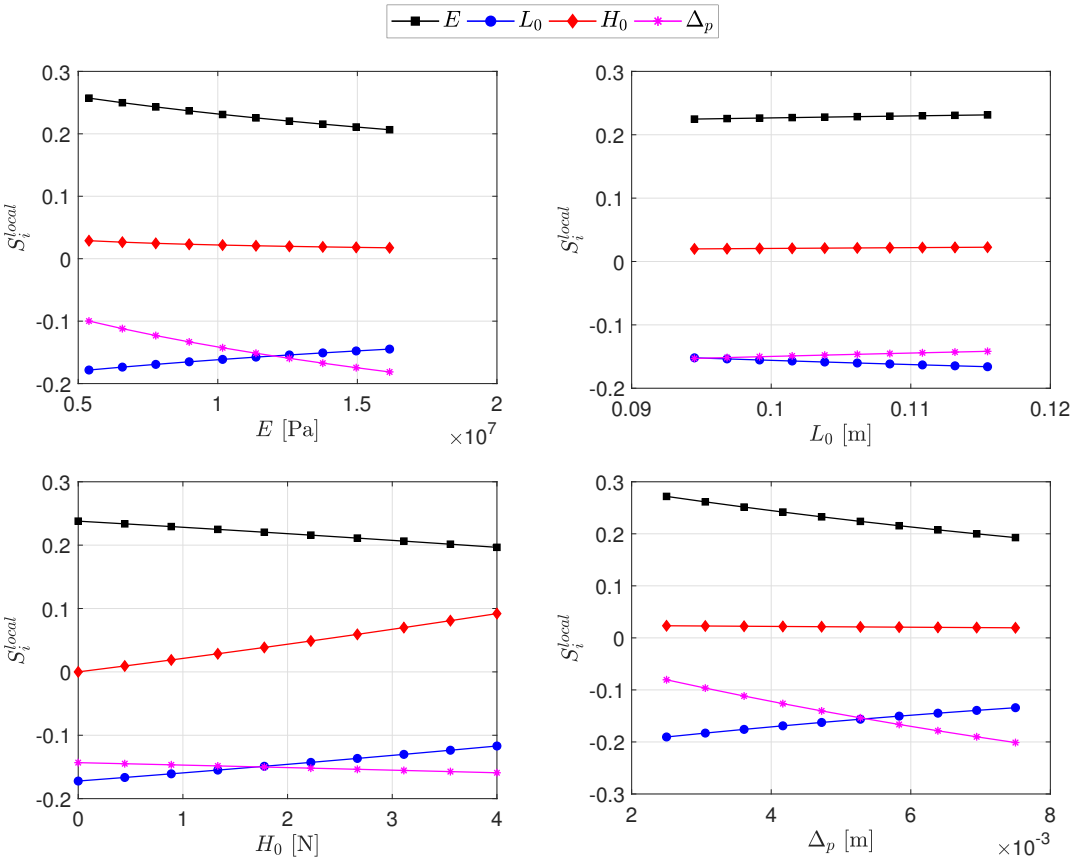

FIGURE 4.1: Local sensitivity indices S_i^{local} for different base points (model 1c)

variable	E	L_0	H_0	Δ_p
S^{Tot}	0.6460	0.0059	0.0942	0.2746

TABLE 4.1: Total sensitivity indices S^{Tot} obtained for model 1c by MC

The local sensitivity indices (4.1) vary with change of base point [168], Figure 4.1). The base point is only changed for one variable at a time while the other variables remain fixed at their initial base point. The ranking of variables in terms of local sensitivity varies as the base point considered is varied. For example, when Δ_p is at the beginning of its considered range, the magnitude of its sensitivity is lower than of E and L_0, but when Δ_p is at the end of its considered range it is the most influential variable. Δ_p results from elasticity of the fascia, which as a human soft tissue is characterized by natural variability so limitation of the analysis to a particular base point may not be sufficient.

Global sensitivity analysis is also performed to investigate the global effect of variations in the domain performed all at once. Table 4.1 presents the total sensitivity Sobol' indices obtained by MC for model 1c.

Figure 4.2 shows scatter plots obtained by the MC method for 4 variables. Ranking of

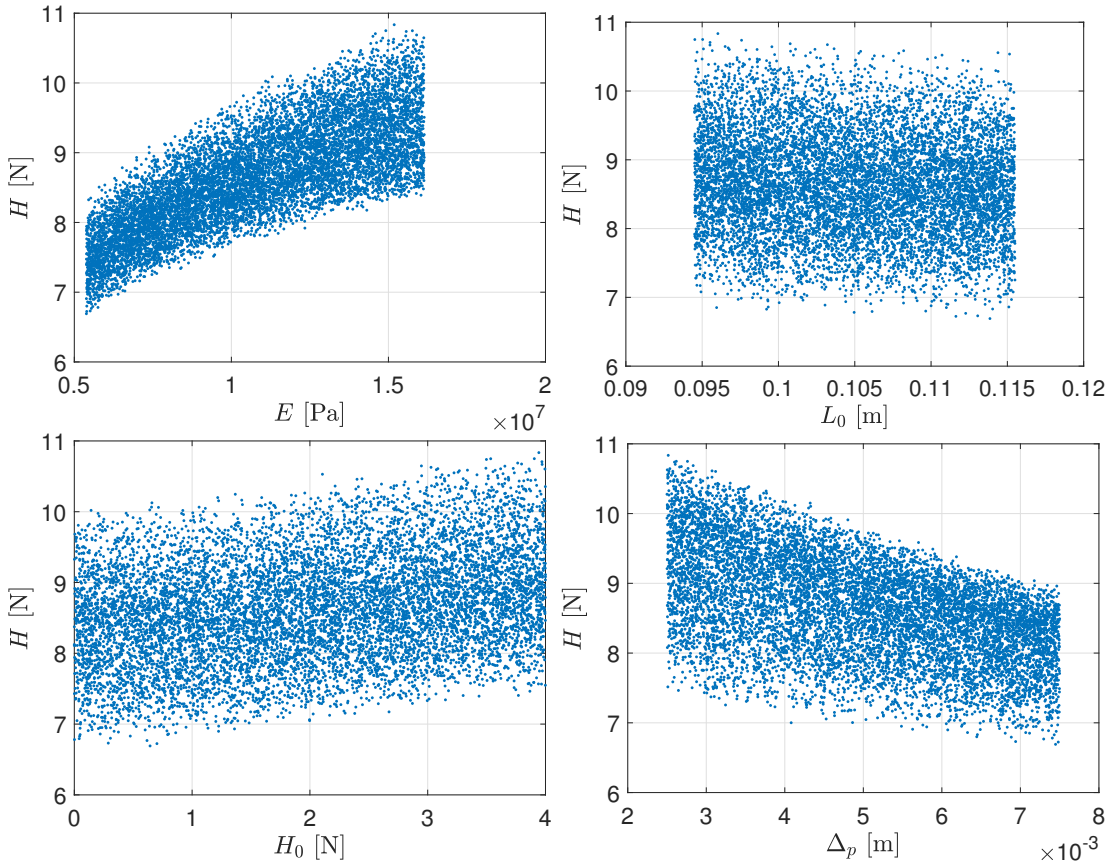

FIGURE 4.2: Scatter plots of model 1c

variables in terms of their significance as obtained from Sobol' indices (Table 4.1) is also visible in the plots.

Globally, E is the most significant. Δ_p is in second place in terms of the sensitivity index. Despite the relatively high local sensitivity index of L_0 around some base points, the variance of L_0 has a minimal effect on the variation of H. Nevertheless, it should be noted that the input variation of L_0 was also low when compared to other variables, which affects its global sensitivity index.

4.2 Model of membrane subjected to forced displacement of supports

The model of the implant subjected to forced displacement has already been presented in section 3.2.1.2 together with a discussion on the DoE. In the following section the outcome of sensitivity analysis will be presented in more detail for the case with 10 variables.

i	1	2	3	4	5	6	7	8	9	10
S_i^{Tot}	0.01	0.0036	0.0009	0.5156	0.0063	0.0055	0.491	0.001	0.0038	0.0106

TABLE 4.2: Total sensitivity index in model 2d, 3rd order PC with $(M-1)P$ point from Sobol' sequence

4.2.1 10-D problem with independent variables

Firstly, as in section 3.2.1.2 all variables are assumed to be independent. Figure 4.3 shows scatter plots obtained for this model by MC (only every tenth point is shown for better clarity of the graph). The strong influence of ξ_4 is visible. Nevertheless, it can be seen that this influence changes over the domain and is greater for higher ξ_4. The displacements of the 4th and 7th supports are also much more influential on the variance of the QoI according to the total Sobol' indices obtained by PC method (Table 4.2). This can be explained by the higher input variation of these two variables when compared to the others.

4.2.2 Reduction of number of variables

The total sensitivity indices are very small for variables other than the 4th (t_4) and 7th (t_7) and indicate that the influence of the uncertainty of the displacement of other supports is negligible in comparison to these two.

This analysis has been repeated for other orientations of the implant that may affect the importance of the variables (Figure 4.4). However, at least one of the two aforementioned variables is always dominant and the sum $S_4^{Tot} + S_7^{Tot}$ is close to 1 for all considered orientations. The influence of other variables on the variation of the output is very small for all considered orientations of the implant.

Therefore for any orientation of the implant the model can be reduced to a model of just 2 variables.

PC metamodels for the model with a reduced number of variables were constructed with different methods of DoE creation. However, since only 2 variables are taken into account, the M2 and M3 methods were not considered because the number of combinations of roots of 5 order is smaller than $2P$ in case of $p = 4$. In this case method M1 consists of taking all possible combinations of D-optimal points of univariate polynomials.

Table 4.3 shows $Err_{\%}$ between the statistics obtained for PC constructed with different approaches for the 2 random-variable model (t_4 and t_7). M5b leads to the highest accuracy in the case of the 2-D problem. It is interesting to compare it with $Err_{\%}$

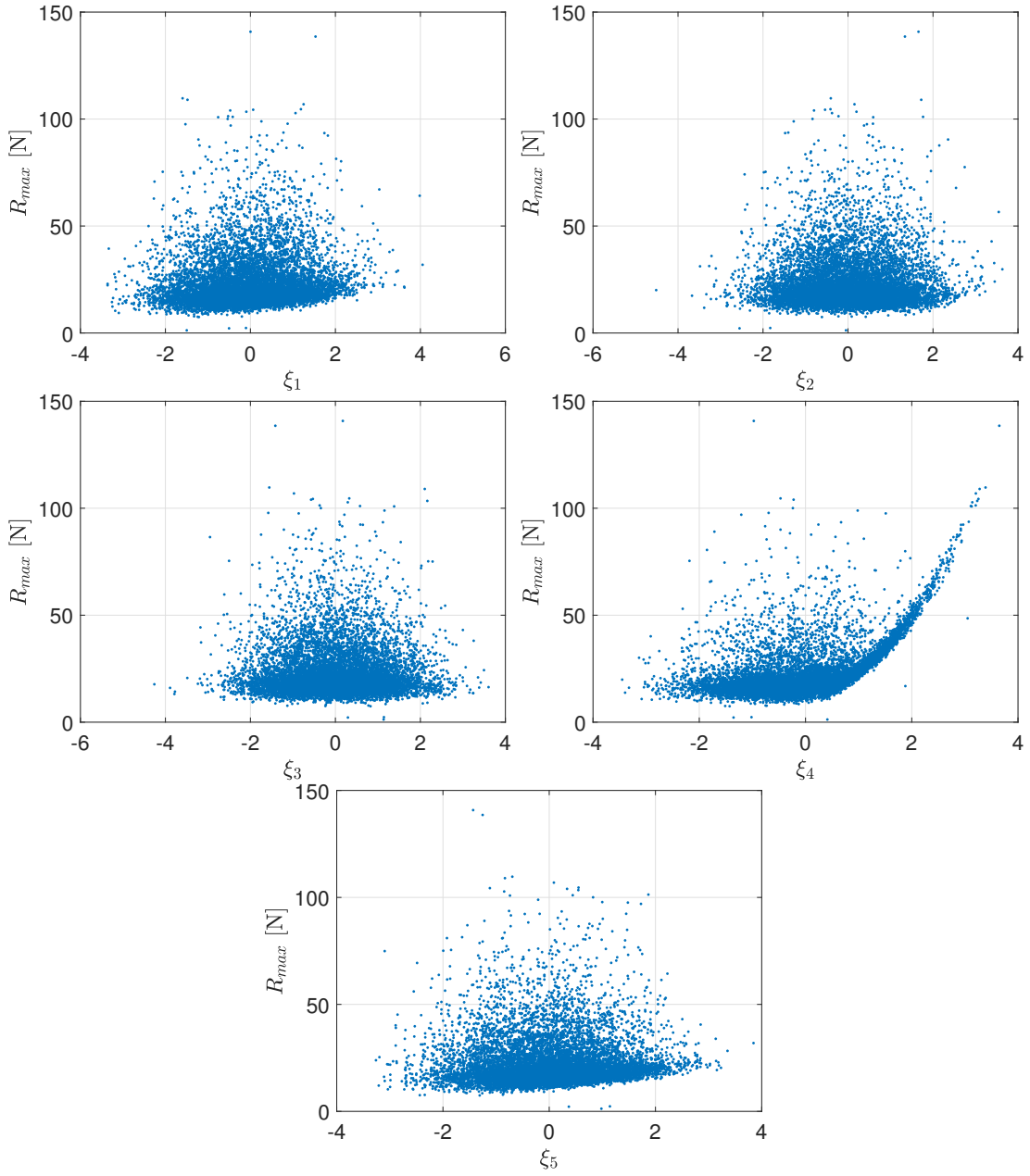

FIGURE 4.3: Scatter plots of model 2d of standardize variables ξ_i related to forced support displacement t_i

obtained for 10D PC (Table 3.8), where in contrast to the reduced 2D problem, the accuracy of M5b was the worst in terms of $Err_{\%}$ of the standard deviation and S_4^{Tot}. Gao and Zhou [53] showed that the best method of DoE in least square polynomial approximation is dependent upon the number of dimensions. They noticed that QMC points are better for high-dimensional problems in terms of convergence and stability. In the model considered of the membrane subjected to forced displacement of supports Sobol'(S1) and Halton(S2) sequences are more efficient in case of 10-D problem than in the reduced model. In this 2D case and also in the 3D model (model 2c, Table 3.6) choosing Sobol' and Halton sequences leads to high $Err_{\%}$ of the standard deviation.

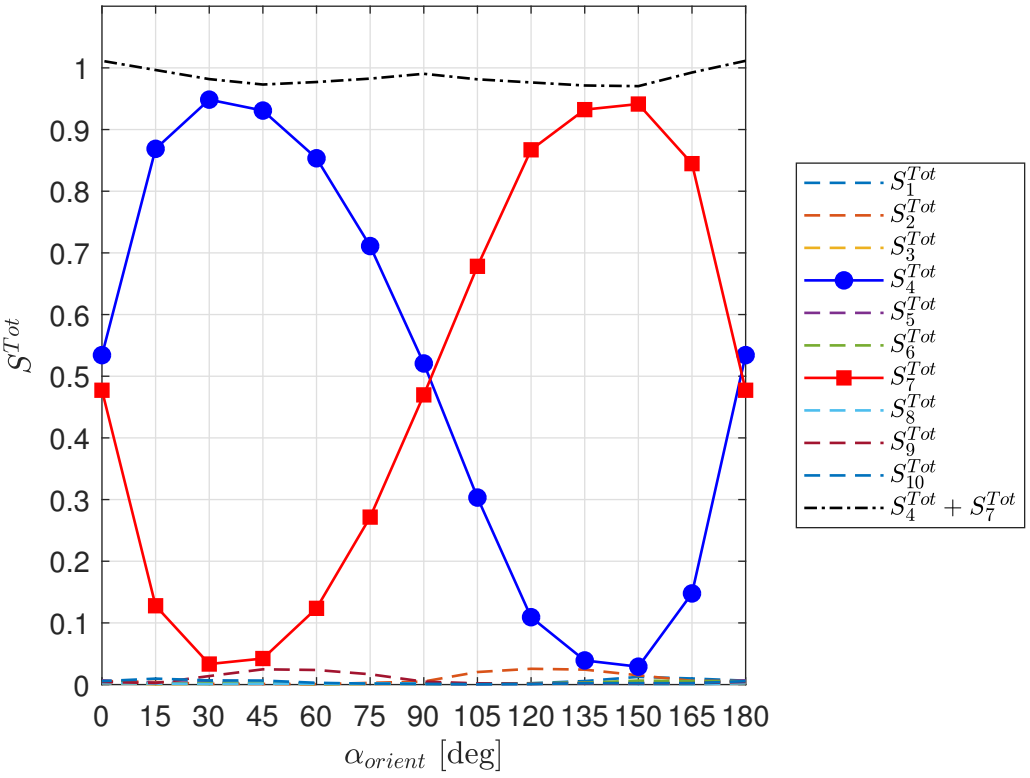

FIGURE 4.4: Total global sensitivity indices vs orientation of implant α_{orient}, model 2d, PC order 3, $2P$ regression points,

method	Mean	Standard deviation	95th percentile
S1	4.51	49.99	10.73
S2	9.09	26.97	0.79
M1 (25 points)	7.75	3.17	4.91
M5b	2.67	2.85	0.62

TABLE 4.3: $Err_{\%}$ between the solution of the reduced 2D model (model 2e) and the MC solution obtained for the 10D model (model 2d), PC order $p = 4$, $2P = 30$ regression points (for method M5b mean $Err_{\%}$ is shown

4.2.3 Correlated variables

Some other analyses have been carried out where a correlation is introduced between the displacements of the supports. Due to lack of a sufficiently large set of experimental data, the correlation matrix is defined based on judgement.

The classic autocorrelation function is based on the distance between points. The correlation matrix in this example corresponds to the positions of the 10 fasteners and is in the form :

$$\mathbf{C}_A = \mathrm{e}^{-\frac{\|\mathbf{z}-\mathbf{z}'\|}{l}}, \tag{4.5}$$

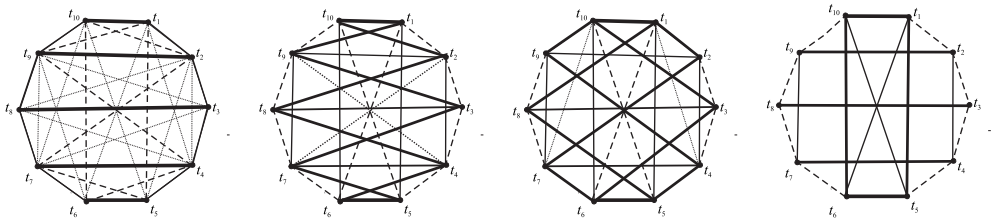

(A) matrix $\mathbf{C}_B$ (B) matrix $\mathbf{C}_C$ (C) matrix $\mathbf{C}_D$ (D) matrix $\mathbf{C}_E$

FIGURE 4.5: Graph representation of correlation. The thicker line, the stronger the correlation. However, no line does not mean no correlation, but only weaker then between other variables (matrices are given in appendix A.3)

where l is the span of the implant and $\mathbf{Z}$ is the position of support. Matrix entry (i,j) is the correlation coefficient between i-th and j-th variable. This is a reasonable approach in many applications. However, the abdominal wall (Figure 1.1) is anisotropic and it is composed of layers with different architectures and orientations of fibres. Linea alba, a tissue playing a key role in ventral hernia problem, is also anisotropic and composed of fibers aligned in different directions [60]. The construction and properties of the abdominal wall affect the values of the displacements of the supports and therefore their level of correlation may depend not only on their distances, but also on their arrangement within the fibres. Therefore, four more correlation matrices are introduced, $\mathbf{C}_B$, $\mathbf{C}_C$, $\mathbf{C}_D$ and $\mathbf{C}_E$ (appendix A.3). Figure 4.5 shows the levels of correlations between forced displacements of the supports for the new matrices.

However, a matrix created manually may not be positive semi-definite and therefore may not fulfill the requirements necessary to be a correlation matrix. This problem is solved by applying the algorithm of finding the nearest semi-definite matrix with elements on the diagonal equal to 1 [73].

4.2.3.1 Results - reduction of number of variables

An example was calculated with the correlation matrix C_B for all variables ($N_{NK} = 10$). Figure 4.6 shows on the left axis eigenvalues corresponding to each variable and on the right axis the total sensitivity indices S^{Tot} to all variables of the maximum reaction force. This calculation was done for polynomial order $p = 5$. Both curves have similar shapes. Starting from the 5th variable, the value of S^{Tot} is smaller than 0.1. Therefore, although the 5th eigenvalue has a similar value to the 4th, truncation at the 4th variable can be considered as reasonable. The influence of truncation for the mean, standard deviation and 95th percentile is presented in Figure 4.7 for different polynomial orders p. The difference between the results obtained for different p is high when only one variable is taken into consideration. These graphs confirm that good accuracy can be obtained for

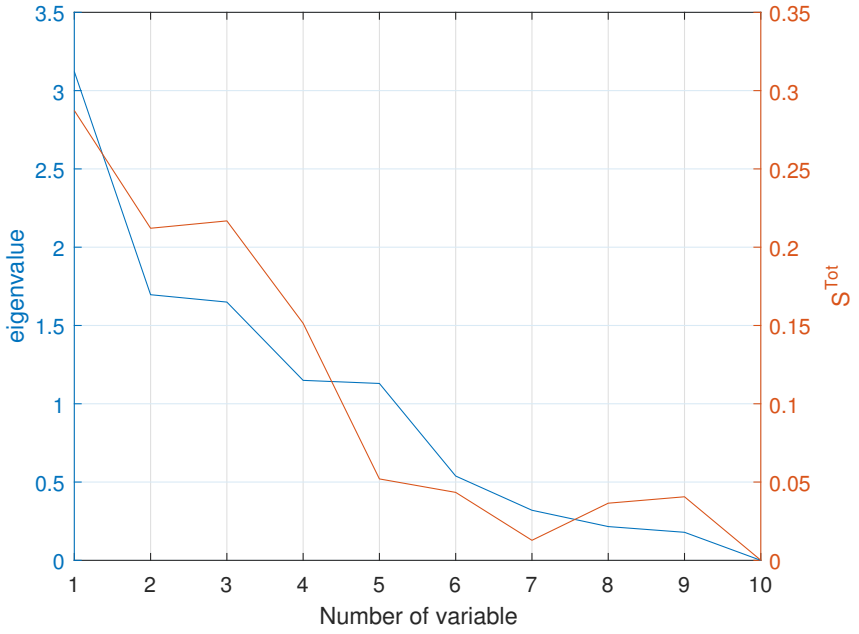

FIGURE 4.6: Eigenvalues and corresponding total sensitivity indices to all variables of the maximum reaction force

truncation at the 4th variable. Global sensitivity analysis can be useful in finding the truncation point efficiently when PC is applied and performing such calculations does not require additional model runs. Based on these results, in further calculations PC of order 2 was applied and 4 variables were taken into account.

4.2.3.2 Results - influence of implant orientation

The orientation of the orthotropic implant within the anisotropic abdominal wall was shown to be important in [106], where the optimal orientation in terms of minimisation of R_{max} was found for different hernia locations and implants. An analysis of implant orientation was also conducted by Hernández-Gascón et al [70] using an FE model of the whole abdominal wall and one hernia location. The conclusion presented there was similar to that obtained in [106], namely that at the hernia location considerd in this thesis, the most compliant axis of the mesh should coincide with cranio-caudal direction of the body. Simón-Allué et al. [145] confirmed this for large hernia defects, but noted that the superiority of any given orientation is not so clear when small and medium hernia defects are considered. All the aforementioned studies were deterministic and conducted for single specific sets of abdominal wall properties.

The influence of the orientation on some quantities obtained by the probabilistic approach has been investigated. The orientation of the implant α_{orient} was modified in the example with 10 independent variables. Figures 4.8 and 4.10 show the mean and 95th percentile

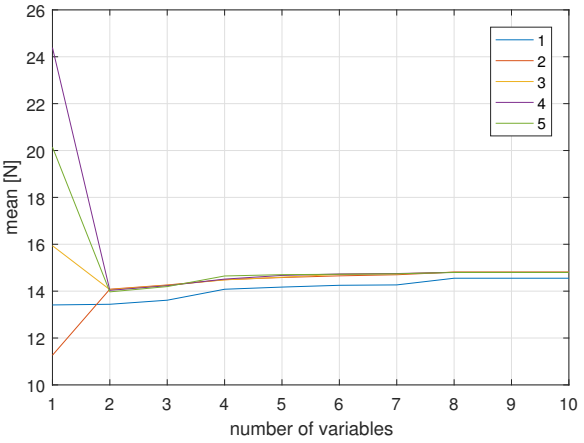

(A) mean

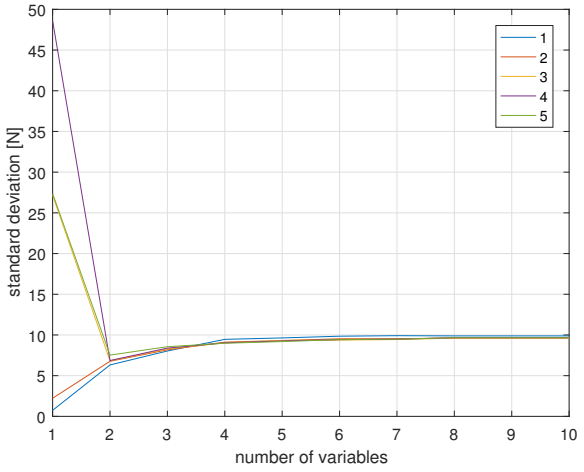

(B) standard deviation

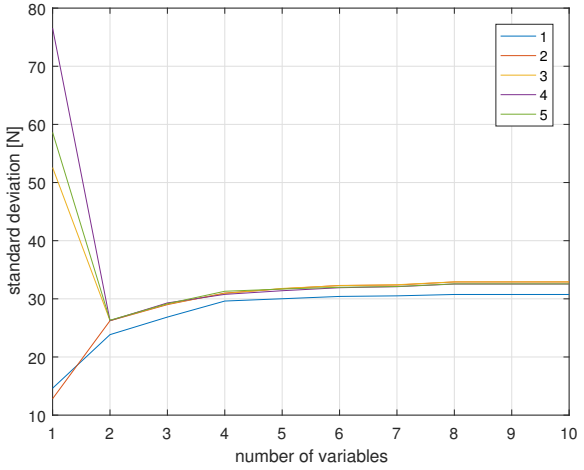

(C) 95th percentile

FIGURE 4.7: Mean (a), standard deviation (b) and percentile 95% (c) with a number of variables for different polynomial orders p from 1 to 5, model 2f

obtained, respectively, of R_{max}. Figure 4.9 shows the change of the standard deviation with orientation. The 95th percentile of R_{max} increases with the orientation angle (0° means that a specified direction of the implant is parallel to the cranio-caudal axis and 90° that is perpendicular), which is in contrast to the solution obtained deterministically for mean input values of the forced displacement [106]. The results as a function of α_{orient} obtained for the model with 10 independent variables do not reproduce the relation obtained by deterministic studies.

The situation is different when correlation between the forced displacements of the supports is introduced. In the same Figures (4.8–4.10) it can be seen, that both mean and 95th percentile decrease with increase of orientation angle. The differences between the mean values obtained from all the considered correlation matrices are small when compared to much higher values obtained for the case with 10 independent variables. The results obtained for the 95th percentile differ more, but the shape of its dependence on α_{orient} is similar for all the matrices considered. It can be seen that the mean and 95th percentile obtained from the calculation with 10 independent variables are higher than the statistics obtained from all the considered correlation matrices. Calculation with independent variables can provide a broader scope of situations, which results in higher variability of R_{max} and can be considered safer, especially when the form of the correlation is not well known. However in such a case, the relation between forced displacements of different supports can change more easily, which may affect conclusions about the proper orientation. The introduction of correlation between the displacements of the supports leads to a change in the shape of the dependency of the quantities considered on the orientation of the implant. Nevertheless the actual choice of correlation matrix does not seem to be important when studying the influence of orientation on the quantity of interest.

4.3 Model of membrane subjected to intraabdominal pressure

4.3.1 Deterministic model

The membrane model of the implant is taken from [105] (Figure 4.11). In place of the overlap of the implant over the fascia, an elastic foundation with elasticity k_{aw} representing the elasticity of the abdominal wall is assumed. In place of the tacks, supports are modelled with springs of elasticity k_f corresponding to the elasticity of the fascia tissue. An impulse of pressure of p_{ia} simulating the intraabdominal pressure during coughing is imposed dynamically. The implicit single-step Houbolt algorithm is

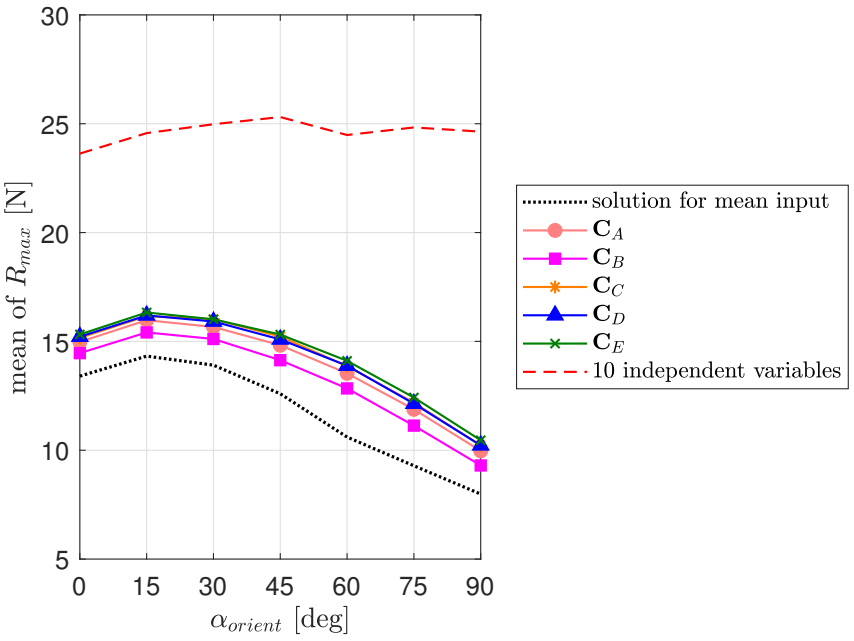

FIGURE 4.8: Mean of QoI obtained from different correlation matrices and the example with independent variables for different orientations of the implant α_{orient}. Additionally the value of the QoI obtained by a single deterministic calculation for mean input is shown. Model with forced displacement of the supports

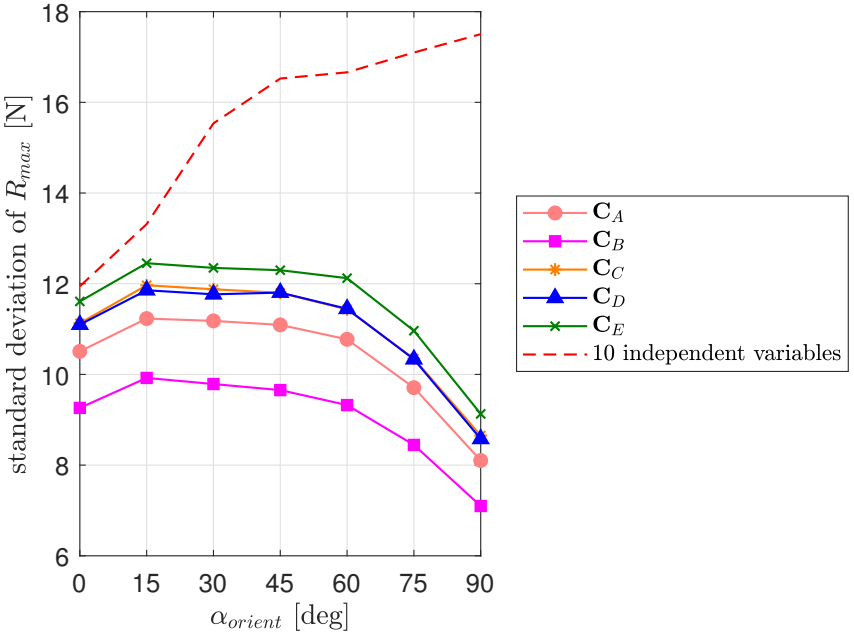

FIGURE 4.9: Standard deviation of QoI obtained from different correlation matrices and the example with independent variables for different orientations of the implant α_{orient}. Model with forced displacement of the supports

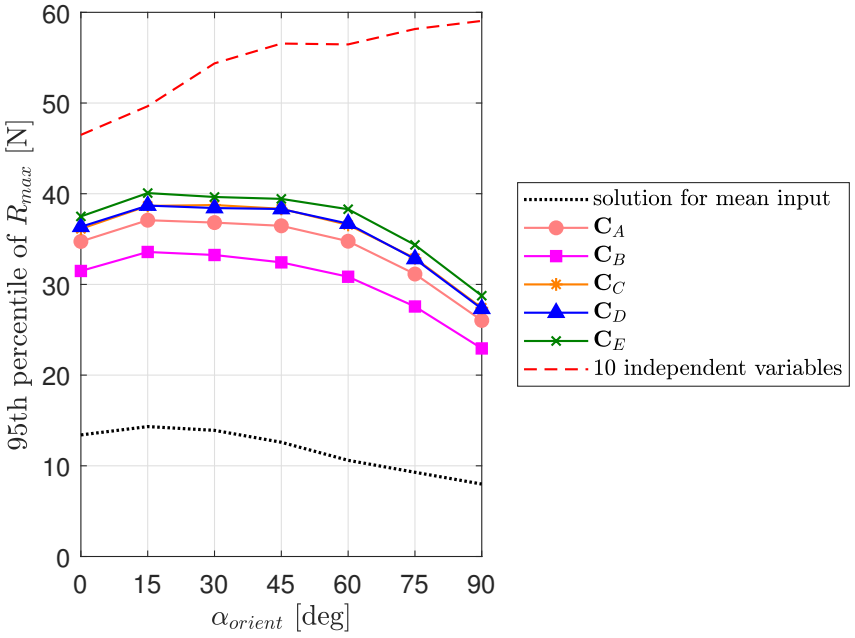

FIGURE 4.10: 95th percentile of QoI obtained from different correlation matrices and the example with independent variables and deterministic results obtained for mean input values for different orientations of the implant α_{orient}. Model with forced displacement of the supports

used. Rayleigh damping is assumed with the damping parameters estimated in [105]. The geometric dimensions, the material model and its parameters are the same as in model 2. The FE model is composed of quadrilateral four-node isoparametric membrane elements [2]. The mesh (Figure 4.12 was chosen based on convergence analysis of the quantities of interest (maximum reaction and deflection of the implant) [105]. The model was validated in [105] by comparison of the simulation with an experiment in a pressure chamber. In that experiment [174] an implant connected to the porcine abdominal wall with hernia was subjected to the impulse of pressure. Displacements were measured by laser sensors and were compared with numerical results obtained from the use of the model.

The quantities of interest are:

- the maximum reaction force R_{max} related to the force in the tacks. The maximum over time and all the supports is found.
- the maximum deflection over time of the center of the implant u_{max}, which is related to problem of excessive mesh bulging.

Two cases of random variables are considered:

- $\mathbf{X} = [p_{ia}, k_f, k_{aw}]^\top$, (model 3a, section 4.3.2);

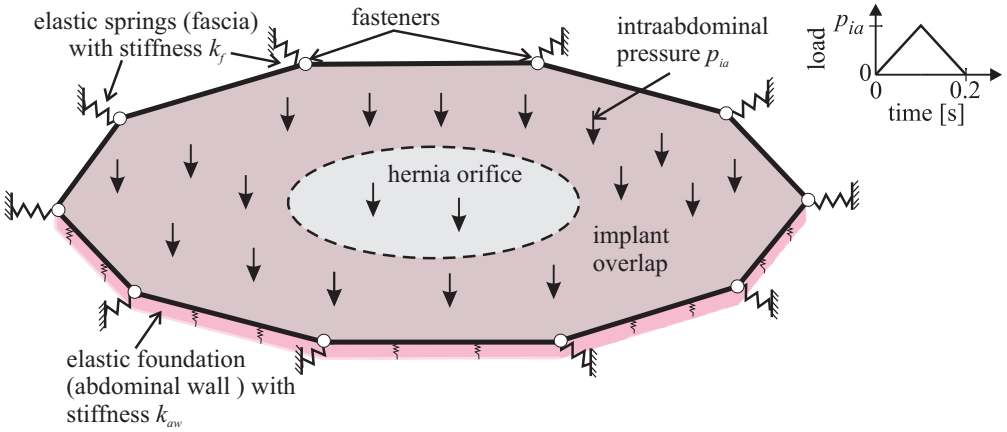

FIGURE 4.11: Scheme of the model of the implant subjected to intraabdominal pressure with the load function

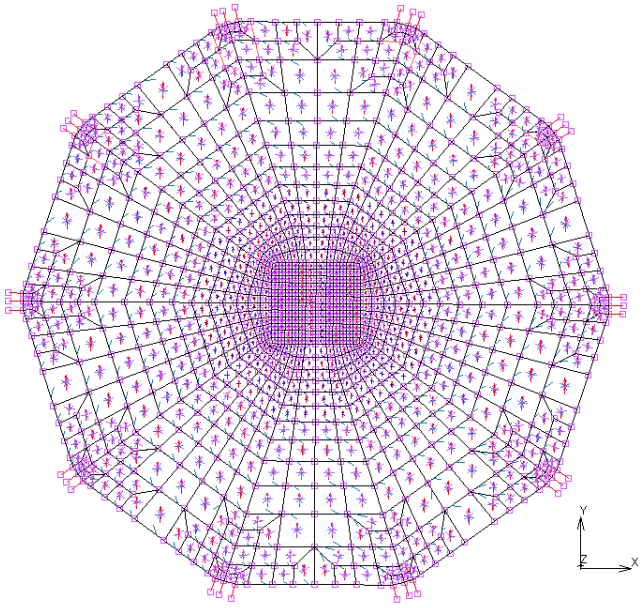

FIGURE 4.12: FE mesh of the model of the implant subjected to the intraabdominal pressure

- random imperfections in the positions of the tacks (model 3b, section 4.3.3).

4.3.2 Uncertainties in pressure and elasticity of the abdominal wall tissues

4.3.2.1 Model

Three independent random variables are assumed $\mathbf{X} = [p_{ia}, k_f, k_{aw}]^\top$.

variable	lower limit	upper limit
p_{ia} [mmHg]	40	127
k_f [kN/m]	0.6	15.5
k_{aw} [kPa]	17	38.5

TABLE 4.4: Limits of uniform distribution, model 3a

Cobb et al. [33] measured the values of intraabdominal pressure during various human activities. They found that the value is correlated with body mass index (BMI) and can also be elevated in people with a chronic cough. The variations in outcome among the 20 subjects reported in that study can be considered high, e.g. for the case of a cough, the relative standard deviation of intraabdominal pressure is 31%. Therefore, the value of the pressure during coughing p_{ia} is assumed to be a uniform random variables in a range taken from [33], where the minimum and maximum values of the pressure was measured in 20 subjects.

k_{aw} and k_f are taken to be uniform random variables because of the uncertainties of the mechanical properties of the abdominal wall tissues. The range of k_{aw} is based on the results reported by Song et al. [153], where the elasticity of abdominal wall was measured *in vivo* in humans. Ranges of k_f are taken from [170], where fascia elasticity was determined.

Table 4.4 presents the ranges of the uniform distribution of each random variable.

4.3.2.2 Results

Monte Carlo simulation was conducted in this example. Polynomial chaos of order 3 was performed with $2P$ points from a Sobol' sequence as the DoE. Figure 4.13 presents normalized histograms obtained by MC and PC of order 3 for two QoI, which shows that PC constructed in this way produces good predictions.

Table 4.5 shows the total Sobol' indices obtained by use of PC coefficients for two QoIs. The uncertainty of p_{ia} has the greatest influence on the variance of the QoIs, whereas the uncertainty of k_{aw} has a negligible one. Figure 4.14 presents scatter plots obtained for model 3a by the PC method. The influence of p_{ia} and lack thereof of k_{aw} are also visible in these graphs.

The results imply that a more detailed study should be performed on intraabdominal pressure in humans. Although the coefficient of variation of k_f was the highest, the significance of k_f variation was much lower than that of p_{ia} so the number of variables in such a study could be reduced to one, namely p_{ia}.

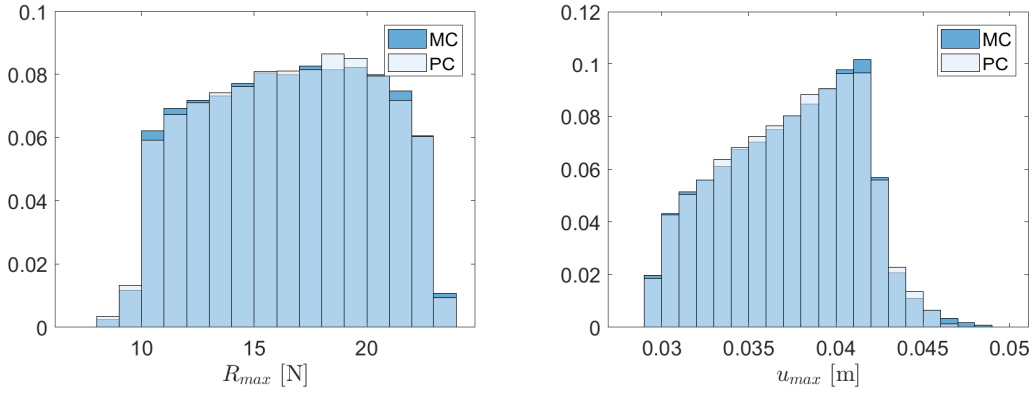

(A) R_{max} (B) u_{max}

FIGURE 4.13: Normalized histograms obtained by MC and PC methods for two considered quantities of interest (R_{max} and u_{max}) in the case of model 3a

Quantity of interest	R_{max}	u_{max}
p_{ia}	0.9503	0.9222
k_f	0.0514	0.0781
k_{aw}	0.0013	0.0011

TABLE 4.5: S^{Tot} obtained by PC for model 3a

4.3.3 Model of membrane subjected to pressure with fixation imperfections

4.3.3.1 Model

Imperfections in fixing can be investigated by using a probabilistic approach. For example, geometric imperfections of shell structures were described by random fields [12, 58, 183, 183]. Here imperfections in discrete fasteners position are covered.

Let the position of the supports referred to their ideal placement be a random variable accounting for the possible imperfection in fixation of the implant under laparoscopic conditions. It is assumed that position of three supports varies (Figure 4.15), which will disturb symmetry. Six independent normal random variables are assumed $\mathbf{X} = [r_1, r_2, r_3, \theta_1, \theta_2, \theta_3]^\top$: the first three describing the radial change $r_i \sim \mathcal{N}(0, 6.4)$ [mm] and the next three the angular change $\delta_i \sim \mathcal{N}(0, 0.08)$, where $i = 1, 2, 3$ is the support number. The quantities of interest are the same as in the model 3a (R_{max} and u_{max}).

In this example, $k_{aw} = 2.775$ MPa (value after [105]), $k_f = 1500$ N/m and $p_{ia} = 11132.4$ Pa. The orientation direction of orthotropic material model is presented in Figure 4.15 ($\alpha_{orient} = 0$).

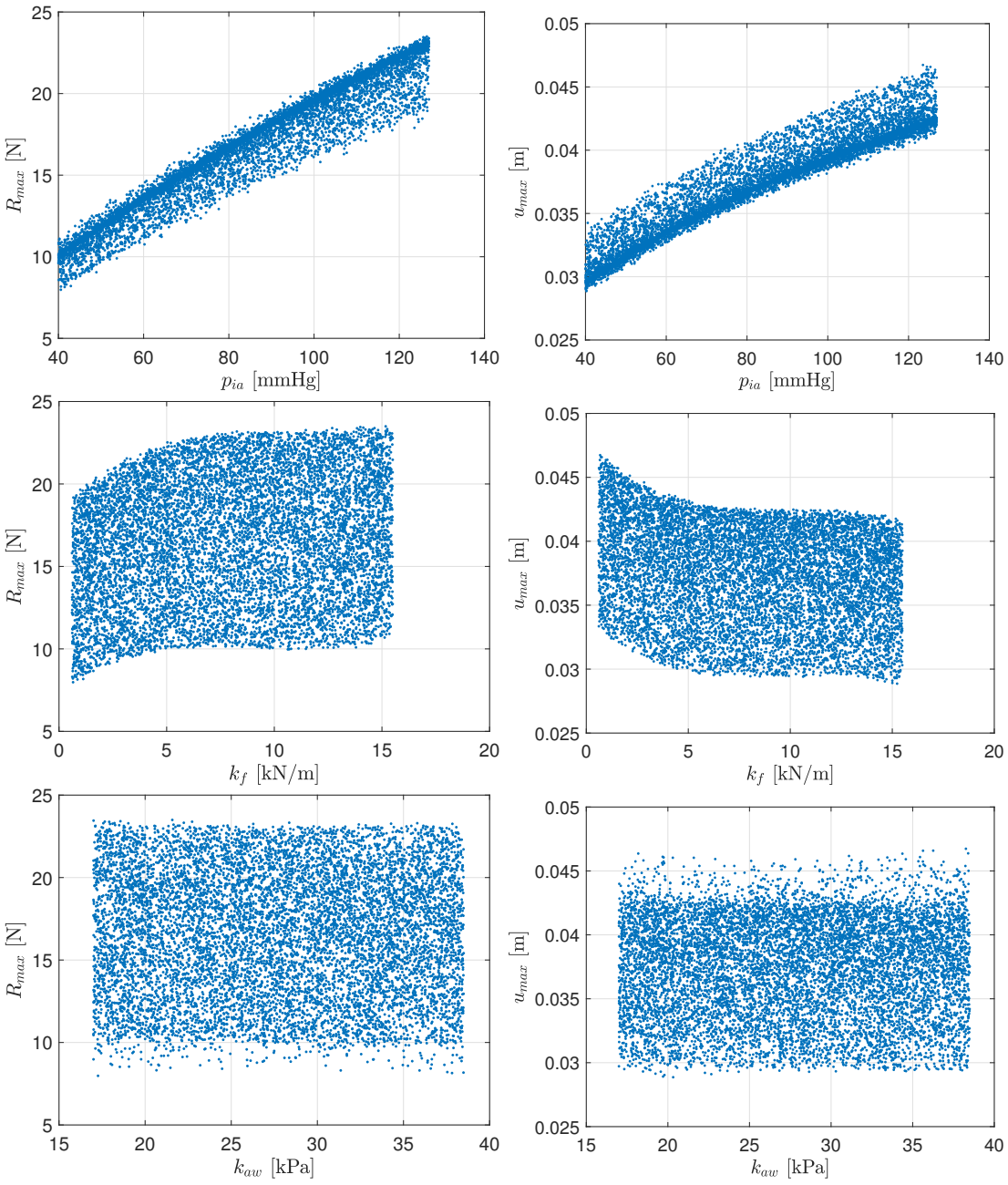

FIGURE 4.14: Scatter plots of model 3a obtained by PC

4.3.3.2 Results

Sobol' sequence points are used to construct the DoE in this model. $(M-1)P$ regression points were chosen.

MC was not performed here because of the high computational cost. Nevertheless in order to estimate the accuracy of the PC metamodel, 100 additional points were taken from a Sobol' sequence to compare their exact solution with the PC prediction. Figure 4.16 shows the normalized root mean square error, $NRMSE$, (3.6) calculated at these

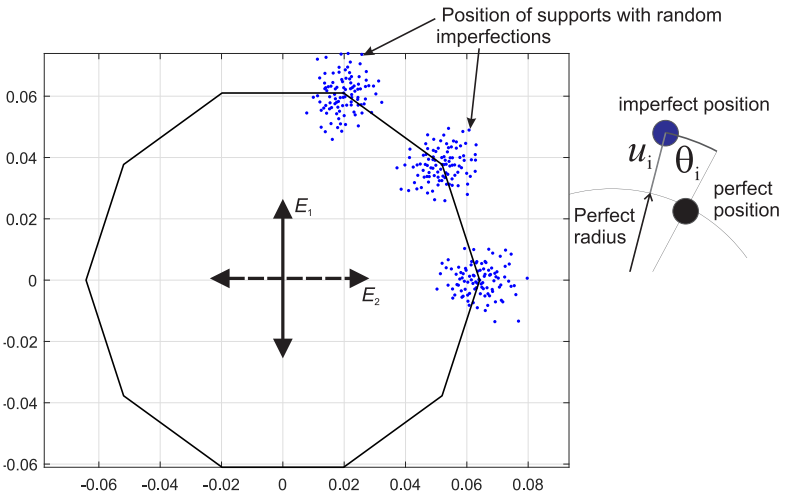

FIGURE 4.15: Scheme of imperfections in model 3b

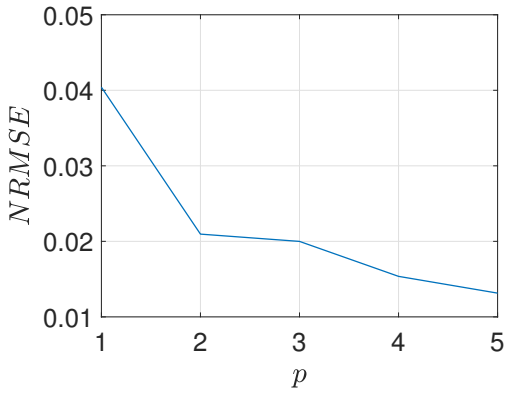

FIGURE 4.16: NRMSE of PC metamodel of R_{max} of order p obtained for 100 extra points for verification purposes, model 3b

additional points. It can been seen to decrease with polynomial order p. Small differences in the values of the mean, standard deviation and 95th percentile of the QoIs (Figure 4.17) with change of order can be seen for $p \geq 2$. There are no significant differences between solutions of S^{Tot} when the QoI is u_{max} (Figure 4.19). The situation is different in the case of the total sensitivity indices of R_{max} as the QoI (Figure 4.18), where a greater difference between results obtained for different PC orders can be observed, especially for the first variable (S_1^{Tot}) although by the 4th and 5th orders the relative difference between values of S_i^{Tot} obtained is already low ($< 3\%$).

Figure 4.20 shows scatter plots obtained for R_{max} generated with points from a Sobol' sequence. The higher sensitivity to ξ_4 (the angular change of the placement of the first support) can be seen, which is confirmed by total Sobol' indices (Figure 4.18). ξ_1 is the second variable in terms of significance. Owing to the orientation of the stiffer direction of the implant, greater importance of the ξ_i positions is expected. The angular change

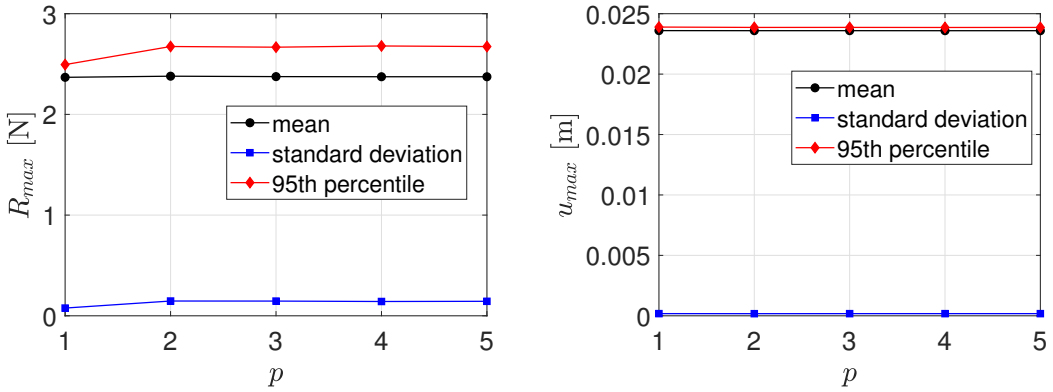

FIGURE 4.17: Mean, standard deviation and 95th percentile of R_{max} and u_{max} obtained by PC of order p, model 3b

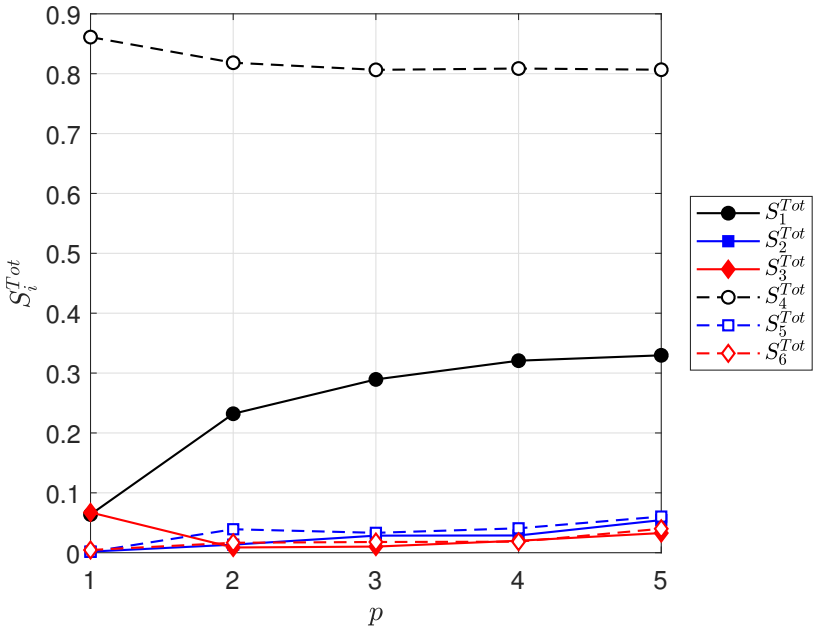

FIGURE 4.18: Total sensitivity indices of R_{max} obtained by PC of order p, model 3b

has a higher impact on R_{max} and u_{max}. For the case of implant orientation considered, imperfections of the second and third fastener have negligible influence on the outcome.

It is interesting to note the large influence in this example of mixed PC terms. The sum of all total indices $\sum_{i=1}^{M} S_i^{tot} = 1.3240$ (in the case of $p = 5$) indicates quite high levels of interaction. Figure 4.21 shows the comparison between total and first order partial Sobol' indices of the two most influential variables (1 and 4) where R_{max} is the QoI. Such large differences between first order and total indices do not appear when u_{max} is the QoI (Figure 4.22). In the case of u_{max} the influence of mixed terms is small as seen from the fact that the sum of total indices barely exceeds 1 ($\sum_{i=1}^{M} S_i^{tot} = 1.0466$ in case of $p = 5$).

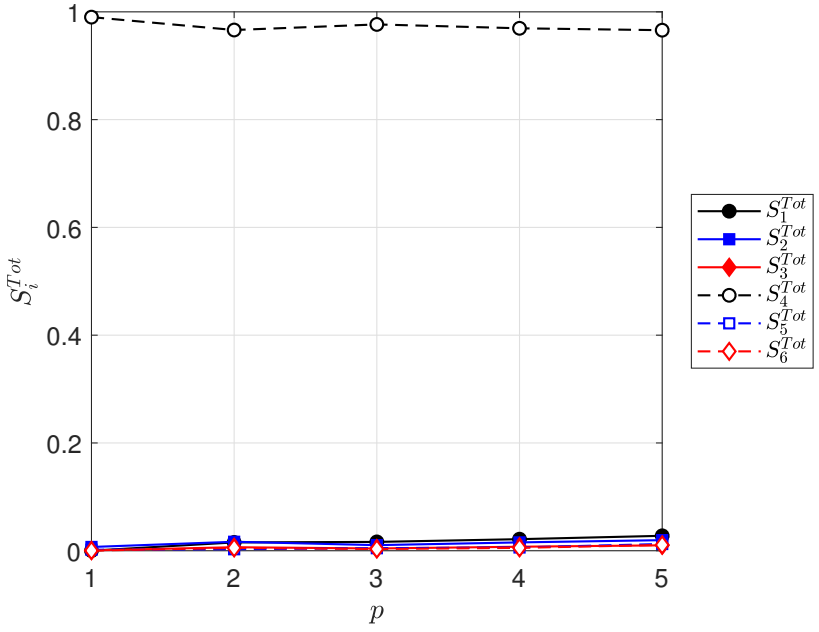

FIGURE 4.19: Total sensitivity indices of u_{max} obtained by PC of order p, model 3b

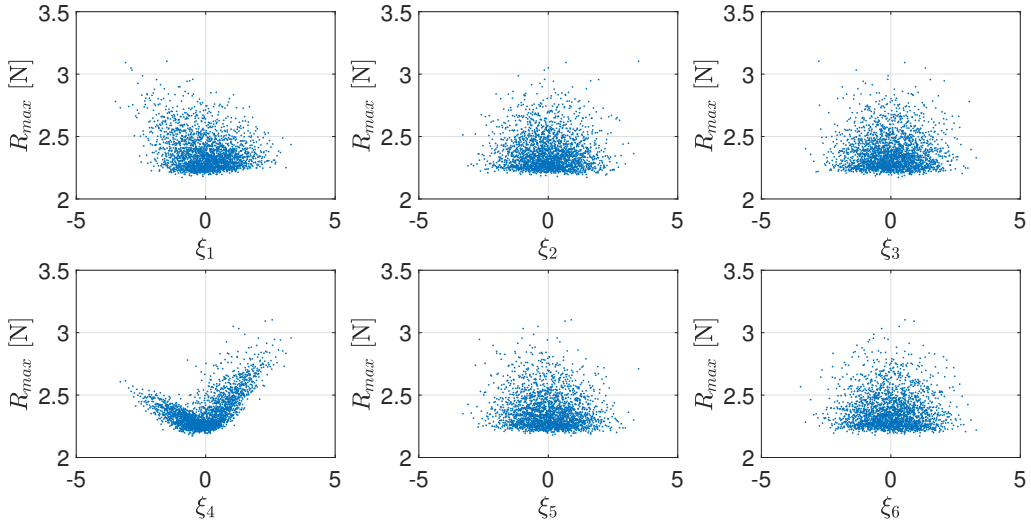

FIGURE 4.20: Scatter plots of R_{max} versus standard random variables in model 3b

The relative standard deviations obtained in models of the system subjected to intraabdominal pressure are presented in Table 4.6. It can be seen that the variation of the QoI for model 3b, the case of imperfections, is low when compared to variation of the QoI caused by the variation of variables considered in the model 3a.

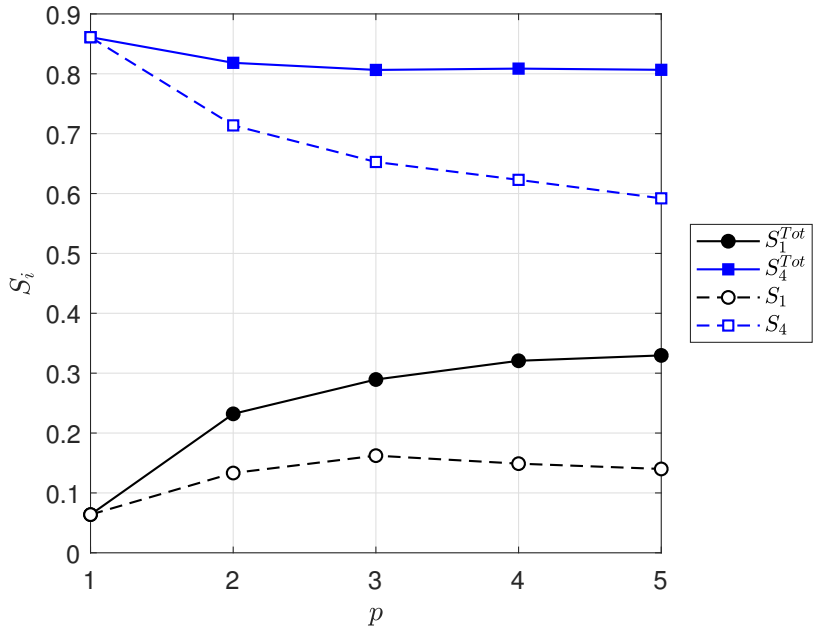

FIGURE 4.21: Total sensitivity indices and first order partial sensitivity indices e of R_{max} obtained by PC of order p, model 3b

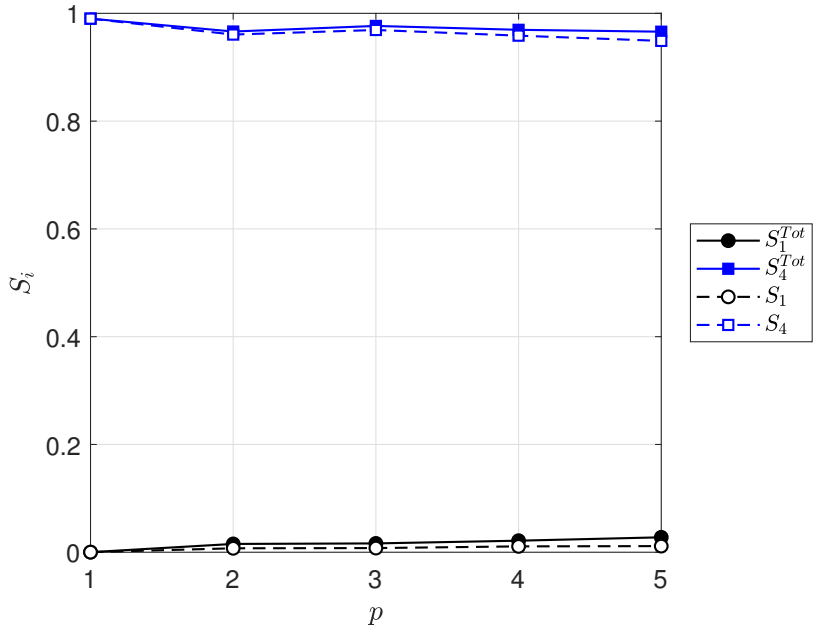

FIGURE 4.22: Total sensitivity indices and first order partial sensitivity indices e of u_{max} obtained by PC of order p, model 3b

	R_{max}	u_{max}
model 3a	0.2234	0.1023
model 3b	0.0614	0.0075

TABLE 4.6: Relative standard deviation of R_{max} and u_{max} in models 3a and 3b

4.4 Membrane model of abdominal wall with implant

4.4.1 Model

Two global FE models of the abdominal wall are considered:

- healthy abdominal wall,
- abdominal wall with hernia repaired with implant.

The geometry of the healthy abdominal wall is taken from the study [169]. Figure 4.23a presents the FE mesh. The model is composed of quadrilateral four-node isoparametric membrane elements. Prediction of abdominal behaviour obtained by the model was compared with displacements of real human abdominal wall acquired in *in vivo* tests and presented in [109].

The thickness of abdominal wall is 3 cm. Translation of the nodes on the edge of the model is fixed. The abdominal wall is subjected to intraabdominal pressure p_{ia}. The material model is taken as linear orthotropic [153]. The model is divided into three zones with different orientations of the material (Figure 4.23b):

- the middle area corresponds to the area of linea alba, rectus abdominis muscle and rectus sheath, where first direction of the material is transverse to the abdominal wall;
- two lateral zones corresponds to the lateral muscles on each side with orientations $\pm\alpha_{aw}$.

The model of the abdominal wall with a hernia repaired with an implant (Figure 4.24) is based on the model of healthy abdominal wall. A hernia orifice was created (Figure 4.24a) and the implant was added (Figure 4.24b) as a membrane structure with the same properties as in the local model 2. The stiffer direction of the implant is in the transverse direction of abdominal wall.

The elasticity moduli of the abdominal wall E_1^{aw}, E_2^{aw} and G_{12}^{aw} and the value of the intraabdominal pressure p_{ia} are assumed to be independent uniform random variables (Table 4.7). The ranges of the distribution are based on a literature study: E_1^{aw} and E_2^{aw} on [153], G_{12}^{aw} on [177] and p_{ia} on [33]. Since the orientation of the composite of lateral muscles and their aponeuroses with different arrangement of fibres is not clear, α_{aw} is assumed to be a uniform random variable as well.

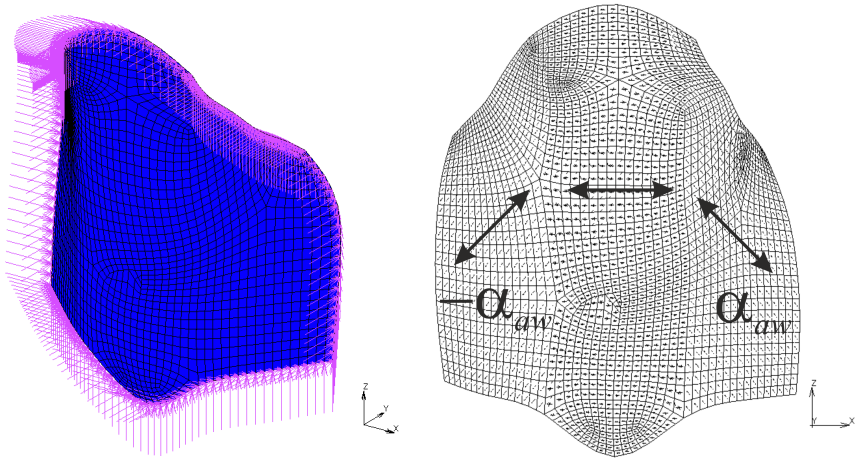

(A) FE model of a healthy abdominal wall 4 with boundary condition

(B) Orientation of material in the described areas of abdominal wall

FIGURE 4.23: FE model of healthy abdominal wall (model 4)

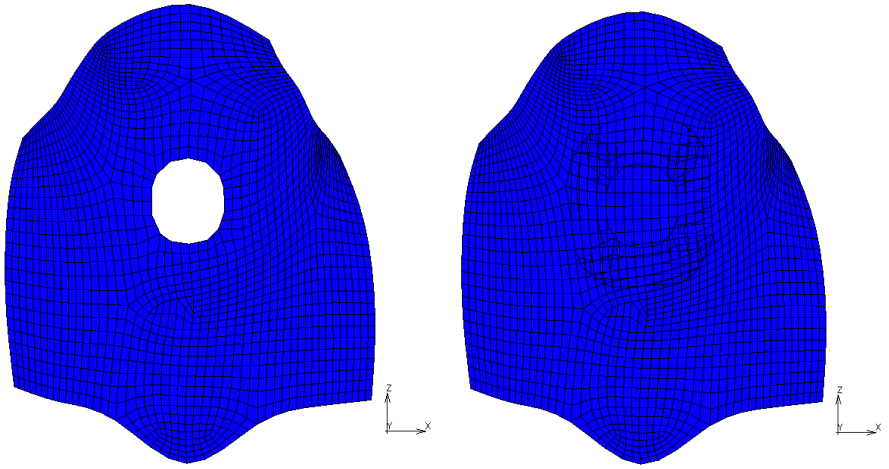

(A) Abdominal wall with hernia

(B) Hernia covered by implant

FIGURE 4.24: FE model of herniated abdominal wall (model 4)

Variable	a	b
E_1^{aw} [Pa]	22000	64000
E_2^{aw} [Pa]	16000	29000
G_{12}^{aw} [Pa]	3000	40000
p_{ia} [Pa]	4800	18625
α_{aw}	0	π

TABLE 4.7: Limits of uniform distribution $\mathcal{U}(a, b)$ for each of the independent variables in model 4

QoI	Variable				
	E_1^{aw}	E_2^{aw}	G_{12}^{aw}	p_{ia}	α_{aw}
	1	2	3	4	5
u_{aw}	0.0756	0.0527	0.0573	0.7534	0.0979
u_i	0.0493	0.0507	0.0795	0.7282	0.1413
$u_{aw} - u_i$	0.5493	0.0507	0.0353	0.3293	0.0786

TABLE 4.8: Total Sobol's indices S_i^{Tot} for different QoI, $p = 3$, model 4

In the ideal case, the behaviour of the repaired abdominal wall should be the same as that of a healthy one. The quantity of interest in the case of this model is the difference between the displacements of the centre of the implant u_i and the corresponding point in the healthy abdominal wall u_{aw}.

4.4.2 Results

PC metamodels were created with $(M-1)P$ Sobol' sequence points as the DoE. The MC simulation was not performed in this case owing to the high computational cost caused by the necessity of computing two models. In order to evaluate PC accuracy, PC metamodels were created with different orders p. As in model 3b, the models were computed for 100 extra points from a Sobol' sequence and the exact value of the QoI was compared with the PC prediction. Figure 4.25a shows the normalized root mean square error, $NRMSE$, (3.6) obtained for different orders for three QoI: the main QoI $u_{aw} - u_i$ and additionally u_{aw} and u_i. PC estimation of the mean, standard deviation and 95th percentile hardly change with order p (Figure 4.25b). Differences between sensitivity indices obtained for different orders become relatively small for order $p > 2$. Therefore PC order 3 has been chosen for the remaining results.

The total Sobol' indices S_i^{Tot} are presented in Table 4.8 for the main QoI ($u_{aw} - u_i$) and additionally for the displacements u_{aw} and u_i. It can be seen that similarly to the case of model 3a, the uncertainty of p_{ia} has the greatest influence on the uncertainty of the displacement of the centre of the implant u_i. However, when the difference between displacements on healthy and repaired abdominal walls is considered as the QoI, E_1^{aw} becomes the most influential variable. The influence of other material parameters is much smaller and can be considered negligible. p_{ia} is in second place in terms of the global sensitivity index. Despite the very wide input variation of α_{aw} in the case of the investigated model, this variable is not important compared to the most significant factors. Similar conclusions can be made based on scatter plots performed for 1000 points of a Sobol' sequence (Figure 4.26).

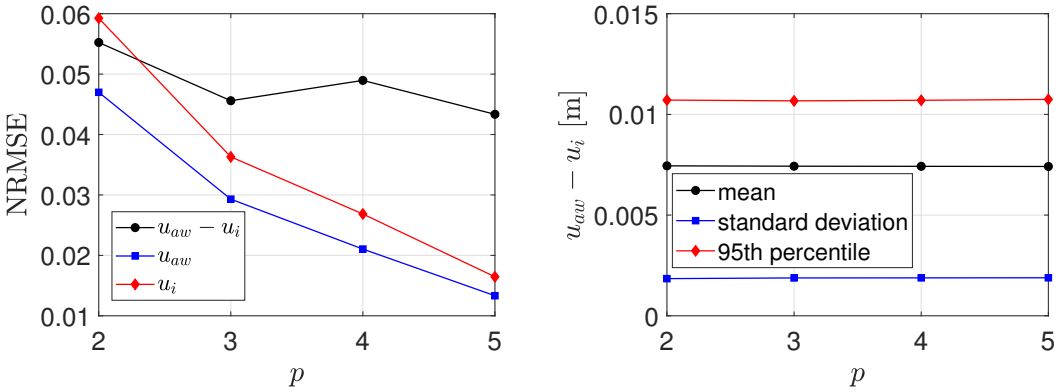

(A) $NRMSE$ obtained for 100 extra validation points

(B) Mean, standard deviation and 95th percentile

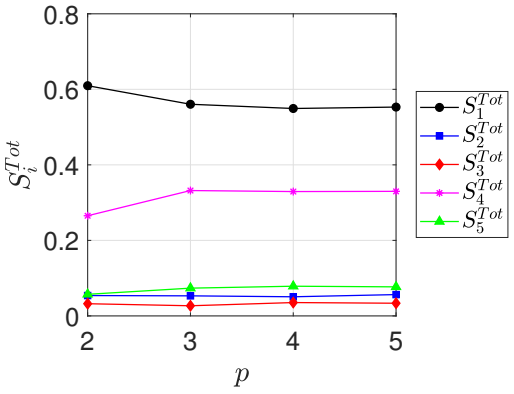

(C) Total sensitivity indices

FIGURE 4.25: PC results for different order p, model 4

The relative standard deviation of $u_{aw} - u_i$ is equal to 25%. Figure 4.27 shows the histogram of $u_{aw} - u_i$ for the point selected in the study. For this implant material, $u_{aw} - u_i$ is relatively low (the maximum obtained value is 0.0145m). This material has already been shown to have satisfactory compatibility with the abdominal wall in terms of stiffness [106] according to an evaluation based on reaction forces in local model 2.

4.5 Civil engineering application: corner joints in historic log houses

4.5.1 Background

Methods of uncertainty propagation and global sensitivity analysis can also be useful in civil engineering problems. The study addresses the topic of timber joints used in log houses and is partially included in a research paper [95].

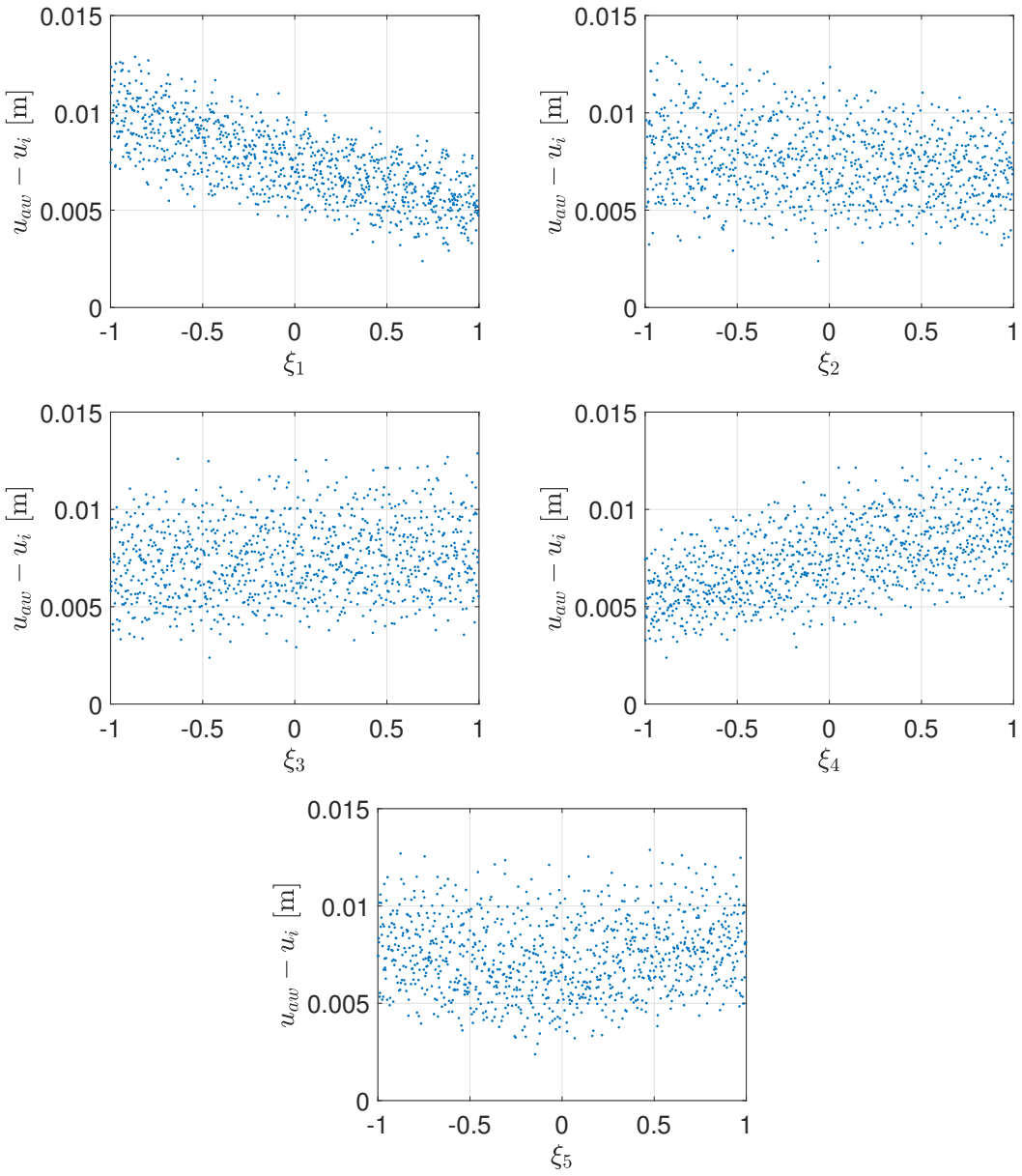

FIGURE 4.26: Scatter plots of model 4 of standardize variables ξ_i

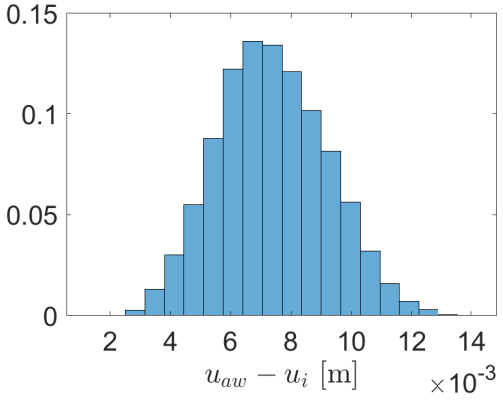

FIGURE 4.27: Histogram of $u_{aw} - u_i$ [m]

In the past, wood was a commonly used construction material owing to its good mechanical properties, high availability and convenience. Log houses were a typical construction in many regions of Europe and beyond. They were usually built not by professionals but by the owners themselves with the help of neighbours. Building traditions were typically transmitted orally to the next generations and written documentation is nowadays hard to come by [92].

One of the main issues in the construction of these buildings is the joints which connect the elements into one structure and ensure the transfer of forces. Many types and variants of joints have evolved over centuries. Some of them are quite complicated and currently it is not clear what was the motivation of such modifications [32]. Employing mechanics can help to satisfy curiosity as to which solutions are the most effective, and what is more, assist conservation works. These days many historical log buildings require renovation or reinforcement. Some of them have been acknowledged as an important part of cultural heritage which should be preserved. Therefore, analysis of timber joints is necessary in order to support the proper conservation of these kinds of buildings.

Some guidelines to assess historic timber structures have already been proposed [39]. The majority of research, both experimental [125] and numerical [180], on joints in timber structures has been focused on roof trusses. However, some experimental and numerical studies on the behaviour of log walls and corner joints have also been performed [9, 62]. The distribution of stresses in corner joints of historic log buildings was studied by [95, 119].

Wood is a natural material, a consequence of which is the high variability of its mechanical properties. They are known to depend on moisture, temperature and age [128]. What is more, wood defects like knots etc. and defects related to fungi or insects increase heterogeneity of the material [39, 123]. The properties of the material are one of the sources of uncertainty in the modelling and design of timber structures. In order to investigate these uncertainties, a probabilistic method has been employed in the design of timber structures and the analysis of robustness [155] and reliability [19]. MC is also an ideal non-intrusive method in this application [19]. PC and the perturbation method have been employed in an application concerned with laminated timber in order to facilitate cost reduction. [88]. Sobol' indices have been calculated to measure the importance of micromechanical parameters for macroscopic properties of wood [76] with the use of a Gaussian process emulator in order to reduce computational cost.

This study is focused on two widely-used historical joints which are typical in southern Poland and western Ukraine: short-corner dovetail (Figure 4.28a) and saddle notch (Figure 4.28b). The aim of this section is to supplement the stress distribution analysis that

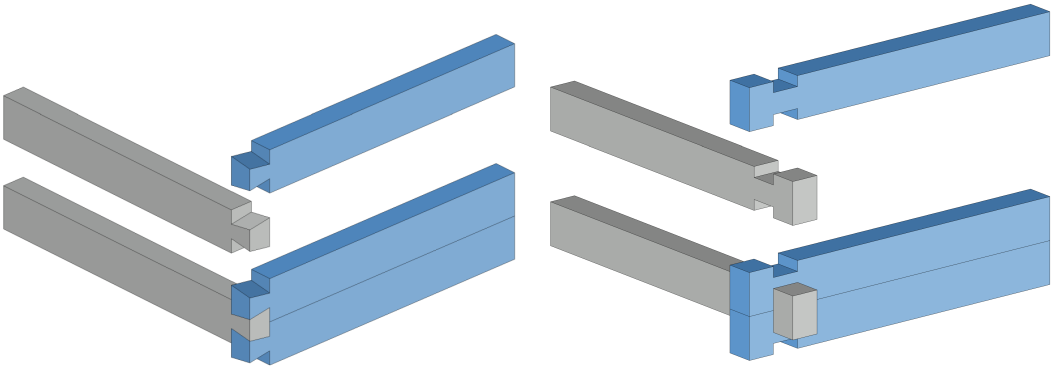

(A) Short-corner dovetail joint (B) Saddle notch joint

FIGURE 4.28: Log carpentry joints

has already been carried out for historic corner joints [95] with a stochastic framework in order to examine uncertainties and study their influence on the mechanical response.

4.5.2 Model

4.5.2.1 Deterministic FE models

The FE models are taken from [95, 119]. The geometry of the joints was at scale 1:2 to be compatible with planned experimental works with joints at this scale. The length of the logs is 1000 mm in the case of dovetail joints and 1075 mm in the case of the saddle notch because of protrusions. The cross-sectional dimensions of a single log are 75x135 mm.

The model is created with the MSC.Marc commercial FE system. The models are built of 4-node linear isoparametric 3-dimensional tetrahedral elements. The dovetail model is composed of 60 847 and the saddle notch of 100 997 elements, respectively. The mesh is finer in the connection area than in the rest of logs (Figure 4.29). The assumed boundary conditions are presented in Figure 4.30. The joint is subjected to forced displacement of 0.05 m in the X direction on the surface marked by the pink colour. Contact is introduced between the logs.

It is assumed that joints are made from pinewood, which is a widely-used material. An orthotropic material model was assumed. The material properties of pinewood in relation to E_L are based on [61] and presented in Table 4.9, where the subscript R denotes the radial, T tangential and L longitudinal direction. E_L was determined in [95, 118] by 4-point bending test of pinewood samples.

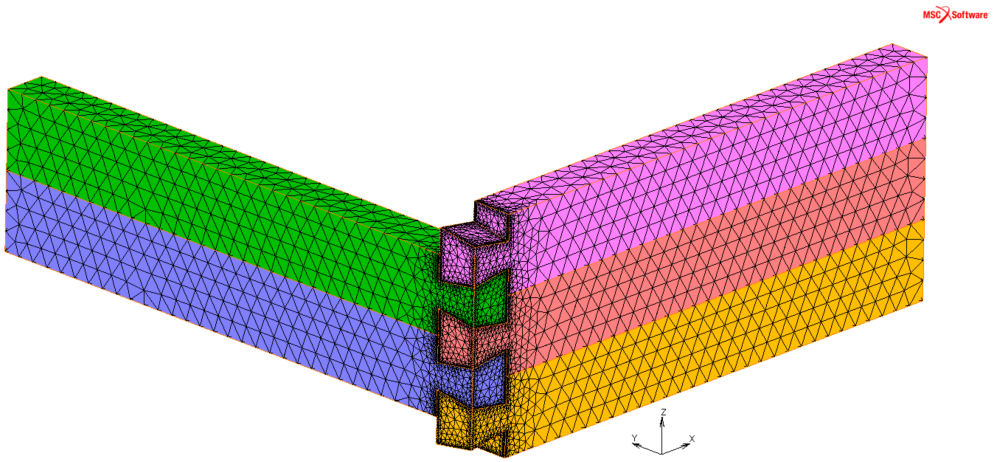

(A) Short-corner dovetail joint model

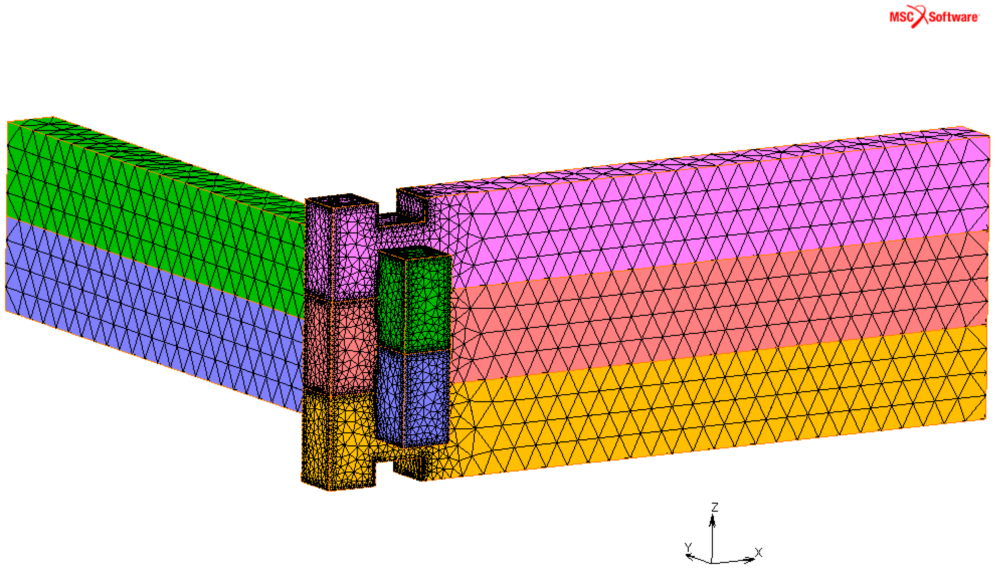

(B) Saddle notch connection model

FIGURE 4.29: FE meshes of carpentry joint models

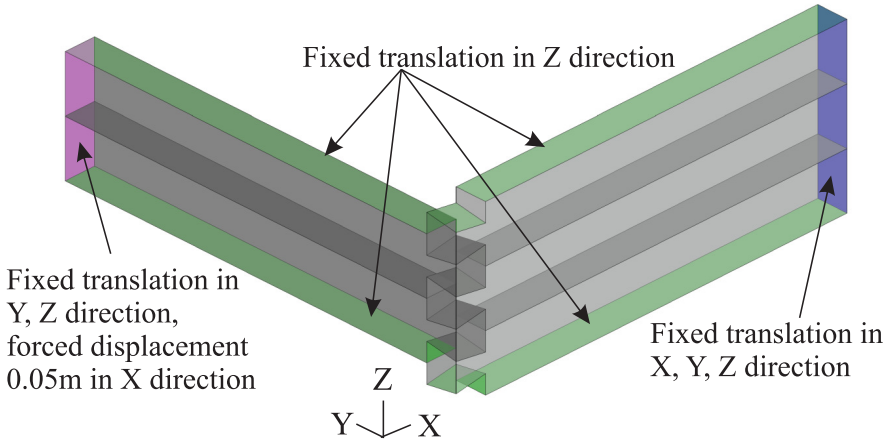

FIGURE 4.30: Assumed boundary conditions in carpentry joints models

E_T/E_L	E_R/E_L	G_{RT}/E_L	G_{TL}/E_L	G_{LR}/E_L	ν_{RT}	ν_{TL}	ν_{LR}
0.068	0.102	0.005	0.046	0.049	0.469	0.024	0.316

TABLE 4.9: Material parameters of pinewood [61]

4.5.2.2 Random variables

Owing to the variability of properties of the natural material – wood – E_L is assumed to be a lognormally distributed variable following the recommendations of [83]. The parameters of the distribution were obtained with the probability distribution fitter toolbox in MATLAB. Two cases of the variability of E_L are considered:

A – lognormal distribution fitted to the pinewood data presented in [118].
$E_L^A \sim \mathcal{LN}(23.01, 0.290)$;

B – lognormal distribution fitted only to data taken from dry samples of pinewood [95] which leads to a narrower range of humidity when compared to **A** and consequently lower variation of $E_L^B \sim \mathcal{LN}(23.18, 0.23)$.

A second variable is related to the uncertainty of the coefficient of friction μ_{cj}. The coefficient of friction between timber elements depends on humidity, roughness, wood grain, age etc. [117, 127, 187]. Values of μ_{cj} reported in the literature for wood-on-wood friction differ significantly and what is more, the coefficient of friction is not only material- but also system- depenent [17]. Grossi et al. [62] investigated friction in corner joints with very similar geometry made from hard wood and showed the high influence of the tolerance of mounting e.g. initial gaps. The coefficient of friction μ_{cj} is assumed to be a uniform random variable $\mu_{cj} \sim \mathcal{U}([0.1, 0.7])$.

To sum up, two random variables are considered in two variants

(A) $\mathbf{X} = [E_L^A, \mu_{cj}]^\top$;

(B) $\mathbf{X} = [E_L^B, \mu_{cj}]^\top$.

4.5.2.3 Quantity of interest

Attention is focused on the principal stresses. In each type of joint, areas of high maximum and minimum principal stress are found (Figure 4.31). More about stress distrbution in the types of joints considered can be found in [95]. n_{max} and n_{min} chosen elements (Figures 4.32 and 4.33) from these areas are assigned to sets I_{max} and I_{min},

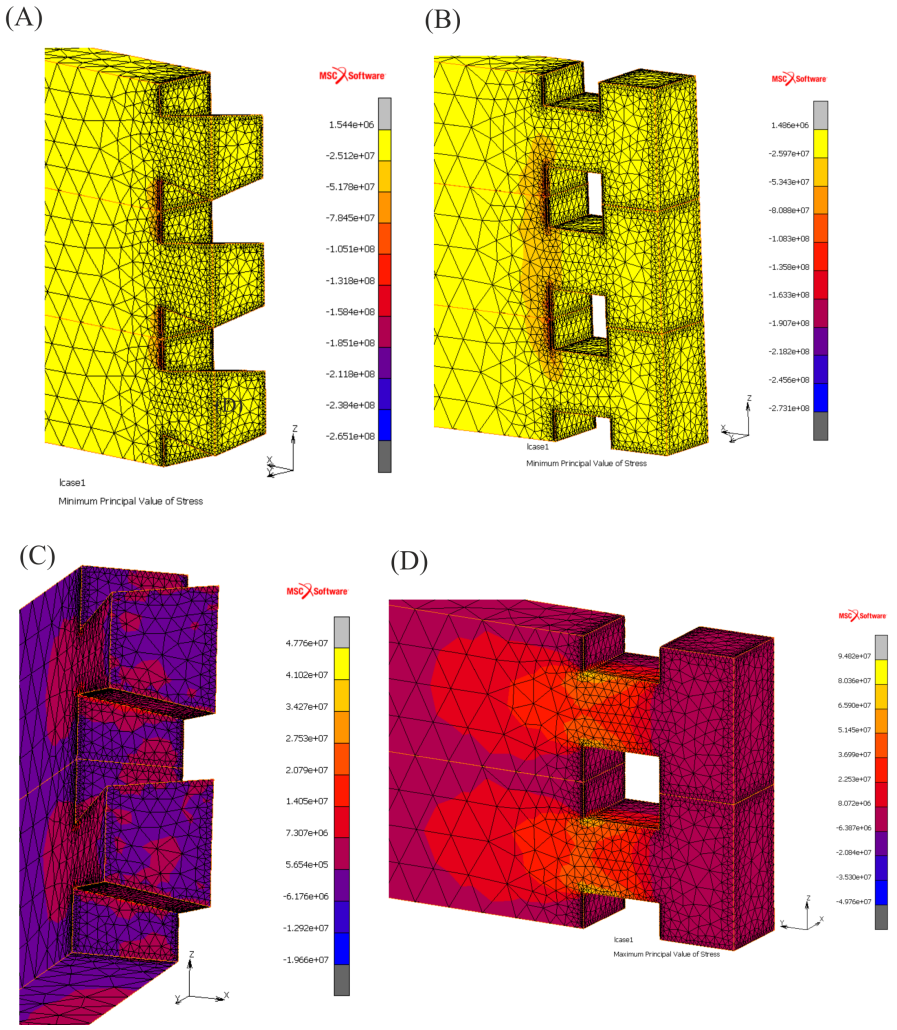

FIGURE 4.31: Areas of high principal stresses in the carpentry joint models (A) σ_{min} in dovetail joint, (B) σ_{min} in saddle notch connection, (C) σ_{max} in dovetail joint, (D) σ_{min} in saddle notch joint

respectively. The chosen quantities of interest are the mean values of the maximum and minimum principal stresses in these elements :

$$\bar{\sigma}_{max} = \frac{1}{n_{max}} \sum_{i=1}^{n_{max}} \sigma^i_{\max}, \tag{4.6}$$

$$\bar{\sigma}_{min} = \frac{1}{n_{min}} \sum_{i=1}^{n_{min}} \sigma^i_{\min}, \tag{4.7}$$

where $\sigma^i_{\max}$ and $\sigma^i_{\min}$ are the values of the maximum and minimum principal stress at the integration point of the i-th element from the I_{max} and I_{min} sets.

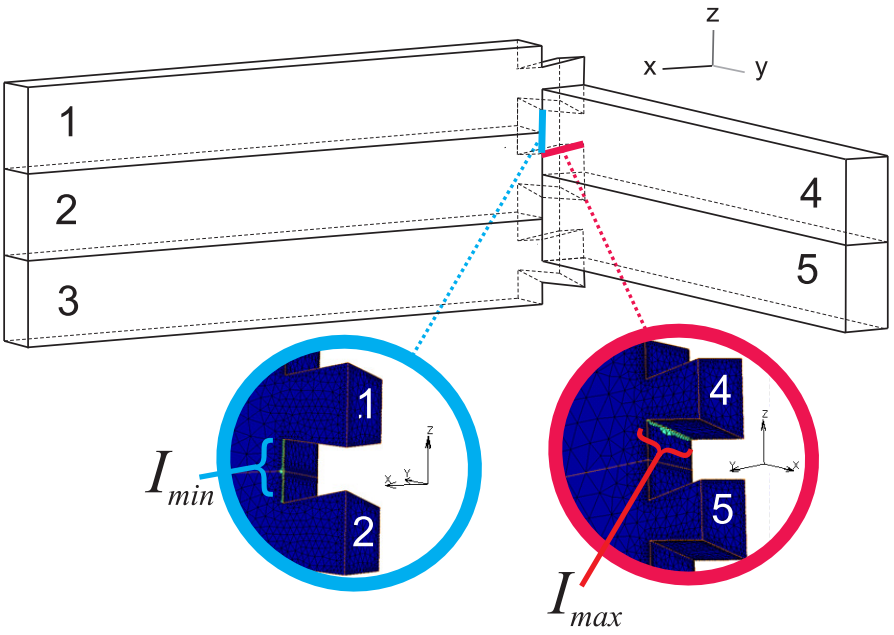

FIGURE 4.32: Elements considered in short-corner dovetail joint

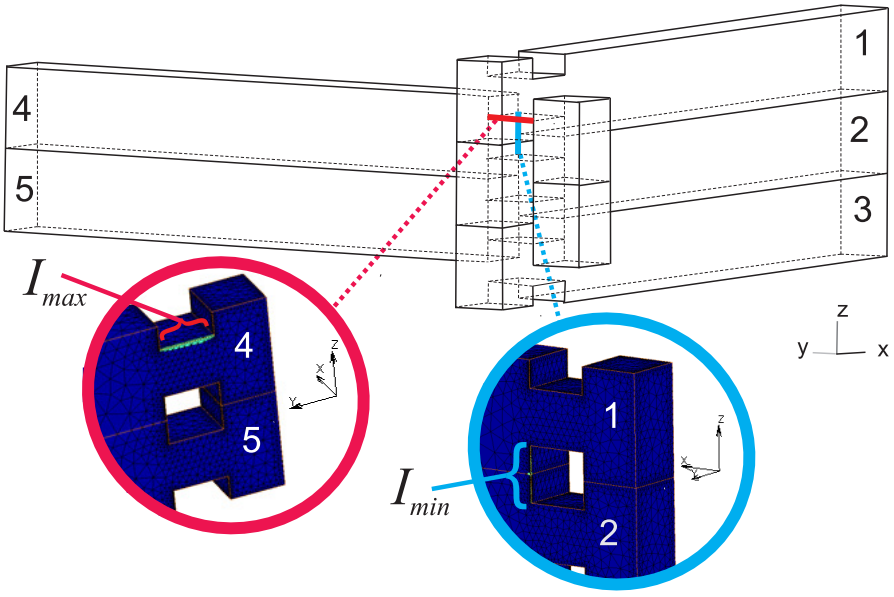

FIGURE 4.33: Elements considered in saddle notch joint

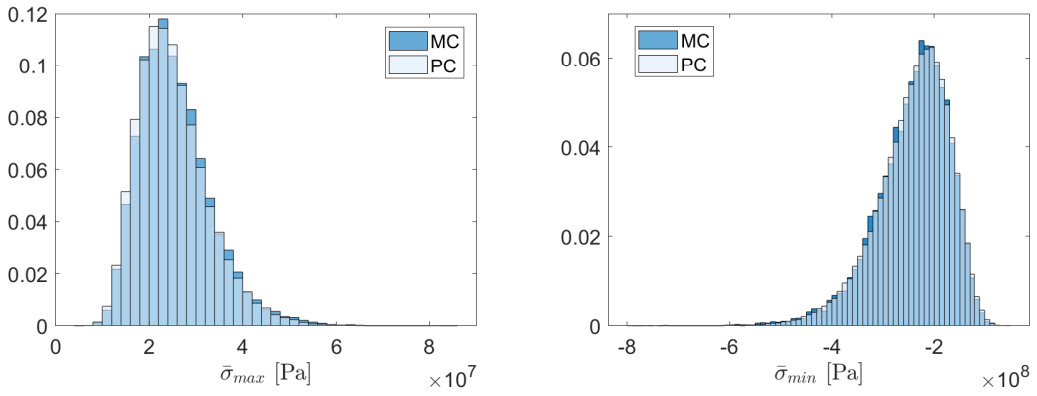

FIGURE 4.34: Normalized histograms of $\bar{\sigma}_{min}$ and $\bar{\sigma}_{min}$ obtained by MC and PC of order 3 in dovetail connection model in variant A

Additionally, some results are also presented for the extreme values of the principal stresses in the areas considered:

$$\max \sigma_{max} = \max_{i \in I_{max}} \sigma^i_{max} \tag{4.8}$$

$$\min \sigma_{min} = \min_{i \in I_{min}} \sigma^i_{min} \tag{4.9}$$

PC is employed to propagate uncertainties and compute Sobol' indices in the models of timber joints. D-optimal selection from set of random candidate points (method M4) was chosen as the DoE. This was based on its efficiency in the example of the implant membrane model with a low number of random variables. The PC order $p = 3$ and $2P = 20$ regression points were used. Nevertheless, since efficiency of DoE in PC is problem-dependent, the accuracy of PC of this order is checked against the MC solution in one of the cases (variant A, dovetail joint). However, 10^4 points were used in MC because 10^5 would be intractable for sensitivity analysis. Scatter plots are also used to confirm the evaluation of the random variables' importance.

4.5.3 Results

4.5.3.1 Variant A

MC was performed for the model of the dovetail joint. Figure 4.34 shows the comparison of histograms of $\bar{\sigma}_{max}$ and $\bar{\sigma}_{min}$ obtained by MC and PC of order 3. Table 4.10 contains the statistics of these distribution. $Err_{\%}$ between the reference MC solution and PC result is very low ($< 1\%$).

V	MC [Pa]		PC [Pa]		$Err_{\%}$ [%]	
	$\bar{\sigma}_{max}$	$\bar{\sigma}_{min}$	$\bar{\sigma}_{max}$	$\bar{\sigma}_{min}$	$\bar{\sigma}_{max}$	$\bar{\sigma}_{min}$
mean	2.51E+07	-2.41E+08	2.51E+07	-2.41E+08	0.12	0.01
standard deviation	7.58E+06	7.17E+07	7.58E+06	7.17E+07	0.00	0.06
95th percentile	3.92E+07	-1.44E+08	3.91E+07	-1.43E+08	0.15	0.24
5th percentile	1.48E+07	-3.73E+08	1.48E+07	-3.75E+08	0.14	0.40

TABLE 4.10: Statistics of $\bar{\sigma}_{max}$ and $\bar{\sigma}_{min}$ in model of dovetail joint in variant A obtained by MC and PC of order 3 and the relative difference between them $Err_{\%}$

Method	Variable	$\bar{\sigma}_{max}$	$\bar{\sigma}_{min}$	$\max \sigma_{max}$	$\min \sigma_{min}$
MC	E_L	1.0174	1.0494	0.8514	1.055
	μ_{cj}	0.0538	0.0075	0.2388	0.0032
PC	E_L	0.96	0.9907	0.8112	0.9956
	μ_{cj}	0.0416	0.01	0.2083	0.005

TABLE 4.11: S_i^{Tot} obtained by MC and PC order 3 for different quantities of interest for dovetail connection model in variant A

	$\bar{\sigma}_{max}$	$\bar{\sigma}_{min}$	$\max \sigma_{max}$	$\min \sigma_{min}$
E_L	0.9998	0.9929	0.9909	0.9994
μ_{cj}	0.0002	0.0076	0.0101	0.0007

TABLE 4.12: Total sensitivity indices S_i^{Tot} obtained for different QoI by PC in the model of the saddle notch joint in variant A

Table 4.11 presents total sensitivity indices S_i^{Tot} obtained by MC and PC of order 3 for different quantities of interest in the case of the dovetail joint model in variant A. Indices obtained by both methods indicate that sensitivity of all QoI to the variation of E_L is much higher than to the variation of μ_{cj}. Only in case of $\max \sigma_{max}$ do both methods show a non-negligible effect of μ_{cj}.

Figure 4.35 shows scatter plots of the variables considered against quantities of interest based on MC solution. The shapes of the plots confirm higher sensitivity to E_L uncertainty than to that of μ_{cj} and slightly higher influence of μ_{cj} variation on $\max \sigma_{max}$ than on other QoI.

PC of the same order ($p = 3$) and the same DoE was used in the approximation of the response of the saddle notch joint. Figure 4.36 shows the comparison of distributions obtained for 2 types of connection. Sensitivity indices related to the variation of μ_{cj} are negligibly small for all considered QoI (Table 4.12).

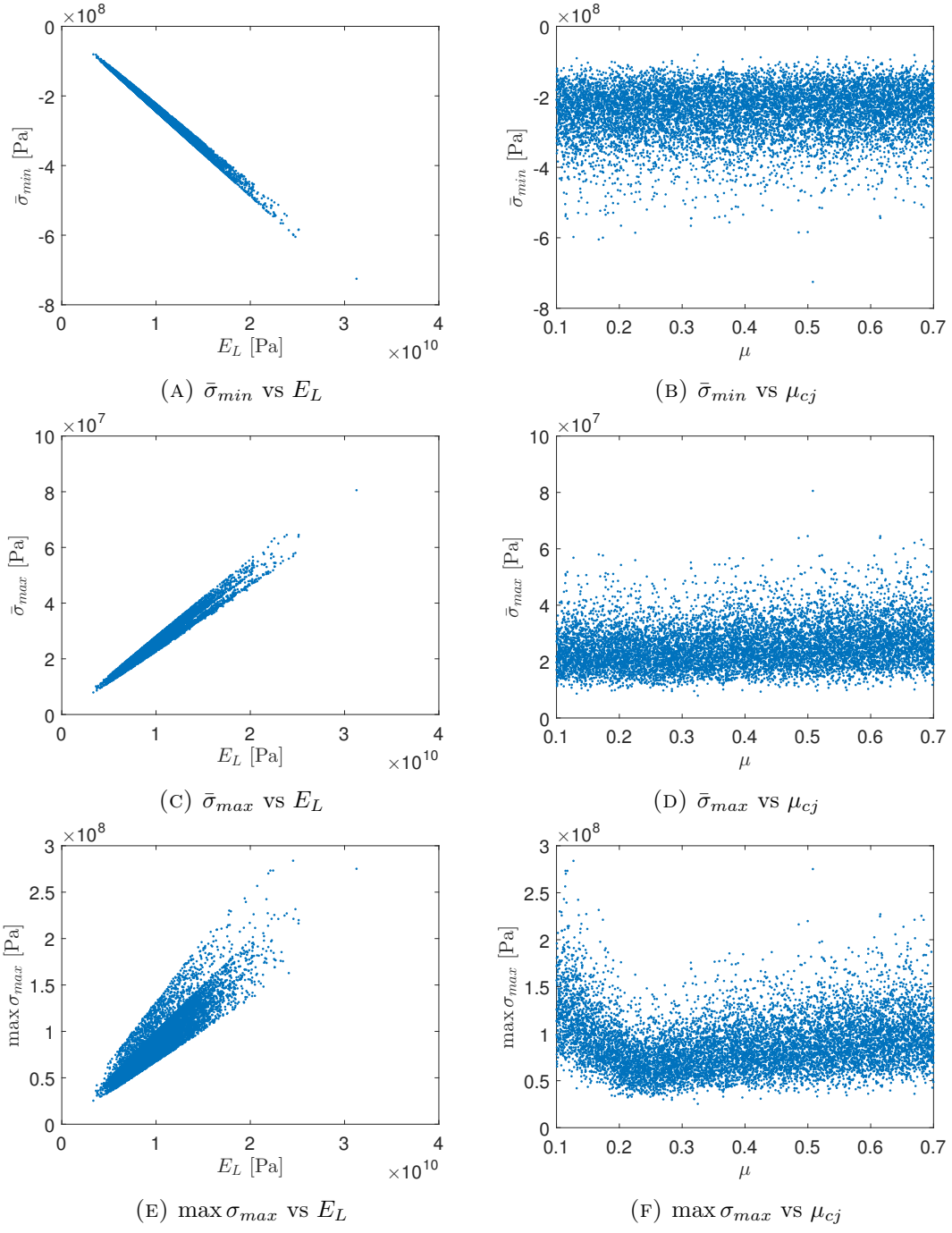

(A) $\bar{\sigma}_{min}$ vs E_L

(B) $\bar{\sigma}_{min}$ vs μ_{cj}

(C) $\bar{\sigma}_{max}$ vs E_L

(D) $\bar{\sigma}_{max}$ vs μ_{cj}

(E) $\max \sigma_{max}$ vs E_L

(F) $\max \sigma_{max}$ vs μ_{cj}

FIGURE 4.35: Scatter plots obtained by MC for short-corner dovetail connection model, variant A

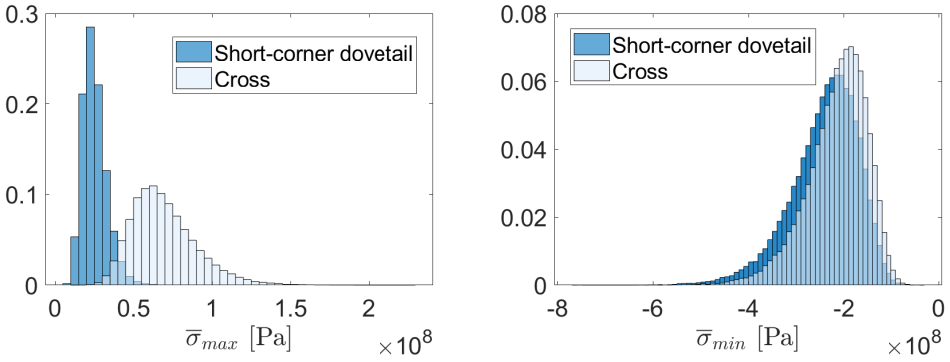

FIGURE 4.36: Normalized histograms of $\bar{\sigma}_{max}$ and $\bar{\sigma}_{min}$ obtained by PC of order $p = 3$ for the short-coner dovetail joint and the saddle notch joint in variant A

Type of joint	Short-corner dovetail		Saddle notch	
Quantity of interest	$\bar{\sigma}_{max}$	$\bar{\sigma}_{min}$	$\bar{\sigma}_{max}$	$\bar{\sigma}_{min}$
Mean	2.95E+07	-2.83E+08	8.12E+07	-2.52E+08
Standard deviation	7.16E+06	6.70E+07	1.90E+07	5.91E+07
5th percentile	1.93E+07	-4.05E+08	5.40E+07	-3.59E+08
95th percentile	4.25E+07	-1.88E+08	1.16E+08	-1.67E+08

TABLE 4.13: Statistics obtained by 3rd order PC for both types of timber joints [Pa], variant B

4.5.3.2 Variant B

The same DoE was used for calculations in variant B with PC of order 3. Figures 4.37 and 4.38 present histograms of $\bar{\sigma}_{max}$ and $\bar{\sigma}_{min}$, respectively. Table 4.13 shows some statistics of the distribution obtained. It can be seen that the results of $\bar{\sigma}_{max}$ differ between the types of joint much more than values of $\bar{\sigma}_{min}$. The mean and 95th percentile of $\bar{\sigma}_{max}$ are higher in case of the saddle notch joint. Nevertheless, $\bar{\sigma}_{min}$, which is higher than $\bar{\sigma}_{max}$ in absolute value, does not differ so significantly between the two types of joint. The coefficient of variation is similar for both quantities of interest and is equal to 24% in the case of the dovetail joint and 23% in the case of the saddle notch joint.

For each type of joint, Table 4.14 shows the Sobol' indices with respect to E_L and μ_{cj} of the mean principle stresses and the extrema of the principal stresses. Although the assumed coefficient of the variation of the input μ_{cj} is higher than of E_L, S_1^{Tot} is much higher than S_2^{Tot}. In the case of the saddle notch and short-corner dovetail joints with quantities of interest related to σ_{min}, S_1^{Tot} is very close to 1 and effect of μ_{cj} is negligibly small ($S_2^{Tot} < 0.02$). In the case of the short-corner dovetail joint related to σ_{max}, S_2^{Tot} is higher, but only where the quantity of interest is $\max \sigma_{max}$, $S_2^{Tot} > 0.1$ (In fact, $S_2^{Tot} = 0.3104$) . The coefficient of friction μ_{cj} has aleading role in work of some types of carpentry joint [126, 127]. Nevertheless, in the case of the joints studied, the uncertainty

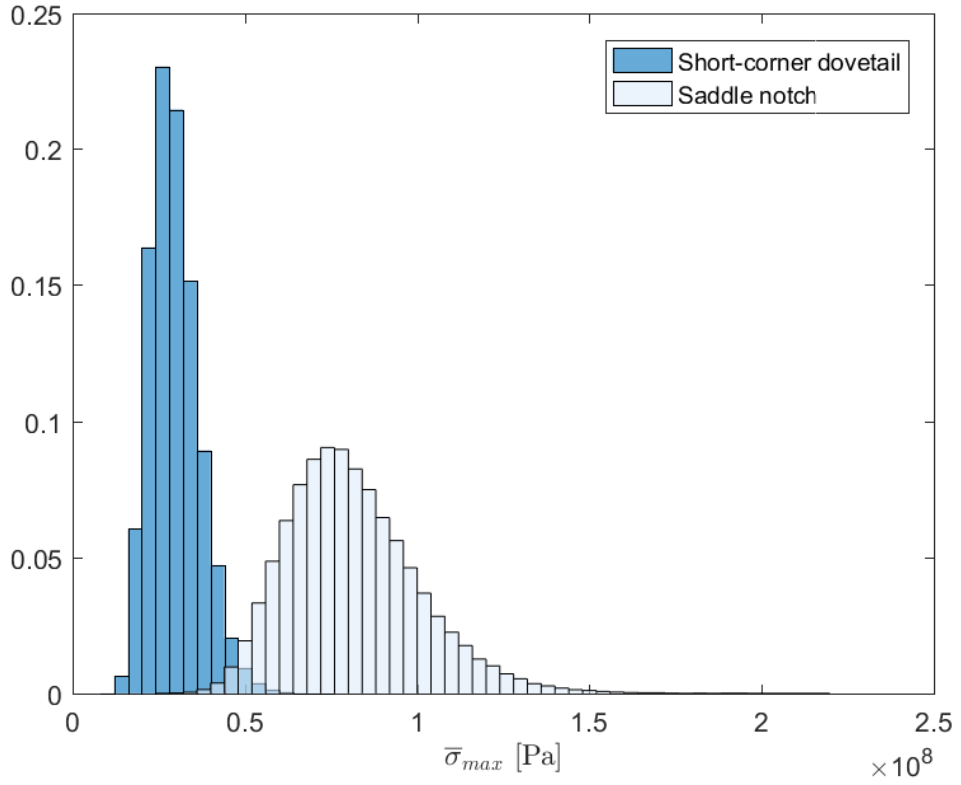

FIGURE 4.37: Normalized histograms of $\bar{\sigma}_{max}$ obtained by PC of order $p = 3$ for the short-coner dovetail joint and the saddle notch joint, variant B

	Short-corner dovetail				Saddle notch			
	$\bar{\sigma}_{max}$	$\bar{\sigma}_{min}$	$\max \sigma_{max}$	$\min \sigma_{min}$	$\bar{\sigma}_{max}$	$\bar{\sigma}_{min}$	$\max \sigma_{max}$	$\min \sigma_{min}$
S_1^{Tot}	0.937	0.9851	0.7101	0.9931	0.9998	0.9886	0.9859	0.999
S_2^{Tot}	0.0641	0.0156	0.3104	0.0075	0.0003	0.0119	0.0151	0.0011

TABLE 4.14: Total Sobol' sensitivity analysis in timber joints models, variant B

of E_L is mostly responsible for variance of the studied quantities of interest (4.6, 4.7). In the light of these results, detailed identification of μ_{cj} is not a priority.

Conclusions obtained for the two variants of the E_L distribution are similar and even for lower variability of E_L, the contribution of the variation of E_L to the total variation of the output is much higher than contribution of μ_{cj}. Values $\bar{\sigma}_{max}$ in the both joints are similar.

4.6 Conclusions

The polynomial chaos expansion method was applied to local and global models of the implant-abdominal wall system in order to propagate uncertainties and measure their effect on the uncertainty of model outputs. The following conclusions can be drawn:

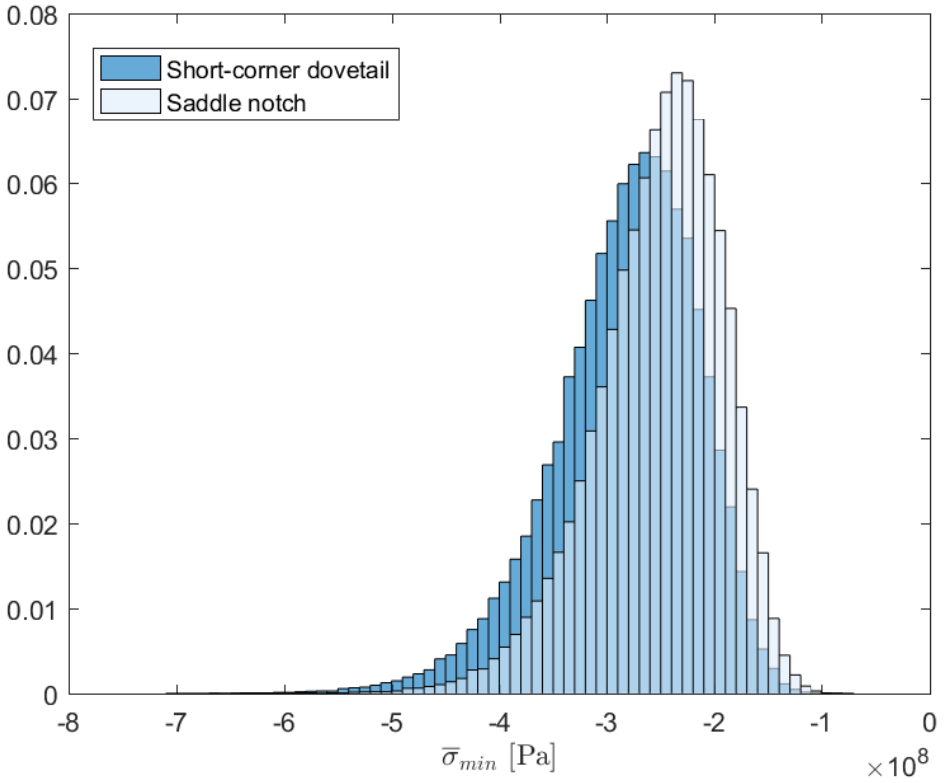

FIGURE 4.38: Normalized histograms of $\bar{\sigma}_{min}$ obtained by PC order $p = 3$ for two types of carpentry joints, variant B

1. Based on global and local sensitivity analysis of the simplified cable model, it can be concluded that:

   - Young's modulus is the most influential variable in both the local and global senses of sensitivity analysis. In further study, its input uncertainty should be characterized in more detail e.g. the significance of load history, ingrowth etc.
   - Despite a low local sensitivity index around some base points, the second most important variable is the displacement of the hernia edges which is related to fascia elasticity. This confirms that proper measurement of the properties of the abdominal wall tissue should not be neglected.
   - Despite high input variability, the uncertainty of the initial force has a low contribution to the variance of the horizontal reaction. This is convenient since it is difficult to introduce a specific value of the initial force in surgical practice, as also concluded in the local sensitivity study by Szymczak et al. [168].
   - The initial length of the cable has negligible effect, but its input variation was also very low.

2. The outcomes of the global sensitivity analysis performed in the membrane model indicate that:

   - The high variability of strains in oblique directions observed by Szymczak et al. [169] leads to high variability of the maximum force in the fasteners connecting the implant to the abdominal wall.
   - The model with 10 random variables (each variable corresponding to a displacement of a support) can be reduced to only 2 variables, which can greatly reduce the computational cost of further analysis.
   - Although the reduced and full models are close to each other, comparison of methods for choosing regression points in the reduced problem lead to different conclusions than for 10 variables. This supports the conclusions made in chapter 3.2 that superiority of methods depends on the number of variables.
   - Treating displacements of all supports as independent is safer owing to the possibilities of wider ranges of scenarios. The mean, standard deviation and 95th percentile are higher in that case than in the examples with correlated variables. However including correlation gives a different relation between the statistics of the maximum force in the fasteners and orientation of the implant. The orientation of the orthotropic surgical mesh within the anisotropic abdominal wall was shown to be important both numerically [106] and experimentally [6]. For the location of hernia considered in this thesis, the stiffer direction of the implant should be placed in the transverse direction of the abdominal wall ($\alpha_{orient} = 90$ deg) according to deterministic studies [70]. Further studies of global models of the abdominal wall with random stiffness and including uncertainties in mechanical properties can help to judge optimal orientation.

3. Uncertainty quantification and sensitivity analysis performed on the local model of the membrane subjected to intraabdominal pressure have shown that:

   - Uncertainty in the intraabdominal pressure was the main contribution to the variance of the quantities of interest. When compared to the influence of intraabdominal pressure, the uncertainty of the stiffness of the abdominal wall and of the fascia are not important. The model could be reduced to only one variable. More detailed studies on intraabdominal pressure and its distribution should be performed.
   - Although relatively large imperfections were imposed on the model, the variance obtained is low when compared to variance obtained in the model with uncertain pressure and stiffness of the abdominal wall and fascia.

- Amongst the considered imperfections in the position of the fasteners, the most influential is the angular change in the support that is closest to the orientation of the stiffer direction of the implant. Imperfections in the positions of the other fasteners have a negligible effect on the variance of the quantities of interest (maximum force in fastener and deflection of the implant).

4. Global sensitivity analysis performed on the global model of the abdominal wall with an implanted surgical mesh lead to the conclusion that although the uncertainty of intraabdominal pressure has the highest influence on the variance of the displacement of the centre of the implant and the displacement of the corresponding point in the abdominal wall, E_1^{aw} is the most influential variable when the difference between the displacements in healthy and repaired abdominal walls is considered. Detailed measurement of E_1^{aw} and intraabdominal pressure values would be beneficial. In the case of this hernia location and this quantity of interest, the orientation of the composite of lateral muscles is not important.

The uncertainty quantification and sensitivity analysis framework was also applied to models of timber joints in which the uncertainty of Young's modulus E_L and the friction coefficient was propagated. The variation of the mean of the principal stress in elements located in the high stress zone is large, 30% in case of variant A (higher input variability) and 23–24% in case of variant B. The effect on the variance of the studied quantities of interest of the uncertainty of the friction coefficient was found negligible, whereas the influence of uncertainty of the Young's modulus dominates the variance of the mean principal stress. Therefore, detailed measurement of the friction coefficient is not of high importance.

Chapter 5

Conclusions

The background of these studies was ventral hernia repair by means of an implanted mesh. One of the issues in computer simulation of the abdominal wall with such a mesh is the uncertainties, which are related for example to the natural variability of the mechanical properties of the abdominal wall, physiological loading and inaccuracies in modelling. However the influence of the high dispersion of results regarding the mechanical behaviour of the abdominal wall on the variability of model outcomes has not been yet studied. The aim of this research was to study these uncertainties and investigate their influence on outcomes of the model.

In this thesis, a probabilistic approach has been proposed to incorporate uncertainties in the modelling of the abdominal wall with an implanted surgical mesh. These uncertainties have been propagated in order to study the variability of the model response. The influence of input uncertainties on the uncertainty of the model outputs has been investigated and influential and non-influential variables have been identified based on global sensitivity analysis outcomes.

Regression-based polynomial chaos expansion method was used to propagate uncertainties and compute Sobol' sensitivity indices. However, the accuracy of such non-intrusive methods depends on the number and choice of regression points. Approaches based on the D-optimal criterion, random approaches and combined ones were amongst the methods of choosing points tested. The methods were firstly tested on univariate examples and then on multivariate examples. The chosen approaches were subsequently applied to another examples. Models with different levels of complexity were studied: from local models of implants such as the simplified cable model and membrane models with various boundary conditions, to global models of the abdominal wall. The methods were also applied to a model of construction made of wood, another natural material exhibiting

high variability. The context here was historic timber joints, where the uncertainties appear in the properties of the wood and in the friction coefficient.

To sum up, the contribution of this thesis is:

- a proposition of methodology to incorporate uncertainties in models related to ventral hernia repair which can be used in further research;
- a comparison of approaches to choosing sampling points for regression-based polynomial chaos expansion from the point of view of their accuracy in the case of ventral hernia-related models;
- an investigation of the influence of uncertainties on the variation of the model output that is important from the point of view of ventral hernia repair optimisation.

The following conclusions can be drawn:

- uncertainties can be incorporated in the modelling of the abdominal wall with an implanted surgical mesh;
- non-intrusive polynomial chaos can be applied to decrease the computational cost of global sensitivity analysis and uncertainty quantification in models related to ventral hernia repair;
- despite nonlinearity, nonsmoothness and high input variability, it is possible to achieve sufficient accuracy by the polynomial chaos expansion method;
- the accuracy of PC depends on the number and position of sampling points. The position which minimises the approximation error is problem dependent. The outcomes obtained can be useful in the choice of the design of experiment (DoE) in similar models of surgical mesh - tissue system:
  - the number of variables should be included in the choice of the DoE. The D-optimal choice from randomly chosen candidate set of points can be recommended for low-dimensional examples, whereas low discrepancy sequences or random choice from univariate polynomials of higher order can be considered in the case of higher dimensional problems;
  - a weight function corresponding to the distribution measure should be included in the D-optimality procedures;
- the global sensitivity and Sobol' indices can be used to efficiently reduce the number of random variables and consequently significantly reduce computational cost;

- an obstacle in correctly performing uncertainty quantification, especially in hydromechanics where experiments usually have to be conducted on a small number of samples/objects, is the lack of sufficient knowledge of the distribution of the input variables. Nevertheless, the output of global sensitivity analysis can help to determine the importance of variables and identify variables of which proper identification of the distribution is not so important.

- global sensitivity analysis can be considered useful in the nonlinear examples studied which have a high input variability since conclusions drawn from local sensitivity may vary with change of base point;

- uncertainty quantification, global sensitivity and Sobol' indices can be used to draw conclusions about the importance of uncertainties and establish priorities for further numerical and experimental studies:

  - uncertainties related to the variability of the properties of the abdominal wall are very influential, which confirms the strong need for proper identification of the mechanical properties of the abdominal wall;
  - a patient-specific approach should be considered in the modelling of the abdominal wall with implanted surgical mesh in order to reduce input variablity. *In vivo* measurement of important parameters can be considered in order to construct patient-specific models. However, uncertainty propagation may be still needed due to challenges of *in vivo* measurement, e.g. uncertain boundary conditions. Studies reported in the literature *in vivo* studies [177] have shown variability amongst results obtained for a single patient.
  - study of imperfections in the connection of the implant to the abdominal wall is less important than incorporating uncertainties related to abdominal wall mechanics;
  - wider studies on intraabdominal pressure and its distribution should be performed;
  - the uncertainties related to friction coefficients are much less influential than uncertainties related to the material properties of wood.

The approach established in this thesis of uncertainty propagation can be used in further studies on the mechanics of the herniated abdominal wall repaired with surgical mesh.

The directions of planned research are as follows:

- application of other truncation schemes of PC including an adaptive one in order to reduce computational cost and the issue of the so-called curse of dimensionality;

- consideration of an adaptive method to DoE;
- application of the established methodology to a more detailed model of abdominal wall with surgical mesh. Work on an FE model based on MRI images is planned.
- incorporation of random fields of material parameters of the abdominal wall and timber joints.
- incorporation of uncertainties into the procedures for optimization of ventral hernia repair parameters like choice of surgical mesh [106, 167].
- it is planned to investigate uncertainties in inverse identification of abdominal wall properties based on measurements described in [109].

Appendix A

Technical information on implementation of probabilistic models and sensitivity analysis

A.1 Used tools

Non-intrusive Polynomial Chaos expansion and sensitivity analysis methods have been implemented in MATLAB. MATLAB random number generator was used to generate all needed random numbers. In fact, there were actually only pseudo-random, since there were generated with deterministic algorithms. However, for the simplicity, in the text such generated number are called just random. In the context of sampling methods (section 3) when numbers were generated simply with a given distribution using standard function are called "purely" random to distinguish them from methods which improve uniformity of distribution, e.g. using low-discrepancy sequences which are called pseudo-random methods.

Marc (MSC.Software) commercial system was used in case of Finite Element models of implant with abdominal wall (models 2, 3, 4) and models of timber joints. PowerShell scripts were written to automatise process of running simulation in MSC.Marc for many random variables and collecting values of considered quantity of interest. Scripts allowed to perform a few simulation in parallel which reduced total time of computations. General scheme of relation is presented in Figure A.1.

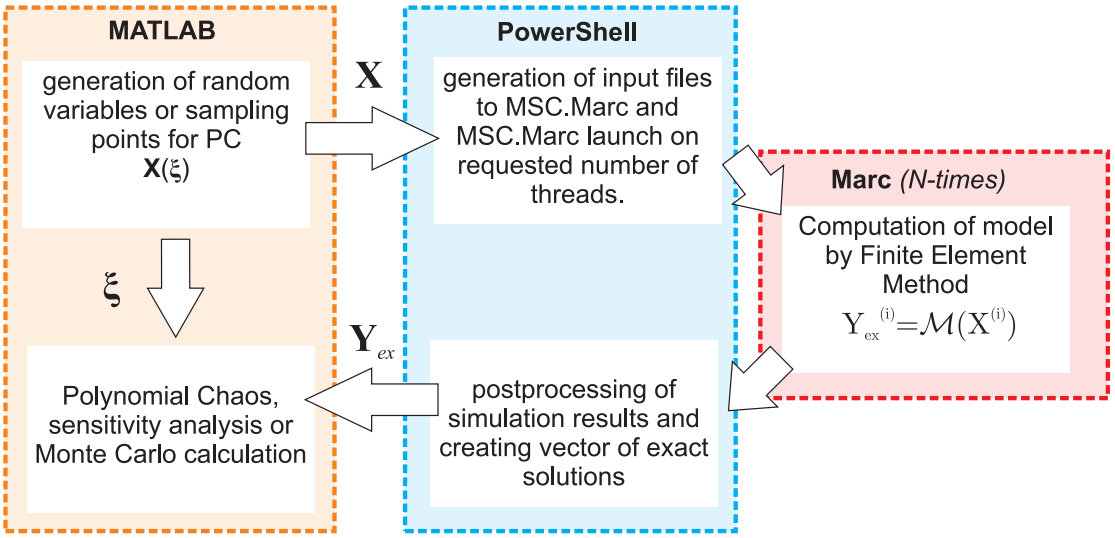

FIGURE A.1: Workflow in case of FE models

A.2 Multivariate polynomials

To create multivariate polynomials, practical implementation (as described in [161]) is to generate univariate polynomials and then create a list of degrees of polynomials corresponding to each variable. On the basis of this list, multiplications of univariate polynomials are constructed. For each degree $q = 1, .., p$ list of all non-negative integers of sum equals q is searched. This is equivalent to the problem of filling $(M + q - 1)$ boxes with $(M - 1)$ balls. Integer is the number of empty boxes between the balls. Initially, all balls are in the first $(M - 1)$ boxes. In the next step, a ball, which is the furthest to the right is shifted to the next place to the right. If the ball is already at the end, then the next furthest to the right ball is shifted and balls which were at the end are brought back to the right side of the ball which has been just shifted. For example, if $M = 3$, $q = 2$, the number of balls is 2 and the number of boxes is 4. Then, the creation of multivariate summands of expansion looks like in Figure A.2. So, if for example polynomial chaos expansion of maximum degree $p = 2$ is searched, $|\mathcal{A}| = 10$ summands are created and the whole expansion with Hermite polynomials is:
$Y^{PC} = a_{0,0,0} + a_{0,0,1}\xi_3 + a_{0,1,0}\xi_2 + a_{1,0,0}\xi_1 + a_{0,0,2}(\xi_3^2 - 1)/\sqrt{2} + a_{0,1,1}\xi_2\xi_3 +$
$+ a_{0,2,0}(\xi_2^2 - 1)/\sqrt{2} + a_{1,0,1}\xi_1\xi_3 + a_{1,1,0}\xi_1\xi_2 + a_{2,0,0}(\xi_1^2 - 1)/\sqrt{2}.$

A.3 Correlation matrices

Figure A.3 presents correlation matrices, which where used in model 2f (section 4.2.3).

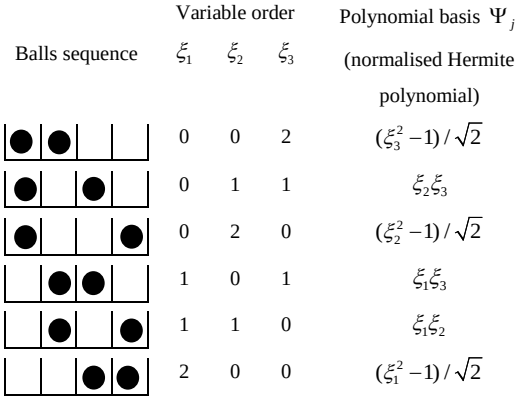

FIGURE A.2: Example of creating multivariate elements of polynomial chaos expansion of order $q = 2$ and number of variables $M = 3$

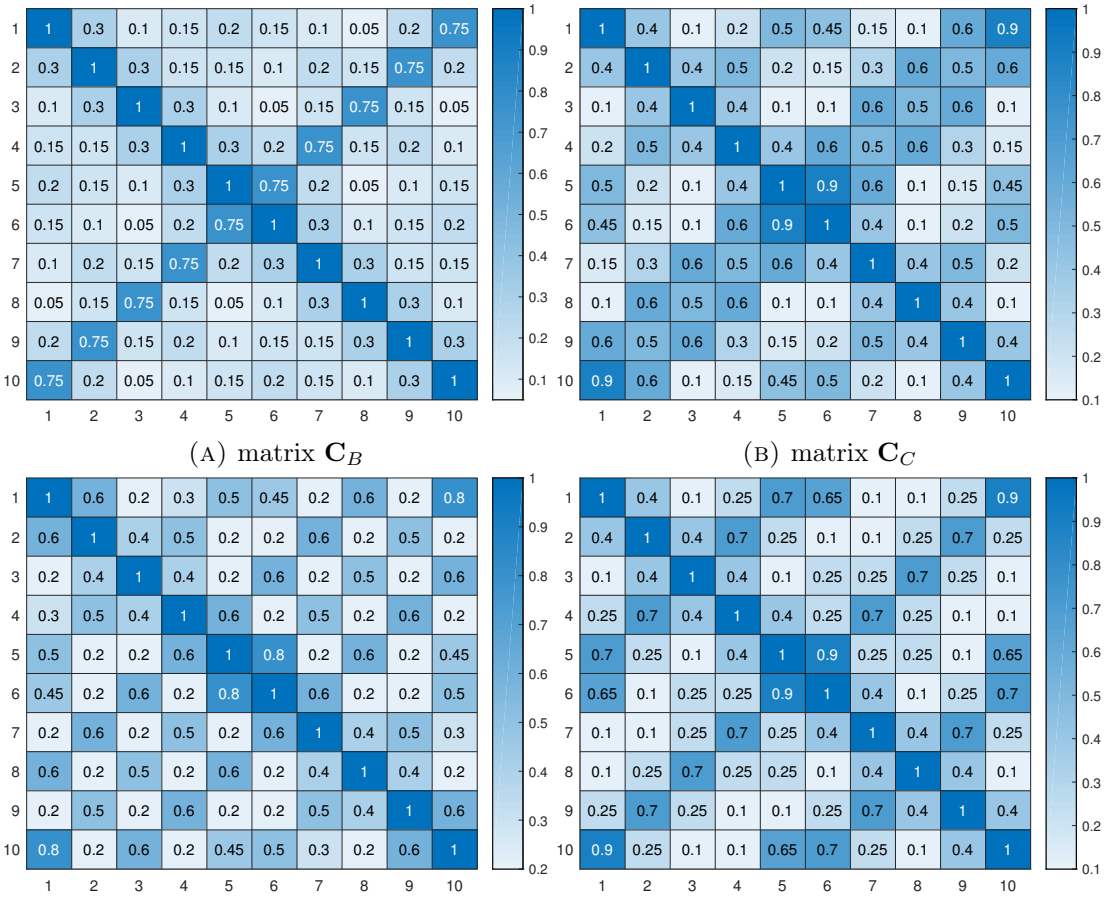

(A) matrix $\mathbf{C}_B$

(B) matrix $\mathbf{C}_C$

(C) matrix $\mathbf{C}_D$

(D) matrix $\mathbf{C}_E$

FIGURE A.3: Correlation matrices in model 2f

Appendix B

Résumé en français

La motivation de cette étude est la nécessité d'une compréhension mécanique, pour venir en soutien aux chirurgiens dans le traitement de la hernie ventrale, notamment dans le cas de récidives de hernie. Des modèles mécaniques sont créés pour prédire le comportement mécanique du système implant-paroi abdominale et peuvent être utilisés dans l'optimisation des paramètres de réparation des hernies ventrales. Cependant, des défis tels que l'incertitude liée à la variabilité naturelle de la mécanique du tissu abdominal ainsi que les difficultés de mesures précises des paramètres du modèle de matériaux viennent interagir avec la modélisation. Cette étude porte donc sur l'application de méthodes de quantification de l'incertitude dans les modèles du système implant-paroi abdominale. Le but de cette thèse est d'étudier les incertitudes dans la modélisation des maillages chirurgicaux au sein de la paroi abdominale et d'évaluer la sensibilité de la réponse du modèle à ces incertitudes.

Dans cette thèse, une approche probabiliste a été proposée pour introduire les incertitudes dans la modélisation de la paroi abdominale à l'aide de l'implant d'un filet chirurgical. La propagation des incertitudes a été menée afin d'étudier la variabilité de la réponse du modèle. L'influence des incertitudes d'entrée sur l'incertitude des quantités d'intérêt de sorties du modèle a été étudiée. Les variables influentes ont été identifiées sur la base des résultats de l'analyse de sensibilité globale. L'approximation par expansion sur le chaos polynomial, basée sur la régression, a été utilisée pour propager les incertitudes et calculer les indices de sensibilité de Sobol. Toutefois, l'exactitude de ces méthodes non intrusives dépend du nombre et du choix des points de régression. Les approches basées sur le critère de D-optimalité, les approches aléatoires ainsi que des approches mixtes ont été testées. Les méthodes ont d'abord été testées sur des exemples simples, puis sur des exemples multivariables. Les approches retenues ont ensuite été appliquées à d'autres exemples. Différents niveaux de complexités ont été étudiés : des modèles

locaux d'implants tels que le modèle de câble simplifié, des modèles de membrane avec différentes conditions limites mais aussi des modèles globaux de la paroi abdominale. Les méthodes ont également été appliquées à un modèle de construction en bois, un matériau naturel présentant également une grande variabilité. Le contexte était dans ce cas les assemblages historiques ou le bois est omniprésent. Des incertitudes apparaissent dans les propriétés intrinsèque du bois et dans le coefficient de frottement.

Les contributions de cette thèse sont :

- une proposition de méthodologie pour introduire les incertitudes dans les modèles liés à la réparation de la hernie ventrale qui peuvent être utilisés dans d'autres domaines d'application ;
- une comparaison des approches pour choisir les points d'échantillonnage utilisés dans la construction de l'approximation par chaos polynomial basé sur la régression. L'étude de l'erreur liée à ce choix quant à l'exactitude des résultats du modèle de hernie ventrale ;
- une étude de l'influence des incertitudes sur la variation des réactions aux appuis, ce qui est primordial du point de vue de choix effectués lors de la réparation de la hernie ventrale.

Les conclusions suivantes peuvent être tirées :

- Les incertitudes peuvent être introduites dans la modélisation de la paroi abdominale avec le filet chirurgical installé ;
- Le chaos polynomial non intrusif peut être mis en oeuvre pour diminuer le coût de calcul de l'analyse de sensibilité globale ainsi que la quantification de l'incertitude dans les modèles liés à la réparation de la hernie ventrale ;
- malgré la non-linéarité et une variabilité d'entrée élevée, il est possible d'obtenir une précision suffisante par la méthode d'expansion du chaos polynomial ;
- la précision du chaos dépend du nombre et de la position des points de régression. La position qui minimise l'erreur d'approximation dépend du problème. Les résultats obtenus peuvent être utiles dans le choix de plan d'expérience dans des modèles similaires d'implant chirurgical - tissu humain :
  - le nombre de variables influe sur le choix du plan d'expérience. Le choix de points D-optimaux à partir d'un ensemble de points pris au hasard est recommandé pour des exemples à faible dimension. Alors qu'un choix aléatoire

basé sur des polynômes d'une seule variable d'ordre élevé peuvent être utilisé dans le cas de problèmes de dimensions plus élevées ;

- il est intéressant d'introduire une fonction de pondération correspondant à la mesure de distribution dans la mesure de D-optimalité ;

- la sensibilité globale et les indices Sobol peuvent être utilisés pour réduire efficacement le nombre de variables aléatoires et, par conséquent, réduire significativement les coûts de calcul ;

- Le manque de connaissances suffisantes sur la distribution des variables d'entrée constitue un obstacle à la quantification correcte de l'incertitude, en particulier en biomécanique, où les expériences doivent généralement être menées sur un petit nombre d'échantillons ou d'objets. Néanmoins, les résultats de l'analyse de sensibilité globale peuvent aider à déterminer l'importance des variables et à identifier les variables dont connaissance parfaite de la distribution n'est pas très importante.

- l'apport de l'analyse de sensitivité globale peut être considéré comme utile sur les exemples nonlinéaires étudiés où les variables d'entrée sont très variables ; étant donné que les conclusions tirées de l'analyse de sensibilité locale varient énormément avec le choix des points effectué.

- La propagation d'incertitude ainsi que l'analyse globale de sensibilité par les indices de Sobol peuvent être utilisées pour tirer des conclusions sur l'importance des incertitudes et établir des priorités pour d'autres études numériques ou expérimentales :

  - Les incertitudes des propriétés de la paroi abdominale sont très influentes sur le résultat, ce qui confirme la nécessité d'identifier correctement les propriétés mécaniques de la paroi abdominale ;
  - une approche spécifique par patient devrait être envisagée dans la modélisation de la paroi abdominale avec implant chirurgical afin de réduire les variabilités d'entrée. Des mesures *In vivo* de paramètres importants peuvent être prises en compte pour construire des modèles spécifiques par patient. Cependant, la propagation de l'incertitude restera sans doute nécessaire car la mesure *in vivo* reste un challenge, par exemple pour les conditions aux limites incertaines. Les études rapportées dans la littérature *in vivo* ont montré une grande variabilité des résultats obtenus, et ce, même pour un seul et même patient.
  - L'étude des imperfections de la connexion de l'implant à la paroi abdominale est moins importante que l'intégration des incertitudes liées à la mécanique de la paroi abdominale ;

- Des études plus larges sur la pression intra-abdominale et sa distribution devraient être effectuées ; Les incertitudes liées aux coefficients de frottement ont beaucoup moins d'influence que les incertitudes liées aux propriétés du bois.

L'approche établie dans cette thèse pour étudier la propagation des incertitudes pourra être utilisée dans d'autres études sur la mécanique de réparation de hernie abdominale par filet chirurgical.

Bibliography

[1] Abdelounis, H. B., Nicolle, S., Ottenio, M., Beillas, P., and Mitton, D. Effect of two loading rates on the elasticity of the human anterior rectus sheath. *Journal of the mechanical behavior of biomedical materials 20* (2013), 1–5.

[2] Ambroziak, A., and Kłosowski, P. A four-node 3d isoparametric membrane element. *Task Quarterly 10*, 1 (2006), 35–47.

[3] Ambroziak, A., and Kłosowski, P. Influence of thermal effects on mechanical properties of pvdf-coated fabric. *Journal of Reinforced Plastics and Composites 33*, 7 (2014), 663–673.

[4] Ambroziak, A., Szepietowska, K., and Lubowiecka, I. Mechanical properties of mosquito nets in the context of hernia repair. *Computer methods in biomechanics and biomedical engineering 19*, 3 (2016), 286–296.

[5] Antille, G., Weinberg, A., et al. *A Study of D-optimal Designs Efficiency for Polynomial Regression*. Université de Genève/Faculté des sciences économiques et sociales, 2000.

[6] Anurov, M., Titkova, S., and Oettinger, A. Impact of position of light mesh endoprosthesis with anisotropic structure for the efficiency of anterior abdominal wall reconstruction. *Bulletin of experimental biology and medicine 149*, 4 (2010), 440–444.

[7] Astruc, L., De Meulaere, M., Witz, J.-F., Nováček, V., Turquier, F., Hoc, T., and Brieu, M. Characterization of the anisotropic mechanical behavior of human abdominal wall connective tissues. *Journal of the mechanical behavior of biomedical materials 82* (2018), 45–50.

[8] Avril, S., and Evans, S. *Material Parameter Identification and Inverse Problems in Soft Tissue Biomechanics*. Springer, 2017.

[9] Bedon, C., Rinaldin, G., and Fragiacomo, M. Non-linear modelling of the in-plane seismic behaviour of timber blockhaus log-walls. *Engineering Structures 91* (2015), 112–124.

[10] Bensley, R. P., Schermerhorn, M. L., Hurks, R., Sachs, T., Boyd, C. A., O'Malley, A. J., Cotterill, P., and Landon, B. E. Risk of late-onset adhesions and incisional hernia repairs after surgery. *Journal of the American College of Surgeons 216*, 6 (2013), 1159–1167.

[11] Berveiller, M., Sudret, B., and Lemaire, M. Stochastic finite element: a non intrusive approach by regression. *Revue européenne de mécanique numérique 15*, 1-2-3 (2006), 81–92.

[12] Bielewicz, E., and Górski, J. Shells with random geometric imperfections simulation—based approach. *International journal of non-linear mechanics 37*, 4-5 (2002), 777–784.

[13] Bielski, P., and Lubowiecka, I. Surface sliding in human abdominal wall numerical models: comparison of single-surface and multi-surface composites. In *Shell Structures. Theory and Applications* (2018), vol. 4, pp. 499–502.

[14] Blatman, G., and Sudret, B. An adaptive algorithm to build up sparse polynomial chaos expansions for stochastic finite element analysis. *Probabilistic Engineering Mechanics 25*, 2 (2010), 183–197.

[15] Blatman, G., and Sudret, B. Efficient computation of global sensitivity indices using sparse polynomial chaos expansions. *Reliability Engineering & System Safety 95*, 11 (2010), 1216–1229.

[16] Blatman, G., Sudret, B., and Berveiller, M. Quasi random numbers in stochastic finite element analysis. *Mécanique & Industries 8*, 3 (2007), 289–297.

[17] Blau, P. J. The significance and use of the friction coefficient. *Tribology International 34*, 9 (2001), 585–591.

[18] Breuing, K., Butler, C. E., Ferzoco, S., Franz, M., Hultman, C. S., Kilbridge, J. F., Rosen, M., Silverman, R. P., Vargo, D., Group, V. H. W., et al. Incisional ventral hernias: review of the literature and recommendations regarding the grading and technique of repair. *Surgery 148*, 3 (2010), 544–558.

[19] Brites, R. D., Neves, L. C., Machado, J. S., Lourenço, P. B., and Sousa, H. S. Reliability analysis of a timber truss system subjected to decay. *Engineering structures 46* (2013), 184–192.

[20] Brown, C., and Finch, J. Which mesh for hernia repair? *The Annals of The Royal College of Surgeons of England 92*, 4 (2010), 272–278.

[21] Brown, S. H. Mechanically relevant consequences of the composite laminate-like design of the abdominal wall muscles and connective tissues. *Medical Engineering and Physics 34*, 4 (2012), 521–523.

[22] Brown, S. H., Carr, J. A., Ward, S. R., and Lieber, R. L. Passive mechanical properties of rat abdominal wall muscles suggest an important role of the extracellular connective tissue matrix. *Journal of Orthopaedic Research 30*, 8 (2012), 1321–1326.

[23] Brown, S. H., and McGill, S. M. Transmission of muscularly generated force and stiffness between layers of the rat abdominal wall. *Spine 34*, 2 (2009), E70–E75.

[24] Brown, S. H., and McGill, S. M. A comparison of ultrasound and electromyography measures of force and activation to examine the mechanics of abdominal wall contraction. *Clinical biomechanics 25*, 2 (2010), 115–123.

[25] Bukała, J., Kwiatkowski, P., and Małachowski, J. Numerical analysis of stent expansion process in coronary artery stenosis with the use of non-compliant balloon. *Biocybernetics and Biomedical Engineering 36*, 1 (2016), 145–156.

[26] Burnaev, E., Panin, I., and Sudret, B. *Effective Design for Sobol Indices Estimation Based on Polynomial Chaos Expansions*. Springer International Publishing, Cham, 2016, pp. 165–184.

[27] Burnaev, E., Panin, I., and Sudret, B. Efficient design of experiments for sensitivity analysis based on polynomial chaos expansions. *Annals of Mathematics and Artificial Intelligence 81*, 1-2 (2017), 187–207.

[28] Calvo, B., Sierra, M., Grasa, J., Muñoz, M., and Peña, E. Determination of passive viscoelastic response of the abdominal muscle and related constitutive modeling: Stress-relaxation behavior. *Journal of the Mechanical Behavior of Biomedical Materials 36* (2014), 47–58.

[29] Chamoin, L., Florentin, E., Pavot, S., and Visseq, V. Robust goal-oriented error estimation based on the constitutive relation error for stochastic problems. *Computers & Structures 106-107*, i (2012), 189–195.

[30] Cho, I., Lee, Y., Ryu, D., and Choi, D.-H. Comparison study of sampling methods for computer experiments using various performance measures. *Structural and Multidisciplinary Optimization 55*, 1 (2017), 221–235.

[31] Choi, S.-K., Grandhi, R. V., Canfield, R. A., and Pettit, C. L. Polynomial chaos expansion with latin hypercube sampling for estimating response variability. *AIAA journal 42*, 6 (2004), 1191–1198.

[32] Cielątkowska, R. *Translocatio. Przeniesienie drewnianych świątyń trzech obrządków. (Translocatio Transfer of wooden temples of the three religions).* Department of Architecture of Gdańsk University of Technology, Gdańsk, 2014.

[33] Cobb, W. S., Burns, J. M., Kercher, K. W., Matthews, B. D., Norton, H. J., and Heniford, B. T. Normal intraabdominal pressure in healthy adults. *Journal of Surgical Research 129*, 2 (2005), 231–235.

[34] Cooney, G., Kiernan, A., Winter, D., and Simms, C. Optimized wound closure using a biomechanical abdominal model. *British Journal of Surgery 105*, 4 (2018), 395–400.

[35] Cooney, G. M., Lake, S. P., Thompson, D. M., Castile, R. M., Winter, D. C., and Simms, C. K. Uniaxial and biaxial tensile stress–stretch response of human linea alba. *Journal of the mechanical behavior of biomedical materials 63* (2016), 134–140.

[36] Cooney, G. M., Moerman, K. M., Takaza, M., Winter, D. C., and Simms, C. K. Uniaxial and biaxial mechanical properties of porcine linea alba. *Journal of the Mechanical Behavior of Biomedical Materials 41* (2015), 68–82.

[37] Cordero, A., Hernández-Gascón, B., Pascual, G., Bellón, J., Calvo, B., and Peña, E. Biaxial mechanical evaluation of absorbable and nonabsorbable synthetic surgical meshes used for hernia repair: physiological loads modify anisotropy response. *Annals of biomedical engineering 44*, 7 (2016), 2181–2188.

[38] Crestaux, T., Le Maître, O., and Martinez, J.-M. Polynomial chaos expansion for sensitivity analysis. *Reliability Engineering & System Safety 94*, 7 (2009), 1161 – 1172. Special Issue on Sensitivity Analysis.

[39] Cruz, H., Yeomans, D., Tsakanika, E., Macchioni, N., Jorissen, A., Touza, M., Mannucci, M., and Lourenço, P. B. Guidelines for on-site assessment of historic timber structures. *International Journal of Architectural Heritage 9*, 3 (2015), 277–289.

[40] de Aguiar, P., Bourguignon, B., Khots, M., Massart, D., and Phan-Than-Luu, R. D-optimal designs. *Chemometrics and Intelligent Laboratory Systems 30*, 2 (1995), 199 – 210.

[41] Deeken, C. R., and Lake, S. P. Mechanical properties of the abdominal wall and biomaterials utilized for hernia repair. *Journal of the mechanical behavior of biomedical materials 74* (2017), 411–427.

[42] Deeken, C. R., Thompson, D. M., Castile, R. M., and Lake, S. P. Biaxial analysis of synthetic scaffolds for hernia repair demonstrates variability in mechanical anisotropy, non-linearity and hysteresis. *Journal of the mechanical behavior of biomedical materials 38* (2014), 6–16.

[43] Diaz, P., Doostan, A., and Hampton, J. Sparse polynomial chaos expansions via compressed sensing and d-optimal design. *Computer Methods in Applied Mechanics and Engineering 336* (2018), 640 – 666.

[44] Drake, R., Vogl, A. W., and Mitchell, A. W. *Gray's Basic Anatomy E-Book: with STUDENT CONSULT Online Access*. Elsevier Health Sciences, 2012.

[45] Dubois, G., Kheireddine, W., Vergari, C., Bonneau, D., Thoreux, P., Rouch, P., Tanter, M., Gennisson, J.-L., and Skalli, W. Reliable protocol for shear wave elastography of lower limb muscles at rest and during passive stretching. *Ultrasound in Medicine and Biology 41*, 9 (2015), 2284–2291.

[46] Eriksen, J., Gögenur, I., and Rosenberg, J. Choice of mesh for laparoscopic ventral hernia repair. *Hernia 11*, 6 (2007), 481–492.

[47] Fajraoui, N., Marelli, S., and Sudret, B. On optimal experimental designs for sparse polynomial chaos expansions. *arXiv preprint arXiv:1703.05312* (2017).

[48] Fedorov, V. V. *Theory of optimal experiments*. Academic Press, INC (english translation), 1972.

[49] Fedorov, V. V., and Hackl, P. *Model-oriented design of experiments*, vol. 125. Springer Science & Business Media, 2012.

[50] Fishman, G. S. *Monte Carlo*. Springer New York, New York, NY, 1996.

[51] Förstemann, T., Trzewik, J., Holste, J., Batke, B., Konerding, M., Wolloscheck, T., and Hartung, C. Forces and deformations of the abdominal wall – A mechanical and geometrical approach to the linea alba. *Journal of Biomechanics 44*, 4 (2011), 600–606.

[52] Frey, C. H., and Patil, S. R. Identification and review of sensitivity analysis methods. *Risk analysis 22*, 3 (2002), 553–578.

[53] Gao, Z., and Zhou, T. On the choice of design points for least square polynomial approximations with application to uncertainty quantification. *Communications in Computational Physics 16*, 2 (2014), 365–381.

[54] Gennisson, J.-L., Deffieux, T., Macé, E., Montaldo, G., Fink, M., and Tanter, M. Viscoelastic and anisotropic mechanical properties of in vivo muscle tissue assessed by supersonic shear imaging. *Ultrasound in medicine and biology 36*, 5 (2010), 789–801.

[55] Ghanem, R. G., and Spanos, P. D. *Stochastic Finite Elements: A Spectral Approach*. Springer-Verlag, 1991.

[56] Gillion, J., Sanders, D., Miserez, M., and Muysoms, F. The economic burden of incisional ventral hernia repair: a multicentric cost analysis. *Hernia 20*, 6 (2016), 819–830.

[57] Giunta, A. A., Wojtkiewicz, S. F., Eldred, M. S., et al. Overview of modern design of experiments methods for computational simulations. In *Proceedings of the 41st AIAA aerospace sciences meeting and exhibit, AIAA-2003-0649* (2003).

[58] Górski, J., Mikulski, T., Oziębło, M., and Winkelmann, K. Effect of geometric imperfections on aluminium silo capacities. *Stahlbau 84*, 1 (2015), 52–57.

[59] Grasa, J., Sierra, M., Lauzeral, N., Muñoz, M., Miana-Mena, F., and Calvo, B. Active behavior of abdominal wall muscles: Experimental results and numerical model formulation. *Journal of the mechanical behavior of biomedical materials 61* (2016), 444–454.

[60] Grässel, D., Prescher, A., Fitzek, S., Keyserlingk, D. G. V., and Axer, H. Anisotropy of human linea alba: A biomechanical study. *Journal of Surgical Research 124*, 1 (2005), 118–125.

[61] Green, D. W., Winandy, J. E., and Kretschmann, D. E. *Wood handbook—Wood as an Engineering Material*. Madison, 1999.

[62] Grossi, P., Sartori, T., Giongo, I., and Tomasi, R. Analysis of timber log-house construction system via experimental testing and analytical modelling. *Construction and Building Materials 102* (2016), 1127–1144.

[63] Guérin, G., and Turquier, F. Impact of the defect size, the mesh overlap and the fixation depth on ventral hernia repairs: a combined experimental and numerical approach. *Hernia 17*, 5 (2013), 647–655.

[64] Hadigol, M., and Doostan, A. Least squares polynomial chaos expansion: A review of sampling strategies. *Computer Methods in Applied Mechanics and Engineering 332* (2017), 382 – 407.

[65] Hadjikov, L., Kirilova, M., Stoytchev, S., and Pashkouleva, D. Visco-elastic mechanical behaviour of human abdominal fascia. *Series on Biomechanics 1*, 1 (2007), 39–46.

[66] Hamby, D. M. A review of techniques for parameter sensitivity analysis of environmental models. *Environmental Monitoring and Assessment 32*, 2 (1994), 135–154.

[67] Hernández, B., Pena, E., Pascual, G., Rodriguez, M., Calvo, B., Doblaré, M., and Bellón, J. Mechanical and histological characterization of the abdominal muscle. a previous step to modelling hernia surgery. *Journal of the mechanical behavior of biomedical materials 4*, 3 (2011), 392–404.

[68] Hernández-Gascón, B., Espés, N., Pena, E., Pascual, G., Bellón, J., and Calvo, B. Computational framework to model and design surgical meshes for hernia repair. *Computer methods in biomechanics and biomedical engineering 17*, 10 (2014), 1071–1085.

[69] Hernández-Gascón, B., Mena, A., Pena, E., Pascual, G., Bellón, J., and Calvo, B. Understanding the passive mechanical behavior of the human abdominal wall. *Annals of biomedical engineering 41*, 2 (2013), 433–444.

[70] Hernández-Gascón, B., Peña, E., Grasa, J., Pascual, G., Bellón, J. M., and Calvo, B. Mechanical response of the herniated human abdomen to the placement of different prostheses. *Journal of biomechanical engineering 135*, 5 (2013), 051004.

[71] Hernández-Gascón, B., Peña, E., Melero, H., Pascual, G., Doblaré, M., Ginebra, M., Bellón, J., and Calvo, B. Mechanical behaviour of synthetic surgical meshes: finite element simulation of the herniated abdominal wall. *Acta Biomaterialia 7*, 11 (2011), 3905–3913.

[72] Hernández-Gascón, B., Peña, E., Pascual, G., Rodríguez, M., Bellón, J., and Calvo, B. Long-term anisotropic mechanical response of surgical meshes used to repair abdominal wall defects. *Journal of the mechanical behavior of biomedical materials 5*, 1 (2012), 257–271.

[73] Higham, N. J. Computing the nearest correlation matrix–a problem from finance. *IMA journal of Numerical Analysis 22*, 3 (2002), 329–343.

[74] Hollinsky, C., and Sandberg, S. Measurement of the tensile strength of the ventral abdominal wall in comparison with scar tissue. *Clinical Biomechanics 22*, 1 (2007), 88–92.

[75] Horbach, A. J., Duong, M. T., and Staat, M. Modelling of compressible and orthotropic surgical mesh implants based on optical deformation measurement. *Journal of the mechanical behavior of biomedical materials 74* (2017), 400–410.

[76] Hristov, P., DiazDelaO, F., Flores, E. S., Guzmán, C., and Farooq, U. Probabilistic sensitivity analysis to understand the influence of micromechanical properties of wood on its macroscopic response. *Composite Structures 181* (2017), 229–239.

[77] Hu, C., and Youn, B. D. Adaptive-sparse polynomial chaos expansion for reliability analysis and design of complex engineering systems. *Structural and Multidisciplinary Optimization 43*, 3 (2011), 419–442.

[78] Huberts, W., Donders, W., Delhaas, T., and Vosse, F. Applicability of the polynomial chaos expansion method for personalization of a cardiovascular pulse wave propagation model. *International Journal for numerical methods in biomedical engineering 30*, 12 (2014), 1679–1704.

[79] Humphrey, J. D. Continuum biomechanics of soft biological tissues. In *Proceedings of the Royal Society of London A: Mathematical, Physical and Engineering Sciences* (2003), vol. 459, The Royal Society, pp. 3–46.

[80] Iooss, B., and Lemaître, P. A review on global sensitivity analysis methods. In *Uncertainty management in simulation-optimization of complex systems*. Springer, 2015, pp. 101–122.

[81] Iooss, B., and Saltelli, A. Introduction to sensitivity analysis. In *Handbook of Uncertainty Quantification*, R. Ghanem, D. Higdon, and H. Owhadi, Eds. Springer International Publishing, 2017.

[82] Isukapalli, S. S. *Uncertainty Analysis of Transport-Transformation Models*. PhD thesis, Graduate School New Brunswick, 1999.

[83] JCSS. Probabilistic Model. Joint committee on structural safety. *www. jcss. ethz. ch* (2001).

[84] Junge, K., Klinge, U., Prescher, A., Giboni, P., Niewiera, M., and Schumpelick, V. Elasticity of the anterior abdominal wall and impact for reparation of incisional hernias using mesh implants. *Hernia 5*, 3 (2001), 113–118.

[85] Junge, K., Klinge, U., Prescher, A., Giboni, P., Niewiera, M., and Schumpelick, V. Elasticity of the anterior abdominal wall and impact for reparation of incisional hernias using mesh implants. *Hernia 5*, 3 (2001), 113–118.

[86] Kahan, L. G., Guertler, C., Blatnik, J. A., and Lake, S. P. Validation of single c-arm fluoroscopic technique for measuring in vivo abdominal wall deformation. *Journal of biomechanical engineering 139*, 8 (2017), 084502.

[87] Kahan, L. G., Lake, S. P., McAllister, J. M., Tan, W. H., Yu, J., Thompson, D., Brunt, L. M., and Blatnik, J. A. Combined in vivo and ex vivo analysis of mesh mechanics in a porcine hernia model. *Surgical endoscopy 32*, 2 (2018), 820–830.

[88] Kandler, G., and Füssl, J. A probabilistic approach for the linear behaviour of glued laminated timber. *Engineering Structures 148* (2017), 673–685.

[89] Karhunen, K. *Über lineare Methoden in der Wahrscheinlichkeitsrechnung*, vol. 37. Universitat Helsinki, 1947.

[90] Khuri, A. I., and Cornell, J. A. *Response surfaces: designs and analyses*, vol. 152. CRC press, 1996.

[91] Kirilova, M., Stoytchev, S., Pashkouleva, D., and Kavardzhikov, V. Experimental study of the mechanical properties of human abdominal fascia. *Medical Engineering & Physics 33*, 1 (2011), 1–6.

[92] Klein, A., and Grabner, M. Analysis of construction timber in rural austria: Wooden log walls. *International Journal of Architectural Heritage 9*, 5 (2015), 553–563.

[93] Klinge, U., Klosterhalfen, B., Conze, J., Limberg, W., Obolenski, B., Öttinger, A., and Schumpelick, V. Modified mesh for hernia repair that is adapted to the physiology of the abdominal wall. *European Journal of Surgery 164*, 12 (1998), 951–960.

[94] Kłosowski, P., Komar, W., and Woźnica, K. Finite element description of nonlinear viscoelastic behaviour of technical fabric. *Construction and Building Materials 23*, 2 (2009), 1133–1140.

[95] Kłosowski, P., Lubowiecka, I., Pestka, A., and Szepietowska, K. Historical carpentry corner log joints—numerical analysis within stochastic framework. (submitted).

[96] Klosterhalfen, B., Junge, K., and Klinge, U. The lightweight and large porous mesh concept for hernia repair. *Expert review of medical devices 2*, 1 (2005), 103–117.

[97] Konerding, M., Chantereau, P., Delventhal, V., Holste, J.-L., and Ackermann, M. Biomechanical and histological evaluation of abdominal wall compliance with intraperitoneal onlay mesh implants in rabbits: A comparison of six different state-of-the-art meshes. *Medical Engineering and Physics 34*, 7 (2012), 806–816.

[98] Kucherenko, S., Tarantola, S., and Annoni, P. Estimation of global sensitivity indices for models with dependent variables. *Computer Physics Communications 183*, 4 (2012), 937–946.

[99] Le Gratiet, L., Marelli, S., and Sudret, B. Metamodel-based sensitivity analysis: Polynomial chaos expansions and gaussian processes. In *Handbook of Uncertainty Quantification*, R. Ghanem, D. Higdon, and H. Owhadi, Eds. Springer International Publishing, 2017.

[100] Le Maître, O. P., and Knio, O. M. *Spectral Methods for Uncertainty Quantification*. Scientific Computation. Springer Netherlands, Dordrecht, 2010.

[101] Le Maître, O. P., Reagan, M. T., Najm, H. N., Ghanem, R. G., and Knio, O. M. A stochastic projection method for fluid flow: II. random process. *Journal of Computational Physics 181*, 1 (2002), 9–44.

[102] Levillain, A., Orhant, M., Turquier, F., and Hoc, T. Contribution of collagen and elastin fibers to the mechanical behavior of an abdominal connective tissue. *Journal of the mechanical behavior of biomedical materials 61* (2016), 308–317.

[103] Loève, M. *Probability Theory I*, vol. 45 of *Graduate Texts in Mathematics*. Springer New York, New York, NY, 1977.

[104] Lubowiecka, I. Behaviour of orthotropic surgical implant in hernia repair due to the material orientation and abdomen surface deformation. *Computer methods in biomechanics and biomedical engineering 18*, 3 (2015), 223–232.

[105] Lubowiecka, I. Mathematical modelling of implant in an operated hernia for estimation of the repair persistence. *Computer methods in biomechanics and biomedical engineering 18*, 4 (2015), 438–445.

[106] Lubowiecka, I., Szepietowska, K., Szymczak, C., and Tomaszewska, A. Preliminary study on the optimal choice of an implant and its orientation in ventral hernia repair. *Journal of Theoretical and Applied Mechanics 54*, 2 (2016), 411–421.

[107] Lubowiecka, I., Szepietowska, K., Tomaszewska, A., and Szymczak, C. Mechanical compatibility of implants used in hernia repair with abdominal wall. In *Shell Structures. Theory and Applications* (2014), vol. 3, pp. 351–354.

[108] Lubowiecka, I., Szymczak, C., Tomaszewska, A., and Śmietański, M. A fem membrane model of human fasciasynthetic implant system in a case of a stiff ventral hernia orifice. In *Shell Structures. Theory and Applications* (2010), vol. 2, pp. 311–314.

[109] Lubowiecka, I., Tomaszewska, A., Szepietowska, K., Szymczak, C., Lochodziejewska-Niemierko, M., and Chmielewski, M. Membrane model of human abdominal wall. simulations vs. in vivo measurements. In *Shell Structures. Theory and Applications* (2018), vol. 4, pp. 503–506.

[110] Lyons, M., Mohan, H., Winter, D., and Simms, C. Biomechanical abdominal wall model applied to hernia repair. *British Journal of Surgery 102*, 2 (2015), e133–e139.

[111] Lyons, M., Winter, D. C., and Simms, C. K. Mechanical characterisation of porcine rectus sheath under uniaxial and biaxial tension. *Journal of biomechanics 47*, 8 (2014), 1876–1884.

[112] Marieb, E. Essentials of human anatomy and physiology 9th ed san francisco, 2009.

[113] Martins, P., Peña, E., Jorge, R. M. N., Santos, a., Santos, L., Mascarenhas, T., and Calvo, B. Mechanical characterization and constitutive modelling of the damage process in rectus sheath. *Journal of the mechanical behavior of biomedical materials 8* (2012), 111–22.

[114] Maurer, M., Röhrnbauer, B., Feola, A., Deprest, J., and Mazza, E. Mechanical biocompatibility of prosthetic meshes: A comprehensive protocol for mechanical characterization. *Journal of the mechanical behavior of biomedical materials 40* (2014), 42–58.

[115] Mazza, E., and Ehret, A. E. Mechanical biocompatibility of highly deformable biomedical materials. *Journal of the mechanical behavior of biomedical materials 48* (2015), 100–124.

[116] McKay, M. D., Beckman, R. J., and Conover, W. J. A comparison of three methods for selecting values of input variables in the analysis of output from a computer code. *Technometrics 42*, 1 (2000), 55–61.

[117] McKenzie, W., and Karpovich, H. The frictional behaviour of wood. *Wood science and technology 2*, 2 (1968), 139–152.

[118] Mleczek, A. Opracowanie wyników badań wytrzymałościowych dotyczących zginania drewna. Tech. rep., Gdańsk University of Technology, Department of Structural Mechanics, 2016.

[119] Mleczek, A., and Kłosowski, P. Numerical analysis of the carpentry joints applied in the traditional wooden structures. In *Advances in Mechanics: Theoretical, Computational and Interdisciplinary Issues: Proceedings of the 3rd Polish Congress of Mechanics (PCM) and 21st International Conference on Computer Methods in Mechanics (CMM), Gdansk, Poland, 8-11 September 2015* (2016), CRC Press, p. 409.

[120] Morokoff, W. J., and Caflisch, R. E. Quasi-Random Sequences and Their Discrepancies. *SIAM J. SCl. COMPUT 15*, 6 (1994), 1251–1279.

[121] Navarro, M., Witteveen, J., and Blom, J. Polynomial chaos expansion for general multivariate distributions with correlated variables. *arXiv preprint arXiv:1406.5483* (2014).

[122] Niederreiter, H. Quasi-monte carlo methods and pseudo-random numbers. *Bulletin of the American Mathematical Society 84*, 6 (1978), 957–1041.

[123] Nowak, T. P., Jasieńko, J., and Hamrol-Bielecka, K. In situ assessment of structural timber using the resistance drilling method–evaluation of usefulness. *Construction and Building Materials 102* (2016), 403–415.

[124] Pachera, P., Pavan, P., Todros, S., Cavinato, C., Fontanella, C., and Natali, A. A numerical investigation of the healthy abdominal wall structures. *Journal of biomechanics 49*, 9 (2016), 1818–1823.

[125] Palma, P., Garcia, H., Ferreira, J., Appleton, J., and Cruz, H. Behaviour and repair of carpentry connections–rotational behaviour of the rafter and tie beam connection in timber roof structures. *Journal of Cultural Heritage 13*, 3 (2012), S64–S73.

[126] Parisi, M. A., and Cordié, C. Mechanical behavior of double-step timber joints. *Construction and Building Materials 24*, 8 (2010), 1364–1371.

[127] Parisi, M. A., and Piazza, M. Mechanics of plain and retrofitted traditional timber connections. *Journal of Structural Engineering 126*, 12 (2000), 1395–1403.

[128] Pestka, A., Kłosowski, P., Lubowiecka, I., and Krajewski, M. Influence of wood moisture on strength and elastic modulus for pine and fir wood subjected to 4-point bending tests. In *Proceedings of World Multidisciplinary Civil Engineering-Architecture-Urban Planning Symposium* (2018). submitted.

[129] Pianosi, F., Beven, K., Freer, J., Hall, J. W., Rougier, J., Stephenson, D. B., and Wagener, T. Sensitivity analysis of environmental models: A systematic review with practical workflow. *Environmental Modelling & Software 79* (2016), 214–232.

[130] Podwojewski, F., Otténio, M., Beillas, P., Guérin, G., Turquier, F., and Mitton, D. Mechanical response of animal abdominal walls in vitro: Evaluation of the influence of a hernia defect and a repair with a mesh implanted intraperitoneally. *Journal of Biomechanics 46*, 3 (2013), 561 – 566.

[131] Podwojewski, F., Otténio, M., Beillas, P., Guérin, G., Turquier, F., and Mitton, D. Mechanical response of human abdominal walls ex vivo: Effect of an incisional hernia and a mesh repair. *Journal of the Mechanical Behavior of Biomedical Materials 38* (2014), 126 – 133.

[132] Poulose, B., Shelton, J., Phillips, S., Moore, D., Nealon, W., Penson, D., Beck, W., and Holzman, M. Epidemiology and cost of ventral hernia repair: making the case for hernia research. *Hernia 16*, 2 (2012), 179–183.

[133] Prasad, A. K., Ahadi, M., Thakur, B. S., and Roy, S. Accurate polynomial chaos expansion for variability analysis using optimal design of experiments. In *Numerical Electromagnetic and Multiphysics Modeling and Optimization (NEMO), 2015 IEEE MTT-S International Conference on* (2015), IEEE, pp. 1–4.

[134] Qadri, S. J. F., Khan, M., Wani, S. N., Nazir, S. S., and Rather, A. Laparoscopic and open incisional hernia repair using polypropylene mesh-a comparative single centre study. *International Journal of Surgery 8*, 6 (2010), 479–483.

[135] Röhrnbauer, B., Kress, G., and Mazza, E. A physically based structural model for a textile prosthetic mesh. *International Journal of Solids and Structures 51*, 3-4 (2014), 633–646.

[136] Röhrnbauer, B., and Mazza, E. A non-biological model system to simulate the in vivo mechanical behavior of prosthetic meshes. *Journal of the mechanical behavior of biomedical materials 20* (2013), 305–315.

[137] Röhrnbauer, B., and Mazza, E. Uniaxial and biaxial mechanical characterization of a prosthetic mesh at different length scales. *Journal of the mechanical behavior of biomedical materials 29* (2014), 7–19.

[138] Saberski, E., Orenstein, S., and Novitsky, Y. Anisotropic evaluation of synthetic surgical meshes. *Hernia 15*, 1 (2011), 47–52.

[139] Saltelli, A., Chan, K., Scott, E. M., et al. *Sensitivity analysis*. Wiley New York, 2000.

[140] Saltelli, A., Ratto, M., Andres, T., Campolongo, F., Cariboni, J., Gatelli, D., Saisana, M., and Tarantola, S. *Global sensitivity analysis: the primer*. John Wiley & Sons, 2008.

[141] Santamaría, V. A., Siret, O., Badel, P., Guerin, G., Novacek, V., Turquier, F., and Avril, S. Material model calibration from planar tension tests on porcine linea alba. *Journal of the Mechanical Behavior of Biomedical Materials 43* (2015), 26 – 34.

[142] Sauerland, S., Walgenbach, M., Habermalz, B., Seiler, C. M., and Miserez, M. Laparoscopic versus open surgical techniques for ventral or incisional hernia repair. *The Cochrane Library* (2011).

[143] Schoenmaeckers, E. J., Wassenaar, E. B., Raymakers, J. T., and Rakic, S. Bulging of the mesh after laparoscopic repair of ventral and incisional hernias. *JSLS: Journal of the Society of Laparoendoscopic Surgeons 14*, 4 (2010), 541.

[144] Simón-Allué, R., Calvo, B., Oberai, A., and Barbone, P. Towards the mechanical characterization of abdominal wall by inverse analysis. *Journal of the Mechanical Behavior of Biomedical Materials 66* (2017), 127–137.

[145] Simón-Allué, R., Hernández-Gascón, B., Lèoty, L., Bellón, J., Peña, E., and Calvo, B. Prostheses size dependency of the mechanical response of the herniated human abdomen. *Hernia 20*, 6 (2016), 839–848.

[146] Simón-Allué, R., Montiel, J., Bellón, J., and Calvo, B. Developing a new methodology to characterize in vivo the passive mechanical behavior of abdominal wall on an animal model. *Journal of the mechanical behavior of biomedical materials 51* (2015), 40–49.

[147] Simón-Allué, R., Ortillés, A., and Calvo, B. Mechanical behavior of surgical meshes for abdominal wall repair: In vivo versus biaxial characterization. *Journal of the mechanical behavior of biomedical materials 82* (2018), 102–111.

[148] Skowronek, M. Probabilistic sensitivity of the limit states of structures using monte carlo simulation. *Meccanica 45*, 6 (2010), 785–796.

[149] Smith, K. On the standard deviations of adjusted and interpolated values of an observed polynomial function and its constants and the guidance they give towards a proper choice of the distribution of observations. *Biometrika 12*, 1-2 (1918), 1–85.

[150] Sobol, I. M. Global sensitivity indices for nonlinear mathematical models and their Monte Carlo estimates. *Mathematics and Computers in Simulation 55*, 1-3 (2001), 271–280.

[151] Sobol, I. M., and Kucherenko, S. Global sensitivity indices for nonlinear mathematical models. review. *Wilmott Mag 1* (2005), 56–61.

[152] Soize, C., and Ghanem, R. Physical systems with random uncertainties: chaos representations with arbitrary probability measure. *SIAM Journal on Scientific Computing 26*, 2 (2004), 395–410.

[153] Song, C., Alijani, A., Frank, T., Hanna, G., and Cuschieri, A. Elasticity of the living abdominal wall in laparoscopic surgery. *Journal of biomechanics 39*, 3 (2006), 587–591.

[154] Song, C., Alijani, A., Frank, T., Hanna, G. B., and Cuschieri, A. Mechanical properties of the human abdominal wall measured in vivo during insufflation for laparoscopic surgery. *Surgical Endoscopy And Other Interventional Techniques 20*, 6 (2006), 987–990.

[155] Sørensen, J. D. Framework for robustness assessment of timber structures. *Engineering Structures 33*, 11 (2011), 3087–3092.

[156] Stefanou, G. The stochastic finite element method: past, present and future. *Computer Methods in Applied Mechanics and Engineering 198*, 9-12 (2009), 1031–1051.

[157] Stoikes, N., Sharpe, J., Tasneem, H., Roan, E., Paulus, E., Powell, B., Webb, D., Handorf, C., Eckstein, E., Fabian, T., et al. Biomechanical evaluation of fixation properties of fibrin glue for ventral incisional hernia repair. *Hernia 19*, 1 (2015), 161–166.

[158] Sudret, B. Uncertainty propagation and sensitivity analysis in mechanical models–contributions to structural reliability and stochastic spectral methods. *Habilitationa diriger des recherches, Université Blaise Pascal, Clermont-Ferrand, France* (2007).

[159] Sudret, B. Global sensitivity analysis using polynomial chaos expansions. *Reliability Engineering & System Safety 93*, 7 (2008), 964–979.

[160] Sudret, B. Polynomial chaos expansions and stochastic finite element methods. *Risk and reliability in geotechnical engineering* (2015), 265–300.

[161] Sudret, B., and Der Kiureghian, A. Stochastic Finite Element Methods and Reliability A State-of-the-Art Report. Tech. Rep. November, 2000.

[162] Sullivan, T. J. *Introduction to uncertainty quantification.* Springer, 2015.

[163] Szepietowska, K., and Lubowiecka, I. Mechanical behaviour of the implant used in human hernia repair under physiological loads. *Acta of bioengineering and biomechanics 15*, 3 (2013).

[164] Szepietowska, K., Magnain, B., Lubowiecka, I., and Florentin, E. Regression points in non-intrusive polynomial chaos expansion method and d-optimal design. *Machine Dynamics Research 41* (2017), 5–16.

[165] Szepietowska, K., Magnain, B., Lubowiecka, I., and Florentin, E. Sensitivity analysis based on non-intrusive regression-based polynomial chaos expansion for surgical mesh modelling. *Structural and Multidisciplinary Optimization 57*, 3 (2018), 1391–1409.

[166] Szymczak, C. *Elementy teorii projektowania.* Wydawnictwo Naukowe PWN, 1998.

[167] Szymczak, C., Lubowiecka, I., Szepietowska, K., and Tomaszewska, A. Two-criteria optimisation problem for ventral hernia repair. *Computer Methods in Biomechanics and Biomedical Engineering 20*, 7 (2017), 760–769.

[168] Szymczak, C., Lubowiecka, I., Tomaszewska, A., and Śmietański, M. Modeling of the fascia-mesh system and sensitivity analysis of a junction force after a laparoscopic ventral hernia repair. *Journal of Theoretical and Applied Mechanics 48*, 4 (2010), 933–950.

[169] Szymczak, C., Lubowiecka, I., Tomaszewska, A., and Śmietański, M. Investigation of abdomen surface deformation due to life excitation: implications for implant selection and orientation in laparoscopic ventral hernia repair. *Clinical Biomechanics 27*, 2 (2012), 105–110.

[170] Szymczak, C., and Śmietański, M. *Selected problems of laparoscopic ventral hernia repair - modeling and simulation.* alfa-medica press Gdańsk, 2012.

[171] Todros, S., Pachera, P., Baldan, N., Pavan, P. G., Pianigiani, S., Merigliano, S., and Natali, A. N. Computational modeling of abdominal hernia laparoscopic repair with a surgical mesh. *International journal of computer assisted radiology and surgery 13*, 1 (2018), 73–81.

[172] Todros, S., Pachera, P., Pavan, P. G., and Natali, A. N. Investigation of the mechanical behavior of polyester meshes for abdominal surgery: A preliminary study. *Journal of Medical and Biological Engineering* (2017), 1–12.

[173] Tomaszewska, A. Mechanical behaviour of knit synthetic mesh used in hernia surgery. *Acta of bioengineering and biomechanics 18*, 1 (2016).

[174] Tomaszewska, A., Lubowiecka, I., Szymczak, C., Śmietański, M., Meronk, B., Kłosowski, P., and Bury, K. Physical and mathematical modelling of implant-fascia system in order to improve laparoscopic repair of ventral hernia. *Clinical Biomechanics 28*, 7 (2013), 743 – 751.

[175] Torre, E., Marelli, S., Embrechts, P., and Sudret, B. A general framework for uncertainty quantification under non-gaussian input dependencies. *arXiv preprint arXiv:1709.08626* (2017).

[176] Tran, D., Mitton, D., Voirin, D., Turquier, F., and Beillas, P. Contribution of the skin, rectus abdominis and their sheaths to the structural response of the abdominal wall ex vivo. *Journal of Biomechanics 47*, 12 (2014), 3056 – 3063.

[177] Tran, D., Podwojewski, F., Beillas, P., Ottenio, M., Voirin, D., Turquier, F., and Mitton, D. Abdominal wall muscle elasticity and abdomen local stiffness on healthy volunteers during various physiological activities. *Journal of the mechanical behavior of biomedical materials 60* (2016), 451–459.

[178] Tse, G., Stutchfield, B., Duckworth, A., De Beaux, A., and Tulloh, B. Pseudo-recurrence following laparoscopic ventral and incisional hernia repair. *Hernia 14*, 6 (2010), 583–587.

[179] Turányi, T. Sensitivity analysis of complex kinetic systems. tools and applications. *Journal of Mathematical Chemistry 5*, 3 (1990), 203–248.

[180] Villar, J., Guaita, M., Vidal, P., and Arriaga, F. Analysis of the stress state at the cogging joint in timber structures. *Biosystems engineering 96*, 1 (2007), 79–90.

[181] Wiener, N. The homogeneous chaos. *American Journal of Mathematics 60*, 4 (1938), 897–936.

[182] Williams, D. F. On the mechanisms of biocompatibility. *Biomaterials 29*, 20 (2008), 2941–2953.

[183] Winkelmann, K., and Górski, J. The use of response surface methodology for reliability estimation of composite engineering structures. *Journal of Theoretical and Applied Mechanics 52*, 4 (2014), 1019–1032.

[184] Xiu, D. *Numerical methods for stochastic computations: a spectral method approach*. Princeton University Press, 2010.

[185] Xiu, D., and Karniadakis, G. E. The Wiener–Askey Polynomial Chaos for Stochastic Differential Equations. *SIAM Journal on Scientific Computing 24*, 2 (2002), 619–644.

[186] Xu, C., and Gertner, G. Z. Uncertainty and sensitivity analysis for models with correlated parameters. *Reliability Engineering & System Safety 93*, 10 (2008), 1563–1573.

[187] Xu, M., Li, L., Wang, M., and Luo, B. Effects of surface roughness and wood grain on the friction coefficient of wooden materials for wood–wood frictional pair. *Tribology Transactions 57*, 5 (2014), 871–878.

[188] Yang, J., Faverjon, B., Dureisseix, D., Swider, P., and Kessissoglou, N. Prediction of the intramembranous tissue formation during perisprosthetic healing with uncertainties. part 1. effect of the variability of each biochemical factor. *Computer methods in biomechanics and biomedical engineering 19*, 13 (2016), 1378–1386.

[189] Yang, J., Faverjon, B., Dureisseix, D., Swider, P., Marburg, S., Peters, H., and Kessissoglou, N. Prediction of the intramembranous tissue formation during perisprosthetic healing with uncertainties. part 2. global clinical healing due to combination of random sources. *Computer methods in biomechanics and biomedical engineering 19*, 13 (2016), 1387–1394.

[190] Zein, S., Colson, B., and Glineur, F. An Efficient Sampling Method for Regression-Based Polynomial Chaos Expansion. *Communications in Computational Physics 13*, 4 (2012), 1173–1188.

[191] Żerdzicki, K., Kłosowski, P., and Woźnica, K. Influence of service ageing on polyester-reinforced polyvinyl chloride-coated fabrics reported through mathematical material models. *Textile Research Journal* (2018), 0040517518773374.

Katarzyna SZEPIETOWSKA

MISE EN OEUVRE DU CHAOS POLYNOMIAL EN BIOMECANIQUE ET EN MECANIQUE DES STRUCTURES

Cette thèse présente une approche probabiliste de la modélisation de la mécanique des matériaux et des structures. Le dimensionnement est influencé par l'incertitude des paramètres d'entrée. Le travail est interdisciplinaire et les méthodes décrites sont appliquées à des exemples de biomécanique et de génie civil. La motivation de ce travail était le besoin d'approches basées sur la mécanique dans la modélisation et la simulation des implants utilisés dans la réparation des hernies ventrales. De nombreuses incertitudes apparaissent dans la modélisation du système implant-paroi abdominale. L'approche probabiliste proposée dans cette thèse permet de propager ces incertitudes et d'étudier leurs influences respectives. La méthode du chaos polynomial basée sur la régression est utilisée dans ce travail. L'exactitude de ce type de méthodes non intrusives dépend du nombre et de l'emplacement des points de calcul choisis. Trouver une méthode universelle pour atteindre un bon équilibre entre l'exactitude et le coût de calcul est encore une question ouverte. Différentes approches sont étudiées dans cette thèse afin de choisir une méthode efficace et adaptée au cas d'étude. L'analyse de sensibilité globale est utilisée pour étudier les influences des incertitudes d'entrée sur les variations des sorties de différents modèles. Les incertitudes sont propagées aux modèles implant-paroi abdominale. Elle permet de tirer des conclusions importantes pour les pratiques chirurgicales. À l'aide de l'expertise acquise à partir de ces modèles biomécaniques, la méthodologie développée est utilisée pour la modélisation de joints de bois historiques et la simulation de leur comportement mécanique. Ce type d'étude facilite en effet la planification efficace des réparations et de la rénovation des bâtiments ayant une valeur historique.
Mots-clés : Propagation d'incertitudes, Analyse de sensibilité globale, Réparation de l'hernie ventrale; Choix des points de regression

POLYNOMIAL CHAOS EXPANSION IN BIO- AND STRUCTURAL MECHANICS

This thesis presents a probabilistic approach to modelling the mechanics of materials and structures where the modelled performance is influenced by uncertainty in the input parameters. The work is interdisciplinary and the methods described are applied to medical and civil engineering problems. The motivation for this work was the necessity of mechanics-based approaches in the modelling and simulation of implants used in the repair of ventral hernias. Many uncertainties appear in the modelling of the implant-abdominal wall system. The probabilistic approach proposed in this thesis enables these uncertainties to be propagated to the output of the model and the investigation of their respective influences. The regression-based polynomial chaos expansion method is used here. However, the accuracy of such non-intrusive methods depends on the number and location of sampling points. Finding a universal method to achieve a good balance between accuracy and computational cost is still an open question so different approaches are investigated in this thesis in order to choose an efficient method. Global sensitivity analysis is used to investigate the respective influences of input uncertainties on the variation of the outputs of different models. The uncertainties are propagated to the implant-abdominal wall models in order to draw some conclusions important for further research. Using the expertise acquired from biomechanical models, modelling of historic timber joints and simulations of their mechanical behaviour is undertaken. Such an investigation is important owing to the need for efficient planning of repairs and renovation of buildings of historical value.
Keywords: uncertainty quantification, global sensitivity analysis, ventral hernia repair; regression points choice

GDAŃSK UNIVERSITY OF TECHNOLOGY
Ul. G.Narutowicza 11/12, 80-233 Gdańsk